

Computational Pathology: A Survey Review and The Way Forward

Mahdi S. Hosseini^{a,*}, Babak Ehteshami Bejnordi^{b,1}, Vincent Quoc-Huy Trinh^c, Danial Hasan^d, Xingwen Li^d, Taehyo Kim^d, Haochen Zhang^d, Theodore Wu^d, Kajanan Chinniah^d, Sina Maghsoudlou^e, Ryan Zhang^d, Stephen Yang^d, Jiadai Zhu^d, Lyndon Chan^d, Samir Khaki^d, Andrei Buin^f, Fatemeh Chaji^g, Ala Salehi^h, Alejandra Zambrano Luna^a, Bich Ngoc Nguyenⁱ, Dimitris Samaras^j, Konstantinos N. Plataniotis^d

^a*Department of Computer Science and Software Engineering (CSSE), Concordia University, Montreal, QC H3H 2R9, Canada*

^b*Qualcomm AI Research, Qualcomm Technologies Netherlands B.V., Amsterdam, The Netherlands*

^c*Institute for Research in Immunology and Cancer of the University of Montreal, Montreal, QC H3T 1J4, Canada*

^d*The Edward S. Rogers Sr. Department of Electrical & Computer Engineering (ECE), University of Toronto, Toronto, ON M5S 3G4, Canada*

^e*Convergent Technologies Research Center (NBIC), University College of Engineering, University of Tehran, Iran*

^f*Huron Digital Pathology, St. Jacobs, ON N0B 2N0, Canada*

^g*Department of Computer Engineering, Ferdowsi University of Mashhad, Mashhad, Iran*

^h*Department of Electrical and Computer Engineering, University of New Brunswick, Fredericton, NB E3B 5A3, Canada*

ⁱ*University of Montreal Hospital Center, Montreal, QC H2X 0C2, Canada*

^j*Department of Computer Science, Stony Brook University, Stony Brook, NY 11794, United States*

*This work is dedicated to the beloved memories of Kuanhou Fang, Shahnaz Habibpanah, Zakiyah Khaliji-Oskoui, James Liang, Mahsa MohammadiMoghaddam, Vily Panoutsakopoulou, Athanasia Samara, Huoyuan Yu, Dexi Zhang
and all people around the world who have lost their lives because of cancer*

Abstract. Computational Pathology (CoPath) is an interdisciplinary science that augments developments of computational approaches to analyze and model medical histopathology images. The main objective for CoPath is to develop infrastructure and workflows of digital diagnostics as an assistive CAD system for clinical pathology facilitating transformational changes in the diagnosis and treatment of cancer diseases. With evergrowing developments in deep learning and computer vision algorithms, and the ease of the data flow from digital pathology, currently CoPath is witnessing a paradigm shift. Despite the sheer volume of engineering and scientific works being introduced for cancer image analysis, there is still a considerable gap of adopting and integrating these algorithms in clinical practice. This raises a significant question regarding the direction and trends that are undertaken in CoPath. In this article we provide a comprehensive review of more than 700 papers to address the challenges faced in problem design all-the-way to the application and implementation viewpoints. We have catalogued each paper into a model-card by examining the key works and challenges faced to layout the current landscape in CoPath. We hope this helps the community to locate relevant works and facilitate understanding of the field's future directions. In a nutshell, we oversee the CoPath developments in cycle of stages which are required to be cohesively linked together to address the challenges associated with such multidisciplinary science. We overview this cycle from different perspectives of data-centric, model-centric, and application-centric problems. We finally sketch remaining challenges and provide directions for future technical developments and clinical integration of CoPath.

Keywords: digital pathology, whole slide image (WSI), deep learning, computer aided diagnosis (CAD), clinical pathology, survey

Contents

1 Introduction	2	3 Data Collection for CoPath	14
2.1 Clinical Pathology Workflow	4	3.1 Tissue Slide Preparation	14
2.2 Diagnostic Tasks	6	3.2 Whole Slide Imaging (WSI)	15
2.3 Prognosis	8	3.3 Cohort Selection, Scale, and Challenges	17
2.4 Prediction of treatment response	9		
2.5 Cancer Statistics	9		
2.6 Organs and Diseases	9		
		4 Domain Expert Knowledge Annotation	19
		4.1 Supervised Annotation	19
		4.2 Optimum Labeling Workflow Design	22
		5 Representational Learning Models in CoPath	23
		5.1 Classification Architectures	23
		5.2 Segmentation Architectures	24
		5.3 Object Detection Architectures	25
		5.4 Multi-Task Learning	25
		5.5 Multi-Modal Learning	26
		5.6 Sequential Models	26
		5.7 Generative Models	27

*Corresponding author.

E-mail address: mahdi.hosseini@concordia.ca

¹Qualcomm AI Research is an initiative of Qualcomm Technologies, Inc.

5.8	Multi-Instance Learning Models	27
5.9	Contrastive Learning	28
5.10	Novel CoPath Architecture	28
5.11	Model Comparison	29
6	Evaluation and Regulations	30
6.1	Clinical Validation	30
6.2	FDA Regulations	31
7	Existing Challenges and Future Opportunities	31
7.1	Comparison to General Computer Vision	31
7.2	Leveraging Existing Datasets	31
7.3	Creating New Datasets	32
7.4	Pre and Post Analytical CAD Tools	32
7.5	Multi Domain Learning	33
7.6	Federated Learning for Multicentral CoPath	33
7.7	CoPath-specific architecture designs	33
7.8	Digital and Computational Pathology Adoption	34
7.9	Institutional Challenges	34
7.10	Clinical Alignment of CoPath Tasks	34
7.11	Concluding Remarks	35
8	Supplementary Material	54
8.1	Surveyed Datasets	54
8.1.1	Table Creation Details	54
8.2	Organ Overview	54
8.3	Technicalities by Task	54
8.4	Model Card Categorization	78
8.4.1	Template	78
8.4.2	Samples	79

1. Introduction

April 2017 marked a turning point for digital pathology when the Philips IntelliSite digital scanner received FDA approval (with limited use case) for diagnostic applications in clinical pathology Release (2017); Evans et al. (2018). A subsequent validation guideline was created to help ensure the produced Whole Slide Image (WSI) scans could be used in clinical settings without compromising patient care, while maintaining similar results to the current gold standard of optical microscopy Araújo et al. (2019); Williams et al. (2018); Großerueschkamp et al. (2021); Kuo and Leo (2019). The use of WSIs offers significant advantages to the pathologist’s workflow: digitally captured images, compared to tissue slides, are immune from accidental physical damage and maintain their quality over time Pell et al. (2019); Al-Janabi et al. (2012). Clinics and practices can share and store these high-resolution images digitally enabling asynchronous viewing/collaboration worldwide Griffin and Treanor (2017); Saco et al. (2016). The development of *digital pathology* shows great promise as a framework to improve work efficiency in the practice of pathology Kaushal et al. (2021); Saco et al. (2016). Adopting a digital workflow also opens immense opportunities for using computational methods to augment and expedite their workflow—the field of *Computational Pathology (CoPath)* is dedicated to researching and developing these methods Van der Laak et al. (2021); Cui and Zhang (2021); Echle et al. (2021); Acs et al. (2020); Salvi et al. (2021); Srinidhi et al. (2021).

However, despite the aforementioned advantages, the adoption of digital pathology, and hence computational pathology, has been slow. Some pathologists consider the analysis of WSIs as opposed to glass slides as an unnecessary change in their workflow Lujan et al. (2022); Liu and Pantanowitz (2019); Griffin and Treanor (2017); Jara-Lazaro et al. (2010) and recent surveys indicate that the switch to digital pathology does not provide enough financial incentive Smith et al. (2022); Sundar et al. (2020); Buabbas et al. (2021); Baidoshvili et al. (2018); Dennis et al. (2005); Al-Janabi et al. (2012). This is where advances from CoPath can address or overpower many of the concerns in adopting a digital workflow. For example, CoPath models to identify morphological features that correlate with breast cancer Dong et al. (2014) provide substantial benefits to clinical accuracy. Further, CoPath models that identify lymph node metastases with better sensitivity while reducing diagnostic time Steiner et al. (2018) can streamline workflows to increase pathologist throughput and generate more revenue Cooper et al. (2012); Kim et al. (2022).

Similar to digital pathology, the adoption of CoPath methods has also lagged despite the many benefits it offers to improve efficiency and accuracy in pathology Abels et al. (2019); Kumar et al. (2020b); Evans et al. (2018); Koohbanani et al. (2021). This lack of adoption and integration into clinical practice raises a significant question regarding the direction and trends of current work in CoPath. This survey looks to review the field of CoPath in a systematic fashion by breaking down the various steps involved in a CoPath workflow and categorizing CoPath works to both determine trends in the field and provide a resource for the community to reference when creating new works.

Existing survey papers in the field of CoPath can be clustered into a few groups. The first focuses on the design and applications of smart diagnosis tools Bera et al. (2019); Niazi et al. (2019); Sobhani et al. (2021); Klein et al. (2021); Go (2022); Rony et al. (2019); Srinidhi et al. (2021); Salvi et al. (2021); Acs et al. (2020); Abinaya and Sivakumar (2022); Bilal et al. (2022); Schneider et al. (2022); Jiang et al. (2020c); Lancellotti et al. (2021). These works focus on designing novel architectures for AI models with regards to specific clinical tasks, although they may briefly discuss clinical challenges and limitations. A second group of works focus on clinical barriers for AI integration discussing specific certifications and regulations required for the development of medical devices under clinical settings Colling et al. (2019); Baxi et al. (2022); Sakamoto et al. (2020); Cheng et al. (2021a); Brixel et al. (2022); Shmatko et al. (2022). Lastly, the final group focuses on both the design and the integration of AI tools with clinical applications Makhlof et al. (2022); Huo et al. (2021); Van der Laak et al. (2021); Cui and Zhang (2021); Serag et al. (2019); Kim et al. (2022); Wong et al. (2022); AlAmir and AlGhamdi (2022); Echle et al. (2021); Cifci et al. (2022); Haggenmüller et al. (2021). These works speak to both the computer vision and pathology communities in developing ML models that can satisfy clinical use cases.

Our work is situated in this final group as we breakdown the end-to-end CoPath workflow into stages and systematically re-

view works related to and addressing those stages. We oversee this as a workflow for CoPath research that breaks down the process of problem definition, data collection, model creation, and clinical validation into a cycle of stages. A visual representation of this cycle is provided in Figure 1. We review over 700 papers from all areas of the CoPath field to examine key works and challenges faced. By reviewing the field so comprehensively, our goal is to layout the current landscape of key developments to allow computer scientists and pathologists alike to situate their work in the overall CoPath workflow, locate relevant works, and facilitate an understanding of the field’s future directions. We also adopt the idea of generating model cards from Mitchell et al. (2019) and designed a card format specifically tailored for CoPath. Each paper we reviewed was catalogued as a model card that concisely describes (1) the organ of application, (2) the compiled dataset, (3) the machine learning model, and (4) the target task. The complete model card categorization of the reviewed publications is provided in Appendix 8.4 for the reader’s use.

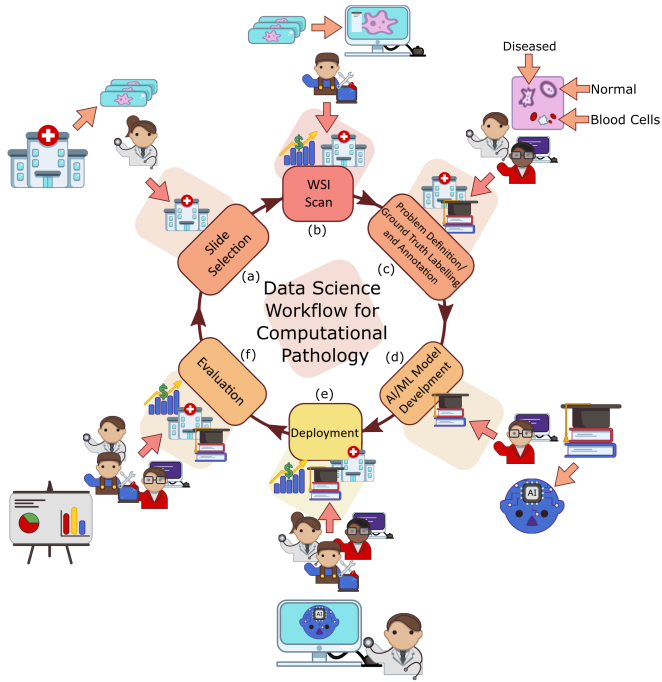


Fig. 1: We divide the data science workflow for pathology into multiple stages, wherein each brings a different level of experience. For example, the problem definition stage (c) is where domain expert knowledge is consulted as to augment images with associated metadata, meanwhile, in the evaluation phase (f), we have computer vision scientists, software developers, and pathologists working in concert to extract meaningful results and implications from the representation learning.

In our review of the CoPath field, we find that two main approaches emerge in works: 1) a data-centric approach and 2) a model-centric approach. Considering a given application area, such as specific cancers, e.g. breast ductal carcinoma in-situ (DCIS), or a specific task, e.g. segmentation of benign and malignant regions of tissue, researchers in the CoPath field focus generally on either improving the data or innovating on the model used.

Works with data-centric approaches focus on collecting

pathology data and compiling datasets to train models on certain tasks based on the premise that the transfer of domain expert knowledge to models is captured by the process of collecting and labeling high-quality data Gu et al. (2021); Huo et al. (2021); Tomaszewski (2021). The motivation behind this approach in CoPath is driven by the need to 1) address the lack of labeled WSI data representing both histology and histopathology cases due to the laborious annotation process Baidoshvili et al. (2018) and 2) capture a predefined pathology ontology provided by domain expert pathologists for the class definitions and relations in tissue samples. Regarding the lack of labeled WSI data our analysis reveals that there are a larger number of datasets with granular labels, but there is a larger total amount of data available for a given organ and disease application that have weakly supervised labels at the Slide or Patient-level. Although some tasks, such as segmentation and detection, require WSI data to have more granular labels at the region-of-interest (ROI) or image mosaic/tiles (known as patch) levels, to capture more precise information for training models, there is a potential gap to leverage the large amount of weakly-supervised data to train models that can be later downstream on smaller strongly-supervised datasets for those tasks. When considering the ontology of pathology as compared to the field of computer vision, we note that pathology has far fewer classes than computer vision (e.g. ImageNet-20K contains 20,000 class categories for natural images Deng et al. (2009a) whereas CAMELYON17 has four classes for breast cancer metastases Litjens et al. (2018)), but has much more variation within class representations and has fuzzy boundaries around the *grade* of cancers. There are also very rare classes in the form of rare diseases and cancers, as presented in Figure 4 and discussed in Section 2, which present a class imbalance challenge when compiling data or training models. If one considers the complexities involved in representational learning of related tissues and diseases, it raises the question of whether there is a clear understanding and consensus in the field of how an efficient dataset should be compiled for model development. Our survey analyzes the availability of CoPath datasets along with what area of application they address and their annotation level in detail in Section 3.3, and the complete table of datasets we have covered is available in Appendix 8.1. Section 4 goes into more depth about the various levels of annotation, the annotation process, and selecting the appropriate annotation level for a task.

The model-centric approach, by contrast, is favoured by computer scientists and engineers, who design algorithmic approaches based on the available pathology data. Selection of a modelling approach, such as self-supervised, weakly-supervised, or strongly-supervised learning, is dictated directly by the amount of data available for a given annotation level and task. Currently, many models are developed on datasets with strongly-supervised labels at the ROI, Patch, or Pixel-levels to address tasks such as tissue type classification or disease detection. However, a recent trend is developing to apply self-supervised and weakly-supervised learning methods to leverage the large amount of data with Slide and Patient-level annotations Campanella et al. (2019b). Models are trained in a self or weakly supervised manner to learn representations on

a wider range of pathology data across organs and diseases, which can be leveraged for other tasks requiring more supervision but without the need for massive labeled datasets Lu et al. (2020a, 2021d); Chen et al. (2022). This trend points to the future direction of CoPath models following a similar trend to that in computer vision, where large-scale models are being pre-trained using self-supervised techniques to achieve state-of-the-art performance in downstream tasks Chen et al. (2020d); Caron et al. (2021a).

Although data and model centric approaches are both important in advancing the performance of models and tools in CoPath, we note a need for much more *application* centric work in CoPath. We define a study to be application centric if the primary focus is on addressing a particularly impactful task or need in the clinical workflow, ideally including clinical validation of the method or tool. To this end, Section 2 details the clinical pathology workflow from specimen collection to report generation, major task categories in CoPath, and specific applications per organ. Particularly, we find that very few works focus on the pre or post-analytical phases of the pathology workflow where many errors can occur, instead focusing on the analytical phase where interpretation tasks take place. Additionally, certain types of cancer with deadly survival rates are underrepresented in CoPath datasets and works. Very few CoPath models and tools have been validated in a clinical setting by pathologists, suggesting that there may still be massive barriers to actually using CoPath tools in practice. All of this points to a severe oversight by the CoPath community towards considering the actual application and implementation of tools in a clinical setting. We suspect this to be a major reason as to why there is a slow uptake in adopting CoPath tools by pathology labs.

The contributions of this survey include the provision of an end-to-end workflow for developing CoPath work which outlines the various stages involved and is reflected within the survey sections. Further, we propose and provide a comprehensive conceptual model card framework for CoPath that clearly categorizes works by their application of interest, dataset usage, and model, enabling consistent and easy comparison and retrieval of papers in relevant areas. Based on our analysis of the field, we highlight several challenges and trends, including the availability of datasets, focus on models leveraging existing data, disregard of impactful application areas, and lack of clinical validation. Finally, we give suggestions for addressing these aforementioned challenges and provide directions for future work in the hopes of aiding the adoption and implementation of CoPath tools in clinical settings.

The structure of this survey closely follows the CoPath data workflow illustrated in Figure 1. Section 2 begins by outlining the clinical pathology workflow and covers the various task domains in CoPath, along with organ specific tasks and diseases. The next step of the workflow involves the processes and methods of histopathology data collection, which is outlined in Section 3. Following data collection, Section 4 details the corresponding annotation and labeling methodology and considerations. Section 5 covers deep learning designs and methodologies for CoPath applications. Section 6 focuses on regulatory measures and clinical validation of CoPath tools. Finally, we

provide our perceived challenges and future outlook of CoPath in Section 7.

2. Clinical Applications for CoPath

The field of CoPath is dedicated to the creation of tools that address and aid steps in the clinical pathology workflow. Thus, a grounded understanding of the clinical workflow is of paramount importance before development of any CoPath tool. The outcomes of clinical pathology are diagnostics, prognostics, and predictions of therapy response. Computational pathology systems that focus on diagnostic tasks aim to assist the pathologists in tasks such as tumour detection, tumour grading, quantification of cell numbers, etc. Prognostic systems aim to predict survival for individual patients while therapy response predictive models aid personalized treatment decisions based on histopathology images. Figure 3 visualizes the goals pertaining to these tasks. In this section, we provide detail on the clinical pathology workflow, the major application areas in diagnostics, prognostics, and therapy response, and finally detail the cancers and CoPath applications in specific organs. The goal is to outline the tasks and areas of application in pathology where CoPath tools and systems can be developed and implemented.

2.1. Clinical Pathology Workflow

This subsection details the clinical workflow in pathology covering the collection of a tissue sample, its subsequent processing into a slide, inspection by a pathologist, and compilation of the analysis and diagnosis into a pathology. Figure 2 summarizes these steps along with suggestions for corresponding CoPath applications, organizing them into the conventional pathology phases for samples: pre-analytical, analytical, and post-analytical. These phases were developed to categorize quality control measures, as each phase has its own set of potential sources of errors Njoroge and Nichols (2014), and thus potential sources of corrections during which CoPath and healthcare artificial intelligence tools could prove useful.

Sample Collection Tissue samples are categorized into two general types a) *small specimens*, normally obtained to diagnose disease and guide subsequent treatment and b) *large specimens*, surgically removed to treat the disease after diagnosis. *Small specimen* biopsies are performed by different specialties in different settings, which can vary from family doctors sampling skin lesions to head and neck specialists performing panendoscopic biopsies under anesthesia. Based on the type of sample required and its originating site, small specimen samples are obtained by different methods: 1) core biopsies, 2) cytological specimens, 3) small excisions, and 4) pincer biopsies. In contrast, *large specimens* are mostly resections performed by surgeons for treatment purposes once the diagnosis has already been obtained. Large specimens are significantly more complex than small specimens and require a high-level of expertise to process before reaching the microscopic interpretation step.

Accessioning The patient-care team fills out request forms which are tagged to the pathology specimen and sent along with the sample to the pathology department to enter the specimen

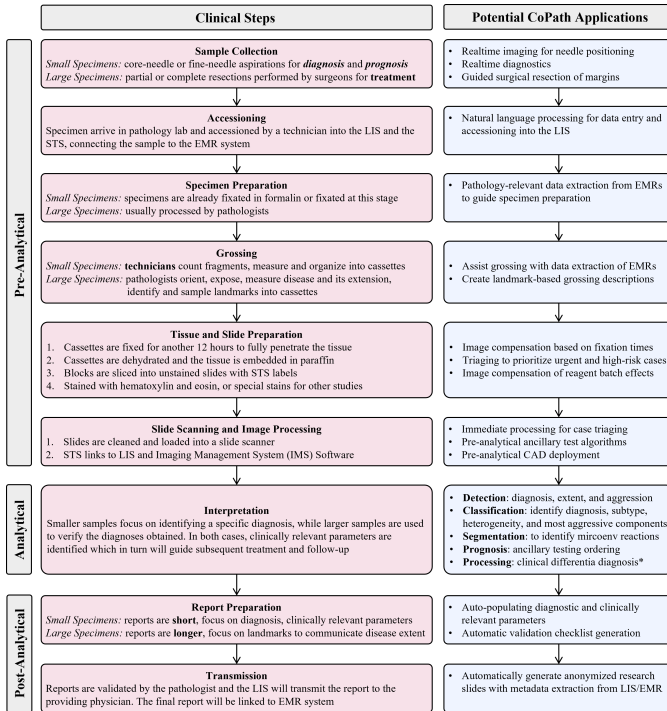


Fig. 2: Quality assurance and control phases developed by pathologists to oversee the clinical pathology workflow into three main phases of pre-analytical, analytical, and post-analytical phases. We further show how each of these processes can be augmented under the potential CoPath applications in an end-to-end pipeline.

and patient information into the laboratory information system (LIS). Depending on the institution, the LIS can then be linked to the electronic medical records (EMR) system to populate basic demographic data, and to a slide tracking system (STS) to locate and time each event in pathology. Ensuring that accessioning is done correctly is essential, as specimen mix-ups or incorrect data entry from request forms are a large source of errors in the workflow Abdollahi et al. (2014).

Specimen Preparation Most samples arrive at the pathology lab having already been preserved in a 4% formalin solution. Other preservation media are used for specific pathology objectives; notably using RPMI to preserve cells for flow cytometry and glutaraldehyde preservation for electron microscopy Smith (2011). Sometimes, the samples are sent to the pathology lab without a preservation medium, and in this “fresh” state the tissue will undergo cold ischemia changes until the pathologist can assess the sample, perform specimen preparation, and fix the tissue in the preservation media. Indeed, each of these events has an impact on the quality of the tissue, which in turn significantly affects the quality of the final WSI. Specifically, large specimens are almost always processed by a pathologist who will open the container, take basic measurements, and open the organ to ensure uniform formalin penetration.

At some medical centers, intra-operative consultations for resection samples are processed in a frozen section procedure, which allows for more rapid diagnosis of the tissue specimens while trading off diagnostic accuracy when compared to fixation in formalin Brender et al. (2005); Ayyagari et al. (2021). Frozen section samples will be rapidly frozen after the pro-

ceeding *grossing* step, therefore they arrive in the lab unprocessed and remain unprocessed until after grossing, undergoing the aforementioned cold ischemia changes in the meantime.

Grossing Once the basic specimen preparation has occurred, the tissue is analyzed by the pathology team without the use of a microscope; a step called grossing. Smaller specimens are often grossed by technicians who fill out a template-based description notably highlighting the number, size, and appearance of the fragments. After grossing, the tissue fragments are placed into tissue cassettes for final fixation. Grossing larger specimens is much more complex, and is usually performed by pathologists, pathologist-assistants, medical residents, or fellows who have undergone extensive training. The grossing starts by orienting the specimen according to the surgical procedure. By cross-referencing the clinical findings and the EMR reports, the operator will localize the disease, locate the pathological landmarks, describe these landmarks, and measure the extent of the disease. Specific sampling of these landmarks is performed, and these samples are then put into cassettes for the final fixation.

Final Tissue and Slide Preparation For non-frozen section samples, the final fixation step will accrue all the samples put into cassettes and will add a last phase of fixation in formalin. Afterwards, the tissue cassettes are removed from formalin and inserted into a tissue processor which dehydrates the tissue through alcohol gradients, subsequently replacing the liquid with melted paraffin wax. These samples are removed from the tissue processor and placed into a mold filled with paraffin which solidifies into a block. A technician then cuts the blocks with a microtome into $4\mu\text{m}$ slices and places them onto positively charged slides. Slides are then deparaffinized, rehydrated by an inverse alcohol gradient, and stained with pigments such as Hematoxylin and Eosin (H&E), or further processed for ancillary testing by immunohistochemistry. Once these steps are complete, the tissue is dehydrated, cleared, and mounted with a coverslip. Note that significant variations will affect the final quality of the slides based on the performance of the prior steps, the experience of the technician who cut the slides, and batch effects from the reagents which are often reused for multiple slides prior to being replaced-known as cross-contamination.

Frozen section samples are rapidly frozen using a freezing medium such as liquid nitrogen, dry ice, or isopentane Brender et al. (2005); Suvarna et al. (2019); Peters (2016); Ayyagari et al. (2021). After freezing, the tissue is cut using a microtome and fixed immediately, most often with formalin Suvarna et al. (2019); Peters (2016). Slides are then stained and covered with a glass coverslip and stored at -80°C Peters (2016).

Slide Scanning and Image Processing The stained slides are cleaned of excess mounting media and scanned with a whole-slide scanner. They are then loaded onto the image management software, which has previously been linked to the LIS and the STS Jahn et al. (2020).

Interpretation After a slide is processed and prepared, a pathologist views the slide to analyze and interpret the sample. The approach to interpretation varies depending on the specimen type. Interpretation of smaller specimens is focused on diagnosis of any disease. Analysis is performed in a decision-

tree style approach to add diagnosis-specific parameters, e.g. esophagus biopsy → type of sampled mucosa → presence of foveolar-type mucosa → identify Barrett's metaplasia → identify degree of dysplasia. Once the main diagnosis has been identified and characterized, the pathologist sweeps the remaining tissue for secondary diagnoses which can also be characterized depending on their nature. Larger specimens are more complex and focus on characterizing the tissue and identifying unexpected diagnoses beyond the prior diagnosis from a small specimen biopsy. Microscopic interpretation of large specimens is highly dependent on the quality of the grossing and the appropriate detection and sampling of landmarks. Each landmark (e.g., tumor surface, tumor at deepest point, surgical margins, lymph node in mesenteric fat) is characterized either according to guidelines, if available, or according to the pathologist's judgment. After the initial microscopic interpretation additional deeper cuts ("levels"), special stains, immunohistochemistry, and/or molecular testing may be performed to hone the diagnosis by generating new material or slides from the original tissue block.

Pathology Report The pathologist synthesizes a diagnosis by aggregating their findings from grossing and microscopic examination in combination with the patient's clinical information, all of which are included in a final pathology report. The classic sections of a pathology report are patient information, a list of specimens included, clinical findings, grossing report, microscopic description, final diagnosis, and comment. The length and degree of complexity of the report again depends on the specimen type. Small specimen reports are often succinct, clearly and unambiguously listing relevant findings which guide treatment and follow-up. Large specimen reports depend on the disease, for example, in cancer resection specimens the grossing landmarks are specifically targeted at elements that will guide subsequent treatment.

In the past, pathology reports had no standardized format, usually taking a narrative-free text form. Free text reports can omit necessary data, include irrelevant information, and contain inconsistent descriptions Renshaw et al. (2018). To combat this, synoptic reporting was introduced to provide a structured and standardized reporting format specific to each organ and cancer of interest Renshaw et al. (2018); Hewer (2020). Over the last 15 years, synoptic reporting has enabled pathologists to communicate information to surgeons, oncologists, patients, and researchers in a consistent manner across institutions and even countries. The College of American Pathologists (CAP) and the International Collaboration on Cancer Reporting (ICCR) are the two major institutions publishing synoptic reporting protocols. The parameters included in these protocols are determined and updated by CAP and ICCR respectively to remain up-to-date and relevant for diagnosis of each cancer type. For the field of computational pathology, synoptic reporting provides a significant advantage in dataset and model creation, as a pre-normalized set of labels exist across a variety of cases and slides in the form of the synoptic parameters filled out in each report. Additionally, suggestion or prediction of synoptic report values are a possible CoPath application area.

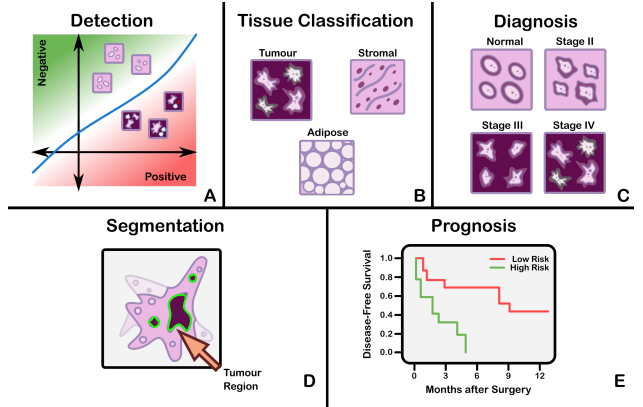


Fig. 3: The categorization of diagnostic tasks in computational pathology along with examples A) **Detection**: common detection task such as differentiating positive from negative classes like malignant from benign, B) **Tissue Subtype Classification**: classification task for tumorous tissue, Stroma tissue, and adipose tissue, C) **Disease Diagnosis**: common disease diagnosis task like cancer staging, D) **Segmentation**: tumor segmentation in WSIs, and E) **Prognosis tasks**: shows a graph comparing survival rate and months after surgery.

2.2. Diagnostic Tasks

Computational pathology systems that focus on diagnostic tasks can broadly be categorized as: (1) disease detection, (2) tissue subtype classification, (3) disease diagnosis, and (4) segmentation, these tasks are visually depicted in Figure 3. Note how the detection tasks all involve visual analysis of the tissue in WSI format. Thus computer vision approach is primarily adopted towards tackling diagnostic tasks in CADs.

Detection We define the detection task as a binary classification problem where inputs are labeled as positive or negative, indicating the presence or absence of a certain feature. There may be variations in the level of annotation required, e.g. slide-level, patch-level, pixel-level detection depending on the feature in question. Although detection tasks may not provide an immediate disease diagnosis, it is a highly relevant task in many pathology workflows as pathologists incorporate the presence or absence of various histological features into synoptic reports that lead to diagnosis. Broadly, detection tasks fall into two main categories: (1) screening the presence of cancers and (2) detecting histopathological features specific to certain diagnoses.

Cancer detection algorithms can assist the pathologists by filtering obviously normal WSIs and directing pathologist's focus to metastatic regions Litjens et al. (2016). An accurate cancer detection CAD would greatly reduce the number of slides reviewed by pathologists, saving both time and effort without sacrificing diagnostic accuracy. Due to this potential impact, cancer detection tasks have been explored in a broad set of organs. Additionally, the simple labeling in binary detection tasks allows for deep learning methods to generalize across different organs where similar cancers form Liu et al. (2019); Khan et al. (2019b); Noorbakhsh et al. (2020).

In contrast to directly predicting the presence of cancers, feature-focused detection tasks can be highly useful in patient diagnosis and treatment planning. For example, identifying microsatellite instability is a crucial factor in determining if immunotherapy will be effective on a patient, and deep learning

methods were shown to be effective at detecting microsatellite instability in Kather et al. (2019b). Similarly, the detection of fibrous regions in liver WSIs is a precursor step to liver tumor classification and a computational approach to detection was demonstrated in Atupelage et al. (2013). Furthermore, the first automatic detection algorithm for keratin pearls, which are valuable biomarkers for oral squamous cell carcinoma grading is presented in Das et al. (2018). Future research into automated detection methods for similar cancer biomarkers could be a valuable step towards developing AI-based pathologist support tools. As an example, lymphocytes, a type of white blood cell, can be detected and quantified to assess the overall health of the immune system. However, manually detecting these cells is a time-consuming task and pathologists rarely identify and count lymphocytes. Thus several computational approaches, including deep learning, are used to provide lymphocyte counts to pathologists Guerrero and Oliveira (2021). Likewise, counting nuclei can contribute towards diagnoses, however, nuclei detection is a difficult task because of the large variations in the shape of different types of nuclei, such as nuclear clutter, heterogeneous chromatin distribution, and irregular and fuzzy boundaries. Addressing these issues, for example, spatially constrained context-aware correlation filters with hierarchical deep features extracted from multiple layers of a pre-trained network were proposed to accurately detect nuclei in Javed et al. (2021).

Tissue Subtype Classification Treatment and patient prognosis can vary widely depending on the stage of cancer, and finely classifying specific tissue structures associated with a specific disease type provides essential diagnostic and prognostic information Wei et al. (2019a). Accordingly, accurately classifying tissue subtypes is a crucial component of the disease diagnosis process. As an example, discriminating between two forms of glioma (a type of brain cancer), glioblastoma multiforme and lower grade glioma, is critical as they differ by over 45% in patient survival rates Barker et al. (2016). Additionally, accurate classification is key in colorectal cancer (CRC) diagnosis, as high morphological variation in tumor cells Sirinukunwattana et al. (2016) makes certain forms of CRC difficult to diagnose by pathologists Korbar et al. (2017). We define this classification of histological features as tissue subtype classification.

Deep neural networks have been shown to be effective at extracting these molecular tumor features from histopathology images, opening new avenues for deep learning applications in computational pathology Rathore et al. (2019). As an extension of the tissue subtype classification task, ML models are often able to identify important correlations between tissue structures and disease. Work on nuclei classification suggests that features regarding the nuclear inner texture are most relevant for high classification accuracy Atupelage et al. (2013). Additionally, a classifier discovered unique chromatin patterns associated with specific types of thyroid follicular lesions in Wang et al. (2010). The potential discovery of similar associations makes tissue subtype classification a relevant task to pursue. Another work presented a computational pathology framework that can localize well-known morphological features on WSIs without the need for spatial labels for each feature us-

ing attention-based multiple-instance learning on WSI classification Lu et al. (2021d). This method outperforms standard weakly-supervised classification algorithms and is adaptable to independent test cohorts, biopsy/resection samples, and varying tissue content. Additionally, the co-representation learning for classification (CoReL) framework is proposed in Pati et al. (2021a) to improve state-of-the-art classification performance for nuclei classification, mitosis detection, and tissue type classification with less data Pati et al. (2021a).

Disease Diagnosis The most frequently explored design of deep learning in digital pathology involves emulating pathologist diagnosis. We define this multi-class diagnosis problem as a disease diagnosis task. Note the similarity with detection–disease diagnosis can be considered a fine-grained classification problem which subdivides the general positive disease class into finer disease-specific labels based on the organ and patient context.

Under this paradigm, research tends to be focused on maximizing performance for reliable clinical applications Kiani et al. (2020); Syrykh et al. (2020); Zhang et al. (2019). Recently, works have begun implementing different emulations of pathologist behaviour in their proposed models. For instance, multi-scale receptive fields were proposed for use in networks to simulate the pathologist viewing process of slides at varying zoom levels Kosaraju et al. (2020). Alternatively, weighted slide-level features were used to classify Barrett's esophagus and esophageal adenocarcinoma, similar to a pathologist assessing the overall impact of various cancer biomarkers Tomita et al. (2019). To emulate how pathologists isolate and focus on salient regions of the slide, the concept of visual attention can be applied to identify the most important regions of tissue slides, thus ignoring diagnostically-irrelevant image regions Xu et al. (2019b); Patil et al. (2019); Xu et al. (2019a). Such methods indicate a positive step towards the clinical implementation of AI-based CAD tools by reinforcing and emulating tested methodologies in pathology. Further, differential diagnoses in complicated cases of metastatic tumors and cancer of unknown primary (CUPs) can require many clinical tests to narrow a differential diagnosis, and a method called Tumor Origin Assessment via Deep Learning (TOAD) is introduced as an assistive tool to assign a differential diagnosis Lu et al. (2021c). This work uses digitized H&E slides of tumors with known primary origins to train a model with transfer learning and weakly supervised multitask learning to simultaneously identify the tumorous or metastatic regions and predicts the site of origin.

Segmentation The segmentation task moves one step beyond classification by adding an element of spatial localization to the predicted label(s). The goal of segmentation is to delineate objects of interest in the image by assigning labels to every pixel. In practice, these pixel-level labels could belong to more than one class, resulting in the more complex semantic segmentation task Chan et al. (2021). Another variant of the segmentation task is instance segmentation, which aims to achieve both pixel-level segmentation accuracy as well as clearly defined object (instance) boundaries. Overall, segmentation provides localization and classification of cancer-specific tumors and of specific histological features that can be meaningful for the pathol-

ogist's clinical interpretation.

Segmentation approaches can accurately capture many morphological statistics Chen et al. (2016a) and textural features Nateghi et al. (2016), both of which are relevant for cancer diagnosis and prognosis. Most frequently, segmentation is used to capture characteristics of individual glands, nuclei, and tumor regions in WSIs. For instance, glandular structure is a critical indicator of the severity of colorectal carcinoma Yan et al. (2020b), thus accurate segmentation could highlight particularly abnormal glands to the pathologist as demonstrated in Sirinukunwattana et al. (2015); Marsh et al. (2018); Yan et al. (2020b). Similarly, nuclear characteristics such as size and shape can help pathologists distinguish between various cell types and consequently, disease severity Hou et al. (2019b); Vahadane et al. (2021). The wide generalizability of this task to various disease types makes it a particularly suitable tool for computational pathology, on which many studies have been conducted Hou et al. (2019a); Naylor et al. (2017); Shin et al. (2016); Graham et al. (2019b); Vu et al. (2019). To address segmentation challenges in histopathology tissue, a generalized deep learning-based framework was proposed in Khened et al. (2021), using a sequence of novel techniques in the preprocessing, training, and inference steps which in conjunction improve the efficiency and the generalizability of model. Similarly, a new framework for WSI analysis in colonoscopy pathology, including lesion segmentation and tissue diagnosis was developed and includes an improved U-Net with a VGG net as the backbone, as well as two training and inference schemes to address the challenge of high resolution images analysis Feng et al. (2020).

There are also some instances of segmentation in different organs. For example, an interactive segmentation model was proposed in which the user-provided squiggles guide the model toward semantic segmentation of tissue regions Jahanifar et al. (2021). Also, they proposed four novel techniques to automatically extract minimalistic and human-drawn-like guiding signals from Ground Truth (GT) masks so that they can be used during the model's training. Similarly for the eye, macular edema (ME) is a common disease where analyzing the fluid lesions is a critical stage of the diagnostic process. The optical coherence tomography (OCT) technique can potentially investigate three fluid types and a novel pipeline for segmentation of the three types of fluid lesions in OCT was proposed in Xing et al. (2021). They presented a multi-layer segmentation to detect the ROI and presented an FCN architecture with attention gate (AG) and spatial pyramid pooling (SPP) module to improve the feature extraction. To predict cellular composition from images, ALBRT is proposed in Dawood et al. (2021), using contrastive learning to learn a compressed and rotation-invariant feature representation which first detects the presence of different cell types in an image patch and then provides cell counts for each type. Another novel deep learning model was developed for simultaneous nuclei instance segmentation in Dogar et al. (2021). The model is based on an encoder-decoder architecture design that performs nuclei segmentation by predicting the distance of pixels from their nuclei centers along with the nuclei probability masks and predicts nuclei classes

when nuclei type annotations are available. Another work in nuclei segmentation is the hard-boundary attention network (HBANet), which identifies hard-boundaries between nuclei, a difficult problem due to overlapped nuclei Cheng et al. (2021b). It presents a background weaken module (BWM) to improve the model's attention to the foreground, and integrates low-level features containing more detailed information into deeper feature layers. Furthermore, a gradient-based boundary adaptive strategy (GS) is designed to generate boundary-weakened data as extra inputs and train the model in an adversarial manner. Finally, segmentation has also been applied to delineate tumorous tissue regions for a variety of cancer types, such as breast Takahama et al. (2019); Priego-Torres et al. (2020), colorectal Qaiser et al. (2019); Xu et al. (2017a), and prostate cancer Eminaga et al. (2019); Avenel et al. (2019). Such works assist in the efficient isolation of tumor tissue, which is a crucial task for making accurate disease predictions.

2.3. Prognosis

Prognosis involves predicting the likely development of a disease based on given patient features. For accurate survival prediction, models must learn to both identify and infer the effects of histological features on patient risk. Prognosis represents a merging of the diagnosis classification task and the disease-survivability regression task.

Training a model for prognosis requires a comprehensive set of both histopathology slides and patient survival data (i.e. a variant of multi-modal representation learning). Despite the complexity of the input data, ML models are still capable of extracting novel histological patterns for disease-specific survivability Zadeh Shirazi et al. (2020); Kather et al. (2019a); Courtiol et al. (2019). Furthermore, strong models can discover novel prognostically-relevant histological features from WSI analysis Bychkov et al. (2018); Wang et al. (2017b).

As the quality and comprehensiveness of data improves, additional clinical factors could be incorporated into deep learning analysis to improve prognosis. For instance, a prognostic model was developed by adjusting a tumor microenvironment-based spatial map with clinical variables such as patient age, gender, health history, and cancer stage Wang et al. (2019b). This multi-domain data analysis approach is advanced by another work, which uses both histopathological image data and cancer genomic data in their novel deep learning framework Hao et al. (2019); Chen et al. (2020b). In Ristanoski et al. (2021), the authors discussed the correlation between platelets and other haematological measures to cancer by assessing patient status and considering the patient features in the primary care dataset, such as age and sex. They demonstrate the model performance with the plot of survival analysis per age group for platelets. Experiments on the publicly available TCGA data demonstrates that prognostic accuracy was maximized when both forms of data were simultaneously considered. Merging information from multiple WSIs of a patient allowed a hybrid aggregation network (HANet), consisting of a self-aggregation module and a WSI-aggregation module, to predict survival risks Chang et al. (2021).

2.4. Prediction of treatment response

With the recent advances in targeted therapy for cancer treatment, clinicians are able to use treatment options that precisely identify and attack certain types of cancer cells. While the number of options for targeted therapy are constantly increasing, it becomes increasingly important to identify patients who are potential therapy responders to a specific therapy option and avoid treating non-responding patients who may experience severe side effects.

Deep learning can be used to detect structures and transformations in tumour tissue that could be used as predictive markers of a positive treatment response. Training such deep learning models usually requires large cohorts of patient data for whom the specific type of treatment option and the corresponding response is known. A deep learning-based biomarker using H&E-stained images was developed to predict pathological complete response (pCR) of breast cancer patients receiving neoadjuvant chemotherapy, which demonstrates a strong prediction ability for guiding treatment decisions Li et al. (2021b). The developed model outperforms conventional biomarkers including stromal tumor-infiltrating lymphocytes and subtype. In another work, the authors propose a method using convolutional neural networks to discover image-based signatures for ipilimumab response prediction in malignant melanoma patients Harder et al. (2019). An immunotherapy response prediction in patients with non-small cell lung cancer from H&E- stained images was proposed in Madabhushi et al. (2021). Similarly, a deep learning method was developed to predict the treatment response to neoadjuvant chemoradiotherapy in local advanced rectal cancer patients, which can provide assistance in making personalized treatment plans Zhang et al. (2020).

2.5. Cancer Statistics

Cancer is the first major cause of death worldwide in 2020, responsible for the death of nearly 10 million or 1 in 6 deaths Organization. As the grey circle in Figure 4 shows, Breast, Prostate, Colon, and Rectum, and Lung are the four most common cancers and they are responsible for half of the diagnosed cases. One of the major setbacks in the clinical pathology workflow is the increasing number of pathology cases. This point shows the importance of computational pathology in these fields as it can help to expedite the pathology workflow and pathologists to overcome the issue of work overload. Some cancers are not only prevalent but also make a considerable proportion of cancer's death toll. Lung cancer is the perfect example for this matter which makes about 12% of the cancers in the United States and its prognosis falls into the lowest bin as Figure 4 shows (0 – 30%). Computational pathology can assist pathologists in nearly every level of their work, from disease detection to segmentation. However, in the case of lung cancer, the true power of CoPath lies within the classification and prognosis task since lung cancer types have major differences between their high-level presentation and prognosis as well as treatment plans. On the other hand, there are cancers which is not prevalent such as liver cancer but they have poor prognosis. By compiling data sets focused on these cancers, CoPath can assist not only pathologists but also clinicians by assembling personalized treatment plans.

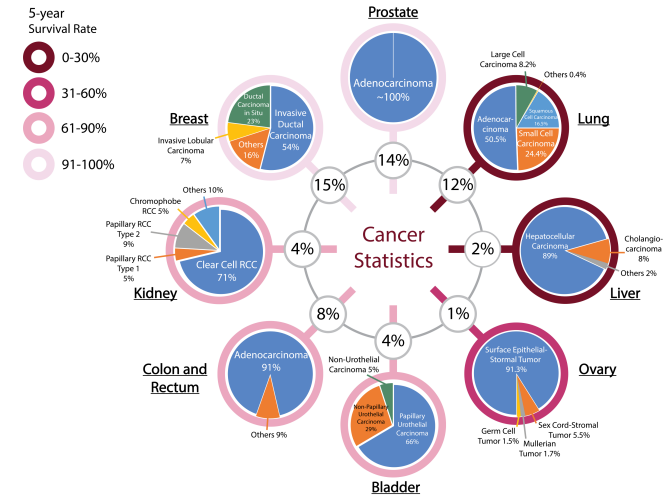


Fig. 4: Demonstration of the cancer statistics, featuring both the 5-Year Survival Rate and Incidence of each cancer in addition to incidence percentage of each subtype. The grey inner circle shows the incidence percentage of the respective cancer. The colored circle around each cancer corresponds to the respective 5-Year Survival Rate bin, showcasing the severity of the cancer. Darker shades (lower survival rate) means fewer people will survive the cancer after 5 years period and the cancer has poor prognosis. On the other hand, lighter shades (higher survival rates) mean more people will survive after 5 years and the cancer has good prognosis. Institute (a); Kenfield et al. (2008); Society (d); Center; Society (c); Andreassen et al. (2016); Society (a); Goodman (2007); Ries et al. (2007); Institute (b); Society (f); Bottaro and Linehan (2005); Srougi et al. (2009); Society (e); Remo et al. (2019); American Cancer Society (i); Society (g); Abbas et al. (2010); Society (b)

2.6. Organs and Diseases

This section presents an overview of the various anatomical application areas for computational pathology grouped by the targeted organ. Each organ section gives a brief overview of the types of cancers typically found and the content of the pathology report as noted from the corresponding CAP synoptic reporting outline (discussed at 2.1); followed by notable CAD designs and biological findings in the field of computational pathology. Figure 5 highlights the intersection between the major diagnostic tasks and the anatomical focuses in state-of-the-art research. The majority of papers are dedicated to the four most common cancer sites: breast, colon, prostate, and lung Siegel et al. (2020). Additionally, a significant amount of research is also done on two of the most severe cancer types: the brain and liver Siegel et al. (2020).

Breast Breast cancers can start from different parts of the breast and majorly consist of 1) Lobular cancers that start from lobular glands, 2) Ductal cancers, 3) Paget cancer which involves the nipple, 4) Phyllodes tumor that stems from fat and connective tissue surrounding the ducts and lobules, and 5) Angiosarcoma which starts in the lining of the blood and lymph vessels. In addition, based on whether the cancer has spread or not, breast cancers can be categorized into *in situ* or *invasive/infiltrating* forms. Ductal carcinoma *in situ* (DCIS) is a precancerous state and is still confined to the ducts. Once the cancerous cells grow out of the ducts, the carcinoma is now considered *invasive* or *infiltrative* and can metastasize American Cancer Society (f).

The synoptic reports for breast cancer diagnosis are divided

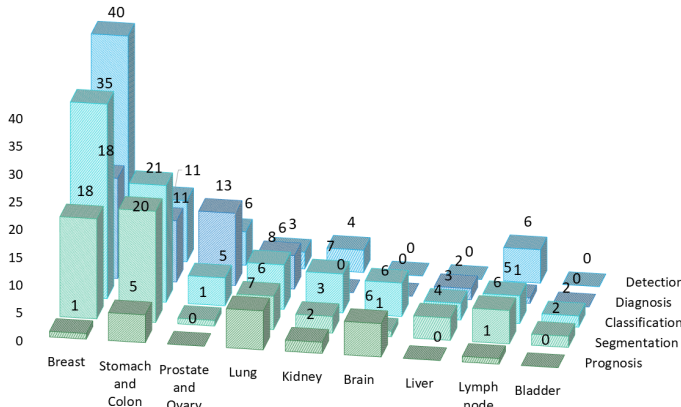


Fig. 5: Distribution of diagnostic tasks in CoPath for different organs from Table 8.3. This distribution includes more than 400 cited works from 2018 to 2022 inclusive. The x-axis covers different organs, the y-axis displays different diagnostic tasks, and the height of the bars along the vertical axis measures the number of works that have examined the specific task and organ. Please refer to Table 8.3 in the supplementary section for more information.

based on the type of cancers mentioned above. For DCIS and invasive breast cancers, the synoptic report focuses on the histologic type and grade, along with the nuclear grade, evidence of necrosis, margin, involvement of regional lymph nodes, and biomarker status. Notably, architectural patterns are no longer a valuable predictive tool compared to nuclear grade and necrosis to determine a relative ordering of diagnostic importance for DCIS Fitzgibbons (2021). In contrast to DCIS and invasive cancers, Phyllodes tumours vary due to their differing origin in the fat and connective tissue, focusing on analyzing the stroma characteristics, existence of heterologous elements, mitotic rate, along with the involvement of lymph nodes. Finally, to determine therapy response and treatments, biomarker tests for Estrogen and Progesterone Allison et al. (2020) receptors, HER-2 Wolff et al. (2018) receptors are recommended, along with occasional tests for Ki67 antigens Dowsett et al. (2011); Healey et al. (2017).

Most breast cancer-focused works in CoPath propose various solutions for carcinoma detection and metastasis detection, an important step for assessing cancer stage and morbidity. Solutions often apply transfer learning techniques with CNN-based models to elevate the performance to clinical-level accuracy. A two-stage CNN, one for patch-level feature extraction and the other for classification, was proposed and achieved 95% accuracy for classifying normal, benign, in situ carcinoma, and invasive carcinomas Nazeri et al. (2018). Additionally, metastasis detection using deep learning methods was shown to outperform pathologists' exhaustive diagnosis by 9% FROC Liu et al. (2017). Breast cancers that have metastasized are amongst the leading causes of death for women worldwide, thus accurate and early diagnoses of when breast cancers have spread to axillary lymph nodes (ALNs) is therefore very critical for patients Turki et al. (2021). An end-to-end deep learning approach was proposed to detect ALN metastases from digital pathology images which compares several deep learning architectures such as DenseNet12, ResNet50, VGG16, Xception, and a customized lightweight convolutional neural network (LCNN)

Turki et al. (2021). Further research has proposed an automated patient-level tumor segmentation and classification system that takes full use of diagnosis information hints from pathologists Wang et al. (2021a). A multi-level view DeepLabV3+ (MLV-DeepLabV3+) was created to investigate the differentiating aspects of cell characteristics between tumor and normal tissue for tumor segmentation. Furthermore, expert segmentation models were chosen and merged using Pareto-front optimization to mimic expert consultation and provide a flawless diagnosis. Outside of diagnosing directly from WSIs, a CAD application called piNET is proposed as a novel proliferation index (PI) calculator for images that highlight the Ki67 biomarker using a U-NET-based deep learning architecture Geread et al. (2021). They suggest an equation for calculating the proliferation index, which requires the counting number of Ki67+ and Ki67 markers present.

Beyond disease diagnosis, a subset of breast-focused research studies the correlation between tissue morphology and molecular differences. Molecular testing can often be preferred over tissue morphology assessments when selecting breast cancer treatments as it provides objective and reproducible disease classifications. For instance, the connection between epithelial patterns with various molecular predictions and heatmaps was used to clearly visualize this correlation Rawat et al. (2020). Future studies could present novel applications that combine molecular analysis with histopathology, and ultimately increase diagnostic and prognostic accuracy for diseases.

Prostate Prostate cancer is the second most prevalent cancer among the total population and the most common cancer among men (both excluding non-melanoma skin cancers), however, most prostate cancers are not lethal. Prostate cancer can occur in any of the three prostate zones: Central (CZ), Peripheral (PZ), and Transition (TZ), in increasing order of aggressiveness. Prostate cancers are almost always adenocarcinomas, which develop from the gland cells that make prostate fluid. The other types of prostate cancers are small cell carcinomas, neuroendocrine tumors, transitional cell carcinomas, isolated intraductal carcinoma, and sarcomas (which are very rare). Other than cancers, there are multiple conditions that are important to identify or diagnose as precursors to cancer or not. Prostatic intraepithelial neoplasia (PIN) is diagnosed as either low-grade PIN or high-grade PIN. Men with high-grade PIN need closely monitored follow-up sessions to screen for prostate cancer. Similarly, atypical small acinar proliferation (ASAP) is another precancerous condition requiring follow-up biopsies. American Cancer Society (i)

To grade and score prostate tumours, pathologists use a Tumor, Nodes, Metastasis (TNM) framework. In the synoptic report, similar to other organs, pathologists identify and report the histologic type and grades, and involvement of regional lymph nodes to help grade and provide prognosis for any tumours. Specifically for prostate analysis, tumour size, and volume are both important factors in prognosis according to multiple studies Ito et al. (2019); Epstein (2011); Salomon et al. (2003); Stamey et al. (1999). Similarly, location is important to note as mentioned previously, for both prognosis and therapy response Lee et al. (2015). Invasion to nearby (except perineural inva-

sion) tissues is noted and can correlate to TMN classification Paner (2021). Additionally, margin analysis is especially important in prostate cancers as a positive margin then cancer recurrence is probable along with metastasis Wright et al. (2010). Finally, intraductal carcinoma (IDC) must be identified and distinguished from PIN and PIA; as it is strongly associated with a high Gleason score, a high-volume tumor, and metastatic disease Varma (2021); Montironi et al. (2018); Zhou (2013); Cohen et al. (2007); Guo and Epstein (2006).

After a prostate cancer diagnosis is established, pathologists assign a Gleason Score to determine the cancer's grade: a grade from 1 to 5 is assigned to the two most common areas and those two grades are summed to make a final Gleason Score American Cancer Society (c). For Gleason scores of 7, where survival and clinical outcomes demonstrate large variance, the identification of Cribriform glands is key in helping to narrow possible outcomes Kweldam et al. (2015); Lee and Ro (2018).

Thus most works focus on prostate aim to classify cancer based on Gleason scoring. To aid in that effort, a U-Net model for object semantic segmentation is created with the goal of precisely labeling each pixel in an image as belonging to foregrounds, which may contain glands or the background in Nour et al. (2021). Additionally, work in Xiong et al. (2021) focused on classifying glands, gland boundary regions, and stroma. The authors opted for two classic classifiers: support vector machines (SVM) and Convolutional Neural Networks (CNNs), finding the SVM to perform best by offering high accuracy and good indicators of regions which are present with high probability. The output of the SVM classifier could help pathologists locate existing glands, saving them a significant amount of time from actively searching for them. However, tasks related to prostate diagnosis are not only time-consuming, but also prone to intra- and inter-observer variation Li et al. (2018b). Specifically, distinguishing between G3 and G4 grades in glands is difficult yet crucial for effective treatment. A method is proposed in Li et al. (2018b) that trains the model on both epithelial cell detection and Gleason grade prediction tasks to achieve better performance in both tasks than models trained on either of the tasks alone. Further, some works have investigated epithelial cell detection to explore data augmentation and stain/color normalization techniques Tellez et al. (2019a); Sethi et al. (2016) which demonstrates the importance of epithelial cell features as an indicator for prostate cancer detection.

Ovary Ovarian cancer is the deadliest gynecologic malignancy and accounts for more than 14,000 deaths each year Bachert et al. (2020). Ovarian cancer manifests in three types: 1) epithelial cell tumors that start from the epithelial cells covering the outer surface of the ovary, 2) germ cell tumors which start from the cells that produce eggs, and 3) stromal tumors which start from cells that hold the ovary together and produce the hormones estrogen and progesterone. Each of these cancer types can be classified into benign, intermediate and malignant categories. Overall, epithelial cell tumors are the most common ovarian cancer and have the worst prognosis American Cancer Society (h).

When compiling a synoptic report for ovarian cancer diagnosis, pathologists focus on histologic type and grade, extra-

organ involvement, regional lymph nodes, T53 gene mutations, and serous tubal intraepithelial carcinoma (STIC). Varying histologic tissue types are vital to determine the pathology characteristics and determining eventual prognosis. For example, generally endometrioid, mucinous, and clear cell carcinomas have better outcomes than serous carcinomas Yang et al. (2021). Additionally, lymph node involvement and metastasis in both regional and distant nodes has a direct correlation to patient survival, grading, and treatment. Determining the presence of STICs correlates directly to the presence of ovarian cancer, as 60% of ovarian cancer patients will also have an associated STIC Bachert et al. (2020). Finally, T53 gene mutations are the most common in epithelial ovarian cancer; which has the worst prognosis among ovarian cancers, so determining their presence is critical to patient cancer risk and therapy response Vermij et al. (2022); Zhang et al. (2016a). There are not a large number of works dedicated to the ovary specifically, but most works on ovary focus on classification of its five most common cancer subtypes: high-grade serous (HGSC), low-grade serous (LGSC), endometriod (ENC), clear cell (CCC), and mucinous (MUC) Wang et al. (2020b); Gamper et al. (2020b).

Lung Lung cancer is the third most common cancer type, next to breast and prostate cancer National Cancer Institute. Lung cancers mostly start in the bronchi, bronchioles, or alveoli and are divided into two major types, non-small cell lung carcinomas (NSCLC) (80 – 85%) and small cell lung carcinomas (SCLC) (10 – 15%). Although NSCLC cancers are different in terms of origin, they are grouped because they have similar outcomes and treatment plans. Common NSCLC cancers are 1) adenocarcinoma, 2) squamous cell carcinoma 3) large cell carcinoma, and some other uncommon subtypes American Cancer Society (d).

For reporting, histologic type helps determine NSCLC vs SCLC and the subtype of NSCLC. Although NSCLC generally has favourable survival rates and prognosis as compared to SCLC, certain subtypes of NSCLC can have lower survival rates due to co-factors Yoshizawa et al. (2011). Histologic patterns are applicable in adenocarcinomas, consisting of favourable types: lepidic, intermediate: acinar and papillary, and unfavourable: micropapillary and solid Moreira et al. (2020). Grading each histologic type aids in categorization but is differentiated based on each type, and thus is out of scope for this paper. Importantly for lung cancers, tumour size is an independent prognostic factor for early cancer stages, lymph node positivity, and locally invasive disease. Additionally, the size of the invasive portion is an important factor for prognosis of non-mucinous adenocarcinoma with lepidic pattern Tsutani et al. (2012); Maeyashiki et al. (2013); Amin et al. (2017b); Wang et al. (2018a); Zhang et al. (2015); Yoshizawa et al. (2011). Other important lung specific features are visceral plural invasion, which is associated with worse prognosis in early-stage lung cancer even with tumors < 3cm Gao et al. (2022), and lymphatic invasion which indicates an unfavourable prognostic finding Tsutani et al. (2012); Amin et al. (2017a).

Most papers that we have reviewed aim to classify NSCLC types. For example, in Coudray et al. (2018), the work not only classifies adenocarcinoma and squamous cell carcinoma,

but also predicts the 10 most commonly mutated genes in adenocarcinoma. The findings indicate the presence of genotype-phenotype correlations for lung cancer tissues, and paves the way for cancer classification and mutation predictions of other types of less common lung cancers. Further, to help determine treatment by classifying NSCLC into squamous and non-squamous histological types, a deep learning model based on the Inception-V3 architecture is introduced Le Page et al. (2021) to analyze whole H&E slides from tumor biopsies. The model was optimized using a thresholding strategy for predictions and a kernel filter to account for the spatial environment of the tiles. Additionally, the prediction was improved using a virtual tissue micro array (TMA) for selecting tumor areas. For determining treatment plans and predicting therapy response, programmed death-ligand 1 (PD-L1) assessment is used in NSCLCs by determining a tumor proportion score (TPS) of PD-L1 expression Garon et al. (2015), but standardization is difficult due to inter-observer variability among pathologists and the use of different antibodies Cooper et al. (2017); Brunnström et al. (2017). An AI system based on a deep learning model of tumor detection was used in Wu et al. (2021) to automatically assess the TPS using whole slide images (WSIs) from the 22c3 assay. To further aid diagnosis, prognosis, and treatment decisions, a novel method for nuclei detection and characterization was introduced in Hou et al. (2019b) using an unsupervised autoencoder network to learn without the use of any annotations. The unsupervised autoencoder is used to construct a CNN which only requires 5% of training data was needed to generate comparable results to state-of-the-art methods on supervised lymphocyte and nuclei tasks, thereby reducing the need for extremely large annotated datasets.

Colon and Rectum Colorectal cancers are two of the five most common cancer types Siegel et al. (2020). Cancer cells usually start to develop in the innermost layer of the colon and rectum walls, known as the mucosa, and continue their way up to other layers. In other layers, there are lymph and blood vessels that can be used by cancer cells to travel to nearby lymph nodes or other organs Society (2020). Colorectal cancers usually start with the creation of different types of polyps, each possessing a unique risk of developing into cancer. Most colorectal cancers are adenocarcinomas, which are split into three well-studied subtypes: classic adenocarcinoma (AC), signet ring cell carcinoma (SRCC), and mucinous adenocarcinoma (MAC). In most cases, AC has a better prognosis than MAC or SRCC. Other types, albeit uncommon, of colorectal cancers are: carcinoid tumors, gastrointestinal stromal tumors (GISTs), lymphomas, and sarcomas American Cancer Society (g).

As in other cancers, histologic grade is the most important factor in cancer prognosis along with regional lymph node status and metastasis. The tumor site is also important in determining survival rates and prognosis You et al. (2020). Vascular invasion of both small and large vessels are important factors in adverse outcomes and metastasis Lim et al. (2010); Santos et al. (2013); Gomez et al. (2014), and perineural invasion has been shown in multiple studies to be an indicator of poor prognosis Liebig et al. (2009); Ueno et al. (2013); Gomez et al. (2014). Additionally, microsatellite instability (MS) is shown to be a

good indicator of prognosis and is divided into three stages in decreasing adversity of Stable (MS-S), Low (MS-L), and High (MS-H) Phipps et al. (2013). Finally, some studies have indicated the usefulness of biomarkers in colorectal cancer treatment, with biomarkers such as BRAF mutations, KRAS mutations, MSI, APC, Micro-RNA, and PIK3CA Vacante et al. (2018).

Similarly to breast pathology research, works are relatively well-distributed among various tasks including disease diagnosis, segmentation, and detection. Expanding on colorectal cancer detection, work from Xu et al. (2017a) used feature analysis for colorectal and mucinous adenocarcinomas using heatmap visualizations. They discovered that adenocarcinoma is often detected by ill-shaped epithelial cells and that misclassification can occur due to lumen regions that resemble the malformed epithelial cells. Similarly for mucinous carcinoma, the model again recognizes the dense epithelium, but this time ignores the primary characteristic of the carcinoma (abundance of extracellular mucin). These findings suggest that a thorough analysis of class activation maps can be helpful for improving the classifier's accuracy and intuitiveness. An interesting detection application for microsatellite instability is implemented Kather et al. (2019b), where the resulting AUC of 0.84 shows that the role of microsatellite instability in patient prognosis could be worth investigating further. Another study presents an image segmentation approach based on principal component analysis (PCA) to H&E staining characteristics to reduce 3-channel RGB data to one channel and applying a discrete wavelet transform (DWT) in the compressed domain Kim et al. (2021). Further, some authors have combined the easiness of off-the-shelf models with one-stop-shop convenience and improved interpretability Schrammen et al. (2022). Simultaneously, the first deep learning application for one-shot tumor localization and genetic subtyping in CRC is developed. All of this work has been done with the goal of unifying tumor diagnosis and subtyping workflows in a single-pass neural network.

Bladder There are several layers within the bladder wall with most cancers starting in the internal layer, called the urothelium or transitional epithelium. Cancers remaining in the inner layer are non-invasive or carcinoma in situ (CIS) or stage 0. If they grow into other layers such as the muscle or fatty layer, the cancer is now *invasive*. Nearly all bladder cancers are urothelial carcinomas or transitional cell carcinomas (TCC). However, there are other types of cancer such as squamous cell carcinomas, adenocarcinomas, small cell carcinomas, and sarcomas which all are very rare. In the early stages, all types of bladder cancers are treated similarly but as their stage progresses, and chemotherapy is needed, different drugs might be used based on the type of the cancer American Cancer Society (e). As with other organs, histologic type and grade also play a role in prognosis and treatment Chalasani et al. (2009), and lymphovascular invasion is independently associated with poor prognosis and recurrence Lotan et al. (2005).

Works focusing on the bladder display promising results that could lead to rapid clinical application. For example, a prediction method for four molecular subtypes (basal, luminal, luminal p53, and double negative) of muscle-invasive bladder can-

cer was proposed in Woerl et al. (2020), outperforming pathologists by 30% in classification accuracy when restricted to a tissue morphology-based assessment. Further improvements in accuracy could help expedite diagnosis by complementing traditional molecular testing methods. Bladder cancer grade classification is explored using a large dataset of 915 WSIs and ends up outperforming 17 pathologists by an average of 10% Zhang et al. (2019). This model has been integrated into an end-to-end diagnostic tool that provides interpretable cellular-level ROI visualization and natural language descriptions of histology slides. However, there was also a diagnostic disagreement of 23% from the pathologists, which could hinder the diagnostic process and consequently limit the overall productivity.

Kidney Each kidney is made up of thousands of glomeruli which feed into the renal tubules. Kidney cancer can occur in the cells that line the tubules (renal cell carcinoma (RCC)), blood vessels and connective tissue (sarcomas), or urothelial cells (Urothelial carcinoma). RCC accounts for about 90% of kidney cancers and comes in two types: 1) clear cell renal carcinoma, which are most common and 2) non-clear cell renal carcinoma consisting of papillary, chromophobe and some very rare subtypes kid (2020).

The College of American Pathologists' cancer protocol template for the kidney is solely focused on RCCs Srigley et al. (2020), likely due to their high probability. Tumour size is directly associated with malignancy rates, with 1cm size increases resulting in 16% increases in malignancy Bonsib (2006). Additionally, the RCC histologic type are correlated with metastasis with clear cell, capillary, collecting ducts (Bellini), and medullary being the most aggressive Muglia and Prando (2015).

For effective patient prognosis, tissue microarray analysis is typically used to identify biomarkers. Currently, this process is time-consuming and prone to error, especially due to the heterogeneity of nuclei. A random forest classifier was proposed to more efficiently detect cancerous nuclei in MIB-1 stained tissue micro-array spots and predict the survival rate for renal cell carcinoma (RCC) patients in Zhang et al. (2019). The results show that there is a significant difference in survival times for patients with high and low proliferating tumors, and further state MIB-1 staining as a key prognostic factor for the survival chance of RCC. Further, frozen kidney sections were used as input data to identify the percentage of glomerulosclerosis, which is a key metric in determining donor organ acceptance in kidney transplants in Marsh et al. (2018). Lastly, many works are focused on glomeruli segmentation, as the number of glomeruli and glomerulosclerosis constitute standard components of a renal pathology report Kannan et al. (2019). In addition to glomeruli detection, some works have also detected other relevant features such as tubules, Bowman's capsules, and arteries Hermsen et al. (2019). The results display strong performance on PAS-stained nephrectomy samples and tissue transplant biopsies, and there seems to be a strong correlation between the visual elements identified by the network and those identified by renal pathologists.

Brain There are two main types of brain tumors: malignant and non-malignant. Malignant tumors can be classified

as primary tumors (originating from the brain) or secondary (metastatic) Gehan and Walker (1977); Li et al. (2021e). The most common type of brain cancers are gliomas, occurring 50.4% of the time, and are classified into four grades American Cancer Society (a). In the synoptic reporting, tumour location is noted as it has some impact on the prognosis, with parietal tumours showing better prognosis compared to other locations Gehan and Walker (1977). Additionally, focality of glioblastomas (a subtype of gliomas) is important to determine as multifocal glioblastoma is far more aggressive and resistant to chemotherapy as compared to unifocal Li et al. (2021e). A recent summary of the World Health Organization's (WHO) classification of tumors of the central nervous system has indicated that biomarkers as both ancillary and diagnostic predictive tools Louis et al. (2021). Additionally, in a recent WHO edition of classification of tumors of the central nervous system, molecular information is now integrated with histologic information into tumor diagnosis for cases such as diffuse gliomas and embryonal tumors Board.

Accordingly, most works focus on gliomas and more specifically glioblastoma, the most aggressive and invasive form of glioma. Due to glioblastoma's extremely low survival rate of 5% after 5 years, compared to a low grade glioma's survival rate of over 50% after 5 years Canadian Cancer Society; Barker et al. (2016), it is critical to distinguish the two forms for improved patient care and prognosis. For instance, the achieved state-of-the-art classification accuracy on the 2014 MICCAI Grand Challenge dataset was achieved in Barker et al. (2016). However, on completely unseen datasets, performance varied from 84% to 93%. This shows the complexity of the diseases; low grade glioma (LGG) versus glioblastoma multiforme (GBM) classification is not a trivial task. Not only do their appearances vary in pathological samples, the diagnosis is often made from a few distinct features in a small slide region Barker et al. (2016). Thus, when building a glioma classification pipeline, selecting relatively small slide regions for the evaluation would be a reasonable procedure.

Liver Liver cancer is one of the most common causes of cancer death World Health Organization. In particular, hepatocellular carcinoma (HCC) is the most common type of primary liver cancer and has various subtypes, but they generally have little impact on treatment Kim et al. (2020a). Histological grade is divided into nuclear features and differentiation, which directly correlate to tumour size, presentation, and metastatic rate Lauwers et al. (2002); Spolverato et al. (2015). Notably, High-grade dysplastic nodules are included in synoptic reports for HCC but are difficult to assess and have high inter-observer disagreement Wanless et al. (1995), and thus is an area where CAD systems could be leveraged to normalize assessments.

Current histological grading of this cancer suffers from an unsatisfactory level of standardization Martins-Filho et al. (2017), likely due to the diversity and complexity of the tissue. This could explain why relatively low number of works are dedicated to liver disease diagnosis and prognosis. Instead, most works focus on the segmentation of cancerous tissues. However, a notable work for liver cancer classification describes where a pathologist's performance using a liver cancer diagnos-

tic tool is evaluated for the diagnosis of hepatocarcinoma and cholangiocarcinoma Kiani et al. (2020). Despite lower performance than pathologists, the tool’s decisions directly affected pathologists’ decisions. Correct model predictions increased pathologists’ average accuracy, while incorrect predictions lowered average accuracy. Furthermore, pathologists frequently consulted the model’s predictions for difficult cases. This confirms the potential benefits of deep learning models as an AI diagnostic tool to provide knowledgeable second opinions.

Lymph Nodes There are hundreds of lymph nodes in the human body that contain immune cells capable of fighting infections. Cancer manifests in lymph nodes in two ways: 1) cancer that originates in the lymph node itself known as lymphoma and 2) cancer cells from different origins that invade lymph nodes American Cancer Society (b). As mentioned in the prior organ sections, lymphocytic infiltration is correlated with cancer recurrence on multiple organs and lymph nodes are the most common site for metastasis. The generalizable impact to multiple organs and importance of detecting lymphocytic infiltration is why many works focused on lymph nodes address metastasis detection Wang et al. (2022). One of the earliest histopathology challenges, ICPR2010, targets lymphocyte and centroblast counting Gurcan et al. (2010). The importance of the lymph nodes in cancer diagnosis is further addressed in the CAMELYON16 and CAMELYON17 Challenges, in which participants classify lymph node metastases Bandi et al. (2018). Metastases in breast regional lymph nodes are classified based on size: micrometastasis, macrometastasis, and isolated tumour cells (ITCs). Results compiled from all challenge submissions indicate that there was extreme difficulty in detecting ITCs, most likely due to the small size and variability. The ITC classification accuracy was less than 40% for all top teams. This suggests that further improvements can be made by introducing more false positives of ITC data, or incorporating IHC stain information as an additional layer of information to improve detection robustness.

Organ Agnostic The remaining papers focus on segmentation, diagnosis, and prognosis tasks that attempt to generalize to multiple organs, or targets organ agnostic applications. For example, nuclei segmentation of epithelial, inflammatory, fibroblast and miscellaneous tissues was performed across seven different organs Graham et al. (2019b). The method attempts to generalize across a large variety of datasets for increased usability and scalability in a clinical setting. Alternatively, an interesting approach to increase the generalization capability of deep learning in histopathology was proposed Hosseini et al. (2019). Currently, publicly available datasets with thorough histological tissue type annotations are organ specific or disease specific and thus constrain the generalizability of CoPath research. To fill this gap, a novel dataset called Atlas of Digital Pathology (ADP) is proposed Hosseini et al. (2019). This dataset contains multi-label patch-level annotations of Histological Tissue Types (HTTs) arranged in a hierarchical taxonomy. Through supervised training on ADP, high performance on multiple tasks is achieved even on unseen tissue types.

3. Data Collection for CoPath

One of the first steps in the workflow for any CoPath research is the collection of a representative dataset. This procedure often requires large volumes of data that should be annotated with ground-truth labels for further analysis Campanella et al. (2019b); Koohbanani et al. (2020); Lu et al. (2021d). However, creating a meaningful dataset with corresponding annotations is a significant challenge faced in the CoPath community Campanella et al. (2019b); Koohbanani et al. (2020); Awan et al. (2017); Lu et al. (2021d); Li et al. (2021d).

This section outlines the entire process of the data-centric design approach in CoPath, including tissue slide preparation and WSI scanning—the first two stages in the proposed workflow shown in Figure 1. Additionally, the trend in dataset compilation across the 700 papers surveyed is discussed regarding dataset sizes, public availability, and annotation types; see Table 8.3 in the Supplementary Material for information regarding the derivations and investigation of said trends.

3.1. Tissue Slide Preparation

For the application development stages in CoPath, the creation of a new WSI dataset must begin with selection of relevant glass slides. High quality WSIs are required for the effective analysis, however, considerations must be made for potential slide artifacts and variations inherently present. As described in Section 2.1, pathology samples are categorized as either biopsy or resection samples, with most samples being prepared as *permanent* samples and some intra-operative resection samples being prepared as *frozen* samples.

Variations and Irregularities Throughout the slide sectioning process, artifacts and irregularities can occur which reduce the slide quality. These can include: a portion of the section being uncovered, or air bubbles in between the glass seal Ghaznavi et al. (2013). Other possible artifacts include: chatter artifacts of the tissue, tissue folding and tears, ink markings present on the slide, and dirt, debris, or microorganisms Ghaznavi et al. (2013); Ianni et al. (2020); Rolls (2016). Cross-contamination of slides by unrelated tissue from other organs is an additional source of error that can cause confusion in the diagnostic process Rolls (2016). As frozen sections follow a different tissue preparation procedure, they present unique irregularities and variations, such as freezing artifacts or cracks in the tissue specimen block Suvarna et al. (2019). Additionally, delay of fixation after cutting a frozen section can produce significant drying artifacts, which reduces clarity of cellular details Peters (2016). Some research has been done in compiling an extensive list of these sources of errors and irregularities from slide preparation Rolls (2016).

Beyond these irregularities, glass slides may vary in stain colour, occurring due to differences in slide thickness, fixation, tissue processing schedule, and patient variation Yagi (2011); Suvarna et al. (2019); Bejnordi et al. (2015, 2014). The irregularities themselves can vary between different labs, causing discrepancies in slides from different pathology centres Zarella et al. (2019). Additionally, differences in the stains themselves, caused by stain age, stain batch, and manufacturer can also cause variation in slide colouration Suvarna et al. (2019).

All such defects and variations are important to keep in mind when selecting glass slides for the development and application process in CoPath, as they can both reduce the quality of the WSI as well as impact the performance of developed CAD tools trained with these WSIs Ghaznavi et al. (2013); Ianni et al. (2020); Bejnordi et al. (2015). A more detailed discussion on the surveyed works in CoPath which seek to identify and correct issues in slide artifacts and colour variation in WSIs is found in Section 3.2. However, prior to digitization, artifacts, and irregularities can be kept at a minimum by following good pathology practices. While an in-depth discussion of this topic is outside the scope of this paper, some research provides an extensive list of recommendations for reducing such errors in slide sectioning Rolls (2016).

3.2. Whole Slide Imaging (WSI)

WSI Scan Once a glass slide is prepared, it must be digitized into a WSI. The digitization and processing workflow for WSIs can be summarized as a four-step process Pantanowitz (2010): (1) Image acquisition via scanning; (2) Image storage; (3) Image editing and annotation; (4) Image display Pantanowitz et al. (2018). As the first two steps of the digitization workflow are the most relevant for WSI collection and with regards to the CoPath workflow, they are discussed to a greater extent below.

Slide scanning is carried out through a dedicated slide scanner device. A plethora of such devices currently exist or are in development; see Table 1 for a collection of commercially available WSI scanners. Notably, scanners from Leica Biosystems and Philips, among others, are FDA-cleared for clinical diagnosis. Additionally, some research has investigated and compared the capabilities and performances of various WSI scanners Hossain et al. (2018); Tabata et al. (2019); Cheng et al. (2019); Lemaillet et al. (2021).

Generally, a WSI scanning device is composed of four major components Zarella et al. (2019): (1) a light source; (2) a slide stage; (3) an objective lens; and (4) a digital camera. In order to produce a WSI that is in focus, which is especially important for CoPath works, appropriate focal points must be chosen across the slide either using a depth map or by selecting arbitrarily spaced tiles in a subset Indu et al. (2016). Once focal points are chosen, the image is scanned by capturing tiles or linear scans of the image, these individual components are then stitched together to form the full image known as the big flat TIFF image Zarella et al. (2019); Indu et al. (2016). To reduce the area needed to be scanned, a segmentation algorithm can be used within the scanner to separate tissue regions from extraneous background regions Bárdi et al. (2019). Additionally, slide can also be scanned at various magnification levels depending on the downstream task and analysis required. The vast majority of WSIs are scanned at $20\times$ ($\sim 0.5\mu\text{m}/\text{pixel}$) or $40\times$ ($\sim 0.25\mu\text{m}/\text{pixel}$) magnification as these are the most useful in practice for general pathologist Zarella et al. (2019).

WSI Storage and Standards WSIs are in giga-pixel dimension format Abels et al. (2019); Herrmann et al. (2018). For instance a tissue in $1\text{cm} \times 1\text{cm}$ size scanned @ $0.25\mu\text{m}/\text{pixel}$ resolution can produce a 4.8GB image (uncompressed) with a $50,000 \times 50,000$ pixels. Due to this large size, hardware constraints may not support viewing entire WSIs at full resolution

Godinho et al. (2017). Therefore, WSIs are most often stored in a tiled format, so that only the viewed portion of the image (tile) is loaded into memory and rendered Godinho et al. (2017). Additionally, to support efficient zooming, WSIs are stored in a pyramidal structure, where higher levels of the pyramid represent lower magnification levels. The highest level of the pyramid is generally a very low resolution thumbnail snapshot of the WSI, while the lowest is the full resolution image (i.e. big-flat TIFF). In this way, different zoom levels can be captured and displayed in a WSI format efficiently—artificially replicating different zooming levels from optical microscopy Singh et al. (2011); Godinho et al. (2017). Additionally, WSIs can be compressed before storage to reduce their filesize, often using JPEG, JPEG 2000, or LZW algorithms, which can reduce an image size by more than seven times Zarella et al. (2019). Alongside the WSI, metadata regarding patient, tissue specimen, scanner, and WSI information is stored for reference Abels et al. (2019); Herrmann et al. (2018); Clunie (2021). Due to their clinical use and importance, it is important to develop effective storage solutions for these WSI data files and metadata, allowing for robust data management, querying of WSIs, and efficient data retrieval Wang et al. (2012); Barron et al. (2018).

To develop CoPath CAD tools in a widespread and general manner, a standardized format for WSIs and their corresponding metadata is essential Herrmann et al. (2018). However, there is a general lack of standardization for WSI formats outputted by various scanners, as shown in Table 1, especially regarding metadata storage. The Digital Imaging and Communications in Medicine (DICOM) standard provides a framework for biomedical image format and data management and has been extended to the CoPath field through Supplement 145 Clunie (2021); Singh et al. (2011). Some research has shown that the use of the DICOM standard allows for efficient data access and greater interoperability between different centres and different CoPath-related devices Herrmann et al. (2018). However there is currently a lack of widespread adoption Herrmann et al. (2018); Abels et al. (2019); Clunie et al. (2018); Clunie (2021), reflected in Table 1 where only two recorded scanners are DICOM-compliant. Notably, with regards to metadata, DICOM provides a systematic format detailing a variety of relevant medical information, consistent with DICOM standards in other medical imaging fields Clunie (2021). The expansion through Supplement 145 also adds pyramid-tiling for WSIs, a format that is directly beneficial to creation of CoPath and CAD tools. While many scanners have adopted the pyramid-type scheme for image data, they have not fully adopted the DICOM image format, outputting in either TIFF, BigTIFF format, or in TIFF-derivatives such as SVS or GTIFF. While the TIFF format allows for semi-structured metadata Godinho et al. (2017), the consistency in metadata structure offered by DICOM is an advantage over the former Clunie (2021).

Apart from storage format, a general system for storing and distributing WSIs is also an important pillar for CoPath. Whereas in other medical imaging fields such as radiology, images are often stored in a picture archiving and communications systems (PACS) in a standardized DICOM format, with

DICOM storage and retrieval protocols Godinho et al. (2017), the need for standardization persists in pathology for WSI storage solutions. Few works have proposed solutions to incorporate DICOM-based WSIs in a PACS, although some research has successfully implemented a WSI PACS consistent using the DICOM standard using a web-based service for viewing and image querying Godinho et al. (2017).

WSI Defects and Variations Certain aspects of the slide scanning process can introduce unfavorable irregularities and variations Kanwal et al. (2022). A major source of defects is out-of-focus regions in a generated WSI. These areas are often caused by glass slide artifacts, such as air bubbles and tissue folds, which interfere with selection of focus points for a slide Ghaznavi et al. (2013); Campanella et al. (2018a). These out-of-focus regions degrade WSI quality and are detrimental to the performance of CAD tools developed with these WSIs and present concerns for performance when deployed in the field and causing high false-positive errors Wang et al. (2020c); Ianni et al. (2020). Additionally, as WSIs are scanned in strips or tiles, any misalignment between tiles can introduce striping/stitching errors in the final image Cross et al. (2018). A further source of error may appear during tissue-background segmentation where the scanner may misidentify some tissue regions as background, potentially missing crucial tissue areas on the glass slide from being digitized Bndi et al. (2019).

Beyond these general sources of error, scanners from different vendors may introduce their own colour variations to WSIs due to variation in sensor design and calibration Zarella et al. (2019). As different pathology centres may use different scanner models, this factor can be a significant source of colour, and therefore strain, variation in a cross-laboratory WSI dataset. These additional sources of error and variation add additional layers of complexity to the WSI processing workflow, and must be kept in mind during slide selection and dataset curation for CAD tool development and deployment.

Addressing Irregularities and Variations Much work has gone into identifying areas of irregularities within WSIs, including most notably blur and tissue fold detection Campanella et al. (2018a); Wang et al. (2020c). Some research has explored automated deep learning tools to identify these irregularities at a more efficient pace than manual inspection Campanella et al. (2018a); Wang et al. (2020c). Further, researchers have created a WSI search engine tool to address the issue of cross-contamination, where a user-identified region is compared with data in a pre-constructed database to identify the most similar WSIs Hegde et al. (2019).

Developing techniques for addressing staining variation has also been a significant research area Khan et al. (2014); Zanjani et al. (2018); Sethi et al. (2016); Bejnordi et al. (2015); Guerrero and Oliveira (2021); Yamashita et al. (2021); Vahadane et al. (2021). Specifically, staining variation refers to differences in colour and contrast of the tissue structures in the final WSI that occurs due to variations in the staining process, staining chemicals, and tissue state. Variations in colour can lead to difficulty in generalizing CAD tools to WSIs from different labs, institutions, and settings Tellez et al. (2019a); Otlora et al. (2019). The use of techniques addressing stain variation is important

Table 1: The following table lists commercially available WSI Scanners grouped by manufacturing company and their respective available compression slide formats.

Company: Scanner Model (Slide Format)
Leica Biosystems: Aperio AT2 / CS2 / GT450 (TIFF (SVS))
Hamamatsu: Nanozoomer SQ / S60 / S360 / S210 (JPEG)
F. Hoffmann-La Roche AG: Ventana DP200 / iScan HT / iScan Coreo (BIF, TIFF, JPG2000, DICOM)
Huron Digital Pathology: TissueScope IQ / LE / LE120 (BigTIFF, DICOM compliant)
Philips: Ultra-Fast Scanner (iSyntax Philips proprietary file)
3DHistech: Pannoramic Series (MRXS, JPG, JPG2000)
Mikroscan Technologies: SL5 (TIFF)
Olympus: SL5 (JPEG, vsl, TIFF)
Somagen Diagnostics: Sakura VisionTek (BigTIFF, TIFF, JPG2000)
Akoya Biosciences: Vectra Polaris (JPEG, single-layer TIFF, BMP, or PNG)
Meyer Instruments: EASYSCAN PRO 6 (SVS, MDS, JPEG, JPEG2000)
Kibio: KF-PRO (JPEG, JPEG2000, BMP, TIFF)
Motic: EasyScan Pro (JPEG, JPEG2000, Aperio Compatible)
Precipoint: PreciPoint O8 (GTIF)
Zeiss: Zeiss Axio (Not specified)
Objective Imaging: Glissando (SVS, BigTIFF)
Microvisioneer: manualWSI (Not specified)

for all future works and we list some computational approaches proposed to address these issues. An example method proposed in Khan et al. (2014) uses a stain normalization technique, attempting to map the original WSI onto a target color profile. In this technique, a color deconvolution matrix is estimated to convert each image to a target H&E color space and each image is normalized to a target image colour profile through spline interpolation Khan et al. (2014). The second approach applies color normalization using the H channel with a threshold on the H channel on a Lymphocyte Detection datasetGuerrero and Oliveira (2021). Alternatively to the aforementioned classical approaches, recent studies have shown promise in having deep neural networks accomplish this task Arvidsson et al. (2019); Shaban et al. (2019b); Zanjani et al. (2018); Mahapatra et al. (2020), commonly applying generative models such as generative adversarial networks (GANs) to stain normalization. Furthermore, Histogram Equalization (HE) technique for contrast enhancement is used in Mehmood et al. (2022). A novel pre-processing technique is also proposed to select and enhance a portion of the images instead of the whole dataset, resulting in improved performance and computational efficiency.

An alternative approach to address the impact of stain variation on training CAD tools is data augmentation. Such methods augment the data with duplicates of the original data, containing adjustments to the color channels of the image, creating images of varying stain coloration, and training train models that are accustomed to stain variationsOtlora et al. (2019). This method has been frequently used as a pre-processing step in the development of training datasets for deep learning Tellez et al. (2019b); Yan et al. (2020c); Wang et al. (2020a). A form of medically-irrelevant data augmentation based on random style transfer, called STRAP, was proposed by researchers and outperformed stain normalization Yamashita et al. (2021). Similar to style transfer, Lin et al. (2022) proposes stain transfer which allows one to virtually generate multiple types of staining from a single stained WSI.

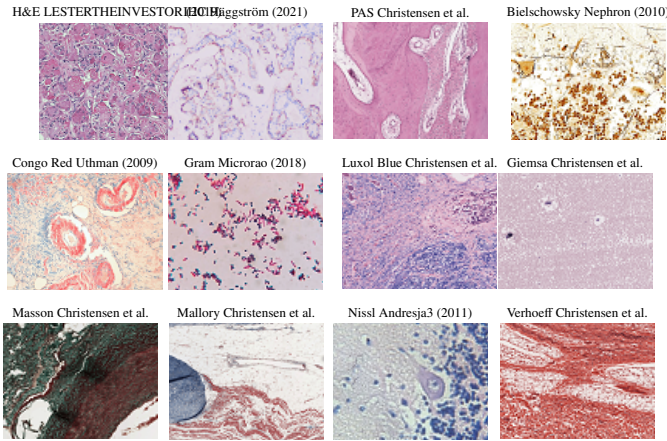


Fig. 6: WSI tissue images with different types of histological stains. Each stain highlights different areas and structures of the tissue in order to aid in visualizing underlying characteristics. Amongst this diversity, there's Hematoxylin and Eosin or H&E which is mainly used in studies as most histopathological processes can be understood from this stain.

3.3. Cohort Selection, Scale, and Challenges

The data used to create/train CoPath CAD tools can greatly impact the performance and success of the tool. Curating the ideal dataset, and thus selecting the ideal set of WSIs for the development of a CAD tool is a nontrivial task. Several works suggest that datasets for deep learning in CoPath should include a large quantity of data with a degree of variation and artifacts in the WSIs Campanella et al. (2019b); Ianni et al. (2020). Some works also recommend the inclusion of difficult or rarely diagnosed cases, however, other works indicate that inclusion of extremely difficult cases may decrease the performance of advanced models Ianni et al. (2020); Wei et al. (2021a).

A study highlighting the results of the 2016 Dataset Session at the first annual Conference on Machine Intelligence in Medical Imaging outlines several key attributes to create an ideal medical imaging dataset Kohli et al. (2017), and while the scope of this conference did not include CoPath, many of the points made regarding medical imaging datasets are also relevant to the development of CoPath datasets. Some key attributes include having a large amount of data to achieve high performance on the desired task, quality ground truth annotations, and being reusable for further efforts in the field Kohli et al. (2017). The session also outlines the impact that class imbalances can have on machine learning models, an issue also prevalent in CoPath as healthy or benign regions often outnumber diseased regions by a significant margin Wahab et al. (2017).

Our survey of past works in the literature reveals some trends in CoPath datasets. Currently, the majority of datasets presented in the literature for CAD tool development are small-scale datasets Campanella et al. (2019b), using a small number of images, images from a small number of pathology laboratories, or both. Examples of these smaller datasets include a dataset with 596 WSIs (401 training, 195 testing) from four centres for breast cancer detection Cruz-Roa et al. (2018) and the BACH2018 dataset, which has 500 ROI images (400 training, 100 testing) and 40 WSIs (30 training, 10 testing) Aresta et al. (2019). Although curating a dataset from fewer pathology labo-

ratories may be simpler, these smaller scale datasets may not be able to effectively generalize to data from other pathology centres Tellez et al. (2019a); Gamper et al. (2020b). An example of this can be seen in which data from different pathology centres are clustered disjointly in a t-SNE representation demonstrated in Ianni et al. (2020). Another alternative was proposed in Saldanha et al. (2022), using a Swarn learning technique multiple AI models can be trained on different small data sets separately and then unified into one central model.

Additionally, stain variations, slide artifacts, and variation of disease prevalence may sufficiently shift the feature space such that a deep learning model may not sustain high performance on unseen data in new settings Gamper et al. (2020b); Willemink et al. (2020). As artifacts in WSIs are inevitable, with some artifacts, such as ink mark-up on glass slides, being an important part of the pathology workflow Ali et al. (2019), the ability of CAD tools to become robust to these artifacts through exposure to a diverse set of images is an important consideration.

Compared to the number of studies conducted on small-scale datasets, relatively fewer studies have been performed using large-scale, multi-centre datasets Campanella et al. (2019b); Iizuka et al. (2020); Ianni et al. (2020). One study uses over 44,715 WSIs from three organ types, with very little curation of the WSIs for multi-instance learning detailed in Campanella et al. (2019b). Stomach and colon epithelial tumors were classified using 8,164 WSIs in Iizuka et al. (2020). A similar study uses 13,537 WSIs from three laboratories to test a machine learning model trained on 5,070 WSIs and achieves high performance Campanella et al. (2019b).

Despite some advancements, there exist major barriers to using such large, multi-centre datasets in CAD development. Notably, for strongly supervised methods of learning, an immense amount of time is needed to acquire granular ground truth annotations on a large amount of data Iizuka et al. (2020). To combat this, some researchers have implemented weakly-supervised learning by harvesting existing slide level annotations to forego the need for further annotation Campanella et al. (2019b). Additionally, it may be difficult to aggregate data from multiple pathology centres due to regulatory, privacy, and attribution concerns, despite the improvements that diverse datasets offer. section 5 discusses model architectures and training techniques that harness curated datasets of various annotation levels.

Dataset Availability In general computer vision, progress can be tracked by increasing the size and availability of datasets used to train models, as noted by the growth of ImageNet from 3.2 million images and 5000 classes in 2009 to 14 million images and 21,000 classes in 2021 Deng et al. (2009b). We can infer that a similar trend should be seen in CoPath to achieve similar progress as compared to general computer vision. In CoPath, availability of datasets for research and development use is a primary concern. Due to the costly nature of acquiring and annotating WSI data, having all CoPath datasets available for public use would be an ideal scenario. To determine the current landscape of collected datasets we have surveyed over 700 CoPath papers, determining the dataset(s) used in each, and tabulated the results into Table 8.3 of the supplementary section.

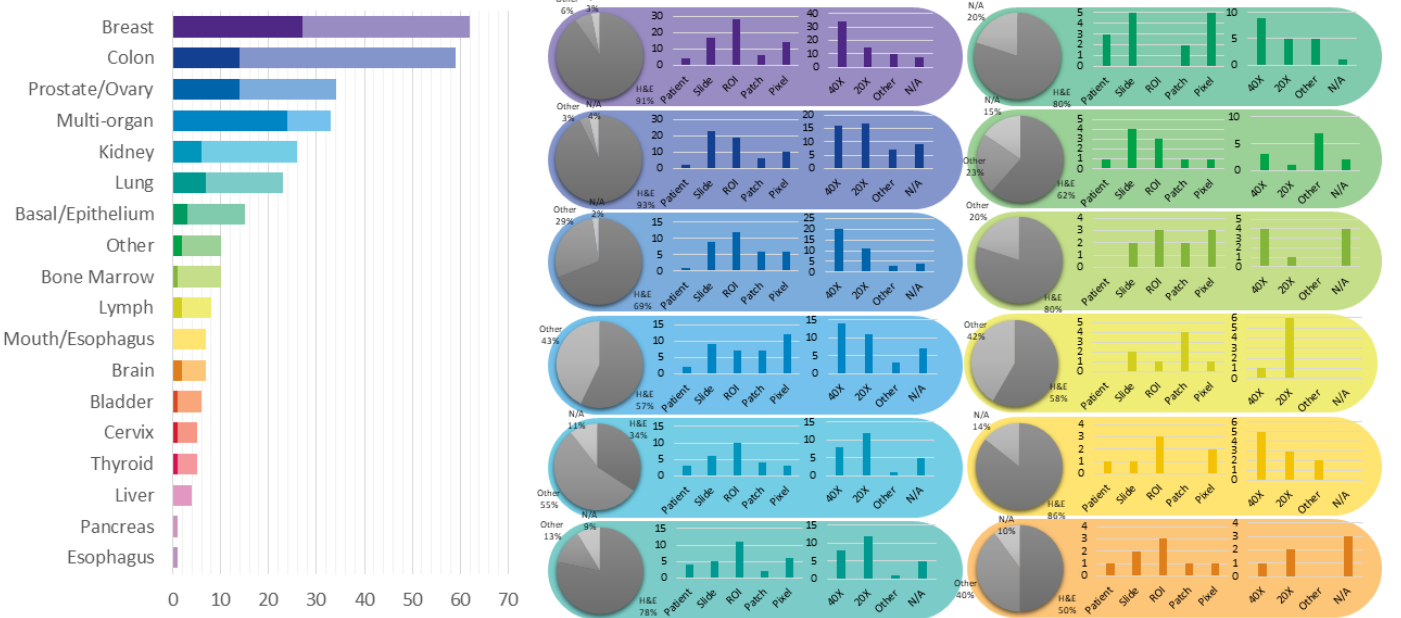


Fig. 7: (left) shows the distribution of datasets per organ. Along the vertical axis, we list different organs, while the horizontal axis shows the number of datasets; wherein the darker color denotes public availability while the light color includes unavailable or by request statuses. (right) Distribution of staining types, annotation levels, and magnification details per organ color coded consistently with the bar graph. Organs have been sorted based on the abundance of datasets. For more details, please refer to Table 8.3 in the supplementary section.

The table includes the name of each dataset, a list of works that reference it, and a corresponding link to the download page (Heading Name & Link). The size of each dataset, the annotation level, number of classes and associated class balance, stain type, and the resolution of the images are also provided. Figure 7 summarizes some of our findings from Table 8.3 and displays the distribution of datasets by availability, organ type, staining type, along with annotation and magnification level.

From Figure 7 we can clearly see that the majority of datasets used for research developments in computational pathology are privately sourced or require additional registration/request. Breaking it down per organ, we see that organs with a small number of datasets in general, such as the liver, thyroid, brain, etc, actually have a smaller proportion of freely accessible datasets. This can be problematic when trying to create CAD tools for cancers in these organs due to a lack of usable data. We additionally note that although data sets requiring registration/request for access can be easily accessible, as in the case of BreakHis Spanhol et al. (2015) being used in multiple works Bardou et al. (2018); Bayramoglu et al. (2016); Li et al. (2020b), the need for registration presents a barrier to access as requests may go unanswered or take much time review.

In our categorization of CoPath datasets, we find that a few prominent datasets have been released publicly for use by the research community. Many such datasets are made available through grand challenges in computational pathology Hartman et al. (2020), such as the CAMELYON16 and CAMELYON17 challenges for breast lymph node metastases detection Bejnordi et al. (2017a); Litjens et al. (2018); Bandi et al. (2019), as well as the GLaS competition for colon gland segmentation, in conjunction with MICCAI 2015 Sirinukunwattana et al. (2017a); Hou et al. (2019b). Notable amongst publicly available data

repositories is the cancer genome atlas (TCGA) Grossman et al. (2016), a very large-scale repository of WSI-data containing many organs and diseases, along with covering a variety of stain types, magnification levels, and scanners. Data collected from TCGA has been used in a large number of works in the literature for the development of CAD tools Otalora et al. (2019); Cho et al. (2020); Hou et al. (2020a). As such, TCGA represents an essential repository for the development of computational pathology. While patient confidentiality is a general concern when compiling and releasing a CoPath dataset, large-scale databases such as TCGA prove that it is possible to provide relatively unrestricted data access without compromising patient confidentiality. Further evaluating public source datasets, it seems that the majority of them use data extracted from large data repositories, such as TCGA, without specifying the IDs of the images used, which provides a challenge in comparing datasets or CAD tool performance across works, however, there are a few datasets that are exceptions to that phenomena Mobadersany et al. (2018); Fischer et al. (2018); Gertych et al. (2019); Lu et al. (2021d).

Figure 7 also provides some insights on the dataset breakdown by organ, stain type, and annotation level. Per organ, it can be seen that the breast, colon, prostate/ovary, and lung tissue datasets are amongst the most common, understandably since cancer occurrence in these regions is the most frequent Siegel et al. (2020)—complying with cancer statistics findings in 2.5. Multi-organ datasets are the other most common type, where we have designated a dataset to be multi-organ if it compiles WSIs from several different organs. To note, multi-organ datasets are especially useful for the development of generalized image analysis tools in computational pathology. The annotation level provided in the datasets did not indicate any pat-

Table 2: Commercially available annotation software along with their manufacturing company and available input slide formats.

Company: Annotation Tool (Input Format)
Leica Biosystems: Aperio eSlide Manager (JFIF, JPEG2000, PMM)
Pathcore: Sedeon Viewer (Aperio SVS, Leica SVN, TIFF, JPEG2000)
Indica: Halo (TIFF/SVS)
Objective Pathology: MyObjective (Scanner-wide compatibility)
ASAP: ASAP (Multiple formats through OpenSlide)
SiliconLotus: SiliconLotus (Not specified)
Augmentiqs: Annotation Software Suite (Not specified)
QuPath: QuPath (Multiple formats, Bio-formats and OpenSlide)
Proscia: Concentriq (Not specified)
Visiopharm A/S: VisioPharm (Not specified)
Hamamatsu: NDP (JPEG)
Roche: Ventana Companion Image Analysis (BIF, TIFF, JPG2000, DICOM compliant)
Huron: HuronViewer (BigTIFF, FlatTIFF, DICOM compliant)
Philips: Intellisite (iSyntax Philips proprietary file)
3DHistech: CaseViewer (JPG, PNG, BMP, TIFF)
AnnotatorJ Hollandi et al. (2020): AnnotatorJ (JPG, PNG, TIFF)
NuClick Koohbanani et al. (2020): NuClick (Not specified)

tern across most organs. Further, the most frequent stain type is H&E, as expected, while a few datasets may contain WSI with other stain types. The most frequently occurring magnification levels are 20 \times and 40 \times , which coincides with most pathology workflows, while a small number of works have used other zoom levels or did not list the specific level (labelled N/A).

4. Domain Expert Knowledge Annotation

A primary goal of CoPath is to capture and distill domain expert knowledge, in this case the expertise of pathologists, into increasingly efficient and accurate CAD tools to aid pathologists everywhere. Much of the domain knowledge transfer is encompassed within the process of human experts, in this case pathologists, generating diagnostically-relevant annotations and labels for WSIs. It must be emphasized, that without some level of label, a WSI dataset is not directly usable to train a model for most CAD tasks that involve the generation of diagnoses, prognoses, or suggestions for pathologists. Thus, the process of obtaining and/or using annotations at the appropriate granularity and quality is paramount in the field. This section focuses on describing various types of ground-truth annotation to cover the spectrum of weak to strong supervision of labels, discussing the practicality of labeling across this supervision spectrum, and how a labeling workflow can be potentially designed to optimize related annotation tasks.

4.1. Supervised Annotation

In contrast to general computer vision, computer scientists do not have expert-level knowledge of histopathology and thus they are not as efficient at generating annotations or labels of pathology images. Further, labels cannot be easily obtained by outsourcing the task to the general public. As a result, pathologists must be leveraged to obtain labels at some stage of the data collection and curation process, and in many annotation pipeline the first step involves recruiting the help of pathologists for their expertise in labelling.

Obtaining Expert Domain Knowledge The knowledge of pathologists is essential in the development of accurate ground

truth annotations—a process most commonly completed by encircling regions of interest (ROI) Cruz-Roa et al. (2018). However, there are studied instances of inter-observer variance between pathologists when determining a diagnosis Faust et al. (2019); Yu et al. (2016); Parvatikar et al. (2020). As obtaining the most correct label is essential when training a model for CAD, this issue must be addressed and a review of the data by several pathologists can result in higher quality ground truth data as compared to that of a single pathologist. As a result, most datasets are curated by involving a group of pathologists in the annotation process. If there exists a disagreement between the expert pathologists on the annotation of a ground truth, one of several methods is usually employed to rectify the discrepancy. A consensus can be reached on the annotation label through discussion amongst pathologists, as is done in the TNBC-CI dataset Naylor et al. (2018), the BCSC dataset Breast Cancer Surveillance Consortium and the MHIST dataset Wei et al. (2021b). Alternatively, images, where disagreements occur, can be discarded, as is done in some works Araújo et al. (2017); Yan et al. (2018). Further, the disagreement between annotators can be recorded to determine the difficulty level of the images, as is done in the MHIST dataset Wei et al. (2021a). This extra metadata aids in the development of CAD tools for analysis.

Pathologists can also be involved indirectly in dataset annotation. Both MoNuSeg Kumar et al. (2017) and ADP Hosseini et al. (2019) have non-expert labelers annotate their respective datasets. A board-certified pathologist is then tasked with reviewing the annotations for correctness. Alternatively, some researchers have employed a pathologist in performing quality control on WSIs for curating a high-quality dataset with minimal artifacts Courtirol et al. (2019); Saltz et al. (2018). To enable the large scale collection of accurate annotated data, Lizard Graham et al. (2021) was developed using a multi-stage pipeline with several significant “pathologist-in-the-loop” refinement steps.

Existing pathological reports, along with the metadata that comes from public large-scale databases like TCGA, can also be leveraged as additional sources of task-dependent annotations without the use of further annotation. For example, TCGA metadata was used to identify desirable slides in Dong et al. (2014), while pathological diagnostic reports were used for breast ductal carcinoma in-situ grading in Idlahcen et al. (2020).

To note, there are some tasks where manual annotation by pathologists can be bypassed altogether. For instance, immunohistochemistry (IHC) was applied to generate mitosis figure labels using a PHH3 slide-restaining approach in Tellez et al. (2018), while immunofluorescence staining was used as annotations to identify nuclei associated with pancreatic adenocarcinoma Chang et al. (2017b). These works parallel the techniques that pathologists often use in clinical practice, such as the use of IHC staining as a supplement to H&E stained slides for difficult to diagnose cases Bandi et al. (2018). They demonstrate high performance on their respective tasks wherein the top-performing models on the TUPAC16 Veta et al. (2019) dataset were achieved Tellez et al. (2018). Importantly, these techniques still utilize supervision, albeit weakly, by leveraging lab

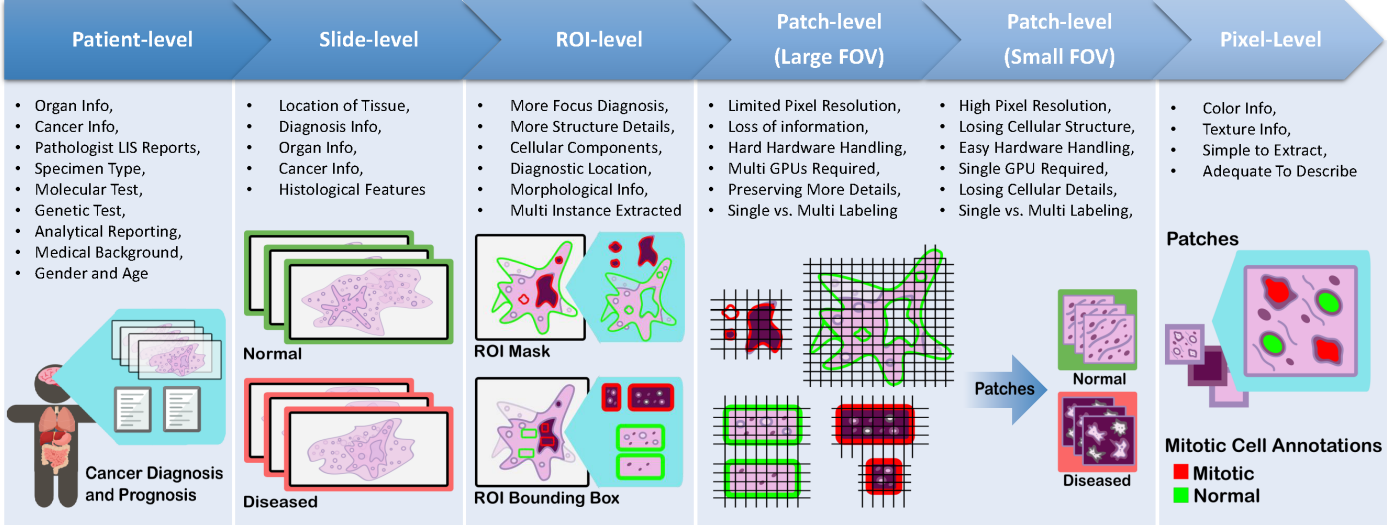


Fig. 8: Details of the five different types of annotations in computational pathology. From left to right: a) **Patient-level annotations:** can include high level information about the patient like status of cancer, test results, etc. b) **Slide-level:** are annotations associated with the whole slide, like a slide of normal tissue or a diseased one c) **ROI-level annotations:** are more focused on diagnosis and structure details d) **Patch-level:** are separated into Large FOV (field of view) and small FOV, each having different computational requirements for processing, and finally e) **Pixel-level:** includes information about color, texture and brightness

techniques that have been developed and refined to identify the desired regions visually.

Ground-Truth Diagnostic Information Understanding different annotation levels and their impact on the procedural development of ML pipelines is an important step in solving tasks within CoPath. There are five possible levels of annotation, in order of increasing granularity (from weakly-supervised to fully-supervised): patient, slide, ROI, patch, and pixel. Figure 8 overviews the benefits and limitations of each level. This section focuses on describing the components and considerations of each granularity level as well as new active learning tools for the development of Ground-Truth Annotations.

Patient-level Annotation Patient-level annotations assign a single label to a single patient and come from case reports that can address multiple WSIs from a primary organ site. In addition to the WSIs, the Laboratory Information System (LIS) may also contain additional metadata, diagnostic information, and analytical or synoptic report information Pantanowitz et al. (2007). Notably, the LIS can store specimen type, molecular and genetic tests, patient medical history, and clinical variables such as the patient's age and gender Narayanan et al. (2019); Lai et al. (2021).

Slide-level Annotation Slide-level annotations designate labels for a single WSI, which encompasses diagnosis and cancer information Lu et al. (2021c); Li et al. (2021a). In comparison to the patient-level, this level of focus provides a more precise tissue location for the provided diagnosis Chen et al. (2021c); Riasatian et al. (2021); Roy et al. (2021).

ROI-level Annotation ROI-level annotation identifies regions within a slide that can be of either diagnostic or analytical relevance to a pathologist. Regions themselves can be designated using two methods: (1) bounding boxes Awan et al. (2017); Yan et al. (2020c); Cruz-Roa et al. (2018) or (2) pixel-wise masks that are augmented on the WSIs Jiang et al. (2020b); Aresta et al. (2019); Litjens et al. (2018). Importantly, each

ROI is considered to be a single class Wang et al. (2019c), but the labels represent more detailed tissue structures providing more specific and detailed diagnostic information than patient and slide levels Lu et al. (2021d), ultimately being more applicable in disease diagnosis tasks Shephard et al. (2021).

Patch-level Annotation Patch-level annotation is done on mosaic tiles (usually in a square shape) extracted from the WSI/ROI with a given field of view (FOV). Most deep-learning models are trained at the patch level, which contains anatomical structures of tissues and cells. Patches are either single-labeled or multi-labeled according to the taxonomical labeling workflow Brieu et al. (2019). One key aspect for patch-level annotation is determining the optimum FOV to encompass enough tissue classes Tokunaga et al. (2019), as considering smaller or bigger FOV can provide different advantages, as demonstrated in Figure 8 for the patch-level.

Patch-Size Selection The choice of the patch size is limited by the computational complexity of the hardware that is used for training CAD tools. For instance, the majority of deep learning pipelines accept image sizes of less than 300×300 pixels Chang et al. (2019); Xiang et al. (2021); Tran et al. (2021); Srinidhi and Martel (2021); Lu et al. (2021d). The size of the FOV needs to be determined such that acceptable levels of morphological tissues will be covered within that patch. Accordingly, the pixel resolution is determined given a certain FOV and patch size. Given the above factors, if a larger FOV is required, then pixel resolution is limited which translates to information loss. In comparison, if higher pixel resolution is required, then the FOV will be limited accordingly which may exclude cellular/architectural relevance pertaining to the underlying class representation Pati et al. (2021a). To mitigate this tradeoff, larger image dimensions are required which consequently increases the computational power required for patch processing (e.g. high RAM GPU memory or parallelized multi-GPU processing) Tokunaga et al. (2019).

Pixel-level Sizing Pixel-level annotation requires labelling each pixel as a specified class. In this level, features are simple to extract and sufficient for describing the images as they encompass color and texture information Shirazi et al. (2018). However, there is a lack of biological interpretability as the other levels of annotation more appropriately describe characteristics of the cellular and tissue structures Li et al. (2021c). A solution based on human-interpretable image features can include histological knowledge and expert annotations that can describe different cell anatomies such as the stroma, the nuclei of the cells, and the size and shape of tumor regions, as well as the texture of the tissues and the location of tumors infiltrating lymphocytes Diao et al. (2021b).

Pixel-wise masks are differentiated from pixel-level annotations in that when an ROI mask of this type is tiled into multiple instances (i.e. patches), each sample is considered a single class. The ROI-level is in contrast to the pixel-level annotations, wherein the latter is defined to include all annotations where each patch can contain several class types.

Picking the Annotation Level Selecting an annotation level depends largely on the specific CoPath task being addressed, as shown in Figure 9. For example, segmentation tasks tend to favor pixel-level annotations as they require precise delineation of a nucleus or tissue ROI. Conversely, disease diagnosis tends to favor datasets with ROI-level annotations, as diagnosis tasks are predominantly associated with the classification of diseased tissue, the higher-level annotations may provide a sufficient level of detail and context for this task Kozierski et al. (2021).

Figure 9 shows that tasks that use stronger supervision are more likely to be used in CAD tool model development. However, due to the high cost of pixel-level annotation, fully supervised annotations are challenging to develop. Even patch-based annotations often require the division and analysis of a WSI into many small individual sub-images resulting in a similar problem to pixel-based annotations Lu et al. (2020a); Tellez et al. (2019b). In contrast, WSI data is most often available with an accompanying slide-level pathology report regarding diagnosis thus making such weakly labeled information at the WSI level significantly more abundant than ROI, patches, or pixel-level data Pinckaers et al. (2021); Li et al. (2021a). Different levels of annotation can be leveraged together, as demonstrated by a framework to use both pixel and slide level annotations to generate pseudo labels Li et al. (2021c). Additionally, it is common in CoPath to further annotate the slide-level WSIs on an ROI or patch level structure Zadeh Shirazi et al. (2020); Phillips et al. (2018); Xu et al. (2020); Koohbanani et al. (2021).

Active Learning Tools Active learning annotation tools bridge the gap between the need for highly supervised labels and the current abundance of less informative annotations. Such works seek to ease the annotation process by using computational approaches to assist the human annotator. For example, in Koohbanani et al. (2020), a platform was developed for creating nuclei and gland segmentation ground truth labels quickly and efficiently. A CNN, trained on similar cohort data, was used to segment nuclei and glands with different mouse actions Koohbanani et al. (2020). Alternatively, Awan et al. Awan et al. (2017) presented the HistoMapr™ platform to assist in diagno-

sis and ground truth data collection. Through this tool, a pathologist selects one of several proposed classes for each given ROI, thus mitigating the need for hand-drawn annotations or manual textual input Awan et al. (2017). Similarly, an active learning model called HALS Diao et al. (2021a) was developed to increase data efficiency by guiding annotators to more informative slide sections. Quick Annotator (QA) Miao et al. (2021) is another tool which provides an easy-to-use online interface for annotating ROIs and was designed to create a significant improvement in the annotation efficiency of histological structures by several orders of magnitude.

There are other active learning annotation tools proposed for different applications in computational histopathology that can be investigated for use in the pathology datasets. In a monocular image, instance-level labeling is provided as a result of analyzing the global labeling problem using a novel densely connected Markov random field Zhang et al. (2016b). DatasetGAN Zhang et al. (2021) generates high-quality semantically segmented images automatically from massive sets of images with minimal human input. Liao et al. Liao et al. (2021) proposed an efficient annotation strategy for colonizing large collections of images into multiple classes. Finally, ScribbleBox Chen et al. (2020a) provides an interactive framework that boosts the efficiency of annotating instances of objects with masks.

These platforms give the pathologist control in the creation of annotations while facilitating dataset creation. Such systems support the necessary relationship between pathologists and computer scientists in the development of CAD tools, and hence may prove to be a valuable contributor to the CAD system development workflow.

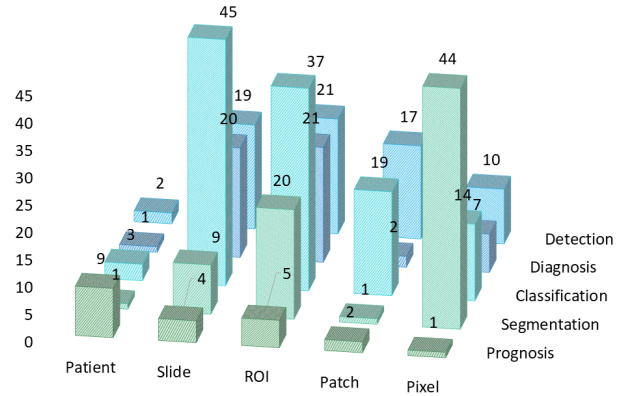


Fig. 9: Distribution of different annotation levels based on the CoPath task being addressed in the surveyed literature. The x-axis displays the different annotation levels studied in the papers (from left to right): Patient, Slide, ROI, Patch, and Pixel. The y-axis shows the different tasks (top to bottom): Detection, Diagnosis, Classification, Segmentation, and Prognosis. The height of the bars along the vertical axis measures the number of works that have examined the specific task and annotation level.

Tissue-Class and Disease Complexity Much of the current CoPath research operates under the umbrella of supervised learning tasks, and correspondingly uses labeled data to develop automated CAD tools. We refer to supervised learning to include a diverse spectrum of annotation i.e. weak-supervision (e.g. patient-level) all the way to strong-supervision (e.g. pixel-

level). Classes within a dataset can be task-dependent, for example as shown in Table 8.3 of the supplementary material, datasets primarily used for segmentation such as MoNuSeg Kumar et al. (2017) and CPM-17 Graham et al. (2019b), have classes for each annotated pixel indicating the presence or absence of nuclei. However, classes need not be task-dependent; datasets such as CAMELYON16 Bejnordi et al. (2017a) outline metastases present in WSIs that can be used for a variety of applications, including disease detection Bejnordi et al. (2017a) and segmentation tasks Takahama et al. (2019).

The current paradigm for dataset compilation in computational pathology, particularly for disease detection and diagnosis, treats different disease tissue types as separate independent classes. For example, BreakHis divides all data into benign/malignant breast tumours Spanhol et al. (2015). At the ROI level, GLaS divides colon tissue into five classes: healthy, adenomatous, moderately differentiated, moderately-to-poorly differentiated, and poorly differentiated Sirinukunwattana et al. (2017a). So far, this approach to class categorization has resulted in high-performing CAD tools Chen et al. (2016a); Bayramoglu et al. (2016); Li et al. (2020b); Javed et al. (2020); Sirinukunwattana et al. (2015); Marsh et al. (2018). However, the treatment of different disease tissue types as an independent class is perceived differently in computer vision domain where the representation learning of normal objects is done differently compared to anomalies. A similar synergy can be found by differentiating healthy tissue classes from diseased ones and one should be mindful about defining meaningful tissue ontology for annotation and labeling.

4.2. Optimum Labeling Workflow Design

This section focuses on the steps required for compilation of a CoPath dataset which is broken into three main sub-tasks: Data Acquisition, Data Annotation, and Data Management, as per Figure 10. Each sub-task is discussed below with reference to its individual components in the hierarchical structure in Figure 10.

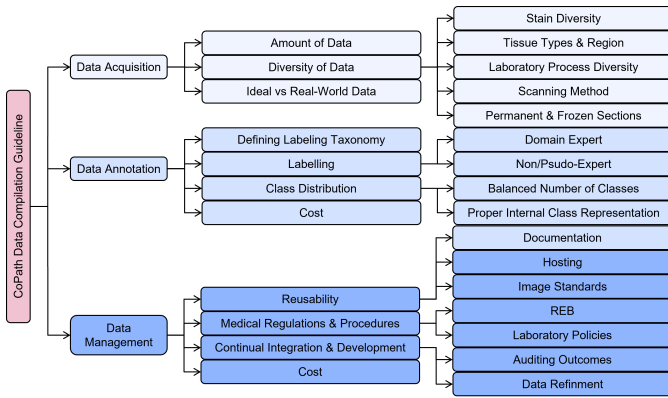


Fig. 10: Tree diagram for the optimum labeling workflow, where a CoPath dataset is divided into tasks and sub-tasks based on its initial characteristics.

Data Acquisition Database compilation starts from data acquisition. When collecting data, it is vital that there are large amounts of data Roh et al. (2019), along with having sufficient

diversity Campanella et al. (2019b); Ianni et al. (2020). Specifically, diversity in CoPath data occurs in multiple ways, such as staining methods, tissue types and regions, laboratory processes, and digital scanners. We advise that CoPath researchers consult expert pathologists on the diversity of data required for various tasks. Ideally, all the data acquired in pathology should be perfect without any irregularity and artifacts. However, some level of artifacts and irregularity are unavoidable and introducing realistic artifacts that are representative of real-world scenarios into the data increases the robustness and generalizability of CAD tools.

Data Annotation After collecting sufficient data, the next task is annotation of the data. Data annotation is a costly process in both time and money, thus a budget and schedule should always be established when generating labels. There are often various approaches for annotating different structures Wahab et al. (2022), so a specific labelling taxonomy should be defined apriori. As mentioned previously, annotation should involve expert pathologists due to the domain knowledge requirement and importance of label correctness.

Once the ontology of class-definitions is defined (in collaboration with expert pathologists), there will be two ways to generate labels or annotations in general: domain expert labelling or non-expert labelling. The domain expert labelling refers to having pathologists annotate data that they are specialized at, which is labor-extensive. On the other hand, non-expert labelling can use crowdsourcing techniques to generate weak labels or have non-experts, such as junior pathologists or students, label the data. This process is cheaper and quicker, but it may be harder to maintain the same level of quality as domain expert labeling Wahab et al. (2022). Regardless of the labelling methodology used, labels generated from both should be validated. Finally, to determine the sufficiency of label quantity, one should consider the balance between the number of classes, representation size of each class, and complexity of class representation. Techniques from active-learning could be also leveraged to compensate for lack of resource management as well as maintain the quality of labeling as discussed above.

Data Management Data management is an important aspect of any dataset creation process, and is the one that is most likely to be overlooked. Proper data management should have considerations for reusability, medical regulations/procedures, and continuous integration and development.

Reusability can be broken down into detailed documentation of the data, accessible and robust hosting of data, and consideration for image standards. Poor cross-organizational documentation can lead to missing metadata, ultimately resulting in discarding entire datasets Sambasivan et al. (2021). Adherence to an established image standard, such as DICOM, can help resolve some of these issues in reusability. Medical regulations/procedures can be broken down into the construction of a Research Ethics Board (REB) and proper consideration for whom is curating the data. Through incentives for data excellence for medical practitioners, the issue of misaligned priorities between data scientists, domain experts, and field partners can be resolved Sambasivan et al. (2021). To ensure that models used on actual patients remain relevant and hidden errors

do not propagate, continuous integration/development (CI/CD) must be implemented. These systems must include at least two components, a method to audit predictions from the model, as well as a way to refine the training data accounting for discrepancies found through auditing. Several algorithms deployed in high-risk environments, including medical diagnosis, proved to only work well when data was updated after initial deployment O’Neil (2016); Sambasivan et al. (2021). Throughout the data management process, consultation with domain experts is a vital step in ensuring the success of data compilations Lones (2021).

5. Representational Learning Models in CoPath

Once an application domain and corresponding dataset have been chosen, the next step of developing a CoPath tool involves designing of an appropriate model and representation learning paradigm. Representation learning refers to a set of algorithmic techniques dedicated to learning feature representations of a certain data domain that can be used in downstream tasks such as classification, segmentation, etc Bengio et al. (2012). In CoPath, the amount of data available for a given annotation level and task are the key determinants to designing a model and learning technique. Neural networks have emerged as the goto models in learning representations of data that are rich enough to avoid hand-crafted features and lead to great performance improvements over other models LeCun et al. (2015a). The annotation level of the data pertaining to the task corresponds to the level of supervision for the learning technique applied. This relationship between data annotation level and learning supervision level is overviewed in Figure 12.

This section details the various types of representation learning models and techniques, along with their corresponding tasks relevant to the CoPath field. Figure 11 highlights the most common backbone architectures used for feature encoding in state-of-the-art research, based on the corresponding tasks. More details are provided in Table 8.3 from the supplementary section. The selection of architectures is then compared to draw useful insights into accuracy, computational complexity, and limitations. Lastly, existing challenges in learning model design are investigated.

5.1. Classification Architectures

In CoPath, general classification architectures are the most prevalent due to their straightforward applicability to a wide range of tasks including tissue subtype classification, disease diagnosis and detection. The definition of each task is detailed in Section 2 while the distribution of tasks for different organs is in Figure 5. The aforementioned tasks are widely present in the computer vision domain and thus general classification architectures are applied to solve the problem. The most common image classification architecture are convolutional neural networks (CNNs) and most of the CNN architectures used in CoPath are transferred from the computer vision domain with pre-trained weights on natural image datasets (e.g. ImageNet) followed by a subsequent fine-tuning/deep-tuning on the specific CoPath task. The process of fine-tuning a neural network

trained in one domain to perform well in another domain is known as transfer learning, and is commonly used in CoPath works Kather et al. (2019b); Tomita et al. (2019); Bauer et al. (2016); Motlagh et al. (2018); Pinckaers et al. (2021); Celik et al. (2020); Liu et al. (2018a); Courtiol et al. (2019); Wei et al. (2019b); Saxena et al. (2020); Bidart and Wong (2019); Holland et al. (2020); Hekler et al. (2019); Lee and Paeng (2018); Kather et al. (2019a); Kumar et al. (2020a); Chan et al. (2019); Faust et al. (2019); Wang et al. (2018b); Idlahcen et al. (2020); Lu et al. (2021c); Gupta et al. (2021); Lu et al. (2021d); Feng et al. (2020); Farahmand et al. (2022); Ciga et al. (2022); Bussoala et al. (2021); Yamashita et al. (2021); Alharbi et al. (2021); Cheng et al. (2022); Teh and Taylor (2022); Su et al. (2022); Yang et al. (2022a). Interestingly, the weights of a neural network trained on natural images are extremely useful for achieving high performance in CoPath. There are two major reasons that make transfer learning a suitable method for CoPath: (1) determining and training neural networks from scratch can produce inferior results compared to fine-tuning an established and performant pre-trained model and (2) transfer learning from a domain with much labeled data to a limited labeled data domain, which is often the case in CoPath, can yield significant performance improvements Tan et al. (2018). Within the subset of CNN architectures, the ResNet architecture is the most commonly used model, unsurprising due to its ability to learn complex features without requiring a significant amount of data Liu et al. (2018a).

In most cases, CNNs are sufficient to complete the task as images possess a well-defined matrix data structure with fixed dimensions, and the convolution operation is precisely suited for this task. However, in some cases, data structures cannot be represented as Euclidean data, i.e. it has a form of a graph. In this case, the convolution operation becomes ill-defined and one may instead use a Graph Convolutional Neural Networks (GCN) Kipf and Welling (2017); Guan et al. (2022), with the convolutional operation being applied directly onto the graphs. One such recent work in the field of CoPath embeds a WSI into a graph-based structure in Euclidean space where the nodes represent patches and edges represent the connections among patches; this work obtained remarkable results on cancer prognosis task outperforming the state of the art in four out of five cancer types Chen et al. (2021c). Similarly, Vision Transformers (ViT) Dosovitskiy et al., only recently introduced, are a direct application of Transformer models Bug et al. (2017) to the image domain. In ViT, images are sub-patched and flattened into a 1D embedding along with a positional encoding which are fed into a Transformer encoding block with an MLP head attached as a classifier. In Gao et al. (2021), ViT models are extended by leveraging pretrained CNN models for nuclei segmentation and classification to extract relevant regions. The relevant regions are fed into a tiny CNN model to produce 1D embeddings that ViT takes in to classify histological subtypes of renal cell carcinoma. When compared to CNN-based models for the same task, this ViT and CNN combination significantly outperformed the competition. Given their impressive performance, it is quite likely that ViTs will be further applied in classification tasks in the near future.

General classification architectures are also commonly used as a baseline for novel architectural design. This design may involve applying changes directly to the architecture or applying the architecture in unique ways. For example, in Wang et al. (2018b); Sali et al. (2020), the VGG architecture was modified to improve performance. A VGG architecture with a global average pooling branch was implemented to be used for disease diagnosis on the BACH dataset Wang et al. (2018b). The global average pooling branch serves to consider “global information” about an image. There are also some interesting technical feats with the ResNet architecture. For example, conditional random fields were introduced Li and Ping (2018) and proved to maintain the same level of computational complexity, while increasing performance. A ResNet architecture was used for the purpose of generating “tissue fingerprints”, vectors that encode important information about an area of tissue, using a technique similar to contrastive learning, wherein a neural network classifies tissues based on the generated fingerprint Rawat et al. (2020). Alternatively, the InceptionV3 architecture was deftly modified wherein the fully convolutional architecture was used to classify patches within the WSI, followed by a k-nearest-neighbour classifier to classify WSIs according to the Gleason Grade Nagpal et al. (2019). A small Squeeze-and-Excitation (SE) ResNet block was introduced Jiang et al. (2019) to reduce the number of parameters while still maintaining a high level of accuracy. Another example of using SE modules can be seen in a DenseNet-focused paper where they used a combination of the DenseNet architecture with SE modules leading to a high performance with fewer parameters compared to ResNet-50 & VGG-16 Li et al. (2020b). Another DenseNet-focused paper systematically compared multiple weakly supervised deep learning approaches for prostate cancer diagnosis, however, they conclude with sub-optimal performance for weakly supervised models Otálora et al. (2020). Lastly, AlexNet was introduced in developing a pipeline that uses both patch sampling and pooling in order to make a deep learning model that operates at the WSI level for disease diagnosis and segmentation Xu et al. (2017a).

In order to achieve superior performance, many researchers often rely on ensembling or multi-stage techniques which combine the predictive power or feature extraction abilities of multiple models to form a final output. These approaches have shown performance improvements compared to traditional single model classifiers Pimkin et al. (2018); Kassani et al. (2019b); Lu et al. (2020b); Lin et al. (2021); Senousy et al. (2021). However, this often comes at the expense of higher computational requirements. One example is a paper that details a model that is built upon simple ensembles called “Deep Hipo” Kosaraju et al. (2020). This network has two branches, each of which takes an image patch at a different resolution and then concatenates the two inputs before the last hidden layer in order to compute a probability. One notable advantage to this approach is the consideration of multiple magnifications in its pipeline.

5.2. Segmentation Architectures

Segmentation is a widely used technique in histopathology image processing, as shown in Figure 5. Architectures per-

forming segmentation require the ability to localize the object of interest, because the desired output has class labels at the pixel-level Ronneberger et al. (2015). Over time, semantic segmentation tasks and architectures have become more common in CoPath, but it remains a very challenging task due to the difficulty of obtaining and predicting pixel-wise annotations.

U-Net is a segmentation architecture which was initially developed for the segmentation of neuronal structures in electron microscopy image stacks Ronneberger et al. (2015), but has become one of the most common architectures for segmentation in CoPath Hou et al. (2019a); Shin et al. (2016); Vu et al. (2019); Chen et al. (2019); Hou et al. (2020a); Bai et al. (2020); Xie et al. (2020); Takahama et al. (2019); Pimkin et al. (2018); Lahiani et al. (2018); Jiménez and Racoceanu (2019); Kausar et al. (2020); Ho et al. (2020); Wetstein et al. (2020); HermSEN et al. (2019); Miao et al. (2021); Qureshi et al. (2008); Geread et al. (2021); Schuchmacher et al. (2021); Feng et al. (2020); Gallego et al. (2021); Wu et al. (2021); Chen et al. (2021a); Nour et al. (2021); Bayat et al. (2021); Guerrero and Oliveira (2021); Khened et al. (2021); Vahadane et al. (2021). U-Net has an encoder-decoder structure: the encoder to contract features spatially and the decoder to expand them again to capture semantically related context and generate pixel-level predictions. With proper data augmentation, the model can be trained end-to-end without requiring a large volume of annotated images Ronneberger et al. (2015). The U-Net model was used to automatically segment nuclei for the purpose of creating a novel dataset with unsupervised learning Hou et al. (2020a), but it should be noted that this process also relies on the Mask R-CNN framework and pathologists for quality checking purposes. In a recent work Wu et al. (2022b), cross-patch dense contrastive learning has been used for semi-supervised nuclei segmentation.

Another common approach for segmentation is to use fully convolutional networks (FCNs) Naylor et al. (2017); Kumar et al. (2017); Sahasrabudhe et al. (2020); Nadeem et al. (2020); Chen et al. (2016a); Dong et al. (2018); Bándi et al. (2019); Phillips et al. (2018); Marsh et al. (2018); van Eekelen et al. (2020); Xing et al. (2021); Khened et al. (2021) or customized architectures constructed by combining multiple components of various architectures or introducing new components to pre-existing architectures Hou et al. (2019b); Khoshdeli et al. (2018); Koohbanani et al. (2020); Abdel-Nasser et al. (2020); Chen et al. (2020c); Graham et al. (2019a); Agarwalla et al. (2017); Li et al. (2019c); Pati et al. (2018); Qaiser et al. (2019); Saltz et al. (2018); Das et al. (2018); Chan et al. (2019); Marsh et al. (2018); Shephard et al. (2021); Wang et al. (2021a); Jahanifar et al. (2021); Schuchmacher et al. (2021); Kim et al. (2021); Gallego et al. (2021); Li et al. (2021c); Koziarski et al. (2021); Dogar et al. (2021); Cheng et al. (2022). For example, two custom CNNs were built known as Object-Net and Separator-Net to perform segmentation Marsh et al. (2018). The former network was used to predict whether a particular pixel is benign or malignant Marsh et al. (2018). The latter network was used to predict structures within the image and refine the prediction of Object-Net through probability fusion Marsh et al. (2018).

5.3. Object Detection Architectures

In this section, we specifically focus on architectures that are used for ROI detection. An example use case is detecting the number of mitosis instances within an input image. This is different from detection using general classification architectures because rather than being interested in a simple binary classification output at the image level, predicting for each ROI in an image is what matters. We note that there is a significant overlap between this task and segmentation depending on the method applied. Segmentation will often output a mask to precisely show where the feature of interest is located at the pixel-level, while object detection will often output points, bounding boxes, or the number of instances for the feature of interest. Object detection has been widely applied to tasks such as mitosis Lafarge et al. (2019); Tellez et al. (2019a); Wahab et al. (2017); Tellez et al. (2018); Wang et al. (2014); Jiménez and Racoceanu (2019); Li et al. (2018a); Otálora et al. (2019); Li et al. (2019a); Sebai et al. (2020); Akram et al. (2018); Lafarge et al. (2021); Alom et al. (2020); Li et al. (2020a); Schuchmacher et al. (2021); Pati et al. (2021a), nuclei Brieu et al. (2019); Fuchs et al. (2008); Sirinukunwattana et al. (2016); Li et al. (2018b); Kashif et al. (2016); Jaume et al. (2021a); Javed et al. (2021), colorectal gland Chen et al. (2016a); Wang et al. (2019a); Qureshi et al. (2008) and glomeruli detection Wu et al. (2019); Yang et al. (2020); Bueno et al. (2020a); however, it can also be applied to the detection of a variety of histopathological objects including tumor-infiltrating lymphocytes Lu et al. (2020c) or keratin pearls Das et al. (2018).

The majority of object detection architectures are custom CNNs or modifications of existing state-of-the-art networks, as shown in Figure 11. A model called CircleNet, which uses a deep layer aggregation network as a backbone, was proposed to detect round objects Yang et al. (2020). Their approach involves using an anchor-free “center point localization” framework in order to output a heatmap with center points followed by a conversion into a bounding circle for the detection of kidney glomeruli. The generation of bounding circles is done using three network heads: a heat map head, local offset head, and circle radius head. A multi-stage deep learning detection model containing two unique stages of progression was proposed Li et al. (2018a). Prior to network training, an FCN based on VGG-16 is used to create bounding box annotations for a centroid labelled mitosis datasets. In the first stage, a modified Fast R-CNN is used to generate region proposals for subsequent classification. In second stage, they used a ResNet-50 based model to eliminate any false positives from the first stage. A Feature Pyramid Network was proposed to detect mitosis in sparsely annotated images using a ResNet backbone Li et al. (2020a). This paper adjusted the object detection loss by introducing a novel factor coined Boxes Density Energy. This proposed factor allowed the network to not penalize the assignment of bounding boxes for non-annotated positive samples, which is a common occurrence in sparsely annotated images.

5.4. Multi-Task Learning

We define multi-task networks as individual models predicting for multiple tasks at once, as defined in Section 2. For exam-

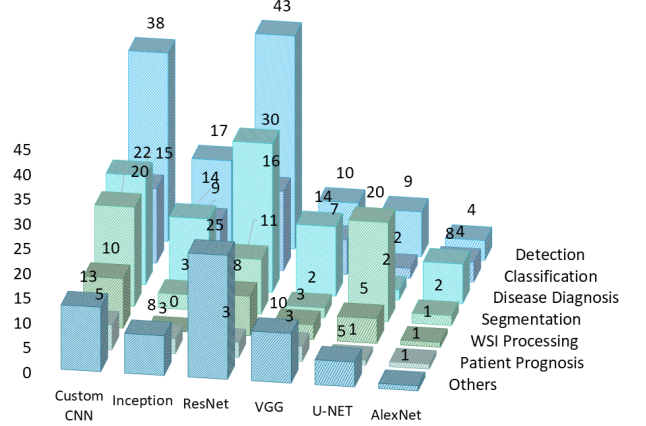


Fig. 11: Distribution of the most common Neural Network architectures used in the surveyed literature, based on the CoPath task. The x-axis displays the Neural Network architectures used in the papers (from left to right): Custom CNN, Inception, ResNet, VGG, U-Net, and AlexNet. The y-axis shows the different tasks (top to bottom): Detection, Classification, Disease Diagnosis, Segmentation, WSI Processing, Patient Prognosis, and Others. For more details, please refer to Table 8.3 in the supplementary section.

ple, this could be a single model that is trained to perform classification and segmentation simultaneously. Multi-task representation learning can be beneficial over independent task learning because sharing representations between related tasks can create more generalizable representations and encourage the task heads to make logically consistent predictions. This type of model, however, is uncommon in CoPath, as it requires annotating multiple tasks for each image—only a few works use multi-task based networks Gamper et al. (2020b); Tellez et al. (2020); Yan et al. (2020b); Alom et al. (2020); Alawad et al. (2020); Koohbanani et al. (2021); Feng et al. (2021b). We discuss a few of these papers in further detail below.

A ResNet-50 acted as a feature extractor and was then passed to a decoder for different tasks Gamper et al. (2020b). For segmentation, a “pyramid scene parsing network” was used and for classification a “single fully connected layer” was used. Notably, their approach relies on multi-task learning by simultaneously training the ResNet model on 11 different tasks (4 segmentation based and 7 classification based). They achieved comparable or better results to single task learning in classification, but comparatively worse results in segmentation. Similarly, a ResNet-50 with two parallel branches to perform segmentation and classification simultaneously, was able to achieve comparable results on both tasks through a multi-task learning approach in Yan et al. (2020b). In this approach, the segmentation branch produces a probability map that is used as the prior for the classification branch; the classification network is a simple 3-layer convolutional architecture. Another work used a single encoder that was shared for four tasks and subsequently an individual MLP for each task Tellez et al. (2020, 2019b). They found that this encoder-based approach led to good results, and was more robust (e.g. transferable to different tasks).

Multi-task networks represent an interesting field of explo-

ration. We believe this is an exciting area because it may reduce the necessity to train multiple deep neural networks to perform different tasks. While the results from the previous works are impressive, there is still work to be done in this field. In Tellez et al. (2020) it was found that model performance may be sensitive to the number and type of tasks used during training. Specifically, combining certain (unrelated) tasks could lead to adverse interference of the features and deteriorate the performance compared to a single-task setting. How to weigh different task objectives during training and select optimal tasks to be trained together is yet to be decided and requires further exploration.

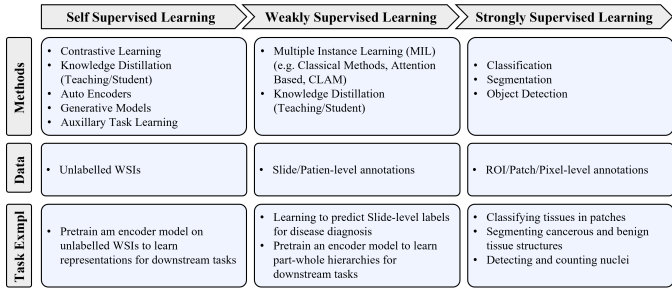


Fig. 12: Details of types of learning using varying levels of supervision. Note that the types of tasks each type of learning can address vary based on the data that is available, as noted in the *Example Task* portion of the figure. However, from left to right, models trained with less supervision can still learn salient representations of the data that can be used to fine-tune models for tasks requiring more supervision. In that sense, for CoPath there is a *spectrum* of supervision from self to strongly supervised learning that aligns well with the annotation levels shown in Figure 8.

5.5. Multi-Modal Learning

As opposed to multi-task networks where multiple tasks are learned simultaneously, the multi-modal approach involves using network input features from multiple domains/modalities at once Ngiam et al. (2011). In the case of CoPath, modalities can be represented as pathologists’ reports, gene expression data, or even WSI images. They are used to learn better unified/shared latent representations which capture correlations not only from a single domain but rather from a set of them, as some information may not be captured in a given domain Li et al. (2022). Originally, the idea of deep learning implied minimal use of hand-crafted feature engineering, instead focusing on features learnt from latent representations. However in practice, one usually obtains best results by combining multiple approaches such as ensemble learning or hand-crafted features and a variety of classifiers. The latter was demonstrated in the case of mitotic cell classification when a new record was set for weakly-annotated MITOS-ATYPIA 2014 dataset with F-score of 86% in Rehman et al. (2022). Another work, which appeared around the same time, showing that CNNs alone can outperform all other hand-crafted feature vectors, namely in the case of MITOS-ATYPIA 2014 dataset where a new F-score of 96% was achieved Sigirci et al. (2021). It is worth noting that one cannot compare these two works directly as they use different classifier heads along with dataset balancing methods; however, one can argue that there is a potential benefit for approaches

emerging from a combination of deep learning, classical ML, and ensemble methods along with multiple modalities. In this regard, each member of a feature vector set can be positioned as a separate modality; in this sense, it is derived from different underlying assumptions. In the case of CoPath multi-modal approaches are slowly gaining traction Weng et al. (2019); Boehm et al. (2021). For example, there are publications that combine gene expression data and WSI images to make better cancer prognosis prediction Shao et al. (2020); Wang et al. (2021b).

5.6. Sequential Models

Recurrent Neural Networks (RNNs) are typically used in tasks with temporally-correlated sequential data, such as speech or time series LeCun et al. (2015b). Since RNNs consider the past through the hidden state, they are suited for handling contextual information. However, RNNs are not very well suited to handle images, which is the default input data in CoPath. Nonetheless, in CoPath, some papers opt to use RNNs, often combined with CNNs as a feature extractor Campanella et al. (2019b); Bychkov et al. (2018); Nahid et al. (2018); Iizuka et al. (2020); Zhang et al. (2019); Saltz et al. (2018); Yao et al. (2019); Yan et al. (2018); Xu et al. (2019b); Raciti et al. (2020); Yan et al. (2020c); BenTaieb and Hamarneh (2018); Zheng et al. (2020). Most commonly, RNNs are applied to aggregate patches or process sequences of features Campanella et al. (2019b); Iizuka et al. (2020); Saltz et al. (2018); Raciti et al. (2020); Qi et al.. Another application of RNNs is to consider spatial relations, as these can be lost during patching Yan et al. (2018, 2020c).

A particularly exciting use of RNNs is in deciding which region within an image should be examined next Xu et al. (2019b,a). A 3-stage model: Look, Investigate, and Classify was built Xu et al. (2019b). In the look stage, a hard attention sensor crops a region from a large patch. The investigative stage consists of a soft attention network that acts as a feature extractor on the cropped region. Afterwards, in the classification stage, an LSTM network is used to classify the cropped region and predict which region should be looked at next. This framework is novel and achieved high performance while only using 15% of pixels from the original image. Similarly, an LSTM network was used to better predict ROIs by treating state features similar to time-series data Xu et al. (2019a). It is used to (1) iteratively crop patches, (2) select which features from a patch will be useful for classification, and (3) predict the next region to look at. Afterwards, these patches are passed into another network for training. Similar sources also found that this approach reduced training time since they only used examples that were valuable for training.

A VGG-19 network was used in parallel to a transformer network that features novel LSTM-based “Feature Aware Normalization” (FAN) units for stain normalization in Bug et al. (2017). The transformer network on the main path outputs feature maps that are then input to the FAN units. These units, along with the VGG network form this paper’s proposed FAN network, which also makes use of the gating units in LSTM. One advantage of this model design is that having the VGG network in a separate path allows it to be replaced by any other

feature extractor. Additionally, simply using larger filter sizes in the transformer network portion gives this model the potential to be used for other style transfers not necessarily related to CoPath.

5.7. Generative Models

Generative models refer to architectures that learn how to create novel instances of samples from a given data distribution. In some research areas including patch synthesis Hou et al. (2019a); Mahmood et al. (2019); Claudio Quiros et al. (2021); Deshpande et al. (2022), stain normalization Cho et al. (2017); Arvidsson et al. (2019); Shaban et al. (2019b); Mahapatra et al. (2020); Schrammen et al. (2022); Yamashita et al. (2021) and style transfer Rawat et al. (2020); Lahiani et al. (2019a,b); Yamashita et al. (2021), and various other tasks Tellez et al. (2019b), Generative Adversarial Networks (GANs) are the dominant models used. Due to the lack of data availability in CoPath, especially with granular labels, having a direct impact on model generalizability, the ability to generate *synthetic* data to further train models is very promising.

Many of the works featuring GANs have produced interesting results. An unsupervised pipeline that is capable of synthesizing annotated data at a very high scale was introduced Hou et al. (2019a). This method relies on a non-GAN based model to create the initial patch, followed by a GAN to refine it. Even pathologists had difficulty distinguishing between real patches and patches generated by this work. In another work, detection was achieved by using two CycleGANs Tavolara et al. (2019), one CycleGAN for tumor regions and the other for non-tumor regions, and the images generated by both were compared to test whether the image was tumor or non-tumor. Another work tested multiple ways to compress gigapixel sized images (i.e. WSIs) using a novel technique called neural image compression using an encoder to map each patch of an image to a spatially consistent feature vector in order to compress the image and finding a BiGAN encoder to perform best Tellez et al. (2019b). In another work, an unsupervised GAN based pipeline is used for bone marrow component classification Hu et al. (2018). This involves the use of classification to cluster cells together, followed by a GAN to generate cell representations for each cluster. Following this, an SVM is applied to perform image-level classification. Further, a study used a self-supervised CycleGAN pipeline to perform stain normalization Mahapatra et al. (2020). It was found that models trained on the normalized images achieved high performance in subsequent detection and segmentation tasks. Similarly, a CycleGAN pipeline was applied to perform artificial immunohistochemistry re-staining Xu et al. (2019c).

There exist numerous opportunities to use generative models in many different ways; but fundamentally they are useful in dataset augmentation tasks, as seen by their application in patch synthesis, stain normalization and style transfer. This can be particularly useful in CoPath due to the challenges around data availability, as discussed in Section 3.3.

5.8. Multi-Instance Learning Models

Multi-instance learning (MIL) involves training on data that comes in labelled sets of bags, each containing unlabelled in-

stances. In the context of CoPath, these labelled bags represent slides and the instances are patches Patil et al. (2019). This approach is especially interesting in CoPath where labels at the WSI level are much more prevalent than patch-level annotations, thus despite being fairly recent, MIL has been applied in CoPath by a significant number of papers Campanella et al. (2019b); Raciti et al. (2020); Mercan et al. (2017); Wang et al. (2019d); Lu et al. (2020a); Xu et al. (2014, 2017b); Li et al. (2019b); Patil et al. (2019); Pinckaers et al. (2021); Yaar et al.; Lerousseau et al. (2020); Chikontwe et al. (2020); Yao et al. (2020); Lu et al. (2022, 2021b); Jewsbury et al. (2021); Alharbi et al. (2021); Li et al. (2021a); Chen et al. (2021c); Riasatian et al. (2021); Lu et al. (2021d); Jewsbury et al. (2021); Pal et al. (2021); Freyre et al. (2021); Marini et al. (2021); Höhne et al. (2021); Anand et al. (2021); Shao et al. (2021).

Most notable work is from Campanella et al. Campanella et al. (2019b) where a novel two stage MIL-based pipeline was introduced to first embed high dimensionality feature vectors using a ResNet MIL-trained model for patch-level encoding and then followed by passing the most “suspicious” (e.g. most likely to be cancerous) patches per slide to an RNN that aggregates those patches to produce a slide level classification. Similarly, a novel multi-stage pipeline called “Recalibrated Multi-instance Deep Learning” (RMDL) was built to output image-level predictions Wang et al. (2019d). This network consists of two stages: The first stage has a network called “localization net” that detects any abnormal regions in the WSI, and outputs a probability map of the WSI. The second stage consists of a novel RMDL network containing three modules: a local-global feature fusion, recalibration module and multi-instance pooling. The recalibration and local-global feature fusion notably contributed to a 7% performance improvement. Further, an attention-MIL model was developed to frame a tumor classification problem as a weakly-supervised MIL problem in Patil et al. (2019). They found that their attention mechanism highlights regions of interest, and gave improved localization relative to other state-of-the-art CNNs. Interestingly enough, MIL models perform better when they utilize representation learning as shown in one work which proposed Dual-stream Multiple Instance Learning Network (DSMIL) by fusing multiple methodologies at once Li et al. (2021a). These included: locally-constrained multiscale attention, multiscale embedding, i.e. patches at 5 \times , 20 \times , 40 \times magnification levels, instance, and bag classifiers along with instance and bag embeddings and self-supervised contrastive learning to learn WSI classifiers. Their approach outperformed previous MIL approaches on CAMELYON16 and TCGA datasets. The result was a 16% increase in classification accuracy in the case of unbalanced bags by using self-supervised contrastive learning alone. Similar to DSMIL a recent study has developed a model dubbed DTFD-MIL Zhang et al. (2022), which brings the concept of pseudo-bags to counter the issues of small cohorts. This method was able to outperform state-of-the-art AUC metrics by 4% on the CAMELYON-16 and TCGA lung cancer datasets.

Another work integrated additional patch features into ML models, such as nuclei grading, learnt from other methods/models, and cumulatively showed that these additional

patch attributes helped in increasing the overall classification accuracy Gao et al. (2021). Surprisingly, grades assigned by segmentation and classification model, outperform hand-crafted features alone. Thus, they show that additional, instance-specific, features could potentially boost accuracy in the MIL regime. A novel framework, called correlated MIL, is proposed by considering the correlation between different instances Shao et al. (2021). Then, a Transformer based MIL (TransMIL) is devised to explore morphological and spatial information among instances. The introduced method conforms with pathologists' actions as they do not neglect the correlation between different areas while making a diagnostic decision. Experiments are performed over three publicly available datasets, which shows the proposed method leads to improved performance and faster convergence compared to the state-of-the-art MIL models.

MIL models show a lot of promise as a research direction for CoPath as they are a weakly supervised approach and predict detailed labels while training on coarser annotations. The research done in this area has the potential to reduce the time associated with labelling since pathologists only need to label at the slide level. While this solves some of the existing challenges with data availability, applications of MIL in CoPath are much less common compared to natural image computer vision because there are few large scale WSI datasets available Campanella et al. (2018b). To conclude, MIL and weakly supervised learning methodologies are currently among the most active research fields in CoPath due to the lack of annotated data.

5.9. Contrastive Learning

The idea of contrastive learning dates back as early as 2005, yet only recently gained momentum in CoPath Hadsell et al. (2006); Schroff et al. (2015); Li et al. (2021a); Tran et al. (2021); Carse et al. (2021); Dawood et al. (2021); Ciga et al. (2022); Feng et al. (2021a). The original idea was to introduce a contrastive loss where hidden representations are learned by attracting similar (positive) examples and repelling distinct (negative) examples Hadsell et al. (2006); Schroff et al. (2015). For example, in the field of CoPath this can be thought of as attracting samples from similar organs or tissue structures and repelling samples from dissimilar organs or tissues. Generally, contrastive learning does not require strongly supervised labels and can learn representations to downstream tasks by fine-tuning on stronger labels with less data. A recently proposed extension to contrastive learning, namely SimCLR Chen et al. (2020d), introduced a set of augmentations that made representation learning harder, but the quality of learned representation became drastically better. The contrastive learning approach is commonly used in self-supervised representation learning Li et al. (2021a); Tran et al. (2021); Ciga et al. (2022) and has recently shown state-of-the-art model performance in a wide array of tasks Ciga et al. (2022). The SimCLR method was applied to digital histopathology Ciga et al. (2022), using 60 varying datasets, and found that self-supervision consistently matches or outperforms state-of-the-art supervised techniques on most histopathology datasets. The performance gap between regression and segmentation tasks, however, is much

smaller, with some models performing better when using supervised pertaining Yang et al. (2022b), and others performing better with self-supervised pretraining. These authors concluded that contrastive pretraining on a dataset with significant visual diversity between images outperforms training on a homogeneous but possibly larger dataset Ciga et al. (2022).

5.10. Novel CoPath Architecture

In this section, we discuss papers that made significant changes to the model design or completely designed an architecture from scratch Graham et al. (2019b); Eminaga et al. (2019); Li et al. (2018b); Hao et al. (2019); Lu et al. (2021d); Abdel-Nasser et al. (2020); Yen et al. (2020); Li et al. (2019c); Tang et al. (2021). In CoPath, many architectures models are adopted from computer vision domain where typically they are developed for the purpose of representing natural images. When adopted, minor changes are applied on the architecture to fit the purpose of CoPath tasks, rather than being designed from scratch for CoPath directly. Unfortunately, general computer vision architectures typically require millions of parameters with large datasets to train successfully Eminaga et al. (2019). In CoPath this is problematic for two reasons: (1) large models can overfit on a smaller CoPath training set and (2) large models require powerful computational resources which may not necessarily be available in clinical settings Eminaga et al. (2019).

To combat this problem, there have been few studies that introduce CoPath-specific architectures. “PlexusNet” was an architecture designed to achieve state-of-the-art performance, while containing significantly less parameters Eminaga et al. (2019). It contains an optional normalization section, a feature extraction section, and a classification section. In order to optimize the network, different model hyperparameters were tested based on the nature of the data given. Another example can be seen where a modified ResNet-50 is first used to downsample an image, and then output it to three distinct, but architecturally identical, branches Graham et al. (2019b). Two of these branches were used for segmentation, while the last branch was for classification. This architecture is called “Hover-Net”. Another work introduced a novel CNN called Path R-CNN which is designed specifically for CoPath applications Li et al. (2018b). In this CNN, a ResNet model is used for generating feature maps. Then, these feature maps are passed into two branches: a Grading Network Head (GNH) and an Epithelial Network Head (ENH). The final prediction depends on the output of these two branches.

To automate the design of novel architectures, one promising field is the neural architecture search (NAS) technique, which is an umbrella term covering evolutionary algorithms (EA), deep learning (specifically Reinforcement Learning), and gradient-based NAS searches. Interestingly enough, EA is a broad term too, covering many optimization algorithms. More specifically, EA encompasses two subfields of neural net searches called Neuroevolution and evolutionary-algorithms based NAS (EANAS) Galván and Mooney (2021); Liu et al. (2021). EANAS adapts well-known neural net building blocks, connections, and activation functions with search imposed only on

mid-sized architectural elements and with training performed after architectural search. In Neuroevolution, the algorithm not only looks for an optimized architecture but also searches optimal weights minimizing the objective and it is more general in applying evolutionary strategies starting from single neuron and single connection Galván and Mooney (2021).

Reinforcement learning is used to conduct NAS to automate model development for cancer prediction Balaprakash et al. (2019). It was found that the discovered models trained faster, had fewer parameters, and had comparable accuracy to manually designed models. As a direct extension of original work on differentiable architecture search (DARTS) Liu et al. (2018b), it is also demonstrated that a model with significantly fewer trainable parameters, can outperform existing SOTA models on a variety of classification tasks with various datasets Tang et al. (2021).

We hypothesize that the field of NAS has yet to be explored significantly due to challenges such as the lack of available annotated data mentioned in Section 3.3, along with its relative novelty as a research area in its own right. We speculate that applications of NAS will provide great improvements in both diagnostic accuracy and speed. Heuristically considering various “no free lunch theorems” Wolpert and Macready (1997); Adam et al. (2019), no single algorithm or architecture can perform best on all machine learning or computer vision tasks. Following from there, it is likely that highly efficient and highly optimized neural network architectures exist that are tailored for CoPath tasks and finding these architectures is best achieved by computational means such as NAS.

5.11. Model Comparison

The various model architectures and types discussed above can and should be compared in terms of performance on the same tasks and datasets, as a fair benchmark is required to determine which models are truly the best for a given task Laleh et al. (2022). There are a number of papers that explicitly tested different CNN models on a specific task to determine which one performs best. In Tellez et al. (2019a), GoogLeNet, AlexNet, VGG16, and FaceNet were all trained for patch-based classification for detection of breast cancer metastases and it was found that deeper networks performed better as expected, with GoogLeNet performing the best. In Wu et al. (2019), the custom P3SGD algorithm worked best with ResNet-34, achieving the highest testing accuracy compared to other traditional and modern architectures such as VGG16, AlexNet, ResNet-18, and MobileNet. Alternatively, five different ImageNet pretrained CNNs of varying model complexities were used for colorectal tissue subtype classification in Kather et al. (2019a). While some of the aforementioned best-performing networks such as GoogLeNet and ResNet were among those tested, it was found that VGG-19 achieved the highest accuracy. This could indicate that while deeper networks often achieve better results, in practice there is not necessarily one state-of-the-art CNN that performs universally better. Which CNN performs best depends on the task, the nature of the data, the metrics used, training time, hyperparameters, and/or hardware constraints.

While existing state-of-the-art CNNs are often sufficient for some tasks, the need for higher accuracy persists, especially as

the field of CoPath advances. Many papers have developed custom CNNs aiming for better performance with respect to certain metrics Zadeh Shirazi et al. (2020); Bidart and Wong (2019); Alom et al. (2020); Yang et al. (2020); Kausar et al. (2020). Existing CNN architectures are often used as baseline models to assess the performance of novel custom CNNs. While these comparisons are with respect to accuracy or AUC, in some other cases, the custom framework could focus on improving computational efficiency and speed Wang et al. (2020c). This is of paramount importance in giga-pixel image processing where hundreds to thousands of image patches could be extracted from WSI (depending on the tissue size and pixel resolution) where the inference speed (number of patches/sec processing) of the deployed architecture becomes the main bottleneck for WSI processing. Performance comparisons can also be drawn between models adopted by different design techniques trained for the same task and on the same dataset in four common task categories—detection, tissue subtype classification, disease diagnosis, and segmentation.

In general, CoPath “grand-challenges” have vastly facilitated comparison between different techniques on a common task and dataset as researchers can develop their own specific techniques and apply it to the same test set provided by the organizers which enables a fair comparison. Among papers that perform breast cancer detection using the CAMELYON16 challenge dataset, the highest AUC was cited in Bejnordi et al. (2017a), while the highest patch-based accuracy was reported in Chen et al. (2016b). Both results were achieved using existing CNNs, namely GoogLeNet and AlexNet. On the contrary, the best performing models for mitosis detection on TUPAC16 Tellez et al. (2019a) and MITOS12 Kausar et al. (2020) both relied on novel CNN architectures designed specifically for the task. The model achieving the highest accuracy for colorectal tissue subtype classification is SqueezeNet, an existing state-of-the-art network. For breast cancer disease diagnosis on the BACH18 (ICIR18) dataset, a test accuracy of 96.1% on ROIs was achieved in the past year with a novel Hybrid CNN architecture pretrained on the same domain Alzubaidi et al. (2020). Also for breast cancer diagnosis, two teams both achieved the highest binary classification accuracy on the BreakHis dataset Celik et al. (2020); Thuy and Hoang (2019). The former paper directly uses a ResNet-50 while the latter uses ensembling of VGG networks. For nuclei segmentation on the Kumar-TCGA dataset, results achieved from Abdel-Nasser et al. (2020) had the highest F1-score out of the paper surveyed using a novel framework developed using ResNet and another existing model. Lastly, results from Koohbanani et al. (2020) scored the best in terms of three metrics for gland segmentation on the GLaS dataset using a custom CNN.

In general, we find that there still exists a lack of common and standardized benchmark datasets in CoPath that can enable more model comparison studies to be performed. As mentioned in Section 3.3 *Dataset Availability*, many works use private datasets and even some public datasets extract from larger repositories without referencing the original WSIs IDs used. As mentioned in the previous section, the development of novel architectures has great potential in finding an optimized model

for CoPath tasks, however, this lack of transparency and standardized benchmark datasets makes it increasingly difficult for new model architectures to be easily compared against existing ones in a systematic way. As models that are hyper-optimized to work on very curated or specific sets of data are unlikely to be robust or generalize well in clinical settings, the lack of more benchmark datasets and model comparison studies is an impediment to progress in the CoPath field.

6. Evaluation and Regulations

6.1. Clinical Validation

Within the domain of CoPath, clinical validation is an essential process for substantiating the decisions produced by deep learning models so that they are more readily accepted by the medical community. Generally, acceptable clinical criteria are determined by authoritative professional guidelines, consensus, or evidence-based sources. However, in CoPath, performance results are generated by the computer scientists and engineers who build the model, who may not be focused on where their model or tool fits into the clinical pathology workflow and their performance implications in clinical settings is often unknown Awan et al. (2017). The process of clinical validation is thus necessary for incorporating the expertise of pathologists to better align the model with clinical objectives.

Despite the importance of this step for real-world deployment, very few works have performed clinical validation with expert pathologists. We identify three prominent types of clinical validation in the CoPath literature: (1) direct performance comparison of CAD tools with pathologists on a similar task, (2) impact of CAD tool assistance on pathologist performance, and (3) pathologist validation of CAD tool outputs. Each topic is further discussed in the sections alongside notable results from various studies.

Direct Performance Comparison with Pathologists It is important to validate the benefits deep learning methods bring in the various tasks performed by pathologists. It is particularly desirable that these methods can achieve near-human performance or even exceed it to increase pathologists' trust in the results from these models, or their willingness to use them as a second opinion. The performance of tools can impact the performance of pathologists when used as a second opinion Kiani et al. (2020). With this in mind, many papers have performed direct comparisons of their models with pathologists in tasks such as prognosis and disease diagnosis.

Disease detection is a particularly time-consuming task. In one study, 11 pathologists with a time constraint of roughly two hours and one expert pathologist without a time constraint were compared to competitors of the CAMELYON16 challenge Bejnordi et al. (2017a). Interestingly, the top teams performed better than the 11 pathologists with a time constraint and similar to the expert pathologist without time constraint. This suggests that deep learning models could be used in clinical scenarios where there are load cases of specific organ/disease for diagnosis and time is critical.

Some papers have also compared tissue subtype classification between pathologists and CoPath ML models. In one paper, the proposed model agreed with all pathologists 66.6% of

the time and had a robust agreement 76.7% of the time, which the paper defines as 2/3 of the pathologists agreeing with the model Wei et al. (2019a). They found that their model performed similarly to, or slightly better than individual pathologists. Additionally, Wang et al. (2020b) cited that their deep learning model outperformed pathologists. This pushes the idea that CAD tools can be used as a second opinion due to the potential of misclassification by a single pathologist.

On disease diagnosis, deep learning models have proven to correctly classify images that even individual pathologists failed to correctly identify Coudray et al. (2018). However, the model generally misclassified examples that pathologists found challenging with 50% of the falsely identified examples also being misclassified by at least one pathologist Coudray et al. (2018). This suggests that deep learning models can serve as a second opinion in order to aid pathologists in their decision-making, but as their model achieved a specificity and sensitivity similar to that of pathologists, there needs to be some caution to not reinforce biases or errors of individual pathologists.

Patient prognosis is a challenging but useful task for deep learning models. Prognosis helps in clinical decision-making, particularly by aiding in decisions regarding treatment. Models have been shown to achieve performance similar to or better than experts Mobadersany et al. (2018); Fuchs et al. (2008); Bauer et al. (2016). For example, results cited in Bauer et al. (2016) indicated an accuracy of 83% and 90% on the two datasets they used, whereas pathologists obtained an accuracy of 80%. This shows that deep learning models and pathologists may perform similarly on patient prognosis.

Overall, AI approaches are not perfect but have approached expert-level ability in performing a variety of tasks. This suggests deep learning could play an important role as a second opinion and in democratizing the knowledge distilled from many pathologists to all pathology centres. Specifically, deep learning models appear to be best used as a tool to enhance the pathologist workflow, and could provide aid in making quick decisions with high accuracy Echle et al. (2021).

Impact of CAD Tool Assistance Much of CoPath research is conducted under the assumption that the resulting AI tools will be intuitive, usable, and beneficial to pathologists and patients. However, CAD tools that are developed without council with pathologists could potentially fail to integrate into a realistic pathologist workflow or fail to make an impact on the most significant diagnostic tasks. Thus, a valuable validation experiment is to compare and comprehend the performance of expert pathologists in clinical tasks before and after a given CAD tool is introduced. Currently, only two types of assistant tools have been validated.

The first approach involves patch triaging, which is used to filter WSIs and display the most diagnostically relevant regions to the pathologist exemplified through some works Raciti et al. (2020). The CAD system, named Paige Prostate Alpha, leverages a weakly-supervised algorithm to recommend patches with the highest probability of cancer Campanella et al. (2019b). When used by pathologists, the proposed CAD system results in significant improvements to sensitivity, average review time, and accuracy.

The second approach involves highlighting important regions of interest to direct pathologist attention. One team uses the LYNA algorithm Liu et al. (2019), to highlight tumor regions in breast cancer WSIs Steiner et al. (2018). The authors compared the performance of six pathologists on a tumor classification test before and after the introduction of LYNA. Results indicate a substantial improvement in sensitivity, average review time, and a subjective “obviousness” score for all breast cancer types.

The similarity between the results of the two approaches is highly suggestive that integration of CAD tools into the clinical workflow will greatly improve pathologist efficiency. However, there is clearly a general lack of research on the clinical impact of CAD tools which leaves the overarching question of *how effective are CAD tools in improving the pathology workflow?* unanswered in the field. Evidently, more research is needed to provide further evidence supporting the integration of CAD tools from CoPath and to examine approaches for implementation in clinical settings.

6.2. FDA Regulations

Despite the ongoing development of CAD tools in CoPath and its potential in triaging cases and providing second opinions, the regulations regarding this technology pose an obstacle to the testing and deployment of these devices. The US Food & Drugs Administration (FDA) currently provides three levels of FDA clearance on AI/ML-based medical technologies - 510(k) clearance, premarket approval, and the De Novo pathway. While one source lists 64 AI/ML-based medical solutions that are currently FDA-approved or cleared, none of these are in the field of CoPath Benjamens et al. (2020). A few companies, such as Paige AI, hold the 510(k) clearance for their digital pathology image viewer; however, an automated diagnostic system is yet to be approved. This may indicate a reluctance to change, and the lack of clarity in the process of FDA approval has prevented numerous impactful technologies from being deployed. There is a need for collaboration between researchers, doctors, and governmental bodies to establish a clear pathway for these novel technologies to be validated and implemented in clinical settings.

7. Existing Challenges and Future Opportunities

7.1. Comparison to General Computer Vision

Typically, the various classes in a given image classification problem represent distinct object types. Examples include natural vision dataset Caltech-256 Griffin et al. (2007), which groups images taken from various search engines into 256 classes (e.g. airplanes, bears, dice, etc.), and ImageNet, which for the LSVRC-2010 competition divided images into 1000 classes Krizhevsky et al. (2012). In the usual computer vision paradigm, there exist abundant “normal” samples and potentially several “anomalous” samples, where an anomaly is considered a data point or collection of data points that are significantly dissimilar to the majority within a given class Pang et al. (2021). Not only these anomalies are out of distribution from general observation of given dataset, but also there is a

lack of consensus on general understanding of anomalous representation. To effectively identify anomalies, machine learning models must learn a feature space that encompasses all samples considered “normal” within each class Pang et al. (2021).

In other words, in general computer vision, each class cannot simply be considered as an anomalous version of any other class. However, in CoPath, since each class is often considered a different disease state on a single tissue type, diseased classes are essentially extensions of the “normal” healthy class into the “anomalous” zone. Yet, from a pathologist’s perspective, similar to the general computer vision approach, the curriculum learning process of a resident pathologist first involves training on histology and gaining a mastery of normal tissue identification, and then train on diseased tissues, so they are able to flag the sample as anomalous and follow up with possible diagnosis.

In light of this, it may be illuminating to approach the problem from an anomaly detection viewpoint. In this mindset, healthy tissue may be considered all normal samples, whereas diseased tissue may be considered anomalous. The output of such an anomaly detection algorithm is dependent on the task at hand. One source describes several meaningful output types that may be produced Pang et al. (2021). The first of these is an anomaly score, which describes how anomalous the input sample is. The second of these is a binary label, indicating whether a sample is normal or anomalous. If only identifying anomalous samples is enough, a binary classification procedure may be sufficient. However, if it is necessary to identify the particular stage of progression of a disease type, then a more granular approach in assigning some *anomaly score* may be more appropriate as explored in a previous work Hosseini et al. (2020). In this paper, it was found that the confidence score in tissue classification was inversely correlated with disease progression. In this way, the confidence score may act as a proxy for an anomaly score. Theoretically, approaches such as this may be able to better replicate the behaviour of pathologists. While several works have used an anomaly detection approach on medical image data, in general, Lu and Xu (2018); Esteva et al. (2017); Iakovidis et al. (2018), few works exist which tackle the problem for WSI data in CoPath. This presents a potential gap that future research work can fill.

7.2. Leveraging Existing Datasets

As mentioned in Section 3.3 of this paper, a minority of datasets in CoPath are available to be freely used by the public. Additionally, the level of annotations varies for each dataset, however as can be noted in Table 8.3 of the supplementary for prominent public datasets such as CAMELYON16, CAMELYON17, GlaS, BreakHis, and TCGA, there is far more available data annotated at the slide level as opposed to more granular predictions. For example, considering breast datasets, there are 399 WSIs annotated at the Slide and ROI levels in CAMELYON16 Cam (2016) and 1399 WSIs annotated at the Patient, Slide, and ROI levels in CAMELYON17 Litjens et al. (2018), in contrast, the TCGA-BRCA dataset contains 1163 diagnostic slides and 1978 tissue slides that are accompanied with labels at the Patient and Slide levels and diagnostic reports with labels for tissue features and tumor grades Grossman et al. (2016).

The lack of publicly available datasets with granular annotations is a major challenge in CoPath. To address this lack some training techniques have been proposed to efficiently obtain labels, such as an active deep learning framework that uses a small amount of labelled data to suggest the most pertinent unlabelled samples to be annotated Qi et al. (2018). Alternatively, other works propose models to synthetically create WSI patches, usually with the use of GANs. For example, Hou et al. Hou et al. (2019a) introduced an unsupervised pipeline that was capable of synthesizing annotated data at a large scale, noting that even pathologists had difficulty distinguishing between real and synthesized patches. However, despite these promising results, the issue of acquiring accurate and large datasets remains a prevalent issue within CoPath.

Generally, tasks such as tissue classification or gland segmentation require labels at the ROI, Patch, or Pixel levels. However, existing data annotated at the Patient and Slide levels can be used for these tasks by leveraging weakly supervised techniques such as MIL Lu et al. (2021d); Patil et al. (2019), or by learning rich representations using self-supervised techniques such as DINO Caron et al. (2021b); Chen et al. (2022) and contrastive learning Ciga et al. (2022) that can be used in downstream tasks. Specifically, work is being done to develop training methodologies and architectures that are more data efficient for Patient and Slide level annotations, such as CLAM which is a MIL technique that is used to train a performant CoPath model with as little as 25% of the training data to get over 0.9 AUC Lu et al. (2021d). Another recent work used self-supervised learning on WSIs without labels to train a hierarchical vision transformer and used the learned representations to fine-tune for cancer subtyping tasks. This finetuned model outperformed other state-of-the-art methods that used supervised learning methods on both the full training set and when all models used only 25% of the training set. These examples demonstrate a recent trend in the application of weakly and self-supervised learning techniques to leverage pre-existing and available data with weak labels, showcasing that a large amount of granular labels are not necessarily required for achieving state-of-the-art performance. We urge researchers in the CoPath field to follow this trend and focus on how to leverage existing weakly labelled datasets, especially to learn rich representations as a pre-training step for learning on smaller strongly labelled datasets.

7.3. Creating New Datasets

Although we mention the availability of many datasets and comment on how to leverage this existing data, there is still a need for new CoPath datasets that address overlooked clinical and diagnostic areas. Therefore, creation of new CoPath datasets should focus on addressing two main goals: (1) tasks that are not addressed adequately by existing datasets and (2) accumulating as large a dataset as possible with maximal variety.

Specifically, the first goal concerns organs, diseases, and workflow steps that do not currently have freely available data or sufficient annotations to develop CAD tools. For example, in Figure 7 we see that brain and liver datasets are not abundant as compared to the breast, and additionally, there are few

publicly available brain datasets and no publicly available liver ones. Collection and release of CoPath datasets for these organs would have significant impact in enabling further works focusing on these applications. Further, analysis of specific organ synoptic reports can guide CoPath researchers to build CAD tools to identify or discriminate the most impactful diagnostic parameters. In the case of the prostate, which is discussed in Section 2.6 *Prostate*, the synoptic report requires distinguishing IDC from PIN and PIA as it correlates to high Gleason scores, additionally, high-grade PIN is a cancer precursor requiring follow-up sessions for screenings. These parameters are identified and noted in the report by the pathologist and factor into the final diagnosis and grading. Thus, collecting annotated datasets for such parameters can be crucial to developing CAD tools that are relevant to clinical workflows and can enrich learned representations.

The second goal is concerned with the scaling laws of deep learning models with respect to the amount of data available and the application of those models to diverse clinical settings. As has been shown in the general computer vision domain, larger datasets have a significant impact on model performance, especially when used to pre-train models to learn rich representations that can be used for various downstream tasks such as classification, semantic segmentation, and pose estimation Sun et al. (2017). Additionally, ensuring that datasets capture the underlying data distribution and thus contain sufficient representation of the test distribution has been shown to be especially important in the medical domain Althnian et al. (2021). For CoPath, this translates to ensuring a dataset captures the variation in tissue structure, disease progression, staining, preparation artifacts, scanners, image processing etc.

7.4. Pre and Post Analytical CAD Tools

In recent years, advances in image analysis, object detection, and segmentation have provided motivation for new approaches to support the analytical phase of the clinical workflow. However, there are two steps of the clinical workflow where CoPath applications could significantly increase efficiency and reduce medical errors: (1) specimen registration and (2) pathology reports. This need is highlighted by a study determining that the pre-analytical and post-analytical phases (as shown in Figure 2 account for up to 77% of medical errors in pathology Abdollahi et al. (2014). Similarly, Meier et al. note that only 14% of medical errors are due to diagnostic errors, with an even smaller proportion being misinterpreted diagnoses in their study Meier et al. (2011). Other authors report approximately 15 – 25% of diagnostic errors being due to slide interpretation Darcy et al. (2016); Nakhleh (2005, 2006, 2008); Nakhleh et al. (2016). These results reinforce the need for CoPath applications that address more than just the analytical phase Nakhleh (2015). Considering post-analytical step of compiling a pathology report, a few natural language processing efforts have been used to analyze completed pathology reports Odisho et al. (2020); López-Úbeda et al. (2022); Kim et al. (2020b), extract primary site codes from reports Qiu et al. (2017), and generate of captions or descriptive texts for WSI patches Zhang et al. (2019). However, to the best of our knowledge, there are no works that reliably extract clinical data from service requests and electronic medical

records to generate a comprehensive backbone of the synoptic or text reports. Development of such a tool would be directly applicable in the clinical workflow of pathologists while also increasing interpretability as CAD tools must explicitly identify and classify the most significant reporting parameters in determining diagnoses and prognoses. We encourage the field of CoPath to expand its efforts in creating tools for pre and post-analytical steps that can reduce the large percentage of clinical errors attributed to those phases, some potential applications are suggested in Figure 2.

7.5. Multi Domain Learning

Multi-domain learning (MDL) is a relatively unexplored topic in the CoPath. In MDL, examples are accompanied by both a class label and a domain indicator. In CoPath, domains represent different datasets which may originate from different organs. Our target is to train a unified architecture that can solve many tasks for data coming from different domains. An example is a single model that is trained using data from multiple organs such as breast, prostate, liver, lung, etc., and is able to solve many tasks such as breast lesion classification, prostate tumor grading, etc. During inference, the model receives an input image and the corresponding domain indicator and is able to solve the corresponding task for the given domain. There are two major reasons that make MDL attractive for CoPath. The first motivation is that the information coming from the training signals of related domains (e.g. Prostate tissue, Lung tissue, etc.) can help us do better on the target domain (Breast tissue). Essentially, by sharing representations between related domains, we can enable our model to generalize better on our original domain. The second motivation is to alleviate the data sparsity problem where one domain has a limited number of labeled data. Through MDL, the domain with limited data can benefit from the features that are jointly learned with other related tasks/domains Zamir et al. (2018); Zhang and Yang (2021). These motivations make MDL particularly well-suited for CoPath.

7.6. Federated Learning for Multicentral CoPath

Data-driven models require a large amount of data to yield strong performance. In CoPath, the performance and generalization of such models increase by incorporating diverse datasets with varying tissue slide preparations, staining quality, and scanners. An obvious solution to train such models is to accumulate the data from multiple medical centers into a centralized repository. However, in practice, data privacy regulations may not allow medical institutions to easily share their data across institutions, especially between countries. A possible set of methods to overcome this issue are privacy-preserving model training algorithms, such as federated learning Bonawitz et al. (2019); Kairouz et al. (2021), which can make use of decentralized data from multiple institutions while keeping the sensitive data private. In federated learning, training starts with a generic machine learning model in a centrally located server. Instead of transferring data to a centralized server to train the model, copies of the model are sent to each institution to train on each institution’s data. The model updates during training are sent

to the central server using encrypted communication and aggregated to combine the learnings from each institution’s data. Ming Lu et al. Lu et al. (2022) demonstrated the feasibility and effectiveness of applying federated, attention-based weakly supervised learning for general-purpose classification and survival prediction on WSIs using data from different sites. Using such algorithms for CoPath can facilitate cross-institutional collaborations and can be a viable solution for future commercial solutions that need to continuously augment and improve their ML models using decentralized data.

7.7. CoPath-specific architecture designs

Many deep learning architectures are not designed for CoPath specifically, which raises a serious question about the optimality of using “borrowed” architectures from general computer vision. For instance, Eminaga et al. (2019) notes that traditional CV architectures may not be well suited for CoPath due to a large number of parameters that risk overfitting. Additionally, the field of pathology has much domain-specific knowledge that should be taken into account before choosing an ML model. For example, under varying magnifications different morphological patterns are captured, from cellular-level details to tissue architecture features Kosaraju et al. (2020). Naively applying an architecture without considering such details could discard key visual information and lead to deteriorated performance.

Unlike natural images, WSIs not only exhibit translational symmetry but also rotational and reflective symmetry Veeling et al. (2018) and CNNs for general vision applications do not exploit this symmetry. The conventional approach to overcome this issue is training the model with augmented rotation and reflections of the data, but this increases training time and does not explicitly restrict CNN kernels to exploit those symmetries. Rotation equivariant CNNs for digital pathology Veeling et al. (2018) were proposed to exploit these symmetries, as they are inherently equivariant to rotations of 90° and reflections, achieving a significant improvement over a comparable CNN on slide level classification and tumor localization tasks. Similarly, Lafarge et al. Lafarge et al. (2021) designed a group convolution layer that leverages the rotational symmetry of pathology data and yields superior performance in mitosis detection, nuclei segmentation, and tumor classification tasks. These results motivate the application and further research of rotation equivariant models for CoPath.

In general, we note that the state-of-the-art architectures used in computational pathology have tended to lag behind those used for computer vision in natural images by a couple of years. This delay in knowledge propagation from the mainline computer vision research in natural images may be due to the data-centric nature of the CoPath field. As data labelling is specialized and expensive to conduct, there may be less incentive to use more advanced architectures where instead further annotations to data or clever training tweaks can be used to train established architectures for better performance. However, we recommend that CoPath researchers should still attempt to use the most recent models available for the simple reason that they tend to be more powerful and efficient over time. While computational efficiency is generally not as important during training,

it is imperative at inference time if models are to be run in real-time on medical devices with limited computational resources.

7.8. Digital and Computational Pathology Adoption

Despite the numerous advantages to the clinical workflow and applications offered by using digital pathology and Co-Path, the adoption of digital pathology remains the first barrier to clinical use. A major reason for adoption hesitancy is consideration of digital slide analysis to be an unnecessary step in a pathologist's workflow Lujan et al. (2022); Liu and Pantanowitz (2019); Griffin and Treanor (2017); Jara-Lazaro et al. (2010), a workflow that may have been refined over decades to hone a process for reproducible and robust diagnoses. In terms of clinical flow efficiency, studies have shown mixed results with two studies indicating an increase in a turnaround time of 19%, which is a reduction in efficiency Schüffler et al. (2021); Hanna et al. (2019), however, another study demonstrated a clear increase in productivity and reduction of turnaround-time Baidoshvili et al. (2018). One of this survey's co-authors (B.N.) has implemented digital pathology at a public tertiary institution, which began as a pilot-study over three years including three experienced academic pathologists and showed a turnaround-time reduction of 18% for biopsies and 25% for resections, with 17% increase in case output. These trial results led to all pathologists not retiring within two years to transition to a digital pathology workflow in 2019. Due to the varied nature of results and outcomes in studies analyzing the effectiveness of digital pathology there is more work to be done to have a multi-institution and lab analysis for more general and concrete results.

Considering CoPath specifically, integration into clinical workflow is relatively understudied as few papers have actually deployed, or performed clinical validation of their results. Works in this area have either proposed methods to deploy their models in the clinic or developed tools/web applications to enable the use of their research in the clinic Kather et al. (2019b); Kiani et al. (2020); Wang et al. (2019b). However, as a primary goal in the field of CoPath is the use of CAD tools in clinical settings more works should consider how to integrate models and tools into the clinical workflow, interfacing with clinicians on how.

7.9. Institutional Challenges

Several institutional challenges may affect the implementation of CoPath tools, and similar challenges in implementing digital pathology workflows at medical institutions have been well-described by many studies Isaacs et al. (2011); Pare et al. (2016); Thorstenson et al. (2014); Cheng et al. (2016); Stathonikos et al. (2013). As noted by multiple studies considering the digital transition of pathology laboratories Isaacs et al. (2011); Pare et al. (2016); Thorstenson et al. (2014); Cheng et al. (2016); Stathonikos et al. (2013), the importance of a common shared goal and frequent communication between the involved parties is necessary to successfully deploy a digital system. These lessons are likely extendable in the context of Co-Path and CAD development as well. Specifically, Cheng et al. Cheng et al. (2016), reported on their experiences and lessons learned as a 7-point-based system to efficiently deploy a digital

pathology system in a large academic center. We believe similar systematic approaches will need to be developed to implement CoPath applications in a clinical setting.

Another institutional challenge concerns the regulatory oversight at the departmental, institutional, accrediting agencies, pathology association, state/provincial, and federal levels. Regulatory measures underlying WSI scanners are well established, as well as the technical and clinical validation of their use Pantanowitz et al. (2013); Abels and Pantanowitz (2017); Parwani et al. (2014). On the other hand, patient confidentiality, ethics, medical data storage regulations, and data encryption laws are equally, if not more, time-consuming and intensive to comply with. These issues can be mitigated by deploying a standardized digital pathology system throughout multiple institutions at the state/provincial level. For example, our co-author (B.N.) has obtained governmental approval and funding to distribute a set of digital pathology systems throughout the province's public anatomical pathology laboratories. Similarly, a unified set of standards for processing and digitizing slides, along with unifying storage and access to WSIs for research use in collaborative efforts is paramount in moving forward in both the development and implementation of CAD systems.

7.10. Clinical Alignment of CoPath Tasks

Researchers in the CoPath field must ensure that the CAD tools they create are clinically relevant and applicable to pathology so that effort and resources are not allocated towards extraneous or clinically irrelevant tasks. For example, certain CADs have been proposed to facilitate case triaging and reduce turnaround time for critical diagnoses Janowczyk and Madabhushi (2016); Liu et al. (2019); Khan et al. (2019b); Noorbakhsh et al. (2020); Sankarapandian et al. (2021)]. However, several regulatory agencies in pathology aim for 90% of cases to be completed within a timeframe of 72 hours for signing-out resection specimens and up to 48 hours for biopsies Alshieban and Al-Surimi (2015); Nakhleh and Fitzgibbons (2005). In this context, triaging becomes extraneous, as signing out cases faster than 48-72 hours has no clinical impact. However, in the context of an institution operating at longer turnaround times or struggling to keep up with the caseload, this method could be lifesaving. Alternatively, identifying mitotic figures and counting positive Ki-67 nuclei are appreciated tools already in use in multiple digital pathology settings, despite these tools being seldom applied to the large caseload proportion of most practicing pathologists.

As noted previously, the overall number of pathologists in the USA has decreased 17% from 2007 to 2017 and caseloads have increased by 41.7% Metter et al. (2019). This trend places further emphasis of developing CAD tools towards specific challenges encountered by pathologists and where sub-specialists may not be readily available. For example, a large consortium generated a prostate cancer CAD that achieved a 86.8% concordance with expert genitourinary pathologists Bulten et al. (2022), a significant breakthrough for healthcare settings where prostate biopsies are not signed out by sub-specialists. Additionally, targeting specific diagnoses with high rates of medical errors and interobserver variance, notably in dermatological, gynecological, and gastrointestinal pathology, should be

prioritized and integrated into practice quickly to support patient care Peck et al. (2018). Finally, advanced CADs capable of diagnosing features out of reach by conventional pathology could have a great impact. For example, identifying the origin of metastases from morphological cues on the WSIs without added immunohistochemistry Lu et al. (2021b) or CADs capable of calculating the exact involvement of cancer on a biopsy core for prognostic purposes Bulten et al. (2022).

7.11. Concluding Remarks

Bringing pathologists and computer scientists together and initiating meaningful collaborations with shared gains between all parties is likely the most efficient path forward for Co-Path and CAD integration. Grounds to facilitate collaborations should be promoted by parties such as the Pathology Innovation Collaborative Community and the Digital Pathology Association. Furthermore, we encourage involved pathologists and computer scientists to communicate and collaborate on studies towards the common goal of providing patients with fast, reproducible, and high-quality care.

Acknowledgment

Authors would like to thank Huron Digital Pathology for providing support and insightful discussions related to digital pathology hardware infrastructures. Authors would like to also thank Xin Zhao, Koosha E. Khorasani, Mona Sharifi, and Kiana Abtahi for their help in revising portions of our model-cards. This work was partly supported from NSERC-CRD (Collaborative and Research Development) funding grant and MITACS-Elevate award.

References

- , . MITOS-ATYPIA-14 Grand Challenge. Available online: <https://mitos-atypia-14.grand-challenge.org/> (accessed June 10, 2021).
- , . The Lung Cancer SPORE. Available at: <https://www.mdanderson.org/research/departments-labs-institutes/spores/lung-cancer-spore.html> (accessed June 10, 2021).
- , 2016. CAMELYON16 ISBI challenge on cancer metastasis detection in lymph node. Available at: <https://camelyon16.grand-challenge.org/> (accessed June 11, 2021).
- , 2017. CAMELYON17. Available at: <https://camelyon17.grand-challenge.org/Organisers/> (accessed June 11, 2021).
- , 2020. What is kidney cancer? URL: <https://www.cancer.org/cancer/kidney-cancer/about/what-is-kidney-cancer>.
- Abbas, A.K., Aster, J.C., Kumar, V., 2010. Robbins and Cotran pathologic basis of disease. Saunders/Elsevier.
- Abdel-Nasser, M., Saleh, A., Puig, D., 2020. Channel-wise aggregation with self-correction mechanism for multi-center multi-organ nuclei segmentation in whole slide imaging., in: VISIGRAPP), pp. 466–473.
- Abdollahi, A., Saffar, H., Saffar, H., 2014. Types and frequency of errors during different phases of testing at a clinical medical laboratory of a teaching hospital in tehran, iran. North American journal of medical sciences 6, 224.
- Abels, E., Pantanowitz, L., 2017. Current state of the regulatory trajectory for whole slide imaging devices in the usa. Journal of pathology informatics 8, 23.
- Abels, E., Pantanowitz, L., Aeffner, F., Zarella, M.D., van der Laak, J., Bui, M.M., Venuri, V.N., Parwani, A.V., Gibbs, J., Agosto-Arroyo, E., et al., 2019. Computational pathology definitions, best practices, and recommendations for regulatory guidance: a white paper from the digital pathology association. The Journal of Pathology 249, 286–294.
- Abinaya, K., Sivakumar, B., 2022. A systematic review: Intellectual detection and prediction of cancer using dl techniques, in: 2022 6th International Conference on Trends in Electronics and Informatics (ICOEI), IEEE. pp. 1497–1504.
- Acs, B., Rantalainen, M., Hartman, J., 2020. Artificial intelligence as the next step towards precision pathology. Journal of internal medicine 288, 62–81.
- Adam, S.P., Alexandropoulos, S.A.N., Pardalos, P.M., Vrahatis, M.N., 2019. No free lunch theorem: A review. Approximation and optimization , 57–82.
- Adnan, M., Kalra, S., Tizhoosh, H.R., 2020. Representation learning of histopathology images using graph neural networks, in: IEEE/CVF Conference on Computer Vision and Pattern Recognition Workshops, pp. 988–989.
- Agarwalla, A., Shaban, M., Rajpoot, N.M., 2017. Representation-aggregation networks for segmentation of multi-gigapixel histology images. ArXiv abs/1707.08814.
- Akram, S.U., Qaiser, T., Graham, S., Kannala, J., Heikkilä, J., Rajpoot, N., 2018. Leveraging unlabeled whole-slide-images for mitosis detection , 69–77.
- Al-Janabi, S., Huisman, A., Van Diest, P.J., 2012. Digital pathology: current status and future perspectives. Histopathology 61, 1–9.
- Al-Milaji, Z., Ersoy, I., Hafiane, A., Palaniappan, K., Bunyak, F., 2019. Integrating segmentation with deep learning for enhanced classification of epithelial and stromal tissues in h&e images. Pattern Recognition Letters 119, 214–221.
- AlAmir, M., AlGhamdi, M., 2022. The role of generative adversarial network in medical image analysis: An in-depth survey. ACM Computing Surveys 55, 1–36.
- Alawad, M., Gao, S., Qiu, J.X., Yoon, H.J., Blair Christian, J., Penberthy, L., Mumphrey, B., Wu, X.C., Coyle, L., Tourassi, G., 2020. Automatic extraction of cancer registry reportable information from free-text pathology reports using multitask convolutional neural networks. Journal of the American Medical Informatics Association 27, 89–98.
- Albertina, B., Watson, M., Holback, C., Jarosz, R., Kirk, S., Lee, Y., Lemmerman, J., 2016. Radiology data from the cancer genome atlas lung adenocarcinoma [tcga-luad] collection. The Cancer Imaging Archive .
- Alharbi, A., Wang, Y., Zhang, Q., 2021. Trans-attention multiple instance learning for cancer tissue classification in digital histopathology images , 79–84.
- Ali, S., Alham, N.K., Verrill, C., Rittscher, J., 2019. Ink removal from histopathology whole slide images by combining classification, detection and image generation models, in: IEEE International Symposium on Biomedical Imaging, IEEE. pp. 928–932.
- Alirezazadeh, P., Hejrat, B., Monsef-Esfahani, A., Fathi, A., 2018. Representation learning-based unsupervised domain adaptation for classification of breast cancer histopathology images. Biocybernetics and Biomedical Engineering 38, 671–683.
- Allison, K.H., Hammond, M.E.H., Dowsett, M., McKernin, S.E., Carey, L.A., Fitzgibbons, P.L., Hayes, D.F., Lakhani, S.R., Chavez-MacGregor, M., Perlmutter, J., et al., 2020. Estrogen and progesterone receptor testing in breast cancer: Asco/cap guideline update. Journal of Clinical Oncology 38, 1346–1366.
- Almansouri, S., Zwyea, S., 2020. Early prognosis of human renal cancer with kaplan-meier plotter data analysis model, in: Journal of physics: conference series, IOP Publishing. p. 012051.
- Alom, M.Z., Aspiras, T., Taha, T.M., Bowen, T., Asari, V.K., 2020. Mitosisnet: End-to-end mitotic cell detection by multi-task learning. IEEE Access 8, 68695–68710.
- Alom, M.Z., Yakopcic, C., Nasrin, M., Taha, T.M., Asari, V.K., et al., 2019. Breast cancer classification from histopathological images with inception recurrent residual convolutional neural network. Journal of digital imaging 32, 605–617.
- Alshieban, S., Al-Surimi, K., 2015. Reducing turnaround time of surgical pathology reports in pathology and laboratory medicine departments. BMJ Open Quality 4, u209223-w3773.
- Althnian, A., AlSaeed, D., Al-Baity, H., Samha, A., Dris, A.B., Alzakari, N., Abou Elwafa, A., Kurdi, H., 2021. Impact of dataset size on classification performance: an empirical evaluation in the medical domain. Applied Sciences 11, 796.
- Alzubaidi, L., Al-Shamma, O., Fadhel, M.A., Farhan, L., Zhang, J., Duan, Y., 2020. Optimizing the performance of breast cancer classification by employing the same domain transfer learning from hybrid deep convolutional neural network model. Electronics 9, 445.
- Amjad, M., Elfandy, H., Hussein, H., Atteya, L.A., Elsebaie, M.A., Abo Elnasr, L.S., Sakr, R.A., Salem, H.S., Ismail, A.F., Saad, A.M., et al., 2019.

- Structured crowdsourcing enables convolutional segmentation of histology images. *Bioinformatics* 35, 3461–3467.
- Amin, M.B., Edge, S.B., Greene, F.L., Byrd, D.R., Brookland, R.K., Washington, M.K., Gershenwald, J.E., Compton, C.C., Hess, K.R., Sullivan, D.C., et al., 2017a. AJCC cancer staging manual, volume 1024. Springer.
- Amin, M.B., Greene, F.L., Edge, S.B., Compton, C.C., Gershenwald, J.E., Brookland, R.K., Meyer, L., Gress, D.M., Byrd, D.R., Winchester, D.P., 2017b. The eighth edition ajcc cancer staging manual: continuing to build a bridge from a population-based to a more “personalized” approach to cancer staging. *CA: a cancer journal for clinicians* 67, 93–99.
- Anand, D., Yashashwi, K., Kumar, N., Rane, S., Gann, P.H., Sethi, A., 2021. Weakly supervised learning on unannotated h&e-stained slides predicts braf mutation in thyroid cancer with high accuracy. *The Journal of Pathology* 255, 232–242.
- Andreassen, B., Aagnes, B., Gislefoss, R., Andreassen, M., Wahlqvist, R., 2016. Incidence and survival of urothelial carcinoma of the urinary bladder in norway 1981–2014. *BMC cancer* 16, 1–11.
- Andresja3, 2011. Nissl cerebelo ampliado. URL: https://commons.wikimedia.org/wiki/File:Nissl_cerebelo_ampliado.png.
- Araújo, A.L.D., Arboleda, L.P.A., Palmier, N.R., Fonseca, J.M., de Pauli Paglioni, M., Gomes-Silva, W., Ribeiro, A.C.P., Brandao, T.B., Simonato, L.E., Speight, P.M., et al., 2019. The performance of digital microscopy for primary diagnosis in human pathology: a systematic review. *Virchows Archiv* 474, 269–287.
- Araújo, T., Aresta, G., Castro, E., Rouco, J., Aguiar, P., Eloy, C., Polónia, A., Campilho, A., 2017. Classification of breast cancer histology images using convolutional neural networks. *PloS one* 12, e0177544.
- Aresta, G., Araújo, T., Kwok, S., Chennamsetty, S.S., Safwan, M., Alex, V., Marami, B., Prastawa, M., Chan, M., Donovan, M., et al., 2019. Bach: Grand challenge on breast cancer histology images. *Medical Image Analysis* 56, 122–139.
- Arvaniti, E., Claassen, M., 2018. Coupling weak and strong supervision for classification of prostate cancer histopathology images. *ArXiv abs/1811.07013*.
- Arvaniti, E., Fricker, K.S., Moret, M., Rupp, N., Hermanns, T., Fankhauser, C., Wey, N., Wild, P.J., Rueschhoff, J.H., Claassen, M., 2018. Automated gleason grading of prostate cancer tissue microarrays via deep learning. *Scientific Reports* 8, 1–11.
- Arvidsson, I., Overgaard, N.C., Åström, K., Heyden, A., 2019. Comparison of different augmentation techniques for improved generalization performance for gleason grading, in: *IEEE International Symposium on Biomedical Imaging*, IEEE. pp. 923–927.
- Atupelage, C., Nagahashi, H., Kimura, F., Yamaguchi, M., Abe, T., Hashiguchi, A., Sakamoto, M., 2013. Computational cell classification methodology for hepatocellular carcinoma, in: *International Conference on Advances in ICT for Emerging Regions (ICTer)*, IEEE. pp. 21–27.
- Avenel, C., Tolf, A., Dragomir, A., Carlom, I.B., 2019. Glandular segmentation of prostate cancer: An illustration of how the choice of histopathological stain is one key to success for computational pathology. *Frontiers in Bioengineering and Biotechnology* 7, 125.
- Awan, R., Koohbanani, N.A., Shaban, M., Lisowska, A., Rajpoot, N., 2018. Context-aware learning using transferable features for classification of breast cancer histology images, in: *International Conference Image Analysis and Recognition*, Springer. pp. 788–795.
- Awan, R., Sirinukunwattana, K., Epstein, D., Jefferyes, S., Qidwai, U., Aftab, Z., Mujeeb, I., Snead, D., Rajpoot, N., 2017. Glandular morphometrics for objective grading of colorectal adenocarcinoma histology images. *Scientific Reports* 7, 1–12.
- Ayyagari, S., Potnuru, A., Saleem, S.A., Marapaka, P., 2021. Analysis of frozen section compared to permanent section: a 2 year study in a single tertiary care hospital. *Journal of Pathology of Nepal* 11, 1854–1858.
- Bachert, S.E., McDowell Jr, A., Piecoro, D., Baldwin Branch, L., 2020. Serous tubal intraepithelial carcinoma: a concise review for the practicing pathologist and clinician. *Diagnostics* 10, 102.
- Bai, T., Xu, J., Xing, F., 2020. Multi-field of view aggregation and context encoding for single-stage nucleus recognition, in: *International Conference on Medical Image Computing and Computer-Assisted Intervention*, Springer. pp. 382–392.
- Baidoshvili, A., Bucur, A., van Leeuwen, J., van der Laak, J., Kluin, P., van Diest, P.J., 2018. Evaluating the benefits of digital pathology implementation: time savings in laboratory logistics. *Histopathology* 73, 784–794.
- Balaprakash, P., Egele, R., Salim, M., Wild, S., Vishwanath, V., Xia, F., Brettin, T., Stevens, R., 2019. Scalable reinforcement-learning-based neural architecture search for cancer deep learning research, in: *International Conference for High Performance Computing, Networking, Storage and Analysis*, pp. 1–33.
- Bándi, P., Balkenhol, M., van Ginneken, B., van der Laak, J., Litjens, G., 2019. Resolution-agnostic tissue segmentation in whole-slide histopathology images with convolutional neural networks. *PeerJ* 7, e8242.
- Bandi, P., Geessink, O., Manson, Q., Van Dijk, M., Balkenhol, M., Hermans, M., Bejnordi, B.E., Lee, B., Paeng, K., Zhong, A., et al., 2018. From detection of individual metastases to classification of lymph node status at the patient level: the camelyon17 challenge. *IEEE Transactions on Medical Imaging* 38, 550–560.
- Bardou, D., Zhang, K., Ahmad, S.M., 2018. Classification of breast cancer based on histology images using convolutional neural networks. *IEEE Access* 6, 24680–24693.
- Barker, J., Hoogi, A., Deppeursinge, A., Rubin, D.L., 2016. Automated classification of brain tumor type in whole-slide digital pathology images using local representative tiles. *Medical Image Analysis* 30, 60–71.
- Barron, D.E.L., Yarlagadda, D.V.K., Rao, P., Tawfik, O., Rao, D., 2018. Scalable storage of whole slide images and fast retrieval of tiles using apache spark, in: *Medical Imaging: Digital Pathology*, International Society for Optics and Photonics. p. 1058113.
- Bauer, S., Carion, N., Schüffler, P., Fuchs, T., Wild, P., Buhmann, J.M., 2016. Multi-organ cancer classification and survival analysis. *arXiv preprint arXiv:1606.00897*.
- Bautista, P.A., Yagi, Y., 2009. Detection of tissue folds in whole slide images, in: *2009 Annual International Conference of the IEEE Engineering in Medicine and Biology Society*, IEEE. pp. 3669–3672.
- Bautista, P.A., Yagi, Y., 2015. Staining correction in digital pathology by utilizing a dye amount table. *Journal of digital imaging* 28, 283–294.
- Baxi, V., Edwards, R., Montalto, M., Saha, S., 2022. Digital pathology and artificial intelligence in translational medicine and clinical practice. *Modern Pathology* 35, 23–32.
- Bayat, A., Anderson, C., Shah, P., 2021. Automated end-to-end deep learning framework for classification and tumor localization from native non-stained pathology images 11596, 115960A.
- Bayramoglu, N., Kannala, J., Heikkilä, J., 2016. Deep learning for magnification independent breast cancer histopathology image classification, in: *International Conference on Pattern Recognition*, IEEE. pp. 2440–2445.
- Beck, A.H., Sangoi, A.R., Leung, S., Marinelli, R.J., Nielsen, T.O., Van De Vijver, M.J., West, R.B., Van De Rijn, M., Koller, D., 2011. Systematic analysis of breast cancer morphology uncovers stromal features associated with survival. *Science translational medicine* 3, 108ra113–108ra113.
- Bejnordi, B.E., Litjens, G., Timofeeva, N., Otte-Höller, I., Homeyer, A., Karssemeijer, N., van der Laak, J.A., 2015. Stain specific standardization of whole-slide histopathological images. *IEEE Transactions on Medical Imaging* 35, 404–415.
- Bejnordi, B.E., Timofeeva, N., Otte-Höller, I., Karssemeijer, N., van der Laak, J.A., 2014. Quantitative analysis of stain variability in histology slides and an algorithm for standardization, in: *Medical Imaging: Digital Pathology*, International Society for Optics and Photonics. p. 904108.
- Bejnordi, B.E., Veta, M., Van Diest, P.J., Van Ginneken, B., Karssemeijer, N., Litjens, G., Van Der Laak, J.A., Hermans, M., Manson, Q.F., Balkenhol, M., et al., 2017a. Diagnostic assessment of deep learning algorithms for detection of lymph node metastases in women with breast cancer. *JAMA network open* 318, 2199–2210.
- Bejnordi, B.E., Zuidhof, G., Balkenhol, M., Hermans, M., Bult, P., van Ginneken, B., Karssemeijer, N., Litjens, G., van der Laak, J., 2017b. Context-aware stacked convolutional neural networks for classification of breast carcinomas in whole-slide histopathology images. *Journal of Medical Imaging* 4, 044504.
- Belharbi, S., Rony, J., Dolz, J., Ayed, I.B., McCaffrey, L., Granger, E., 2021a. Deep interpretable classification and weakly-supervised segmentation of histology images via max-min uncertainty. *IEEE Transactions on Medical Imaging* 41, 702–714.
- Belharbi, S., Rony, J., Dolz, J., Ayed, I.B., McCaffrey, L., Granger, E., 2021b. Deep interpretable classification and weakly-supervised segmentation of histology images via max-min uncertainty. *IEEE Transactions on Medical Imaging*.
- Bengio, Y., Courville, A., Vincent, P., 2012. Representation learning: A review and new perspectives. URL: <https://arxiv.org/abs/1206.5538>, doi:10.48550/ARXIV.1206.5538.

- Benjamins, S., Dhunnoo, P., Meskó, B., 2020. The state of artificial intelligence-based fda-approved medical devices and algorithms: an online database. *NPJ Digital Medicine* 3, 1–8.
- BenTaieb, A., Hamarneh, G., 2018. Predicting cancer with a recurrent visual attention model for histopathology images, in: International Conference on Medical Image Computing and Computer-Assisted Intervention, Springer. pp. 129–137.
- Bera, K., Schalper, K.A., Rimm, D.L., Velcheti, V., Madabhushi, A., 2019. Artificial intelligence in digital pathology—new tools for diagnosis and precision oncology. *Nature reviews Clinical oncology* 16, 703–715.
- Bidart, R., Wong, A., 2019. Triresnet: A deep triple-stream residual network for histopathology grading, in: International Conference on Image Analysis and Recognition, Springer. pp. 369–382.
- Bilal, M., Nimir, M., Snead, D., Taylor, G.S., Rajpoot, N., 2022. Role of ai and digital pathology for colorectal immuno-oncology. *British Journal of Cancer*, 1–9.
- Bilal, M., Raza, S.E.A., Azam, A., Graham, S., Ilyas, M., Cree, I.A., Snead, D., Minhas, F., Rajpoot, N.M., 2021. Development and validation of a weakly supervised deep learning framework to predict the status of molecular pathways and key mutations in colorectal cancer from routine histology images: a retrospective study. *The Lancet Digital Health* 3, e763–e772.
- Board, W.C.o.T.E., . Central Nervous System Tumours. URL: <https://publications.iarc.fr/Book-And-Report-Series/Who-Classification-Of-Tumours/Central-Nervous-System-Tumours-2021>.
- Boehm, K.M., Khosravi, P., Vanguri, R., Gao, J., Shah, S.P., 2021. Harnessing multimodal data integration to advance precision oncology. *Nature Reviews Cancer*, 1–13.
- Bonawitz, K., Eichner, H., Grieskamp, W., Huba, D., Ingberman, A., Ivanov, V., Kiddon, C., Konečný, J., Mazzocchi, S., McMahan, B., et al., 2019. Towards federated learning at scale: System design. *Proceedings of machine learning and systems* 1, 374–388.
- Bonsib, S.M., 2006. Renal lymphatics, and lymphatic involvement in sinus vein invasive (pt3b) clear cell renal cell carcinoma: a study of 40 cases. *Modern pathology* 19, 746–753.
- Borkowski, A.A., Bui, M.M., Thomas, L.B., Wilson, C.P., DeLand, L.A., Mastorides, S.M., . Lc25000 lung and colon histopathological image dataset URL: https://github.com/tampapath/lung_colon_image_set.
- Borovec, J., Kybic, J., Arganda-Carreras, I., Sorokin, D., Bueno, G., Khvostikov, A., Bakas, S., Chang, E., Heldmann, S., Kartasalo, K., Latonen, L., Lotz, J., Noga, M., Pati, S., Punithakumar, K., Ruusuvuori, P., Skalski, A., Tahmasebi, N., Valkonen, M., Muñoz-Barrutia, A., 2020. Anhir: Automatic non-rigid histological image registration challenge. *IEEE Transactions on Medical Imaging* PP, 1–1. doi:10.1109/TMI.2020.2986331.
- Bottaro, D.P., Linehan, W.M., 2005. Multifocal renal cancer: genetic basis and its medical relevance. *Clinical Cancer Research* 11, 7206–7208.
- Boyd, J., Liashuhua, M., Deutsch, E., Paragios, N., Christodoulidis, S., Vakalopoulou, M., 2021. Self-supervised representation learning using visual field expansion on digital pathology, in: IEEE/CVF International Conference on Computer Vision, pp. 639–647.
- Brancati, N., Anniciello, A.M., Pati, P., Riccio, D., Scognamiglio, G., Jaume, G., De Pietro, G., Di Bonito, M., Foncubierta, A., Botti, G., et al., 2021. Bracs: A dataset for breast carcinoma subtyping in h&e histology images. arXiv preprint arXiv:2111.04740.
- Brancati, N., De Pietro, G., Frucci, M., Riccio, D., 2019. A deep learning approach for breast invasive ductal carcinoma detection and lymphoma multi-classification in histological images. *IEEE Access* 7, 44709–44720.
- Breast Cancer Surveillance Consortium, . Available at: <https://www.bccs-research.org/> (accessed June 10, 2021).
- Brender, E., Burke, A., Glass, R.M., 2005. Frozen section biopsy. *Jama* 294, 3200–3200.
- Brieu, N., Meier, A., Kapil, A., Schoenmeyer, R., Gavriel, C.G., Cai, P.D., Schmidt, G., 2019. Domain adaptation-based augmentation for weakly supervised nuclei detection. arXiv preprint arXiv:1907.04681.
- Brixtel, R., Bougleux, S., Lézoray, O., Caillot, Y., Lemoine, B., Fontaine, M., Nebati, D., Renouf, A., 2022. Whole slide image quality in digital pathology: review and perspectives. *IEEE Access*.
- Brunnström, H., Johansson, A., Westbom-Fremer, S., Backman, M., Djureinovic, D., Patthey, A., Isaksson-Mettävainio, M., Gulyas, M., Micke, P., 2017. Pd-l1 immunohistochemistry in clinical diagnostics of lung cancer: inter-pathologist variability is higher than assay variability. *Modern Pathology* 30, 1411–1421.
- Buabbas, A.J., Mohammad, T., Ayed, A.K., Mallah, H., Al-Shawaf, H., Khal- fan, A.M., 2021. Evaluating the success of the tele-pathology system in governmental hospitals in kuwait: an explanatory sequential mixed methods design. *BMC Medical Informatics and Decision Making* 21, 1–12.
- Budak, Ü., Cömert, Z., Rashid, Z.N., Şengür, A., Çubuk, M., 2019. Computer-aided diagnosis system combining fcn and bi-lstm model for efficient breast cancer detection from histopathological images. *Applied Soft Computing* 85, 105765.
- Bueno, G., Fernandez-Carrobles, M.M., Gonzalez-Lopez, L., Deniz, O., 2020a. Glomerulosclerosis identification in whole slide images using semantic segmentation. *Computer methods and programs in biomedicine* 184, 105273.
- Bueno, G., Gonzalez-Lopez, L., Garcia-Rojo, M., Laurinavicius, A., Deniz, O., 2020b. Data for glomeruli characterization in histopathological images. *Data in brief* 29, 105314.
- Bug, D., Schneider, S., Grote, A., Oswald, E., Feuerhake, F., Schüller, J., Mershof, D., 2017. Context-based normalization of histological stains using deep convolutional features, in: Deep Learning in Medical Image Analysis and Multimodal Learning for Clinical Decision Support. Springer, pp. 135–142.
- Bulten, W., Bárdi, P., Hoven, J., van de Loo, R., Lotz, J., Weiss, N., van der Laak, J., van Ginneken, B., Hulsbergen-van de Kaa, C., Litjens, G., 2018. Peso: Prostate epithelium segmentation on h&e-stained prostatectomy whole slide images.
- Bulten, W., Bárdi, P., Hoven, J., Loo, R.v.d., Lotz, J., Weiss, N., Laak, J.v.d., Ginneken, B.v., Hulsbergen-van de Kaa, C., Litjens, G., 2019. Epithelium segmentation using deep learning in h&e-stained prostate specimens with immunohistochemistry as reference standard. *Scientific reports* 9, 1–10.
- Bulten, W., Kartasalo, K., Chen, P.H.C., Ström, P., Pinckaers, H., Nagpal, K., Cai, Y., Steiner, D.F., van Boven, H., Vink, R., et al., 2022. Artificial intelligence for diagnosis and gleason grading of prostate cancer: the panda challenge. *Nature medicine* 28, 154–163.
- Bulten, W., Litjens, G., Pinckaers, H., Ström, P., Eklund, M., Kartasalo, K., Demkin, M., Dane, S., 2020. The PANDA challenge: Prostate cANcer graDe Assessment using the Gleason grading system. URL: <https://doi.org/10.5281/zenodo.3715938>. doi:10.5281/zenodo.3715938.
- Bussola, N., Marcolini, A., Maggio, V., Jurman, G., Furlanello, C., 2021. Ai slipping on tiles: Data leakage in digital pathology , 167–182.
- Bychkov, D., Linder, N., Turkki, R., Nordling, S., Kovanen, P.E., Verrill, C., Wallander, M., Lundin, M., Haglund, C., Lundin, J., 2018. Deep learning based tissue analysis predicts outcome in colorectal cancer. *Scientific Reports* 8, 1–11.
- Bárdi, P., Geessink, O., Manson, Q., Van Dijk, M., Balkenhol, M., HermSEN, M., Ehteshami Bejnordi, B., Lee, B., Paeng, K., Zhong, A., Li, Q., Zanjani, F.G., Zinger, S., Fukuta, K., Komura, D., Ovtcharov, V., Cheng, S., Zeng, S., Thagaard, J., Dahl, A.B., Lin, H., Chen, H., Jacobsson, L., Hedlund, M., Çetin, M., Halıcı, E., Jackson, H., Chen, R., Both, F., Franke, J., Küsters-Vandeveldé, H., Vreuls, W., Bult, P., van Ginneken, B., van der Laak, J., Litjens, G., 2019. From detection of individual metastases to classification of lymph node status at the patient level: The camelyon17 challenge. *IEEE Transactions on Medical Imaging* 38, 550–560. doi:10.1109/TMI.2018.2867350.
- Caicedo, J.C., Goodman, A., Karhohs, K.W., Cimini, B.A., Ackerman, J., Haghghi, M., Heng, C., Becker, T., Doan, M., McQuin, C., et al., 2019. Nucleus segmentation across imaging experiments: the 2018 data science bowl. *Nature methods* 16, 1247–1253.
- Campanella, G., Hanna, M.G., Brogi, E., Fuchs, T.J., 2019a. Breast metastases to axillary lymph nodes. *Cancer Imaging Arch*.
- Campanella, G., Hanna, M.G., Geneslaw, L., Miraflor, A., Werneck Krauss Silva, V., Busam, K.J., Brogi, E., Reuter, V.E., Klimstra, D.S., Fuchs, T.J., 2019b. Clinical-grade computational pathology using weakly supervised deep learning on whole slide images. *Nature medicine* 25, 1301–1309.
- Campanella, G., Rajanna, A.R., Corsale, L., Schüffler, P.J., Yagi, Y., Fuchs, T.J., 2018a. Towards machine learned quality control: A benchmark for sharpness quantification in digital pathology. *Computerized Medical Imaging and Graphics* 65, 142–151.
- Campanella, G., Silva, V.W.K., Fuchs, T.J., 2018b. Terabyte-scale deep multiple instance learning for classification and localization in pathology. arXiv preprint arXiv:1805.06983.
- Canadian Cancer Society, . Survival statistics for brain and spinal cord tumours. Available at: <https://www.cancer.ca/en/cancer-information/cancer-type/brain-spinal/prognosis-and-survival/survival-statistics/?region=on#~:~text=InCanada,the5-year,surviveatleast5years>. (accessed June 10, 2021).
- Caron, M., Touvron, H., Misra, I., Jégou, H., Mairal, J., Bojanowski, P., Joulin, A., 2021a. Emerging properties in self-supervised vision transformers, in:

- Proceedings of the IEEE/CVF International Conference on Computer Vision, pp. 9650–9660.
- Caron, M., Touvron, H., Misra, I., Jégou, H., Mairal, J., Bojanowski, P., Joulin, A., 2021b. Emerging properties in self-supervised vision transformers, in: Proceedings of the IEEE/CVF international conference on computer vision, pp. 9650–9660.
- Carse, J., Carey, F., McKenna, S., 2021. Unsupervised representation learning from pathology images with multi-directional contrastive predictive coding, in: IEEE International Symposium on Biomedical Imaging, IEEE. pp. 1254–1258.
- Celik, Y., Talo, M., Yildirim, O., Karabatak, M., Acharya, U.R., 2020. Automated invasive ductal carcinoma detection based using deep transfer learning with whole-slide images. *Pattern Recognition Letters* 133, 232–239.
- Center, C., . Bladder cancer types. Available at: <https://www.cancercenter.com/cancer-types/bladder-cancer/types> (accessed Feb 10, 2023).
- Chalasani, V., Chin, J.L., Izawa, J.I., 2009. Histologic variants of urothelial bladder cancer and nonurothelial histology in bladder cancer. *Canadian Urological Association Journal* 3, S193.
- Chan, L., Hosseini, M.S., Plataniotis, K.N., 2021. A comprehensive analysis of weakly-supervised semantic segmentation in different image domains. *International Journal of Computer Vision* 129, 361–384.
- Chan, L., Hosseini, M.S., Rowsell, C., Plataniotis, K.N., Damaskinos, S., 2019. Histosegnet: Semantic segmentation of histological tissue type in whole slide images, in: IEEE/CVF International Conference on Computer Vision, pp. 10662–10671.
- Chandradevan, R., Aljudi, A.A., Drumheller, B.R., Kunananthaseelan, N., Amgad, M., Gutman, D.A., Cooper, L.A., Jaye, D.L., 2020. Machine-based detection and classification for bone marrow aspirate differential counts: initial development focusing on nonneoplastic cells. *Laboratory Investigation* 100, 98–109.
- Chang, H., Han, J., Zhong, C., Snijders, A.M., Mao, J.H., 2017a. Unsupervised transfer learning via multi-scale convolutional sparse coding for biomedical applications. *IEEE Transactions on Pattern Analysis and Machine Intelligence* 40, 1182–1194.
- Chang, H.Y., Jung, C.K., Woo, J.I., Lee, S., Cho, J., Kim, S.W., Kwak, T.Y., 2019. Artificial intelligence in pathology. *Journal of pathology and translational medicine* 53, 1.
- Chang, J.R., Lee, C.Y., Chen, C.C., Reischl, J., Qaiser, T., Yeh, C.Y., 2021. Hybrid aggregation network for survival analysis from whole slide histopathological images , 731–740.
- Chang, Y.H., Thibault, G., Madin, O., Azimi, V., Meyers, C., Johnson, B., Link, J., Margolin, A., Gray, J.W., 2017b. Deep learning based nucleus classification in pancreas histological images, in: International Conference of the IEEE Engineering in Medicine and Biology Society (EMBC), IEEE. pp. 672–675.
- Chen, B., Ling, H., Zeng, X., Gao, J., Xu, Z., Fidler, S., 2020a. Scribblebox: Interactive annotation framework for video object segmentation, in: European Conference on Computer Vision, Springer. pp. 293–310.
- Chen, H., Qi, X., Yu, L., Heng, P.A., 2016a. Dcan: deep contour-aware networks for accurate gland segmentation , 2487–2496.
- Chen, K., Zhang, N., Powers, L., Roveda, J., 2019. Cell nuclei detection and segmentation for computational pathology using deep learning, in: Spring Simulation Conference (SpringSim), IEEE. pp. 1–6.
- Chen, P., Liang, Y., Shi, X., Yang, L., Gader, P., 2021a. Automatic whole slide pathology image diagnosis framework via unit stochastic selection and attention fusion. *Neurocomputing* 453, 312–325.
- Chen, R., Jing, Y., Jackson, H., 2016b. Identifying metastases in sentinel lymph nodes with deep convolutional neural networks. *arXiv preprint arXiv:1608.01658*.
- Chen, R.J., Chen, C., Li, Y., Chen, T.Y., Trister, A.D., Krishnan, R.G., Mahmood, F., 2022. Scaling vision transformers to gigapixel images via hierarchical self-supervised learning, in: Proceedings of the IEEE/CVF Conference on Computer Vision and Pattern Recognition, pp. 16144–16155.
- Chen, R.J., Lu, M.Y., Chen, T.Y., Williamson, D.F., Mahmood, F., 2021b. Synthetic data in machine learning for medicine and healthcare. *Nature Biomedical Engineering* 5, 493–497.
- Chen, R.J., Lu, M.Y., Shaban, M., Chen, C., Chen, T.Y., Williamson, D.F., Mahmood, F., 2021c. Whole slide images are 2d point clouds: Context-aware survival prediction using patch-based graph convolutional networks, in: International Conference on Medical Image Computing and Computer-Assisted Intervention, Springer. pp. 339–349.
- Chen, R.J., Lu, M.Y., Wang, J., Williamson, D.F., Rodig, S.J., Lindeman, N.I., Mahmood, F., 2020b. Pathomic fusion: an integrated framework for fusing histopathology and genomic features for cancer diagnosis and prognosis. *IEEE Transactions on Medical Imaging* .
- Chen, S., Ding, C., Tao, D., 2020c. Boundary-assisted region proposal networks for nucleus segmentation , 279–288.
- Chen, T., Kornblith, S., Norouzi, M., Hinton, G., 2020d. A simple framework for contrastive learning of visual representations, in: International conference on machine learning, PMLR. pp. 1597–1607.
- Cheng, C.L., Azhar, R., Sng, S.H.A., Chua, Y.Q., Hwang, J.S.G., Chin, J.P.F., Seah, W.K., Loke, J.C.L., Ang, R.H.L., Tan, P.H., 2016. Enabling digital pathology in the diagnostic setting: navigating through the implementation journey in an academic medical centre. *Journal of clinical pathology* 69, 784–792.
- Cheng, J., Tian, S., Yu, L., Gao, C., Kang, X., Ma, X., Wu, W., Liu, S., Lu, H., 2022. Resganet: Residual group attention network for medical image classification and segmentation. *Medical Image Analysis* 76, 102313.
- Cheng, J.Y., Abel, J.T., Balis, U.G., McClintock, D.S., Pantanowitz, L., 2021a. Challenges in the development, deployment, and regulation of artificial intelligence in anatomic pathology. *The American Journal of Pathology* 191, 1684–1692.
- Cheng, W.C., Saleheen, F., Badano, A., 2019. Assessing color performance of whole-slide imaging scanners for digital pathology. *Color Research & Application* 44, 322–334.
- Cheng, Y., Qiao, P., He, H., Song, G., Chen, J., 2021b. Hard-boundary attention network for nuclei instance segmentation , 1–7.
- Chikontwe, P., Kim, M., Nam, S.J., Go, H., Park, S.H., 2020. Multiple instance learning with center embeddings for histopathology classification, in: International Conference on Medical Image Computing and Computer-Assisted Intervention, Springer. pp. 519–528.
- Cho, H., Lim, S., Choi, G., Min, H., 2017. Neural stain-style transfer learning using gan for histopathological images. *arXiv preprint arXiv:1710.08543* .
- Cho, K.O., Lee, S.H., Jang, H.J., 2020. Feasibility of fully automated classification of whole slide images based on deep learning. *The Korean Journal of Physiology & Pharmacology* 24, 89–99.
- Christensen, K., Velkey, M., Stoolman, L.M., Hessler, L., Mosley-Brower, D., . Michigan histology and virtual microscopy learning resources - virtual slide list. URL: <https://histology.medicine.umich.edu/full-slide-list>.
- Cicalese, P.A., Mobiny, A., Yuan, P., Becker, J., Mohan, C., Nguyen, H.V., 2020. Styopath: Style-transfer data augmentation for robust histology image classification, in: Medical Image Computing and Computer Assisted Intervention – MICCAI, Springer. p. 351–361.
- Cifci, D., Foersch, S., Kather, J.N., 2022. Artificial intelligence to identify genetic alterations in conventional histopathology. *The Journal of Pathology* 257, 430–444.
- Ciga, O., Xu, T., Martel, A.L., 2022. Self supervised contrastive learning for digital histopathology. *Machine Learning with Applications* 7, 100198.
- Ciompi, F., Geessink, O., Bejnordi, B.E., De Souza, G.S., Baidoshvili, A., Litjens, G., Van Ginneken, B., Nagtegaal, I., Van Der Laak, J., 2017. The importance of stain normalization in colorectal tissue classification with convolutional networks, in: IEEE International Symposium on Biomedical Imaging, IEEE. pp. 160–163.
- Clark, K., Vendt, B., Smith, K., Freymann, J., Kirby, J., Koppel, P., Moore, S., Phillips, S., Maffitt, D., Pringle, M., et al., 2013. The cancer imaging archive (tcia): maintaining and operating a public information repository. *Journal of digital imaging* 26, 1045–1057.
- Claudio Quiros, A., Murray-Smith, R., Yuan, K., 2021. Pathologygan: Learning deep representations of cancer tissue. *Journal of Machine Learning for Biomedical Imaging* 2021, 1–48.
- Clunie, D., Hosseinzadeh, D., Wintell, M., De Mena, D., Lajara, N., Garcia-Rojo, M., Bueno, G., Saligrama, K., Stearrett, A., Toomey, D., et al., 2018. Digital imaging and communications in medicine whole slide imaging connectathon at digital pathology association pathology visions 2017. *Journal of Pathology Informatics* 9.
- Clunie, D.A., 2021. Dicom format and protocol standardization—a core requirement for digital pathology success. *Toxicologic Pathology* 49, 738–749.
- Cohen, R.J., Wheeler, T.M., Bonkhoff, H., Rubin, M.A., 2007. A proposal on the identification, histologic reporting, and implications of intraductal prostatic carcinoma. *Archives of pathology & laboratory medicine* 131, 1103–1109.
- Colling, R., Pitman, H., Oien, K., Rajpoot, N., Macklin, P., in Histopathology Working Group, C.P.A., Bachtiar, V., Booth, R., Bryant, A., Bull, J., et al.,

2019. Artificial intelligence in digital pathology: a roadmap to routine use in clinical practice. *The Journal of pathology* 249, 143–150.
- Cooper, L.A., Carter, A.B., Farris, A.B., Wang, F., Kong, J., Gutman, D.A., Widener, P., Pan, T.C., Cholleti, S.R., Sharma, A., et al., 2012. Digital pathology: Data-intensive frontier in medical imaging. *Proceedings of the IEEE* 100, 991–1003.
- Cooper, W.A., Russell, P.A., Cherian, M., Duhig, E.E., Godbolt, D., Jessup, P.J., Khoo, C., Leslie, C., Maher, A., Moffat, D.F., et al., 2017. Intra-and interobserver reproducibility assessment of pd-l1 biomarker in non-small cell lung cancer reproducibility of pd-l1 biomarker assessment in nsclc. *Clinical Cancer Research* 23, 4569–4577.
- Corredor, G., Toro, P., Bera, K., Rasmussen, D., Viswanathan, V.S., Buzzy, C., Fu, P., Barton, L.M., Stroberg, E., Duval, E., et al., 2021. Computational pathology reveals unique spatial patterns of immune response in h&e images from covid-19 autopsies: preliminary findings. *Journal of Medical Imaging* 8, 017501.
- Corvo, A., Caballero, H.S.C., Westenberg, M.A., van Driel, M.A., van Wijk, J., 2020. Visual analytics for hypothesis-driven exploration in computational pathology. *IEEE Transactions on Visualization and Computer Graphics*.
- Coudray, N., Ocampo, P.S., Sakellaropoulos, T., Narula, N., Snuderl, M., Fenyo, D., Moreira, A.L., Razavian, N., Tsirigos, A., 2018. Classification and mutation prediction from non-small cell lung cancer histopathology images using deep learning. *Nature medicine* 24, 1559–1567.
- Courtial, P., Maussion, C., Moarii, M., Pronier, E., Pilcer, S., Sefta, M., Manceron, P., Toldo, S., Zaslavskiy, M., Le Stang, N., et al., 2019. Deep learning-based classification of mesothelioma improves prediction of patient outcome. *Nature medicine* 25, 1519–1525.
- Cross, S., Furness, P., Igali, L., Snead, D., Treanor, D., 2018. Best practice recommendations for implementing digital pathology. Technical Report G162. The Royal College of Pathologists. 4th Floor 21 Prescott Street, London, United Kingdom E1 8BB.
- Cruz-Roa, A., Basavanhally, A., González, F., Gilmore, H., Feldman, M., Ganeshan, S., Shih, N., Tomaszewski, J., Madabhushi, A., 2014. Automatic detection of invasive ductal carcinoma in whole slide images with convolutional neural networks, in: *Medical Imaging: Digital Pathology*, International Society for Optics and Photonics. p. 904103.
- Cruz-Roa, A., Gilmore, H., Basavanhally, A., Feldman, M., Ganeshan, S., Shih, N., Tomaszewski, J., Madabhushi, A., González, F., 2018. High-throughput adaptive sampling for whole-slide histopathology image analysis (hashi) via convolutional neural networks: Application to invasive breast cancer detection. *PloS one* 13, e0196828.
- Cruz-Roa, A., Gilmore, H., Basavanhally, A., Feldman, M., Ganeshan, S., Shih, N.N., Tomaszewski, J., González, F.A., Madabhushi, A., 2017. Accurate and reproducible invasive breast cancer detection in whole-slide images: a deep learning approach for quantifying tumor extent. *Scientific Reports* 7, 1–14.
- Cruz-Roa, A.A., Arevalo Ovalle, J.E., Madabhushi, A., González Osorio, F.A., 2013. A deep learning architecture for image representation, visual interpretability and automated basal-cell carcinoma cancer detection , 403–410.
- Cui, M., Zhang, D.Y., 2021. Artificial intelligence and computational pathology. *Laboratory Investigation* 101, 412–422.
- Darcy, T.P., Barasch, S.P., Souers, R.J., Perrotta, P.L., 2016. Test cancellation: a college of american pathologists q-probes study. *Archives of pathology & laboratory medicine* 140, 125–129.
- Das, D.K., Bose, S., Maiti, A.K., Mitra, B., Mukherjee, G., Dutta, P.K., 2018. Automatic identification of clinically relevant regions from oral tissue histological images for oral squamous cell carcinoma diagnosis. *Tissue and Cell* 53, 111–119.
- Dastidar, T.R., Ethirajan, R., 2020. Whole slide imaging system using deep learning-based automated focusing. *Biomedical Optics Express* 11, 480–491.
- Dawood, M., Branson, K., Rajpoot, N.M., Minhas, F., 2021. Alprt: Cellular composition prediction in routine histology images, in: *IEEE/CVF International Conference on Computer Vision*, pp. 664–673.
- Deng, J., Dong, W., Socher, R., Li, L.J., Li, K., Fei-Fei, L., 2009a. Imagenet: A large-scale hierarchical image database, in: *IEEE Conference on Computer Vision and Pattern Recognition*, pp. 248–255.
- Deng, J., Dong, W., Socher, R., Li, L.J., Li, K., Fei-Fei, L., 2009b. ImageNet: A Large-Scale Hierarchical Image Database, in: *CVPR09*.
- Dennis, T., Start, R.D., Cross, S.S., 2005. The use of digital imaging, video conferencing, and telepathology in histopathology: a national survey. *Journal of Clinical Pathology* 58, 254–258.
- Deshpande, S., Minhas, F., Graham, S., Rajpoot, N., 2022. Safron: Stitching across the frontier network for generating colorectal cancer histology images. *Medical Image Analysis* 77, 102337.
- Diao, J.A., Chen, R.J., Kvedar, J.C., 2021a. Efficient cellular annotation of histopathology slides with real-time ai augmentation.
- Diao, J.A., Chui, W.F., Wang, J.K., Mitchell, R.N., Rao, S.K., Resnick, M.B., Lahiri, A., Maheshwari, C., Glass, B., Mountain, V., et al., 2020. Dense, high-resolution mapping of cells and tissues from pathology images for the interpretable prediction of molecular phenotypes in cancer. *bioRxiv*.
- Diao, J.A., Wang, J.K., Chui, W.F., Mountain, V., Gullapally, S.C., Srinivasan, R., Mitchell, R.N., Glass, B., Hoffman, S., Rao, S.K., et al., 2021b. Human-interpretable image features derived from densely mapped cancer pathology slides predict diverse molecular phenotypes. *Nature communications* 12, 1–15.
- Dimitropoulos, K., Barmoutis, P., Zioga, C., Kamas, A., Patsiaoura, K., Grammalidis, N., 2017. Grading of invasive breast carcinoma through grassmannian vlad encoding. *PloS one* 12, e0185110.
- Dogar, G.M., Fraz, M.M., Javed, S., 2021. Feature attention network for simultaneous nuclei instance segmentation and classification in histology images , 1–6.
- Dong, F., Irshad, H., Oh, E.Y., Lerwill, M.F., Brachtel, E.F., Jones, N.C., Knoblauch, N.W., Montaser-Kouhsari, L., Johnson, N.B., Rao, L.K., et al., 2014. Computational pathology to discriminate benign from malignant intraductal proliferations of the breast. *PloS one* 9, e114885.
- Dong, N., Kampffmeyer, M., Liang, X., Wang, Z., Dai, W., Xing, E., 2018. Reinforced auto-zoom net: Towards accurate and fast breast cancer segmentation in whole-slide images, in: *Deep Learning in Medical Image Analysis and Multimodal Learning for Clinical Decision Support*. Springer, pp. 317–325.
- Dosovitskiy, A., Beyer, L., Kolesnikov, A., Weissenborn, D., Zhai, X., Unterthiner, T., Dehghani, M., Minderer, M., Heigold, G., Gelly, S., et al., . An image is worth 16x16 words: Transformers for image recognition at scale, in: *International Conference on Learning Representations*.
- Dowsett, M., Nielsen, T.O., A'Hern, R., Bartlett, J., Coombes, R.C., Cuzick, J., Ellis, M., Henry, N.L., Hugh, J.C., Lively, T., et al., 2011. Assessment of ki67 in breast cancer: recommendations from the international ki67 in breast cancer working group. *Journal of the National cancer Institute* 103, 1656–1664.
- Doyle, S., Feldman, M.D., Shih, N., Tomaszewski, J., Madabhushi, A., 2012. Cascaded discrimination of normal, abnormal, and confounder classes in histopathology: Gleason grading of prostate cancer. *BMC bioinformatics* 13, 1–15.
- Doyle, S., Monaco, J., Feldman, M., Tomaszewski, J., Madabhushi, A., 2011. An active learning based classification strategy for the minority class problem: application to histopathology annotation. *BMC bioinformatics* 12, 1–14.
- Echle, A., Rindtorff, N.T., Brinker, T.J., Luedde, T., Pearson, A.T., Kather, J.N., 2021. Deep learning in cancer pathology: a new generation of clinical biomarkers. *British journal of cancer* 124, 686–696.
- van Eekelen, L., Pinckaers, H., Hebeda, K.M., Litjens, G., 2020. Multi-class semantic cell segmentation and classification of aplasia in bone marrow histology images 11320, 113200B.
- Ehteshami Bejnordi, B., Mullooly, M., Pfeiffer, R.M., Fan, S., Vacek, P.M., Weaver, D.L., Herschorn, S., Brinton, L.A., van Ginneken, B., Karssemeijer, N., et al., 2018. Using deep convolutional neural networks to identify and classify tumor-associated stroma in diagnostic breast biopsies. *Modern Pathology* 31, 1502–1512.
- Eminaga, O., Abbas, M., Kunder, C., Loening, A.M., Shen, J., Brooks, J.D., Langlotz, C.P., Rubin, D.L., 2019. Plexus convolutional neural network (plexusnet): A novel neural network architecture for histologic image analysis. *arXiv preprint arXiv:1908.09067*.
- Epstein, J.I., 2011. Prognostic significance of tumor volume in radical prostatectomy and needle biopsy specimens. *The Journal of urology* 186, 790–797.
- Ertsosun, M.G., Rubin, D.L., 2015. Automated grading of gliomas using deep learning in digital pathology images: a modular approach with ensemble of convolutional neural networks, in: *AMIA Annual Symposium Proceedings*, American Medical Informatics Association. p. 1899.
- Esteva, A., Kuprel, B., Novoa, R.A., Ko, J., Swetter, S.M., Blau, H.M., Thrun, S., 2017. Dermatologist-level classification of skin cancer with deep neural networks. *nature* 542, 115–118.
- Evans, A.J., Bauer, T.W., Bui, M.M., Cornish, T.C., Duncan, H., Glassy, E.F., Hipp, J., McGee, R.S., Murphy, D., Myers, C., et al., 2018. Us food and drug

- administration approval of whole slide imaging for primary diagnosis: a key milestone is reached and new questions are raised. *Archives of pathology & laboratory medicine* 142, 1383–1387.
- Failmezger, H., Muralidhar, S., Rullan, A., de Andrea, C.E., Sahai, E., Yuan, Y., 2020. Topological tumor graphs: a graph-based spatial model to infer stromal recruitment for immunosuppression in melanoma histology. *Cancer research* 80, 1199–1209.
- Farahani, H., Boschman, J., Farnell, D., Darbandsari, A., Zhang, A., Ahmadvand, P., Jones, S.J., Huntsman, D., Köbel, M., Gilks, C.B., et al., 2022. Deep learning-based histotype diagnosis of ovarian carcinoma whole-slide pathology images. *Modern Pathology* 35, 1983–1990.
- Farahmand, S., Fernandez, A.I., Ahmed, F.S., Rimm, D.L., Chuang, J.H., Reisenbichler, E., Zarringhalam, K., 2022. Deep learning trained on hematoxylin and eosin tumor region of interest predicts her2 status and trastuzumab treatment response in her2+ breast cancer. *Modern Pathology* 35, 44–51.
- Faust, K., Bala, S., Van Ommeren, R., Portante, A., Al Qawahmed, R., Djuric, U., Diamandis, P., 2019. Intelligent feature engineering and ontological mapping of brain tumour histomorphologies by deep learning. *Nature Machine Intelligence* 1, 316–321.
- Feng, C., Vanderbilt, C., Fuchs, T., 2021a. Nuc2vec: Learning representations of nuclei in histopathology images with contrastive loss , 179–189.
- Feng, R., Liu, X., Chen, J., Chen, D.Z., Gao, H., Wu, J., 2020. A deep learning approach for colonoscopy pathology wsi analysis: accurate segmentation and classification. *IEEE Journal of Biomedical and Health Informatics* 25, 3700–3708.
- Feng, Z., Wang, Z., Wang, X., Mao, Y., Li, T., Lei, J., Wang, Y., Song, M., 2021b. Mutual-complementing framework for nuclei detection and segmentation in pathology image, in: *Proceedings of the IEEE/CVF International Conference on Computer Vision*, pp. 4036–4045.
- Fischer, W., Moudgalya, S.S., Cohn, J.D., Nguyen, N.T., Kenyon, G.T., 2018. Sparse coding of pathology slides compared to transfer learning with deep neural networks. *BMC bioinformatics* 19, 9–17.
- Fitzgibbons, C., 2021. Protocol for the examination of resection specimens from patients with ductal carcinoma in situ (dcis) of the breast. URL: https://documents.cap.org/protocols/Breast.DCIS_4.4.0.0.REL_CAPCP.pdf.
- Folmsbee, J., Liu, X., Brandwein-Weber, M., Doyle, S., 2018. Active deep learning: Improved training efficiency of convolutional neural networks for tissue classification in oral cavity cancer, in: *IEEE International Symposium on Biomedical Imaging*, IEEE. pp. 770–773.
- Foucart, A., Debeir, O., Decaestecker, C., 2019. Snow: Semi-supervised, noisy and/or weak data for deep learning in digital pathology, in: *IEEE International Symposium on Biomedical Imaging*, IEEE. pp. 1869–1872.
- Frankel, A.O., Lathara, M., Shaw, C.Y., Wogmon, O., Jackson, J.M., Clark, M.M., Eshraghi, N., Keenen, S.E., Woods, A.D., Purohit, R., et al., 2022. Machine learning for rhabdomyosarcoma histopathology. *Modern Pathology* , 1–11.
- Freyre, C.A., Spiegel, S., Gubser Keller, C., Vandemeulebroecke, M., Hoefling, H., Dubost, V., Cörek, E., Moulin, P., Hossain, I., 2021. Biomarker-based classification and localization of renal lesions using learned representations of histology—a machine learning approach to histopathology. *Toxicologic Pathology* 49, 798–814.
- Fuchs, T.J., Wild, P.J., Moch, H., Buhmann, J.M., 2008. Computational pathology analysis of tissue microarrays predicts survival of renal clear cell carcinoma patients , 1–8.
- Gadermayr, M., Dombrowski, A.K., Klinkhammer, B.M., Boor, P., Merhof, D., 2019. Cnn cascades for segmenting sparse objects in gigapixel whole slide images. *Computerized Medical Imaging and Graphics* 71, 40–48.
- Gallego, J., Swiderska-Chadaj, Z., Markiewicz, T., Yamashita, M., Gabaldon, M.A., Gertych, A., 2021. A u-net based framework to quantify glomerulosclerosis in digitized pas and h&e stained human tissues. *Computerized Medical Imaging and Graphics* 89, 101865.
- Galván, E., Mooney, P., 2021. Neuroevolution in deep neural networks: Current trends and future challenges. *IEEE Transactions on Artificial Intelligence* 2, 476–493.
- Gamper, J., Koohbanani, N.A., Benet, K., Khurram, A., Rajpoot, N., 2019. Pan-nuke: an open pan-cancer histology dataset for nuclei instance segmentation and classification, in: *European Congress on Digital Pathology*, Springer. pp. 11–19.
- Gamper, J., Koohbanani, N.A., Graham, S., Jahanifar, M., Khurram, S.A., Azam, A., Hewitt, K., Rajpoot, N.M., 2020a. Pannuke dataset extension, insights and baselines. *CoRR* abs/2003.10778.
- Gamper, J., Koohbanani, N.A., Rajpoot, N., 2020b. Multi-task learning in histo-pathology for widely generalizable model. *arXiv preprint arXiv:2005.08645*.
- Gandomkar, Z., Brennan, P.C., Mello-Thoms, C., 2018. Mudern: Multi-category classification of breast histopathological image using deep residual networks. *Artificial intelligence in medicine* 88, 14–24.
- Gao, Y., Dong, Y., Zhou, Y., Chen, G., Hong, X., Zhang, Q., et al., 2022. Peripheral tumor location predicts a favorable prognosis in patients with resected small cell lung cancer. *International Journal of Clinical Practice* 2022.
- Gao, Z., Hong, B., Zhang, X., Li, Y., Jia, C., Wu, J., Wang, C., Meng, D., Li, C., 2021. Instance-based vision transformer for subtyping of papillary renal cell carcinoma in histopathological image, in: *International Conference on Medical Image Computing and Computer-Assisted Intervention*, Springer. pp. 299–308.
- Garon, E.B., Rizvi, N.A., Hui, R., Leighl, N., Balmanoukian, A.S., Eder, J.P., Patnaik, A., Aggarwal, C., Gubens, M., Horn, L., et al., 2015. Pembrolizumab for the treatment of non-small-cell lung cancer. *New England Journal of Medicine* 372, 2018–2028.
- Gehan, E.A., Walker, M.D., 1977. Prognostic factors for patients with brain tumors. *National Cancer Inst Monograph* 46, 189–195.
- Genovese, A., Hosseini, M.S., Piuri, V., Plataniotis, K.N., Scotti, F., 2021. Histopathological transfer learning for acute lymphoblastic leukemia detection, in: *2021 IEEE International Conference on Computational Intelligence and Virtual Environments for Measurement Systems and Applications (CIVEMSA)*, IEEE. pp. 1–6.
- Geread, R.S., Sivanandarajah, A., Brouwer, E.R., Wood, G.A., Androutsov, D., Faragalla, H., Khademi, A., 2021. pinet—an automated proliferation index calculator framework for ki67 breast cancer images. *Cancers* 13, 11.
- Gertych, A., Swiderska-Chadaj, Z., Ma, Z., Markiewicz, T., Cierniak, S., Salemi, H., Guzman, S., Walts, A.E., Knudsen, B.S., et al., 2019. Convolutional neural networks can accurately distinguish four histologic growth patterns of lung adenocarcinoma in digital slides. *Scientific Reports* 9, 1–12.
- Ghahremani, P., Marino, J., Dodds, R., Nadeem, S., 2022. Deeplif: An online platform for quantification of clinical pathology slides, in: *Proceedings of the IEEE/CVF Conference on Computer Vision and Pattern Recognition*, pp. 21399–21405.
- GHaznavi, F., Evans, A., Madabhushi, A., Feldman, M., 2013. Digital imaging in pathology: whole-slide imaging and beyond. *Annual Review of Pathology: Mechanisms of Disease* 8, 331–359.
- Gildenblat, J., Klaiman, E., 2019. Self-supervised similarity learning for digital pathology. *arXiv preprint arXiv:1905.08139*.
- Giuste, F., Venkatesan, M., Zhao, C., Tong, L., Zhu, Y., Deshpande, S.R., Wang, M.D., 2020. Automated classification of acute rejection from endomyocardial biopsies, in: *Proceedings of the 11th ACM International Conference on Bioinformatics, Computational Biology and Health Informatics*, pp. 1–9.
- Go, H., 2022. Digital pathology and artificial intelligence applications in pathology. *Brain Tumor Research and Treatment* 10, 76.
- Godinho, T.M., Lebre, R., Silva, L.B., Costa, C., 2017. An efficient architecture to support digital pathology in standard medical imaging repositories. *Journal of biomedical informatics* 71, 190–197.
- Gomez, D., Zaitoun, A.M., De Rosa, A., Hossaini, S., Beckingham, I.J., Brooks, A., Cameron, I.C., 2014. Critical review of the prognostic significance of pathological variables in patients undergoing resection for colorectal liver metastases. *HPB* 16, 836–844.
- Goodman, Z.D., 2007. Neoplasms of the liver. *Modern Pathology* 20, S49–S60.
- Graham, S., Chen, H., Gamper, J., Dou, Q., Heng, P.A., Snead, D., Tsang, Y.W., Rajpoot, N., 2019a. Mild-net: Minimal information loss dilated network for gland instance segmentation in colon histology images. *Medical Image Analysis* 52, 199–211.
- Graham, S., Epstein, D., Rajpoot, N., 2020. Dense steerable filter cnns for exploiting rotational symmetry in histology images. *IEEE Transactions on Medical Imaging* 39, 4124–4136.
- Graham, S., Jahanifar, M., Azam, A., Nimir, M., Tsang, Y.W., Dodd, K., Hero, E., Sahota, H., Tank, A., Benes, K., et al., 2021. Lizard: A large-scale dataset for colonic nuclear instance segmentation and classification, in: *IEEE/CVF International Conference on Computer Vision*, pp. 684–693.
- Graham, S., Shaban, M., Qaiser, T., Koohbanani, N.A., Khurram, S.A., Rajpoot, N., 2018. Classification of lung cancer histology images using patch-level summary statistics, in: *Medical Imaging: Digital Pathology*, International Society for Optics and Photonics. p. 1058119.
- Graham, S., Vu, Q.D., Raza, S.E.A., Azam, A., Tsang, Y.W., Kwak, J.T., Rajpoot, N., 2019b. Hover-net: Simultaneous segmentation and classification

- of nuclei in multi-tissue histology images. *Medical Image Analysis* 58, 101563.
- Griffin, G., Holub, A., Perona, P., 2007. Caltech-256 object category dataset .
- Griffin, J., Treanor, D., 2017. Digital pathology in clinical use: where are we now and what is holding us back? *Histopathology* 70, 134–145.
- Großerueschkamp, F., Jütte, H., Gerwert, K., Tannapfel, A., 2021. Advances in digital pathology: from artificial intelligence to label-free imaging. *Visceral Medicine*, 1–9.
- Grossman, R.L., Heath, A.P., Ferretti, V., Varmus, H.E., Lowy, D.R., Kibbe, W.A., Staudt, L.M., 2016. Toward a shared vision for cancer genomic data. *New England Journal of Medicine* 375, 1109–1112.
- Gu, H., Huang, J., Hung, L., Chen, X., 2021. Lessons learned from designing an ai-enabled diagnosis tool for pathologists. *Proceedings of the ACM on Human-Computer Interaction* 5, 1–25.
- Guan, Y., Zhang, J., Tian, K., Yang, S., Dong, P., Xiang, J., Yang, W., Huang, J., Zhang, Y., Han, X., 2022. Node-aligned graph convolutional network for whole-slide image representation and classification, in: *Proceedings of the IEEE/CVF Conference on Computer Vision and Pattern Recognition*, pp. 18813–18823.
- Gueréndel, C., Arnold, P., Torben-Nielsen, B., 2021. Creating small but meaningful representations of digital pathology images, in: *MICCAI Workshop on Computational Pathology*, PMLR. pp. 206–215.
- Guerrero, R.E.D., Oliveira, J.L., 2021. Improvements in lymphocytes detection using deep learning with a preprocessing stage , 178–182.
- Gunduz-Demir, C., Kandemir, M., Tosun, A.B., Sokmensuer, C., 2010. Automatic segmentation of colon glands using object-graphs. *Medical image analysis* 14, 1–12.
- Guo, C.C., Epstein, J.I., 2006. Intraductal carcinoma of the prostate on needle biopsy: histologic features and clinical significance. *Modern pathology* 19, 1528–1535.
- Guo, X., Wang, F., Teodoro, G., Farris, A.B., Kong, J., 2019. Liver steatosis segmentation with deep learning methods, in: *IEEE International Symposium on Biomedical Imaging*, pp. 24–27.
- Gupta, P., Huang, Y., Sahoo, P.K., You, J.F., Chiang, S.F., Onthoni, D.D., Chern, Y.J., Chao, K.Y., Chiang, J.M., Yeh, C.Y., et al., 2021. Colon tissues classification and localization in whole slide images using deep learning. *Diagnostics* 11, 1398.
- Gurcan, M.N., Madabhushi, A., Rajpoot, N., 2010. Pattern recognition in histopathological images: An icpr 2010 contest, in: *International Conference on Pattern Recognition*, Springer. pp. 226–234.
- Hadsell, R., Chopra, S., LeCun, Y., 2006. Dimensionality reduction by learning an invariant mapping, in: *IEEE Computer Society Conference on Computer Vision and Pattern Recognition (CVPR'06)*, IEEE. pp. 1735–1742.
- Hägele, M., Seegerer, P., Lapuschkin, S., Bockmayr, M., Samek, W., Klauschen, F., Müller, K.R., Binder, A., 2020. Resolving challenges in deep learning-based analyses of histopathological images using explanation methods. *Scientific Reports* 10, 1–12.
- Haggenmüller, S., Maron, R.C., Hekler, A., Utikal, J.S., Barata, C., Barnhill, R.L., Beltraminelli, H., Berking, C., Betz-Stablein, B., Blum, A., et al., 2021. Skin cancer classification via convolutional neural networks: systematic review of studies involving human experts. *European Journal of Cancer* 156, 202–216.
- Hameed, Z., Garcia-Zapirain, B., Aguirre, J.J., Isaza-Ruget, M.A., 2022. Multiclass classification of breast cancer histopathology images using multilevel features of deep convolutional neural network. *Scientific Reports* 12, 1–21.
- Han, Z., Wei, B., Zheng, Y., Yin, Y., Li, K., Li, S., 2017. Breast cancer multi-classification from histopathological images with structured deep learning model. *Scientific Reports* 7, 1–10.
- Hanna, M.G., Reuter, V.E., Hameed, M.R., Tan, L.K., Chiang, S., Sigel, C., Hollmann, T., Giri, D., Samboy, J., Moradel, C., et al., 2019. Whole slide imaging equivalency and efficiency study: experience at a large academic center. *Modern Pathology* 32, 916–928.
- Hao, J., Kosaraju, S.C., Tsaku, N.Z., Song, D.H., Kang, M., 2019. Page-net: interpretable and integrative deep learning for survival analysis using histopathological images and genomic data, in: *Pacific Symposium on Bio-computing*, World Scientific. pp. 355–366.
- Harder, N., Schönmeyer, R., Nekolla, K., Meier, A., Brieu, N., Vanegas, C., Madonna, G., Capone, M., Botti, G., Ascierto, P.A., et al., 2019. Automatic discovery of image-based signatures for ipilimumab response prediction in malignant melanoma. *Scientific Reports* 9, 1–19.
- Hart, S.N., Flotte, W., Norgan, A.P., Shah, K.K., Buchan, Z.R., Mounajjid, T., Flotte, T.J., 2019. Classification of melanocytic lesions in selected and whole-slide images via convolutional neural networks. *Journal of Pathology Informatics* 10.
- Hartman, D.J., Van Der Laak, J.A., Gurcan, M.N., Pantanowitz, L., 2020. Value of public challenges for the development of pathology deep learning algorithms. *Journal of Pathology Informatics* 11.
- Healey, M.A., Hirko, K.A., Beck, A.H., Collins, L.C., Schnitt, S.J., Eliassen, A.H., Holmes, M.D., Tamimi, R.M., Hazra, A., 2017. Assessment of ki67 expression for breast cancer subtype classification and prognosis in the nurses' health study. *Breast cancer research and treatment* 166, 613–622.
- Hegde, N., Hipp, J.D., Liu, Y., Emmert-Buck, M., Reif, E., Smilkov, D., Terry, M., Cai, C.J., Amin, M.B., Mermel, C.H., et al., 2019. Similar image search for histopathology: Smily. *NPJ Digital Medicine* 2, 1–9.
- Hekler, A., Utikal, J.S., Enk, A.H., Solass, W., Schmitt, M., Klode, J., Schaden-dorf, D., Sondermann, W., Franklin, C., Bestvater, F., et al., 2019. Deep learning outperformed 11 pathologists in the classification of histopathological melanoma images. *European Journal of Cancer* 118, 91–96.
- Hermsen, M., de Bel, T., Den Boer, M., Steenbergen, E.J., Kers, J., Florquin, S., Roelofs, J.J., Stegall, M.D., Alexander, M.P., Smith, B.H., et al., 2019. Deep learning-based histopathologic assessment of kidney tissue. *Journal of the American Society of Nephrology* 30, 1968–1979.
- Herrmann, M.D., Clunie, D.A., Fedorov, A., Doyle, S.W., Pieper, S., Kleipeis, V., Le, L.P., Mutter, G.L., Milstone, D.S., Schultz, T.J., et al., 2018. Implementing the dicom standard for digital pathology. *Journal of Pathology Informatics* 9.
- Hewer, E., 2020. The oncologist's guide to synoptic reporting: a primer. *Oncology* 98, 396–402.
- Ho, D.J., Agaram, N.P., Schüffler, P.J., Vanderbilt, C.M., Jean, M.H., Hameed, M.R., Fuchs, T.J., 2020. Deep interactive learning: an efficient labeling approach for deep learning-based osteosarcoma treatment response assessment, in: *International Conference on Medical Image Computing and Computer-Assisted Intervention*, Springer. pp. 540–549.
- Ho, D.J., Yarlagadda, D.V., D'Alfonso, T.M., Hanna, M.G., Grabenstetter, A., Ntiamoah, P., Brogi, E., Tan, L.K., Fuchs, T.J., 2021. Deep multi-magnification networks for multi-class breast cancer image segmentation. *Computerized Medical Imaging and Graphics* 88, 101866.
- Höhn, J., Krieghoff-Henning, E., Jutzi, T.B., von Kalle, C., Utikal, J.S., Meier, F., Gellrich, F.F., Hobelsberger, S., Hauschild, A., Schlager, J.G., et al., 2021. Combining cnn-based histologic whole slide image analysis and patient data to improve skin cancer classification. *European Journal of Cancer* 149, 94–101.
- Höhne, J., de Zoete, J., Schmitz, A.A., Bal, T., di Tomaso, E., Lenga, M., 2021. Detecting genetic alterations in braf and ntrk as oncogenic drivers in digital pathology images: towards model generalization within and across multiple thyroid cohorts , 105–116.
- Holland, L., Wei, D., Olson, K.A., Mitra, A., Graff, J.P., Jones, A.D., Durbin-Johnson, B., Mitra, A.D., Rashidi, H.H., 2020. Limited number of cases may yield generalizable models, a proof of concept in deep learning for colon histology. *Journal of Pathology Informatics* 11.
- Hollandi, R., Diósdí, Á., Hollandi, G., Moshkov, N., Horváth, P., 2020. Annotatorj: an imagej plugin to ease hand annotation of cellular compartments. *Molecular biology of the cell* 31, 2179–2186.
- Hossain, M.S., Nakamura, T., Kimura, F., Yagi, Y., Yamaguchi, M., 2018. Practical image quality evaluation for whole slide imaging scanner, in: *Biomedical Imaging and Sensing Conference*, International Society for Optics and Photonics. p. 107111S.
- Hosseini, M.S., Chan, L., Huang, W., Wang, Y., Hasan, D., Rowsell, C., Damaskinos, S., Plataniotis, K.N., 2020. On transferability of histological tissue labels in computational pathology, in: *European Conference on Computer Vision*, Springer. pp. 453–469.
- Hosseini, M.S., Chan, L., Tse, G., Tang, M., Deng, J., Norouzi, S., Rowsell, C., Plataniotis, K.N., Damaskinos, S., 2019. Atlas of digital pathology: A generalized hierarchical histological tissue type-annotated database for deep learning, in: *IEEE Conference on Computer Vision and Pattern Recognition*, pp. 11747–11756.
- Hou, L., Agarwal, A., Samaras, D., Kure, T.M., Gupta, R.R., Saltz, J.H., 2019a. Robust histopathology image analysis: to label or to synthesize? , 8533–8542.
- Hou, L., Gupta, R., Van Arnam, J.S., Zhang, Y., Sivalenka, K., Samaras, D., Kure, T.M., Saltz, J.H., 2020a. Dataset of segmented nuclei in hematoxylin and eosin stained histopathology images of ten cancer types. *Scientific data* 7, 1–12.
- Hou, L., Gupta, R., Van Arnam, J.S., Zhang, Y., Sivalenka, K., Samaras, D.,

- Kurc, T.M., Saltz, J.H., 2020b. Dataset of segmented nuclei in hematoxylin and eosin stained histopathology images of ten cancer types. *Scientific data* 7, 1–12.
- Hou, L., Nguyen, V., Kanevsky, A.B., Samaras, D., Kurc, T.M., Zhao, T., Gupta, R.R., Gao, Y., Chen, W., Foran, D., et al., 2019b. Sparse autoencoder for unsupervised nucleus detection and representation in histopathology images. *Pattern Recognition Letters* 86, 188–200.
- Hou, L., Samaras, D., Kurc, T.M., Gao, Y., Davis, J.E., Saltz, J.H., 2016. Patch-based convolutional neural network for whole slide tissue image classification, in: *Proceedings of the IEEE conference on computer vision and pattern recognition*, pp. 2424–2433.
- Hu, B., Tang, Y., Eric, I., Chang, C., Fan, Y., Lai, M., Xu, Y., 2018. Unsupervised learning for cell-level visual representation in histopathology images with generative adversarial networks. *IEEE Journal of Biomedical and Health Informatics* 23, 1316–1328.
- Huang, Y., Chung, A., 2019. Evidence localization for pathology images using weakly supervised learning, in: *International Conference on Medical Image Computing and Computer-Assisted Intervention*, Springer, pp. 613–621.
- Huang, Y., Chung, A.C.S., 2018. Improving high resolution histology image classification with deep spatial fusion network, in: *Computational Pathology and Ophthalmic Medical Image Analysis*. Springer, pp. 19–26.
- Huo, Y., Deng, R., Liu, Q., Fogo, A.B., Yang, H., 2021. Ai applications in renal pathology. *Kidney international* 99, 1309–1320.
- Häggström, M., 2021. Chromogenic immunohistochemistry for calponin in sclerosing adenosis. URL: https://commons.wikimedia.org/wiki/File:Chromogenic_immunohistochemistry_for_calponin_in_sclerosing_adenosis.jpg.
- Iakovidis, D.K., Georgakopoulos, S.V., Vasilakakis, M., Koulaouzidis, A., Plagianakos, V.P., 2018. Detecting and locating gastrointestinal anomalies using deep learning and iterative cluster unification. *IEEE Transactions on Medical Imaging* 37, 2196–2210.
- Ianni, J.D., Soans, R.E., Sankarapandian, S., Chamarthi, R.V., Ayyagari, D., Olsen, T.G., Bonham, M.J., Stavish, C.C., Motaparthi, K., Cockerell, C.J., et al., 2020. Tailored for real-world: a whole slide image classification system validated on uncurated multi-site data emulating the prospective pathology workload. *Scientific Reports* 10, 1–12.
- Ildahcen, F., Himmi, M.M., Mahmoudi, A., 2020. Cnn-based approach for cervical cancer classification in whole-slide histopathology images. *arXiv preprint arXiv:2005.13924*.
- Iesmantas, T., Alzbutas, R., 2018. Convolutional capsule network for classification of breast cancer histology images, in: *International Conference Image Analysis and Recognition*, Springer, pp. 853–860.
- Iizuka, O., Kanavati, F., Kato, K., Rambeau, M., Arihiro, K., Tsuneki, M., 2020. Deep learning models for histopathological classification of gastric and colonic epithelial tumours. *Scientific Reports* 10, 1–11.
- Indu, M., Rathy, R., Binu, M., 2016. “slide less pathology”: Fairy tale or reality? *Journal of oral and maxillofacial pathology: JOMFP* 20, 284.
- Institute, N.C., a. Cancer stat facts: Common cancer sites. Available at: <https://seer.cancer.gov/statfacts/html/common.html> (accessed Feb 12, 2023).
- Institute, N.C., b. Cancer stat facts: Ovarian cancer. Available at: <https://seer.cancer.gov/statfacts/html/ovary.html> (accessed Feb 14, 2023).
- Isaacs, M., Lennerz, J.K., Yates, S., Clermont, W., Rossi, J., Pfeifer, J.D., 2011. Implementation of whole slide imaging in surgical pathology: A value added approach. *Journal of Pathology Informatics* 2, 39.
- Ito, Y., Vertosick, E.A., Sjoberg, D.D., Vickers, A.J., Al-Ahmadie, H.A., Chen, Y.B., Gopalan, A., Sirintrapan, S.J., Tickoo, S.K., Eastham, J.A., et al., 2019. In organ-confined prostate cancer, tumor quantitation not found to aid in prediction of biochemical recurrence. *The American journal of surgical pathology* 43, 1061.
- Jaber, M.I., Song, B., Taylor, C., Vaske, C.J., Benz, S.C., Rabizadeh, S., Soon-Shiong, P., Szeto, C.W., 2020. A deep learning image-based intrinsic molecular subtype classifier of breast tumors reveals tumor heterogeneity that may affect survival. *Breast Cancer Research* 22, 1–10.
- Jahanifar, M., Tajeddin, N.Z., Koohbanani, N.A., Rajpoot, N.M., 2021. Robust interactive semantic segmentation of pathology images with minimal user input, in: *IEEE/CVF International Conference on Computer Vision*, pp. 674–683.
- Jahn, S.W., Plass, M., Moinfar, F., 2020. Digital pathology: advantages, limitations and emerging perspectives. *Journal of Clinical Medicine* 9, 3697.
- Janowczyk, A., Doyle, S., Gilmore, H., Madabhushi, A., 2018. A resolution adaptive deep hierarchical (radical) learning scheme applied to nuclear segmentation of digital pathology images. *Computer Methods in Biomechanics and Biomedical Engineering: Imaging & Visualization* 6, 270–276.
- Janowczyk, A., Madabhushi, A., 2016. Deep learning for digital pathology image analysis: A comprehensive tutorial with selected use cases. *Journal of Pathology Informatics* 7.
- Jara-Lazaro, A.R., Thamboo, T.P., Teh, M., Tan, P.H., 2010. Digital pathology: exploring its applications in diagnostic surgical pathology practice. *Pathology* 42, 512–518.
- Jaume, G., Pati, P., Anklin, V., Foncubierta, A., Gabrani, M., 2021a. *Histo-cartography: A toolkit for graph analytics in digital pathology*, in: *MICCAI Workshop on Computational Pathology*, PMLR, pp. 117–128.
- Jaume, G., Pati, P., Bozorgtabar, B., Foncubierta, A., Anniciello, A.M., Ferroce, F., Rau, T., Thiran, J.P., Gabrani, M., Goksel, O., 2021b. Quantifying explainers of graph neural networks in computational pathology, in: *IEEE/CVF Conference on Computer Vision and Pattern Recognition*, pp. 8106–8116.
- Jaume, G., Pati, P., Foncubierta-Rodríguez, A., Ferroce, F., Scognamiglio, G., Anniciello, A.M., Thiran, J.P., Goksel, O., Gabrani, M., 2020. Towards explainable graph representations in digital pathology, in: *ICML*, pp. 1–5.
- Javed, S., Mahmood, A., Dias, J., Werghi, N., Rajpoot, N., 2021. Spatially constrained context-aware hierarchical deep correlation filters for nucleus detection in histology images. *Medical Image Analysis* 72, 102104.
- Javed, S., Mahmood, A., Fraz, M.M., Koohbanani, N.A., Benes, K., Tsang, Y.W., Hewitt, K., Epstein, D., Snead, D., Rajpoot, N., 2020. Cellular community detection for tissue phenotyping in colorectal cancer histology images. *Medical Image Analysis* 63, 101696.
- Jayachandran, S., Ghosh, A., 2020. Deep transfer learning for texture classification in colorectal cancer histology, in: *IAPR Workshop on Artificial Neural Networks in Pattern Recognition*, Springer, pp. 173–186.
- Jewsbury, R., Bhalerao, A., Rajpoot, N.M., 2021. A quadtree image representation for computational pathology, in: *IEEE/CVF International Conference on Computer Vision*, pp. 648–656.
- Ji, M.Y., Yuan, L., Lu, S.M., Gao, M.T., Zeng, Z., Zhan, N., Ding, Y.J., Liu, Z.R., Huang, P.X., Lu, C., et al., 2020. Glandular orientation and shape determined by computational pathology could identify aggressive tumor for early colon carcinoma: a triple-center study. *Journal of translational medicine* 18, 1–12.
- Jiang, C., Liao, J., Dong, P., Ma, Z., Cai, D., Zheng, G., Liu, Y., Bu, H., Yao, J., 2020a. Blind deblurring for microscopic pathology images using deep learning networks. *CoRR abs/2011.11879*.
- Jiang, Y., Chen, L., Zhang, H., Xiao, X., 2019. Breast cancer histopathological image classification using convolutional neural networks with small se-resnet module. *PLoS one* 14, e0214587.
- Jiang, Y., Xiong, J., Li, H., Yang, X., Yu, W., Gao, M., Zhao, X., Ma, Y., Zhang, W., Guan, Y., et al., 2020b. Recognizing basal cell carcinoma on smartphone-captured digital histopathology images with a deep neural network. *British Journal of Dermatology* 182, 754–762.
- Jiang, Y., Yang, M., Wang, S., Li, X., Sun, Y., 2020c. Emerging role of deep learning-based artificial intelligence in tumor pathology. *Cancer communications* 40, 154–166.
- Jiménez, G., Racocceanu, D., 2019. Deep learning for semantic segmentation versus classification in computational pathology: Application to mitosis analysis in breast cancer grading. *Frontiers in Bioengineering and Biotechnology* 7, 145.
- Kainz, P., Urschler, M., Schulter, S., Wohlhart, P., Lepetit, V., 2015. You should use regression to detect cells, in: *International Conference on Medical Image Computing and Computer-Assisted Intervention*, Springer, pp. 276–283.
- Kairouz, P., McMahan, H.B., Avent, B., Bellet, A., Bennis, M., Bhagoji, A.N., Bonawitz, K., Charles, Z., Cormode, G., Cummings, R., et al., 2021. Advances and open problems in federated learning. *Foundations and Trends® in Machine Learning* 14, 1–210.
- Kalra, S., Tizhoosh, H.R., Shah, S., Choi, C., Damaskinos, S., Safarpoor, A., Shafiei, S., Babaie, M., Diamandis, P., Campbell, C.J., et al., 2020. Pan-cancer diagnostic consensus through searching archival histopathology images using artificial intelligence. *NPJ Digital Medicine* 3, 1–15.
- Kannan, S., Morgan, L.A., Liang, B., Cheung, M.G., Lin, C.Q., Mun, D., Nader, R.G., Belghasem, M.E., Henderson, J.M., Francis, J.M., et al., 2019. Segmentation of glomeruli within trichrome images using deep learning. *Kidney international reports* 4, 955–962.
- Kanwal, N., Pérez-Bueno, F., Schmidt, A., Engan, K., Molina, R., 2022. The devil is in the details: Whole slide image acquisition and processing for artifacts detection, color variation, and data augmentation: A review. *IEEE Access* 10, 58821–58844.

- Karimi, D., Nir, G., Fazli, L., Black, P.C., Goldenberg, L., Salcudean, S.E., 2019. Deep learning-based gleason grading of prostate cancer from histopathology images—role of multiscale decision aggregation and data augmentation. *IEEE Journal of Biomedical and Health Informatics* 24, 1413–1426.
- Kashif, M.N., Raza, S.E.A., Sirinukunwattana, K., Arif, M., Rajpoot, N., 2016. Handcrafted features with convolutional neural networks for detection of tumor cells in histology images, in: *IEEE International Symposium on Biomedical Imaging*, IEEE. pp. 1029–1032.
- Kassani, S.H., Kassani, P.H., Wesolowski, M.J., Schneider, K.A., Deters, R., 2019a. Breast cancer diagnosis with transfer learning and global pooling, in: *International Conference on Information and Communication Technology Convergence (ICTC)*, IEEE. pp. 519–524.
- Kassani, S.H., Kassani, P.H., Wesolowski, M.J., Schneider, K.A., Deters, R., 2019b. Classification of histopathological biopsy images using ensemble of deep learning networks, in: *International Conference on Computer Science and Software Engineering*. pp. 92–99.
- Kather, J., Weis, C.A., Bianconi, F., Melchers, S., Schad, L., Gaiser, T., Marx, A., Zöllner, F., 2016a. Multi-class texture analysis in colorectal cancer histology. *Scientific Reports* 6, 27988.
- Kather, J.N., Krisam, J., Charoentong, P., Luedde, T., Herpel, E., Weis, C.A., Gaiser, T., Marx, A., Valous, N.A., Ferber, D., et al., 2019a. Predicting survival from colorectal cancer histology slides using deep learning: A retrospective multicenter study. *PLoS medicine* 16, e1002730.
- Kather, J.N., Pearson, A.T., Halama, N., Jäger, D., Krause, J., Loosen, S.H., Marx, A., Boor, P., Tacke, F., Neumann, U.P., et al., 2019b. Deep learning can predict microsatellite instability directly from histology in gastrointestinal cancer. *Nature medicine* 25, 1054–1056.
- Kather, J.N., Zöllner, F., Bianconi, F., Melchers, S., Schad, L., Gaiser, T., Marx, A., Weis, C., 2016b. Collection of textures in colorectal cancer histology. *Zenodo* 5281.
- Kausar, T., MingJiang, W., Ashraf, M.A., Kausar, A., 2020. Smallmitosis: Small size mitotic cells detection in breast histopathology images. *IEEE Access*.
- Kaushal, R.K., Rajaganesan, S., Rao, V., Sali, A., More, B., Desai, S.B., 2021. Validation of a portable whole-slide imaging system for frozen section diagnosis. *Journal of Pathology Informatics* 12, 33.
- Kenfield, S.A., Wei, E.K., Stampfer, M.J., Rosner, B.A., Colditz, G.A., 2008. Comparison of aspects of smoking among the four histological types of lung cancer. *Tobacco control* 17, 198–204.
- Khan, A., Atzori, M., Otárla, S., Andreczyk, V., Müller, H., 2020. Generalizing convolution neural networks on stain color heterogeneous data for computational pathology, in: *Medical Imaging: Digital Pathology*, International Society for Optics and Photonics. p. 113200R.
- Khan, A.M., Rajpoot, N., Treanor, D., Magee, D., 2014. A nonlinear mapping approach to stain normalization in digital histopathology images using image-specific color deconvolution. *IEEE Transactions on Biomedical Engineering* 61, 1729–1738.
- Khan, S., Islam, N., Jan, Z., Din, I.U., Rodrigues, J.J.C., 2019a. A novel deep learning based framework for the detection and classification of breast cancer using transfer learning. *Pattern Recognition Letters* 125, 1–6.
- Khan, U.A.H., Stürenberg, C., Gencoglu, O., Sandeman, K., Heikkinen, T., Rannikko, A., Mirtti, T., 2019b. Improving prostate cancer detection with breast histopathology images, in: *European Congress on Digital Pathology*, Springer. pp. 91–99.
- Khened, M., Kori, A., Rajkumar, H., Krishnamurthi, G., Srinivasan, B., 2021. A generalized deep learning framework for whole-slide image segmentation and analysis. *Scientific Reports* 11, 1–14.
- Khoshdeli, M., Winkelmaier, G., Parvin, B., 2018. Fusion of encoder-decoder deep networks improves delineation of multiple nuclear phenotypes. *BMC bioinformatics* 19, 1–11.
- Kiani, A., Uyumazturk, B., Rajpurkar, P., Wang, A., Gao, R., Jones, E., Yu, Y., Langlotz, C.P., Ball, R.L., Montine, T.J., et al., 2020. Impact of a deep learning assistant on the histopathologic classification of liver cancer. *NPJ Digital Medicine* 3, 1–8.
- Kieffer, B., Babaie, M., Kalra, S., Tizhoosh, H.R., 2017. Convolutional neural networks for histopathology image classification: Training vs. using pre-trained networks, in: *International Conference on Image Processing Theory, Tools and Applications (IPTA)*, IEEE. pp. 1–6.
- Kim, H., Jang, M., Park, Y.N., 2020a. Histopathological variants of hepatocellular carcinomas: an update according to the 5th edition of the who classification of digestive system tumors. *Journal of Liver Cancer* 20, 17–24.
- Kim, H., Yoon, H., Thakur, N., Hwang, G., Lee, E.J., Kim, C., Chong, Y., 2021. Deep learning-based histopathological segmentation for whole slide images of colorectal cancer in a compressed domain. *Scientific Reports* 11, 1–14.
- Kim, I., Kang, K., Song, Y., Kim, T.J., 2022. Application of artificial intelligence in pathology: Trends and challenges. *Diagnostics* 12, 2794.
- Kim, Y., Lee, J.H., Choi, S., Lee, J.M., Kim, J.H., Seok, J., Joo, H.J., 2020b. Validation of deep learning natural language processing algorithm for keyword extraction from pathology reports in electronic health records. *Scientific reports* 10, 1–9.
- Kipf, T.N., Welling, M., 2017. Semi-supervised classification with graph convolutional networks, in: *International Conference on Learning Representations*, OpenReview.net.
- Kirby, J., . MICCAI 2014 Grand Challenges. Available at: <https://wiki.cancerimagingarchive.net/display/Public/MICCAI2014GrandChallenges> (accessed June 10, 2021).
- Klein, C., Zeng, Q., Arbaretz, F., Devêvre, E., Calderaro, J., Lomenie, N., Maiuri, M.C., 2021. Artificial intelligence for solid tumour diagnosis in digital pathology. *British Journal of Pharmacology* 178, 4291–4315.
- Kloeckner, J., Sansonowicz, T.K., Rodrigues, Á.L., Nunes, T.W., 2020. Multicategorical classification using deep learning applied to the diagnosis of gastric cancer. *Jornal Brasileiro de Patologia e Medicina Laboratorial* 56.
- Köbel, M., Kalloger, S.E., Baker, P.M., Ewanowich, C.A., Arseneau, J., Zherebitskiy, V., Abdulkarim, S., Leung, S., Duggan, M.A., Fontaine, D., et al., 2010. Diagnosis of ovarian carcinoma cell type is highly reproducible: a transcanadian study. *The American journal of surgical pathology* 34, 984–993.
- Kohli, M.D., Summers, R.M., Geis, J.R., 2017. Medical image data and datasets in the era of machine learning—whitepaper from the 2016 c-mimi meeting dataset session. *Journal of digital imaging* 30, 392–399.
- Kong, B., Sun, S., Wang, X., Song, Q., Zhang, S., 2018. Invasive cancer detection utilizing compressed convolutional neural network and transfer learning, in: *International Conference on Medical Image Computing and Computer-Assisted Intervention*, Springer. pp. 156–164.
- Koohbanani, N.A., Jahanifar, M., Tajadin, N.Z., Rajpoot, N., 2020. Nuclick: a deep learning framework for interactive segmentation of microscopic images. *Medical Image Analysis* 65, 101771.
- Koohbanani, N.A., Unnikrishnan, B., Khurram, S.A., Krishnaswamy, P., Rajpoot, N., 2021. Self-path: Self-supervision for classification of pathology images with limited annotations. *IEEE Transactions on Medical Imaging* 40, 2845–2856.
- Korbar, B., Olfson, A.M., Miraflor, A.P., Nicka, C.M., Suriawinata, M.A., Torresani, L., Suriawinata, A.A., Hassanzpour, S., 2017. Deep learning for classification of colorectal polyps on whole-slide images. *Journal of Pathology Informatics* 8.
- Kosaraju, S.C., Hao, J., Koh, H.M., Kang, M., 2020. Deep-hipo: Multi-scale receptive field deep learning for histopathological image analysis. *Methods* 179, 3–13.
- Kociarski, M., Cyganek, B., Olborski, B., Antosz, Z., Zydek, M., Kwolek, B., Wąsowicz, P., Bukała, A., Swadźba, J., Sitkowski, P., 2021. Diagset: a dataset for prostate cancer histopathological image classification. arXiv preprint arXiv:2105.04014.
- Krizhevsky, A., Sutskever, I., Hinton, G.E., 2012. Imagenet classification with deep convolutional neural networks. *Advances in neural information processing systems* 25.
- Kulkarni, P.M., Robinson, E.J., Pradhan, J.S., Gartrell-Corrado, R.D., Rohr, B.R., Trager, M.H., Geskin, L.J., Kluger, H.M., Wong, P.F., Acs, B., et al., 2020. Deep learning based on standard h&e images of primary melanoma tumors identifies patients at risk for visceral recurrence and death. *Clinical Cancer Research* 26, 1126–1134.
- Kumar, A., Singh, S.K., Saxena, S., Lakshmanan, K., Sangaiah, A.K., Chauhan, H., Shrivastava, S., Singh, R.K., 2020a. Deep feature learning for histopathological image classification of canine mammary tumors and human breast cancer. *Information Sciences* 508, 405–421.
- Kumar, N., Gupta, R., Gupta, S., 2020b. Whole slide imaging (wsi) in pathology: current perspectives and future directions. *Journal of Digital Imaging* 33, 1034–1040.
- Kumar, N., Verma, R., Sharma, S., Bhargava, S., Vahadane, A., Sethi, A., 2017. A dataset and a technique for generalized nuclear segmentation for computational pathology. *IEEE Transactions on Medical Imaging* 36, 1550–1560.
- Kuo, K.H., Leo, J.M., 2019. Optical versus virtual microscope for medical education: a systematic review. *Anatomical Sciences Education* 12, 678–685.

- Kweldam, C.F., Wildhagen, M.F., Steyerberg, E.W., Bangma, C.H., Van Der Kwast, T.H., Van Leenders, G.J., 2015. Cribriform growth is highly predictive for postoperative metastasis and disease-specific death in gleason score 7 prostate cancer. *Modern pathology* 28, 457–464.
- Van der Laak, J., Litjens, G., Ciompi, F., 2021. Deep learning in histopathology: the path to the clinic. *Nature medicine* 27, 775–784.
- Labati, R.D., Piuri, V., Scotti, F., 2011. All-idb: The acute lymphoblastic leukemia image database for image processing, in: 2011 18th IEEE international conference on image processing, IEEE. pp. 2045–2048.
- Lafarge, M.W., Bekkers, E.J., Pluim, J.P., Duits, R., Veta, M., 2021. Roto-translation equivariant convolutional networks: Application to histopathology image analysis. *Medical Image Analysis* 68, 101849.
- Lafarge, M.W., Pluim, J.P., Eppenhof, K.A., Veta, M., 2019. Learning domain-invariant representations of histological images. *Frontiers in medicine* 6, 162.
- Lagree, A., Shiner, A., Alera, M.A., Fleshner, L., Law, E., Law, B., Lu, F.I., Dodington, D., Gandhi, S., Slodkowska, E.A., et al., 2021. Assessment of digital pathology imaging biomarkers associated with breast cancer histologic grade. *Current Oncology* 28, 4298–4316.
- Lahiani, A., Gildenblat, J., Klaman, I., Albarqouni, S., Navab, N., Klaiman, E., 2019a. Virtualization of tissue staining in digital pathology using an unsupervised deep learning approach, in: European Congress on Digital Pathology, Springer. pp. 47–55.
- Lahiani, A., Gildenblat, J., Klaman, I., Navab, N., Klaiman, E., 2018. Generalizing multistain immunohistochemistry tissue segmentation using one-shot color deconvolution deep neural networks. *arXiv preprint arXiv:1805.06958*
- Lahiani, A., Klaman, I., Navab, N., Albarqouni, S., Klaiman, E., 2020. Seamless virtual whole slide image synthesis and validation using perceptual embedding consistency. *IEEE Journal of Biomedical and Health Informatics*
- Lahiani, A., Navab, N., Albarqouni, S., Klaiman, E., 2019b. Perceptual embedding consistency for seamless reconstruction of tilewise style transfer, in: International Conference on Medical Image Computing and Computer-Assisted Intervention, Springer. pp. 568–576.
- Lai, Z., Wang, C., Oliveira, L.C., Dugger, B.N., Cheung, S.C., Chuah, C.N., 2021. Joint semi-supervised and active learning for segmentation of gigapixel pathology images with cost-effective labeling, in: IEEE/CVF International Conference on Computer Vision, pp. 591–600.
- Laleh, N.G., Muti, H.S., Loeffler, C.M.L., Echle, A., Saldanha, O.L., Mahmood, F., Lu, M.Y., Trautwein, C., Langer, R., Dislich, B., et al., 2022. Benchmarking weakly-supervised deep learning pipelines for whole slide classification in computational pathology. *Medical image analysis* 79, 102474.
- Lancellotti, C., Cancian, P., Savevski, V., Kotha, S.R.R., Fraggetta, F., Graziano, P., Di Tommaso, L., 2021. Artificial intelligence & tissue biomarkers: advantages, risks and perspectives for pathology. *Cells* 10, 787.
- Lara, J.S., O., V.H.C., Otálora, S., Müller, H., González, F.A., 2020. Multi-modal latent semantic alignment for automated prostate tissue classification and retrieval, in: Medical Image Computing and Computer Assisted Intervention – MICCAI, Springer. p. 572–581.
- Lauwers, G.Y., Terris, B., Balis, U.J., Batts, K.P., Regimbreau, J.M., Chang, Y., Graeme-Cook, F., Yamabe, H., Imai, I., Cleary, K.R., et al., 2002. Prognostic histologic indicators of curatively resected hepatocellular carcinomas: a multi-institutional analysis of 425 patients with definition of a histologic prognostic index. *The American journal of surgical pathology* 26, 25–34.
- Le Page, A.L., Ballot, E., Truntzer, C., Derangère, V., Ilie, A., Rageot, D., Bibeau, F., Ghiringhelli, F., 2021. Using a convolutional neural network for classification of squamous and non-squamous non-small cell lung cancer based on diagnostic histopathology images. *Scientific Reports* 11, 1–8.
- LeCun, Y., Bengio, Y., Hinton, G., 2015a. Deep learning. *nature* 521, 436–444.
- LeCun, Y., Bengio, Y., Hinton, G., 2015b. Deep learning. *Nature* 521, 436–444.
- Lee, B., Paeng, K., 2018. A robust and effective approach towards accurate metastasis detection and pn-stage classification in breast cancer, in: International Conference on Medical Image Computing and Computer-Assisted Intervention, Springer. pp. 841–850.
- Lee, J.J., Thomas, I.C., Nolley, R., Ferrari, M., Brooks, J.D., Leppert, J.T., 2015. Biologic differences between peripheral and transition zone prostate cancer. *The Prostate* 75, 183–190.
- Lee, T.K., Ro, J.Y., 2018. Spectrum of cribriform proliferations of the prostate: from benign to malignant. *Archives of Pathology & Laboratory Medicine* 142, 938–946.
- Lei, G., Xia, Y., Zhai, D.H., Zhang, W., Chen, D., Wang, D., 2020. Staincnn: An efficient stain feature learning method. *Neurocomputing* 406, 267–273.
- Lemaitre, P., Takeda, K., Lamont, A.C., Agrawal, A., 2021. Colorimetric uncertainty estimation for the performance assessment of whole slide imaging scanners. *Journal of Medical Imaging* 8, 057501.
- Lerousseau, M., Vakalopoulou, M., Classe, M., Adam, J., Battistella, E., Carré, A., Estienne, T., Henry, T., Deutsch, E., Paragios, N., 2020. Weakly supervised multiple instance learning histopathological tumor segmentation , 470–479.
- LESTERTHEINVESTOR, 2019. High power h&e stained image of a parotid sclerosing polycystic adenoma. URL: https://commons.wikimedia.org/wiki/File:High_power_H%26E_stained_image_of_a_parotid_sclerosing_polycystic_adenoma.tif.
- Levine, A.B., Peng, J., Farnell, D., Nursey, M., Wang, Y., Naso, J.R., Ren, H., Farahani, H., Chen, C., Chiu, D., et al., 2020. Synthesis of diagnostic quality cancer pathology images by generative adversarial networks. *The Journal of Pathology* 252, 178–188.
- Levy, J.J., Jackson, C.R., Sriharan, A., Christensen, B.C., Vaickus, L.J., 2020. Preliminary evaluation of the utility of deep generative histopathology image translation at a mid-sized ncicancer center. *bioRxiv* .
- Lewis Jr, J.S., Ali, S., Luo, J., Thorstad, W.L., Madabhushi, A., 2014. A quantitative histomorphometric classifier (quhbic) identifies aggressive versus indolent p16-positive oropharyngeal squamous cell carcinoma. *The American journal of surgical pathology* 38, 128.
- Li, B., Li, Y., Eliceiri, K.W., 2021a. Dual-stream multiple instance learning network for whole slide image classification with self-supervised contrastive learning, in: IEEE/CVF Conference on Computer Vision and Pattern Recognition, pp. 14318–14328.
- Li, C., Wang, X., Liu, W., Latecki, L.J., 2018a. Deepmitosis: Mitosis detection via deep detection, verification and segmentation networks. *Medical Image Analysis* 45, 121–133.
- Li, C., Wang, X., Liu, W., Latecki, L.J., Wang, B., Huang, J., 2019a. Weakly supervised mitosis detection in breast histopathology images using concentric loss. *Medical Image Analysis* 53, 165–178.
- Li, C., Zhu, X., Yao, J., Huang, J., 2022. Hierarchical transformer for survival prediction using multimodality whole slide images and genomics, in: 2022 26th International Conference on Pattern Recognition (ICPR), IEEE. pp. 4256–4262.
- Li, F., Yang, Y., Wei, Y., He, P., Chen, J., Zheng, Z., Bu, H., 2021b. Deep learning-based predictive biomarker of pathological complete response to neoadjuvant chemotherapy from histological images in breast cancer. *Journal of translational medicine* 19, 1–13.
- Li, H., Han, X., Kang, Y., Shi, X., Yan, M., Tong, Z., Bu, Q., Cui, L., Feng, J., Yang, L., 2020a. A novel loss calibration strategy for object detection networks training on sparsely annotated pathological datasets, in: International Conference on Medical Image Computing and Computer-Assisted Intervention, Springer. pp. 320–329.
- Li, J., Chen, W., Huang, X., Yang, S., Hu, Z., Duan, Q., Metaxas, D.N., Li, H., Zhang, S., 2021c. Hybrid supervision learning for pathology whole slide image classification, in: International Conference on Medical Image Computing and Computer-Assisted Intervention, Springer. pp. 309–318.
- Li, J., Li, W., Gertych, A., Knudsen, B.S., Speier, W., Arnold, C.W., 2019b. An attention-based multi-resolution model for prostate whole slide image classification and localization. *ArXiv abs/1905.13208*.
- Li, J., Sarma, K.V., Ho, K.C., Gertych, A., Knudsen, B.S., Arnold, C.W., 2017. A multi-scale u-net for semantic segmentation of histological images from radical prostatectomies 2017, 1140.
- Li, W., Li, J., Sarma, K.V., Ho, K.C., Shen, S., Knudsen, B.S., Gertych, A., Arnold, C.W., 2018b. Path r-cnn for prostate cancer diagnosis and gleason grading of histological images. *IEEE Transactions on Medical Imaging* 38, 945–954.
- Li, W., Li, J., Wang, Z., Polson, J., Sisk, A.E., Sajed, D.P., Speier, W., Arnold, C.W., 2021d. Pathal: An active learning framework for histopathology image analysis. *IEEE Transactions on Medical Imaging* 41, 1176–1187.
- Li, X., Shen, X., Zhou, Y., Wang, X., Li, T.Q., 2020b. Classification of breast cancer histopathological images using interleaved densenet with senet (id-snet). *PloS one* 15, e0232127.
- Li, Y., Ping, W., 2018. Cancer metastasis detection with neural conditional random field. *arXiv preprint arXiv:1806.07064* .
- Li, Y., Zhang, Z.X., Huang, G.H., Xiang, Y., Yang, L., Pei, Y.C., Yang, W., Lv, S.Q., 2021e. A systematic review of multifocal and multicentric glioblastoma. *Journal of Clinical Neuroscience* 83, 71–76.

- Li, Z., Tao, R., Wu, Q., Li, B., 2019c. Da-refinenet: A dual input whole slide image segmentation algorithm based on attention. *arXiv*, arXiv–1907.
- Liang, Y., Yang, J., Quan, X., Zhang, H., 2019. Metastatic breast cancer recognition in histopathology images using convolutional neural network with attention mechanism, in: Chinese Automation Congress (CAC), IEEE. pp. 2922–2926.
- Liao, Y.H., Kar, A., Fidler, S., 2021. Towards good practices for efficiently annotating large-scale image classification datasets, in: IEEE/CVF Conference on Computer Vision and Pattern Recognition, pp. 4350–4359.
- Liebig, C., Ayala, G., Wilks, J., Verstovsek, G., Liu, H., Agarwal, N., Berger, D.H., Albo, D., 2009. Perineural invasion is an independent predictor of outcome in colorectal cancer. *Journal of clinical oncology* 27, 5131.
- Liechty, B., Xu, Z., Zhang, Z., Slocum, C., Bahadir, C.D., Sabuncu, M.R., Pisapia, D.J., 2022. Machine learning can aid in prediction of idh mutation from h&e-stained histology slides in infiltrating gliomas. *Scientific Reports* 12, 22623.
- Lim, S.B., Yu, C.S., Jang, S.J., Kim, T.W., Kim, J.H., Kim, J.C., 2010. Prognostic significance of lymphovascular invasion in sporadic colorectal cancer. *Diseases of the colon & rectum* 53, 377–384.
- Lin, J., Han, G., Pan, X., Chen, H., Li, D., Jia, X., Shi, Z., Wang, Z., Cui, Y., Li, H., et al., 2021. Pdbl: Improving histopathological tissue classification with plug-and-play pyramidal deep-broad learning. *arXiv preprint arXiv:2111.03063*.
- Lin, Y., Zeng, B., Wang, Y., Chen, Y., Fang, Z., Zhang, J., Ji, X., Wang, H., Zhang, Y., 2022. Unpaired multi-domain stain transfer for kidney histopathological images .
- Litjens, G., Bandi, P., Bejnordi, B.E., Geessink, O., Balkenhol, M., Bult, P., Halilovic, A., Hermans, M., van de Loo, R., Vogels, R., Manson, Q.F., Stathonikos, N., Baidoshvili, A., van Diest, P., Wauters, C., van Dijk, M., van der Laak, J., 2018. 1399 h&e-stained sentinel lymph node sections of breast cancer patients: the camelyon dataset. *Gigascience* 7, giy065. doi:<https://doi.org/10.1093/gigascience/giy065>.
- Litjens, G., Sánchez, C.I., Timofeeva, N., Hermans, M., Nagtegaal, I., Kovacs, I., Hulsbergen-Van De Kaa, C., Bult, P., Van Ginneken, B., Van Der Laak, J., 2016. Deep learning as a tool for increased accuracy and efficiency of histopathological diagnosis. *Scientific Reports* 6, 26286.
- Liu, B., Yao, K., Huang, M., Zhang, J., Li, Y., Li, R., 2018a. Gastric pathology image recognition based on deep residual networks, in: IEEE Annual Computer Software and Applications Conference (COMPSAC), IEEE. pp. 408–412.
- Liu, H., Simonyan, K., Yang, Y., 2018b. Darts: Differentiable architecture search, in: International Conference on Learning Representations.
- Liu, Y., Gadepalli, K., Norouzi, M., Dahl, G.E., Kohlberger, T., Boyko, A., Venugopalan, S., Timofeev, A., Nelson, P.Q., Corrado, G.S., et al., 2017. Detecting cancer metastases on gigapixel pathology images. *arXiv preprint arXiv:1703.02442* .
- Liu, Y., Kohlberger, T., Norouzi, M., Dahl, G.E., Smith, J.L., Mohtashamian, A., Olson, N., Peng, L.H., Hipp, J.D., Stumpe, M.C., 2019. Artificial intelligence-based breast cancer nodal metastasis detection: Insights into the black box for pathologists. *Archives of pathology & laboratory medicine* 143, 859–868.
- Liu, Y., Pantanowitz, L., 2019. Digital pathology: Review of current opportunities and challenges for oral pathologists. *Journal of Oral Pathology & Medicine* 48, 263–269.
- Liu, Y., Sun, Y., Xue, B., Zhang, M., Yen, G.G., Tan, K.C., 2021. A survey on evolutionary neural architecture search. *IEEE transactions on neural networks and learning systems* .
- Lones, M.A., 2021. How to avoid machine learning pitfalls: a guide for academic researchers. *arXiv preprint arXiv:2108.02497* .
- López-Úbeda, P., Martín-Noguerol, T., Aneiros-Fernández, J., Luna, A., 2022. Natural language processing in pathology: Current trends and future insights. *The American Journal of Pathology* .
- Lotan, Y., Gupta, A., Shariat, S.F., Palapattu, G.S., Vazina, A., Karakiewicz, P.I., Bastian, P.J., Rogers, C.G., Amiel, G., Perotte, P., et al., 2005. Lymphovascular invasion is independently associated with overall survival, cause-specific survival, and local and distant recurrence in patients with negative lymph nodes at radical cystectomy. *Journal of clinical oncology* 23, 6533–6539.
- Louis, D.N., Perry, A., Wesseling, P., Brat, D.J., Cree, I.A., Figarella-Branger, D., Hawkins, C., Ng, H., Pfister, S.M., Reifenberger, G., et al., 2021. The 2021 who classification of tumors of the central nervous system: a summary. *Neuro-oncology* 23, 1231–1251.
- Lu, C., Koyuncu, C., Corredor, G., Prasanna, P., Leo, P., Wang, X., Janowczyk, A., Bera, K., Lewis Jr, J., Velcheti, V., et al., 2021a. Feature-driven local cell graph (FLocK): New computational pathology-based descriptors for prognosis of lung cancer and hpv status of oropharyngeal cancers. *Medical Image Analysis* 68, 101903.
- Lu, M.Y., Chen, R.J., Kong, D., Lipkova, J., Singh, R., Williamson, D.F., Chen, T.Y., Mahmood, F., 2022. Federated learning for computational pathology on gigapixel whole slide images. *Medical Image Analysis* 76, 102298.
- Lu, M.Y., Chen, R.J., Mahmood, F., 2020a. Semi-supervised breast cancer histology classification using deep multiple instance learning and contrast predictive coding, in: Medical Imaging: Digital Pathology, International Society for Optics and Photonics. p. 113200J.
- Lu, M.Y., Chen, T.Y., Williamson, D.D., Zhao, M., Shady, M., Lipkova, J., Mahmood, F., 2021b. Abstract po-007: Deep learning-based computational pathology predicts origins for cancers of unknown primary.
- Lu, M.Y., Chen, T.Y., Williamson, D.F., Zhao, M., Shady, M., Lipkova, J., Mahmood, F., 2021c. Ai-based pathology predicts origins for cancers of unknown primary. *Nature* 594, 106–110.
- Lu, M.Y., Williamson, D.F., Chen, T.Y., Chen, R.J., Barbieri, M., Mahmood, F., 2021d. Data-efficient and weakly supervised computational pathology on whole-slide images. *Nature Biomedical Engineering* 5, 555–570.
- Lu, M.Y., Williamson, D.F., Chen, T.Y., Chen, R.J., Barbieri, M., Mahmood, F., 2021e. Data-efficient and weakly supervised computational pathology on whole-slide images. *Nature Biomedical Engineering* 5, 555–570.
- Lu, W., Graham, S., Bilal, M., Rajpoot, N., Minhas, F., 2020b. Capturing cellular topology in multi-gigapixel pathology images, in: IEEE/CVF Conference on Computer Vision and Pattern Recognition Workshops, pp. 260–261.
- Lu, Y., Xu, P., 2018. Anomaly detection for skin disease images using variational autoencoder. *CoRR abs/1807.01349*.
- Lu, Z., Xu, S., Shao, W., Wu, Y., Zhang, J., Han, Z., Feng, Q., Huang, K., 2020c. Deep-learning-based characterization of tumor-infiltrating lymphocytes in breast cancers from histopathology images and multiomics data. *JCO Clinical Cancer Informatics* 4, 480–490.
- Lujan, G., Li, Z., Parwani, A.V., 2022. Challenges in implementing a digital pathology workflow in surgical pathology. *Human Pathology Reports* 29, 300673.
- Lutnick, B., Manthey, D., Becker, J.U., Ginley, B., Moos, K., Zuckerman, J.E., Rodrigues, L., Gallan, A.J., Barisoni, L., Alpers, C.E., et al., 2022. A user-friendly tool for cloud-based whole slide image segmentation with examples from renal histopathology. *Communications medicine* 2, 105.
- Madabhushi, A., Wang, X., Barrera, C., Velcheti, V., 2021. Predicting response to immunotherapy using computer extracted features of cancer nuclei from hematoxylin and eosin (h&e) stained images of non-small cell lung cancer (nsclc). US Patent 11,055,844.
- Maeyashiki, T., Suzuki, K., Hattori, A., Matsunaga, T., Takamochi, K., Oh, S., 2013. The size of consolidation on thin-section computed tomography is a better predictor of survival than the maximum tumour dimension in resectable lung cancer. *European Journal of Cardio-Thoracic Surgery* 43, 915–918.
- Mapahapatra, D., Bozorgtabar, B., Thiran, J.P., Shao, L., 2020. Structure preserving stain normalization of histopathology images using self supervised semantic guidance, in: International Conference on Medical Image Computing and Computer-Assisted Intervention, Springer. pp. 309–319.
- Mahmood, F., Borders, D., Chen, R.J., McKay, G.N., Salimian, K.J., Baras, A., Durr, N.J., 2019. Deep adversarial training for multi-organ nuclei segmentation in histopathology images. *IEEE Transactions on Medical Imaging* 39, 3257–3267.
- Makhlof, Y., Salto-Tellez, M., James, J., O'Reilly, P., Maxwell, P., 2022. General roadmap and core steps for the development of ai tools in digital pathology. *Diagnostics* 12, 1272.
- Marinelli, R.J., Montgomery, K., Liu, C.L., Shah, N.H., Pappong, W., Nitzberg, M., Zachariah, Z.K., Sherlock, G.J., Natkunam, Y., West, R.B., et al., 2007. The stanford tissue microarray database. *Nucleic acids research* 36, D871–D877.
- Marini, N., Otálora, S., Ciompi, F., Silvello, G., Marchesin, S., Vatrano, S., Buttafuoco, G., Atzori, M., Müller, H., 2021. Multi-scale task multiple instance learning for the classification of digital pathology images with global annotations, in: MICCAI Workshop on Computational Pathology, PMLR. pp. 170–181.
- Marsh, J.N., Matlock, M.K., Kudose, S., Liu, T.C., Stappenbeck, T.S., Gaut, J.P., Swamiadass, S.J., 2018. Deep learning global glomerulosclerosis in transplant kidney frozen sections. *IEEE Transactions on Medical Imaging*

- 37, 2718–2728.
- Martins-Filho, S.N., Paiva, C., Azevedo, R.S., Alves, V.A.F., 2017. Histological grading of hepatocellular carcinoma—a systematic review of literature. *Frontiers in medicine* 4, 193.
- Matek, C., Schwarz, S., Spiekermann, K., Marr, C., 2019. Human-level recognition of blast cells in acute myeloid leukaemia with convolutional neural networks. *Nature Machine Intelligence* 1, 538–544.
- Mehmood, S., Ghazal, T.M., Khan, M.A., Zubair, M., Naseem, M.T., Faiz, T., Ahmad, M., 2022. Malignancy detection in lung and colon histopathology images using transfer learning with class selective image processing. *IEEE Access* 10, 25657–25668.
- Meier, F.A., Varney, R.C., Zarbo, R.J., 2011. Study of amended reports to evaluate and improve surgical pathology processes. *Advances in anatomic pathology* 18, 406–413.
- Meng, Z., Zhao, Z., Su, F., 2019. Multi-classification of breast cancer histology images by using gravitation loss, in: *IEEE International Conference on Acoustics, Speech and Signal Processing (ICASSP)*, IEEE. pp. 1030–1034.
- Mercan, C., Aksoy, S., Mercan, E., Shapiro, L.G., Weaver, D.L., Elmore, J.G., 2017. Multi-instance multi-label learning for multi-class classification of whole slide breast histopathology images. *IEEE Transactions on Medical Imaging* 37, 316–325.
- Metter, D.M., Colgan, T.J., Leung, S.T., Timmons, C.F., Park, J.Y., 2019. Trends in the us and canadian pathologist workforces from 2007 to 2017. *JAMA network open* 2, e194337–e194337.
- Miao, R., Toth, R., Zhou, Y., Madabhushi, A., Janowczyk, A., 2021. Quick annotator: an open-source digital pathology based rapid image annotation tool. *The Journal of Pathology* 7, 542–547.
- Microrao, 2018. Gram positive cocci and gram negative bacilli. URL: https://commons.wikimedia.org/wiki/File:Gram_positive_cocci_and_Gram_negative_bacilli.jpg.
- Mirzazadeh, A., Mohseni, A., Ibrahim, S., Giuste, F.O., Zhu, Y., Shehata, B.M., Deshpande, S.R., Wang, M.D., 2021. Improving heart transplant rejection classification training using progressive generative adversarial networks, in: *IEEE EMBS International Conference on Biomedical and Health Informatics (BHI)*, IEEE. pp. 1–4.
- Mitchell, M., Wu, S., Zaldivar, A., Barnes, P., Vasserman, L., Hutchinson, B., Spitzer, E., Raji, I.D., Gebru, T., 2019. Model cards for model reporting, in: *Proceedings of the conference on fairness, accountability, and transparency*, pp. 220–229.
- Mobadersany, P., Yousefi, S., Amgad, M., Gutman, D.A., Barnholtz-Sloan, J.S., Vega, J.E.V., Brat, D.J., Cooper, L.A., 2018. Predicting cancer outcomes from histology and genomics using convolutional networks. *National Academy of Sciences* 115, E2970–E2979.
- Mohapatra, P., Panda, B., Swain, S., 2019. Enhancing histopathological breast cancer image classification using deep learning. *Int J Innov Technol Explor Eng* 8, 2024–2032.
- Montironi, R., Zhou, M., Magi-Galluzzi, C., Epstein, J.I., 2018. Features and prognostic significance of intraductal carcinoma of the prostate. *European Urology Oncology* 1, 21–28.
- Moreira, A.L., Ocampo, P.S., Xia, Y., Zhong, H., Russell, P.A., Minami, Y., Cooper, W.A., Yoshida, A., Bubendorf, L., Papotti, M., et al., 2020. A grading system for invasive pulmonary adenocarcinoma: a proposal from the international association for the study of lung cancer pathology committee. *Journal of Thoracic Oncology* 15, 1599–1610.
- Motlagh, M.H., Jannesari, M., Aboukhayr, H., Khosravi, P., Elemento, O., Totonchi, M., Hajirasouliha, I., 2018. Breast cancer histopathological image classification: A deep learning approach. *BioRxiv* , 242818.
- Mu, Y., Tizhoosh, H.R., Tayebi, R.M., Ross, C., Sur, M., Leber, B., Campbell, C.J., 2021. A bert model generates diagnostically relevant semantic embeddings from pathology synopses with active learning. *Communications Medicine* 1, 1–13.
- Muglia, V.F., Prando, A., 2015. Renal cell carcinoma: histological classification and correlation with imaging findings. *Radiologia brasileira* 48, 166–174.
- Nadeem, S., Hollmann, T., Tannenbaum, A., 2020. Multimarginal wasserstein barycenter for stain normalization and augmentation, in: *International Conference on Medical Image Computing and Computer-Assisted Intervention*, Springer. pp. 362–371.
- Nagpal, K., Foote, D., Liu, Y., Chen, P.H.C., Wulczyn, E., Tan, F., Olson, N., Smith, J.L., Mohtashamian, A., Wren, J.H., et al., 2019. Development and validation of a deep learning algorithm for improving gleason scoring of prostate cancer. *NPJ Digital Medicine* 2, 1–10.
- Nahid, A.A., Kong, Y., 2018. Histopathological breast-image classification using local and frequency domains by convolutional neural network. *Information* 9, 19.
- Nahid, A.A., Mehrabi, M.A., Kong, Y., 2018. Histopathological breast cancer image classification by deep neural network techniques guided by local clustering. *BioMed research international* 2018.
- Nakhleh, R.E., 2005. A prelude to error reduction in anatomic pathology.
- Nakhleh, R.E., 2006. Error reduction in surgical pathology. *Archives of pathology & laboratory medicine* 130, 630–632.
- Nakhleh, R.E., 2008. Patient safety and error reduction in surgical pathology. *Archives of pathology & laboratory medicine* 132, 181–185.
- Nakhleh, R.E., 2015. Role of informatics in patient safety and quality assurance. *Surgical Pathology Clinics* 8, 301–307.
- Nakhleh, R.E., Fitzgibbons, P.L., 2005. Quality management in anatomic pathology: promoting patient safety through systems improvement and error reduction. *College of American Pathologists*.
- Nakhleh, R.E., Nosé, V., Colasacco, C., Fatheree, L.A., Lillemoe, T.J., McCrory, D.C., Meier, F.A., Otis, C.N., Owens, S.R., Raab, S.S., et al., 2016. Interpretive diagnostic error reduction in surgical pathology and cytology: guideline from the college of american pathologists pathology and laboratory quality center and the association of directors of anatomic and surgical pathology. *Archives of Pathology & Laboratory Medicine* 140, 29–40.
- Narayanan, P.L., Raza, S.E.A., Hall, A.H., Marks, J.R., King, L., West, R.B., Hernandez, L., Dowsett, M., Gusterson, B., Maley, C., et al., 2019. Unmasking the tissue microecology of ductal carcinoma in situ with deep learning. *BioRxiv* , 812735.
- Nasrin, S., Alom, M.Z., Taha, T.M., Asari, V.K., 2020. Pcolornet: investigating the impact of different color spaces for pathological image classification, in: *Medical Imaging: Digital Pathology*, International Society for Optics and Photonics. p. 113201A.
- Nateghi, R., Danyali, H., Helfroush, M.S., 2016. A systematic approach for glandular structure segmentation from colon histopathology images, in: *Iranian Conference on Electrical Engineering (ICEE)*, IEEE. pp. 1505–1509.
- National Cancer Institute, . Common cancer types. Available at: <https://www.cancer.gov/types/common-cancers#:~:text=Themostcommonlytypeofarecombinedforthelist/> (accessed June 10, 2021).
- Nawaz, M., Sewissy, A.A., Soliman, T.H.A., 2018. Multi-class breast cancer classification using deep learning convolutional neural network. *Int. J. Adv. Comput. Sci. Appl* 9, 316–332.
- Naylor, P., Laé, M., Reyal, F., Walter, T., 2017. Nuclei segmentation in histopathology images using deep neural networks , 933–936.
- Naylor, P., Laé, M., Reyal, F., Walter, T., 2018. Segmentation of nuclei in histopathology images by deep regression of the distance map. *IEEE Transactions on Medical Imaging* 38, 448–459.
- Nazeri, K., Aminpour, A., Ebrahimi, M., 2018. Two-stage convolutional neural network for breast cancer histology image classification, in: *International Conference Image Analysis and Recognition*, Springer. pp. 717–726.
- Nephron, 2010. High power h&e stained image of a parotid sclerosing polycystic adenoma. URL: https://commons.wikimedia.org/wiki/File:Cerebellum_-biel_-_very_high_mag.jpg.
- Ngiam, J., Khosla, A., Kim, M., Nam, J., Lee, H., Ng, A.Y., 2011. Multimodal deep learning, in: *ICML*.
- Nguyen, E.H., Yang, H., Deng, R., Lu, Y., Zhu, Z., Roland, J.T., Lu, L., Landman, B.A., Fogo, A.B., Huo, Y., 2021. Circle representation for medical object detection. *IEEE transactions on medical imaging* 41, 746–754.
- Nguyen, H.G., Blank, A., Lugli, A., Zlobec, I., 2020. An effective deep learning architecture combination for tissue microarray spots classification of h&e stained colorectal images, in: *IEEE International Symposium on Biomedical Imaging*, IEEE. pp. 1271–1274.
- Niazi, M.K.K., Parwani, A.V., Gurcan, M.N., 2019. Digital pathology and artificial intelligence. *The lancet oncology* 20, e253–e261.
- Nirschl, J.J., Janowczyk, A., Peyster, E.G., Frank, R., Margulies, K.B., Feldman, M.D., Madabhushi, A., 2018. A deep-learning classifier identifies patients with clinical heart failure using whole-slide images of h&e tissue. *PloS one* 13, e0192726.
- Njoroge, S.W., Nichols, J.H., 2014. Risk management in the clinical laboratory. *Annals of laboratory medicine* 34, 274.
- Noorbakhsh, J., Farahmand, S., Namburi, S., Caruana, D., Rimm, D., Soltanieh-ha, M., Zarringhalam, K., Chuang, J.H., et al., 2020. Deep learning-based cross-classifications reveal conserved spatial behaviors within tumor histological images. *Nature communications* 11, 1–14.
- Nour, A., Saad, S., Boufama, B., 2021. Prostate biomedical images segmentation and classification by using u-net cnn model, in: *ACM Conference on*

- Bioinformatics, Computational Biology, and Health Informatics, pp. 1–7.
- Odisho, A.Y., Park, B., Altieri, N., DeNero, J., Cooperberg, M.R., Carroll, P.R., Yu, B., 2020. Natural language processing systems for pathology parsing in limited data environments with uncertainty estimation. *JAMIA open* 3, 431–438.
- Oliveira, S.P., Neto, P.C., Fraga, J., Montezuma, D., Monteiro, A., Monteiro, J., Ribeiro, L., Gonçalves, S., Pinto, I.M., Cardoso, J.S., 2021. Cad systems for colorectal cancer from wsi are still not ready for clinical acceptance. *Scientific Reports* 11, 1–15.
- O’Neil, C., 2016. Weapons of Math Destruction: How Big Data Increases Inequality and Threatens Democracy. Crown Publishing Group, USA.
- Organization, W.H., . Cancer. Available at: <https://www.who.int/news-room/factsheets/detail/cancer> (accessed Feb 13, 2023).
- Otalora, S., Atzori, M., Andrarczyk, V., Khan, A., Müller, H., 2019. Staining invariant features for improving generalization of deep convolutional neural networks in computational pathology. *Frontiers in Bioengineering and Biotechnology* , 198.
- Otalora, S., Atzori, M., Khan, A., Jimenez-del Toro, O., Andrarczyk, V., Müller, H., 2020. Systematic comparison of deep learning strategies for weakly supervised gleason grading, in: *Medical Imaging: Digital Pathology*, International Society for Optics and Photonics, p. 113200L.
- Öztürk, Ş., Akdemir, B., 2019. Hic-net: A deep convolutional neural network model for classification of histopathological breast images. *Computers & Electrical Engineering* 76, 299–310.
- Pal, A., Xue, Z., Desai, K., Banjo, A.A.F., Adeputi, C.A., Long, L.R., Schiffman, M., Antani, S., 2021. Deep multiple-instance learning for abnormal cell detection in cervical histopathology images. *Computers in Biology and Medicine* 138, 104890.
- Paner, S., 2021. Protocol for the examination of radical prostatectomy specimens from patients with carcinoma of the prostate gland. URL: https://documents.cap.org/protocols/Prostate_4.2.0.1.REL_CAPCP.pdf.
- Pang, G., Shen, C., Cao, L., Hengel, A.V.D., 2021. Deep learning for anomaly detection: A review. *ACM Comput. Surv.* 54.
- Pantanowitz, L., 2010. Digital images and the future of digital pathology. *Journal of Pathology Informatics* 1.
- Pantanowitz, L., Henricks, W.H., Beckwith, B.A., 2007. Medical laboratory informatics. *Clinics in laboratory medicine* 27, 823–843.
- Pantanowitz, L., Sharma, A., Carter, A.B., Kurc, T., Sussman, A., Saltz, J., 2018. Twenty years of digital pathology: an overview of the road travelled, what is on the horizon, and the emergence of vendor-neutral archives. *Journal of pathology informatics* 9.
- Pantanowitz, L., Sinard, J.H., Henricks, W.H., Fatheree, L.A., Carter, A.B., Contis, L., Beckwith, B.A., Evans, A.J., Lal, A., Parwani, A.V., 2013. Validating whole slide imaging for diagnostic purposes in pathology: guideline from the college of american pathologists pathology and laboratory quality center. *Archives of Pathology and Laboratory Medicine* 137, 1710–1722.
- Pare, G., Meyer, J., Trudel, M.C., Tetu, B., 2016. Impacts of a large decentralized telepathology network in canada. *Telemedicine and e-Health* 22, 246–250.
- Parvatikar, A., Choudhary, O., Ramanathan, A., Navolotskaia, O., Carter, G., Tosun, A.B., Fine, J.L., Chennubhotla, S.C., 2020. Modeling histological patterns for differential diagnosis of atypical breast lesions, in: *Medical Image Computing and Computer Assisted Intervention – MICCAI*, Springer, pp. 550–560.
- Parwani, A.V., Hassell, L., Glassy, E., Pantanowitz, L., 2014. Regulatory barriers surrounding the use of whole slide imaging in the united states of america. *Journal of pathology informatics* 5.
- Pati, P., Andani, S., Pediaditis, M., Viana, M.P., Rüschoff, J.H., Wild, P., Gabrani, M., 2018. Deep positive-unlabeled learning for region of interest localization in breast tissue images, in: *Medical Imaging: Digital Pathology*, International Society for Optics and Photonics, p. 1058107.
- Pati, P., Foncubierta-Rodríguez, A., Goksel, O., Gabrani, M., 2021a. Reducing annotation effort in digital pathology: A co-representation learning framework for classification tasks. *Medical Image Analysis* 67, 101859.
- Pati, P., Foncubierta-Rodríguez, A., Goksel, O., Gabrani, M., 2021b. Reducing annotation effort in digital pathology: A co-representation learning framework for classification tasks. *Medical Image Analysis* 67, 101859.
- Patil, A., Tamboli, D., Meena, S., Anand, D., Sethi, A., 2019. Breast cancer histopathology image classification and localization using multiple instance learning, in: *IEEE International WIE Conference on Electrical and Computer Engineering (WIECON-ECE)*, IEEE, pp. 1–4.
- Peck, M., Moffat, D., Latham, B., Badrick, T., 2018. Review of diagnostic error in anatomical pathology and the role and value of second opinions in error prevention. *Journal of clinical pathology* 71, 995–1000.
- Peikari, M., Gangeh, M.J., Zubovits, J., Clarke, G., Martel, A.L., 2015. Triaging diagnostically relevant regions from pathology whole slides of breast cancer: A texture based approach. *IEEE transactions on medical imaging* 35, 307–315.
- Pell, R., Oien, K., Robinson, M., Pitman, H., Rajpoot, N., Rittscher, J., Snead, D., Verrill, C., quality assurance working group, U.N.C.R.I.N.C.M.P.C.P., Driskell, O.J., et al., 2019. The use of digital pathology and image analysis in clinical trials. *The Journal of Pathology: Clinical Research* 5, 81–90.
- Peters, S.R., 2016. A Practical guide to Frozen Section Technique. SPRINGER.
- Peyster, E.G., Arabaymohammadi, S., Janowczyk, A., Azarianpour-Esfahani, S., Sekulic, M., Cassol, C., Blower, L., Parwani, A., Lal, P., Feldman, M.D., et al., 2021. An automated computational image analysis pipeline for histological grading of cardiac allograft rejection. *European Heart Journal* 42, 2356–2369.
- Phillips, A., Teo, I., Lang, J., 2018. Fully convolutional network for melanoma diagnostics. *arXiv preprint arXiv:1806.04765*.
- Phipps, A.I., Lindor, N.M., Jenkins, M.A., Baron, J.A., Win, A.K., Gallinger, S., Gryfe, R., Newcomb, P.A., 2013. Colon and rectal cancer survival by tumor location and microsatellite instability: the colon cancer family registry. *Diseases of the colon and rectum* 56, 937.
- Pimkin, A., Makarchuk, G., Kondratenko, V., Pisov, M., Krivov, E., Belyaev, M., 2018. Ensembling neural networks for digital pathology images classification and segmentation, in: *International Conference Image Analysis and Recognition*, Springer, pp. 877–886.
- Pinckaers, H., Bulten, W., van der Laak, J., Litjens, G., 2021. Detection of prostate cancer in whole-slide images through end-to-end training with image-level labels. *IEEE Transactions on Medical Imaging* 40, 1817–1826.
- Ponzi, F., Deodato, G., Macii, E., Di Cataldo, S., Ficarra, E., 2020. Exploiting “uncertain” deep networks for data cleaning in digital pathology, in: *IEEE International Symposium on Biomedical Imaging*, IEEE, pp. 1139–1143.
- Priego-Torres, B.M., Sanchez-Morillo, D., Fernandez-Granero, M.A., Garcia-Rojo, M., 2020. Automatic segmentation of whole-slide h&e stained breast histopathology images using a deep convolutional neural network architecture. *Expert Systems With Applications* 151, 113387.
- Qaiser, T., Tsang, Y.W., Taniyama, D., Sakamoto, N., Nakane, K., Epstein, D., Rajpoot, N., 2019. Fast and accurate tumor segmentation of histology images using persistent homology and deep convolutional features. *Medical Image Analysis* 55, 1–14.
- Qi, J., Burnside, G., Charnley, P., Coenen, F., . Event-based pathology data prioritisation: A study using multi-variate time series classification .
- Qi, Q., Li, Y., Wang, J., Zheng, H., Huang, Y., Ding, X., Rohde, G.K., 2018. Label-efficient breast cancer histopathological image classification. *IEEE Journal of Biomedical and Health Informatics* 23, 2108–2116.
- Qiu, J.X., Yoon, H.J., Fearn, P.A., Tourassi, G.D., 2017. Deep learning for automated extraction of primary sites from cancer pathology reports. *IEEE journal of biomedical and health informatics* 22, 244–251.
- Qureshi, H., Sertel, O., Rajpoot, N., Wilson, R., Gurcan, M., 2008. Adaptive discriminant wavelet packet transform and local binary patterns for meningioma subtype classification, in: *International Conference on Medical Image Computing and Computer-Assisted Intervention*, Springer, pp. 196–204.
- Raciti, P., Sue, J., Ceballos, R., Godrich, R., Kunz, J.D., Kapur, S., Reuter, V., Grady, L., Kanan, C., Klimstra, D.S., et al., 2020. Novel artificial intelligence system increases the detection of prostate cancer in whole slide images of core needle biopsies. *Modern Pathology* 33, 2058–2066.
- Rączkowski, Ł., Możejko, M., Zambonelli, J., Szczurek, E., 2019. Ara: accurate, reliable and active histopathological image classification framework with bayesian deep learning. *Scientific Reports* 9, 1–12.
- Rakhlin, A., Shvets, A., Iglovikov, V., Kalinin, A.A., 2018. Deep convolutional neural networks for breast cancer histology image analysis, in: *International Conference Image Analysis and Recognition*, Springer, pp. 737–744.
- Rathore, S., Iftikhar, M., Nasrallah, M., Gurcan, M., Rajpoot, N., Mourelatos, Z., 2019. Tmod-35, prediction of overall survival, and molecular markers in gliomas via analysis of digital pathology images using deep learning. *Neuro-oncology* 21, vi270–vi270.
- Rathore, S., Niazi, T., Iftikhar, M.A., Chaddad, A., 2020. Glioma grading via analysis of digital pathology images using machine learning. *Cancers* 12, 578.
- Rawat, R.R., Ortega, I., Roy, P., Sha, F., Shibata, D., Ruderman, D., Agus, D.B., 2020. Deep learned tissue “fingerprints” classify breast cancers by er/pr/her2 status from h&e images. *Scientific Reports* 10, 1–13.

- Rehman, M.U., Akhtar, S., Zakwan, M., Mahmood, M.H., 2022. Novel architecture with selected feature vector for effective classification of mitotic and non-mitotic cells in breast cancer histology images. *Biomedical Signal Processing and Control* 71, 103212.
- Release, F.N., 2017. Fda allows marketing of first whole slide imaging system for digital pathology. <https://www.fda.gov/news-events/press-announcements/fda-allows-marketing-first-whole-slide-imaging-system-digital-pathology>.
- Remo, A., Fassan, M., Vanoli, A., Bonetti, L.R., Barresi, V., Tatangelo, F., Gafa, R., Giordano, G., Pancione, M., Grillo, F., et al., 2019. Morphology and molecular features of rare colorectal carcinoma histotypes. *Cancers* 11, 1036.
- Ren, J., Hacihaliloglu, I., Singer, E.A., Foran, D.J., Qi, X., 2019. Unsupervised domain adaptation for classification of histopathology whole-slide images. *Frontiers in Bioengineering and Biotechnology* 7, 102.
- Renshaw, A.A., Mena-Allauca, M., Gould, E.W., Sirintrapun, S.J., 2018. Synoptic reporting: Evidence-based review and future directions. *JCO Clinical Cancer Informatics*, 1–9URL: <https://doi.org/10.1200/CCCI.17.00088>, doi:10.1200/CCCI.17.00088, pMID: 30652566, arXiv:<https://doi.org/10.1200/CCCI.17.00088>.
- Riasatian, A., Babaie, M., Maleki, D., Kalra, S., Valipour, M., Hemati, S., Zaveri, M., Safarpoor, A., Shafiei, S., Afshari, M., et al., 2021. Fine-tuning and training of densenet for histopathology image representation using tcga diagnostic slides. *Medical Image Analysis* 70, 102032.
- Ries, L.G., Young, J., Keel, G., Eisner, M., Lin, Y., Horner, M., et al., 2007. Seer survival monograph: cancer survival among adults: Us seer program, 1988–2001, patient and tumor characteristics. National Cancer Institute, SEER Program, NIH Pub 7, 133–144.
- Ristanoski, G., Emery, J., Martinez Gutierrez, J., McCarthy, D., Aickelin, U., 2021. Handling uncertainty using features from pathology: opportunities in primary care data for developing high risk cancer survival methods, in: Australasian Computer Science Week Multiconference, pp. 1–7.
- Roh, Y., Heo, G., Whang, S.E., 2019. A survey on data collection for machine learning: a big data-ai integration perspective. *IEEE Transactions on Knowledge and Data Engineering* 33, 1328–1347.
- Rolls, G., 2016. 101 steps to better histology - a practical guide to good histology practice.
- Ronneberger, O., Fischer, P., Brox, T., 2015. U-net: Convolutional networks for biomedical image segmentation, in: International Conference on Medical Image Computing and Computer-Assisted Intervention, Springer, pp. 234–241.
- Rony, J., Belharbi, S., Dolz, J., Ayed, I.B., McCaffrey, L., Granger, E., 2019. Deep weakly-supervised learning methods for classification and localization in histology images: a survey. *arXiv preprint arXiv:1909.03354*.
- Roux, L., Racocceanu, D., Loménie, N., Kulikova, M., Irshad, H., Klossa, J., Capron, F., Genestie, C., Le Naour, G., Gurcan, M.N., 2013. Mitosis detection in breast cancer histological images an icpr 2012 contest. *Journal of Pathology Informatics* 4.
- Roy, K., Banik, D., Bhattacharjee, D., Nasipuri, M., 2019. Patch-based system for classification of breast histology images using deep learning. *Computerized Medical Imaging and Graphics* 71, 90–103.
- Roy, M., Kong, J., Kashyap, S., Pastore, V.P., Wang, F., Wong, K.C., Mukherjee, V., 2021. Convolutional autoencoder based model histocae for segmentation of viable tumor regions in liver whole-slide images. *Scientific Reports* 11, 1–10.
- Ryu, J., Puche, A.V., Shin, J., Park, S., Brattoli, B., Lee, J., Jung, W., Cho, S.I., Paeng, K., Ock, C.Y., Yoo, D., Pereira, S., 2023. Ocelot: Overlapped cell on tissue dataset for histopathology, in: Proceedings of the IEEE conference on computer vision and pattern recognition.
- Saco, A., Bombi, J.A., Garcia, A., Ramírez, J., Ordi, J., 2016. Current status of whole-slide imaging in education. *Pathobiology* 83, 79–88.
- Sahasrabudhe, M., Christodoulidis, S., Salgado, R., Michiels, S., Loi, S., André, F., Paragios, N., Vakalopoulou, M., 2020. Self-supervised nuclei segmentation in histopathological images using attention, in: International Conference on Medical Image Computing and Computer-Assisted Intervention, Springer, pp. 393–402.
- Sakamoto, T., Furukawa, T., Lami, K., Pham, H.H.N., Uegami, W., Kuroda, K., Kawai, M., Sakanashi, H., Cooper, L.A.D., Bychkov, A., et al., 2020. A narrative review of digital pathology and artificial intelligence: focusing on lung cancer. *Translational Lung Cancer Research* 9, 2255.
- Saldanha, O.L., Quirke, P., West, N.P., James, J.A., Loughrey, M.B., Grabsch, H.I., Salto-Tellez, M., Alwers, E., Cifci, D., Ghaffari Laleh, N., et al., 2022. Swarm learning for decentralized artificial intelligence in cancer histopathology. *Nature Medicine* , 1–8.
- Sali, R., Adewole, S., Ehsan, L., Denson, L.A., Kelly, P., Amadi, B.C., Holtz, L., Ali, S.A., Moore, S.R., Syed, S., et al., 2020. Hierarchical deep convolutional neural networks for multi-category diagnosis of gastrointestinal disorders on histopathological images, in: IEEE International Conference on Healthcare Informatics (ICHI), IEEE, pp. 1–6.
- Sali, R., Ehsan, L., Kowsari, K., Khan, M., Moskaluk, C.A., Syed, S., Brown, D.E., 2019. Celiacnet: Celiac disease severity diagnosis on duodenal histopathological images using deep residual networks, in: IEEE International Conference on Bioinformatics and Biomedicine (BIBM), IEEE, pp. 962–967.
- Salomon, L., Levrel, O., Anastasiadis, A.G., Irani, J., De La Taille, A., Saint, F., Vordos, D., Cicco, A., Hoznek, A., Chopin, D., et al., 2003. Prognostic significance of tumor volume after radical prostatectomy: a multivariate analysis of pathological prognostic factors. *European urology* 43, 39–44.
- Saltz, J., Gupta, R., Hou, L., Kurc, T., Singh, P., Nguyen, V., Samaras, D., Shroyer, K.R., Zhao, T., Batiste, R., et al., 2018. Spatial organization and molecular correlation of tumor-infiltrating lymphocytes using deep learning on pathology images. *Cell reports* 23, 181–193.
- Salvi, M., Acharya, U.R., Molinari, F., Meiburger, K.M., 2021. The impact of pre- and post-image processing techniques on deep learning frameworks: A comprehensive review for digital pathology image analysis. *Computers in Biology and Medicine* 128, 104129. URL: <https://www.sciencedirect.com/science/article/pii/S0010482520304601>.
- Salvi, M., Michielli, N., Molinari, F., 2020. Stain color adaptive normalization (scan) algorithm: separation and standardization of histological stains in digital pathology. *Computer methods and programs in biomedicine* 193, 105506.
- Sambasivan, N., Kapania, S., Highfill, H., Akrong, D., Paritosh, P.K., Aroyo, L.M., 2021. "everyone wants to do the model work, not the data work": Data cascades in high-stakes ai.
- Sankarapandian, S., Kohn, S., Spurrier, V., Grullon, S., Soans, R.E., Ayyagari, K.D., Chamarthi, R.V., Motaparthi, K., Lee, J.B., Shon, W., et al., 2021. A pathology deep learning system capable of triage of melanoma specimens utilizing dermatopathologist consensus as ground truth, in: Proceedings of the IEEE/CVF International Conference on Computer Vision, pp. 629–638.
- Santos, C., López-Doriga, A., Navarro, M., Mateo, J., Biondo, S., Martínez Vilalacampa, M., Soler, G., Sanjuan, X., Paules, M., Laquente, B., et al., 2013. Clinicopathological risk factors of stage ii colon cancer: results of a prospective study. *Colorectal Disease* 15, 414–422.
- Sarnecki, J.S., Burns, K.H., Wood, L.D., Waters, K.M., Hruban, R.H., Wirtz, D., Wu, P.H., 2016. A robust nonlinear tissue-component discrimination method for computational pathology. *Laboratory Investigation* 96, 450–458.
- Saxena, S., Shukla, S., Gyanchandani, M., 2020. Pre-trained convolutional neural networks as feature extractors for diagnosis of breast cancer using histopathology. *International Journal of Imaging Systems and Technology* 30, 577–591.
- Schmauch, B., Romagnoni, A., Pronier, E., Saillard, C., Maillé, P., Calderaro, J., Kamoun, A., Sefta, M., Toldo, S., Zaslavskiy, M., et al., 2020. A deep learning model to predict rna-seq expression of tumours from whole slide images. *Nature communications* 11, 1–15.
- Schneider, L., Laiouar-Pedari, S., Kuntz, S., Krieghoff-Henning, E., Hekler, A., Kather, J.N., Gaiser, T., Fröhling, S., Brinker, T.J., 2022. Integration of deep learning-based image analysis and genomic data in cancer pathology: A systematic review. *European Journal of Cancer* 160, 80–91.
- Schömig-Markiefka, B., Pryalukhin, A., Hull, W., Bychkov, A., Fukuoka, J., Madabhushi, A., Achter, V., Nieroda, L., Büttner, R., Quaas, A., et al., 2021. Quality control stress test for deep learning-based diagnostic model in digital pathology. *Modern Pathology* 34, 2098–2108.
- Schrammen, P.L., Ghaffari Laleh, N., Echle, A., Truhn, D., Schulz, V., Brinker, T.J., Brenner, H., Chang-Claude, J., Alwers, E., Brobeil, A., et al., 2022. Weakly supervised annotation-free cancer detection and prediction of genotype in routine histopathology. *The Journal of Pathology* 256, 50–60.
- Schroff, F., Kalenichenko, D., Philbin, J., 2015. Facenet: A unified embedding for face recognition and clustering, in: IEEE Conference on Computer Vision and Pattern Recognition, pp. 815–823.
- Schuchmacher, D., Schoerner, S., Kuepper, C., Grosserueschkamp, F., Sternemann, C., Lugnier, C., Kraeft, A.L., Juette, H., Tannapfel, A., Reinacher-Schick, A., et al., 2021. A framework for falsifiable explanations of machine learning models with an application in computational pathology. *medRxiv*.

- Schüffler, P.J., Geneslaw, L., Yarlagadda, D.V.K., Hanna, M.G., Samboy, J., Stamelos, E., Vanderbilt, C., Philip, J., Jean, M.H., Corsale, L., et al., 2021. Integrated digital pathology at scale: A solution for clinical diagnostics and cancer research at a large academic medical center. *Journal of the American Medical Informatics Association* 28, 1874–1884.
- Sebai, M., Wang, X., Wang, T., 2020. Maskmitosis: a deep learning framework for fully supervised, weakly supervised, and unsupervised mitosis detection in histopathology images. *Medical & Biological Engineering & Computing* 58, 1603–1623.
- Senousy, Z., Abdelsamea, M.M., Gaber, M.M., Abdar, M., Acharya, U.R., Khosravi, A., Nahavandi, S., 2021. Mcua: Multi-level context and uncertainty aware dynamic deep ensemble for breast cancer histology image classification. *IEEE Transactions on Biomedical Engineering* 69, 818–829.
- Serag, A., Ion-Margineanu, A., Qureshi, H., McMillan, R., Saint Martin, M.J., Diamond, J., O'Reilly, P., Hamilton, P., 2019. Translational ai and deep learning in diagnostic pathology. *Frontiers in medicine* 6, 185.
- Sethi, A., Sha, L., Vahadane, A.R., Deaton, R.J., Kumar, N., Macias, V., Gann, P.H., 2016. Empirical comparison of color normalization methods for epithelial-stromal classification in h and e images. *Journal of Pathology Informatics* 7.
- Shaban, M., Awan, R., Fraz, M.M., Azam, A., Tsang, Y.W., Snead, D., Rajpoot, N.M., 2020. Context-aware convolutional neural network for grading of colorectal cancer histology images. *IEEE Transactions on Medical Imaging* 39, 2395–2405.
- Shaban, M., Khurram, S.A., Fraz, M.M., Alsubaie, N., Masood, I., Mushtaq, S., Hassan, M., Loya, A., Rajpoot, N.M., 2019a. A novel digital score for abundance of tumour infiltrating lymphocytes predicts disease free survival in oral squamous cell carcinoma. *Scientific Reports* 9, 1–13.
- Shaban, M.T., Baur, C., Navab, N., Albarqouni, S., 2019b. Staingan: Stain style transfer for digital histological images, in: *IEEE International Symposium on Biomedical Imaging*, IEEE, pp. 953–956.
- Shao, W., Wang, T., Sun, L., Dong, T., Han, Z., Huang, Z., Zhang, J., Zhang, D., Huang, K., 2020. Multi-task multi-modal learning for joint diagnosis and prognosis of human cancers. *Medical Image Analysis* 65, 101795.
- Shao, Z., Bian, H., Chen, Y., Wang, Y., Zhang, J., Ji, X., et al., 2021. Transmil: Transformer based correlated multiple instance learning for whole slide image classification. *Advances in Neural Information Processing Systems* 34, 2136–2147.
- Shen, Y., Ke, J., 2020. A deformable crf model for histopathology whole-slide image classification, in: *International Conference on Medical Image Computing and Computer-Assisted Intervention*, Springer, pp. 500–508.
- Shen, Y., Shen, D., Ke, J., 2022. Identify representative samples by conditional random field of cancer histology images. *IEEE Transactions on Medical Imaging* 41, 3835–3848.
- Shephard, A.J., Graham, S., Bashir, S., Jahanifar, M., Mahmood, H., Khurram, A., Rajpoot, N.M., 2021. Simultaneous nuclear instance and layer segmentation in oral epithelial dysplasia, in: *IEEE/CVF International Conference on Computer Vision*, pp. 552–561.
- Shin, H.C., Roth, H.R., Gao, M., Lu, L., Xu, Z., Nogues, I., Yao, J., Mollura, D., Summers, R.M., 2016. Deep convolutional neural networks for computer-aided detection: Cnn architectures, dataset characteristics and transfer learning. *IEEE Transactions on Medical Imaging* 35, 1285–1298.
- Shirazi, S.H., Naz, S., Razzaq, M.I., Umar, A.I., Zaib, A., 2018. Automated pathology image analysis, in: *Soft Computing Based Medical Image Analysis*. Elsevier, pp. 13–29.
- Shmatko, A., Ghaffari Laleh, N., Gerstung, M., Kather, J.N., 2022. Artificial intelligence in histopathology: enhancing cancer research and clinical oncology. *Nature cancer* 3, 1026–1038.
- Siegel, R.L., Miller, K.D., Jemal, A., 2020. Cancer statistics, 2020. *CA: A Cancer Journal for Clinicians* 70, 7–30.
- Sigirci, I.O., Albayrak, A., Bilgin, G., 2021. Detection of mitotic cells in breast cancer histopathological images using deep versus handcrafted features. *Multimedia Tools and Applications*, 1–24.
- Silva-Rodríguez, J., Colomer, A., Sales, M.A., Molina, R., Naranjo, V., 2020. Going deeper through the gleason scoring scale: An automatic end-to-end system for histology prostate grading and cribriform pattern detection. *Computer Methods and Programs in Biomedicine* 195, 105637.
- Singh, R., Chubb, L., Pantanowitz, L., Parwani, A., 2011. Standardization in digital pathology: Supplement 145 of the dicom standards. *Journal of Pathology Informatics* 2.
- Sirinukunwattana, K., Pluim, J.P., Chen, H., Qi, X., Heng, P.A., Guo, Y.B., Wang, L.Y., Matuszewski, B.J., Bruni, E., Sanchez, U., et al., 2017a. Gland segmentation in colon histology images: The glas challenge contest. *Medical Image Analysis* 35, 489–502.
- Sirinukunwattana, K., Pluim, J.P., Chen, H., Qi, X., Heng, P.A., Guo, Y.B., Wang, L.Y., Matuszewski, B.J., Bruni, E., Sanchez, U., et al., 2017b. Gland segmentation in colon histology images: The glas challenge contest. *Medical Image Analysis* 35, 489–502.
- Sirinukunwattana, K., Raza, S.E.A., Tsang, Y.W., Snead, D.R., Cree, I.A., Rajpoot, N.M., 2016. Locality sensitive deep learning for detection and classification of nuclei in routine colon cancer histology images. *IEEE Transactions on Medical Imaging* 35, 1196–1206.
- Sirinukunwattana, K., Snead, D.R., Rajpoot, N.M., 2015. A stochastic polygons model for glandular structures in colon histology images. *IEEE Transactions on Medical Imaging* 34, 2366–2378.
- Smith, J., Johnsen, S., Zeuthen, M.C., Thomsen, L.K., Marcussen, N., Hansen, S., Jensen, C.L., 2022. On the road to digital pathology in denmark—national survey and interviews. *Journal of Digital Imaging*, 1–18.
- Smith, J.H., 2011. Cytology, liquid-based cytology and automation. *Best Practice & Research Clinical Obstetrics & Gynaecology* 25, 585–596.
- Sobhani, F., Robinson, R., Hamidinekoo, A., Roxanis, I., Somaiah, N., Yuan, Y., 2021. Artificial intelligence and digital pathology: Opportunities and implications for immuno-oncology. *Biochimica et Biophysica Acta (BBA)-Reviews on Cancer* 1875, 188520.
- American Cancer Society, a. Brain tumors – classifications, symptoms, diagnosis and treatments. Available at: <https://www.aans.org/en/Patients/Neurosurgical-Conditions-and-Treatments/Brain-Tumors> (accessed Jan 30, 2023).
- American Cancer Society, b. Lymph nodes and cancer. Available at: <https://www.cancer.org/treatment/understanding-your-diagnosis/lymph-nodes-and-cancer.html> (accessed Jan 25, 2023).
- American Cancer Society, c. Tests to diagnose and stage prostate cancer. Available at: <https://www.cancer.org/cancer/prostate-cancer/detection-diagnosis-staging/how-diagnosed.html> (accessed Jan 21, 2023).
- American Cancer Society, d. Tests to diagnose and stage prostate cancer. Available at: <https://www.cancer.org/cancer/lung-cancer/about/what-is.html> (accessed Jan 21, 2023).
- American Cancer Society, e. What is bladder cancer? Available at: <https://www.cancer.org/cancer/bladder-cancer/about/what-is-bladder-cancer.html> (accessed Jan 25, 2023).
- American Cancer Society, f. What is breast cancer? Available at: <https://www.cancer.org/cancer/breast-cancer/about/what-is-breast-cancer.html> (accessed Jan 22, 2023).
- American Cancer Society, g. What is colorectal cancer? Available at: <https://www.cancer.org/cancer/colon-rectal-cancer/about/what-is-colorectal-cancer.html> (accessed Jan 21, 2023).
- American Cancer Society, h. What is ovarian cancer? Available at: <https://www.cancer.org/cancer/ovarian-cancer/about/what-is-ovarian-cancer.html> (accessed Jan 21, 2023).
- American Cancer Society, i. What is prostate cancer? Available at: <https://www.cancer.org/cancer/prostate-cancer/about/what-is-prostate-cancer.html> (accessed Jan 21, 2023).
- Society, A.C., a. Liver cancer survival rates. Available at: <https://www.cancer.org/cancer/liver-cancer/detection-diagnosis-staging/survival-rates.html> (accessed Feb 10, 2023).
- Society, A.C., b. Lung cancer survival rates. Available at: <https://www.cancer.org/cancer/lung-cancer/detection-diagnosis-staging/survival-rates.html> (accessed Feb 11, 2023).
- Society, A.C., c. Survival rates for bladder cancer. Available at: <https://www.cancer.org/cancer/bladder-cancer/detection-diagnosis-staging/survival-rates.html> (accessed Feb 10, 2023).
- Society, A.C., d. Survival rates for breast cancer. Available at: <https://www.cancer.org/cancer/breast-cancer/understanding-a-breast-cancer-diagnosis/breast-cancer-survival-rates.html> (accessed Feb 9, 2023).
- Society, A.C., e. Survival rates for colorectal cancer. Available at: <https://www.cancer.org/cancer/colon-rectal-cancer/detection-diagnosis-staging/survival-rates.html> (accessed Feb 9, 2023).
- Society, A.C., f. Survival rates for kidney cancer. Available at: <https://www.cancer.org/cancer/kidney-cancer/detection-diagnosis-staging/survival-rates.html> (accessed Feb 9, 2023).
- Society, A.C., g. Survival rates for prostate cancer. Available at: <https://www.cancer.org/cancer/prostate-cancer/detection-diagnosis-staging/survival-rates.html> (accessed Feb 8, 2023).
- Society, A.C., 2020. Colorectal cancer facts & figures 2020–2022. Published

- online , 48.
- Song, Z., Zou, S., Zhou, W., Huang, Y., Shao, L., Yuan, J., Gou, X., Jin, W., Wang, Z., Chen, X., et al., 2020. Clinically applicable histopathological diagnosis system for gastric cancer detection using deep learning. *Nature communications* 11, 1–9.
- Spanhol, F.A., Oliveira, L.S., Cavalin, P.R., Petitjean, C., Heutte, L., 2017. Deep features for breast cancer histopathological image classification, in: IEEE International Conference on Systems, Man, and Cybernetics (SMC), IEEE, pp. 1868–1873.
- Spanhol, F.A., Oliveira, L.S., Petitjean, C., Heutte, L., 2015. A dataset for breast cancer histopathological image classification. *IEEE Transactions on Biomedical Engineering* 63, 1455–1462.
- Spolverato, G., Kim, Y., Alexandrescu, S., Popescu, I., Marques, H.P., Aldrighetti, L., Clark Gamblin, T., Miura, J., Maithel, S.K., Squires, M.H., et al., 2015. Is hepatic resection for large or multifocal intrahepatic cholangiocarcinoma justified? results from a multi-institutional collaboration. *Annals of surgical oncology* 22, 2218–2225.
- Strigley, J.R., Zhou, M., Allan, R., et al., 2020. Protocol for the examination of resection specimens from patients with invasive carcinoma of renal tubular origin. The College of American Pathologists (CAP) Cancer Protocols, v4 1.
- Srinidhi, C.L., Ciga, O., Martel, A.L., 2021. Deep neural network models for computational histopathology: A survey. *Medical Image Analysis* 67, 101813. URL: <https://www.sciencedirect.com/science/article/pii/S1361841520301778>; doi:<https://doi.org/10.1016/j.media.2020.101813>.
- Srinidhi, C.L., Kim, S.W., Chen, F.D., Martel, A.L., 2022. Self-supervised driven consistency training for annotation efficient histopathology image analysis. *Medical Image Analysis* 75, 102256.
- Srinidhi, C.L., Martel, A.L., 2021. Improving self-supervised learning with hardness-aware dynamic curriculum learning: An application to digital pathology, in: IEEE/CVF International Conference on Computer Vision, pp. 562–571.
- Srougi, V., Kato, R.B., Salvatore, F.A., Ayres, P.P., Dall’Oglio, M.F., Srougi, M., 2009. Incidence of benign lesions according to tumor size in solid renal masses. *International braz j urol* 35, 427–431.
- Stacke, K., Eilertsen, G., Unger, J., Lundström, C., 2019. A closer look at domain shift for deep learning in histopathology. arXiv preprint arXiv:1909.11575 .
- Stamey, T.A., McNeal, J.E., Yemoto, C.M., Sigal, B.M., Johnstone, I.M., 1999. Biological determinants of cancer progression in men with prostate cancer. *Jama* 281, 1395–1400.
- Stathonikos, N., Veta, M., Huisman, A., van Diest, P.J., 2013. Going fully digital: Perspective of a dutch academic pathology lab. *Journal of pathology informatics* 4, 15.
- Steiner, D.F., MacDonald, R., Liu, Y., Truszkowski, P., Hipp, J.D., Gammie, C., Thng, F., Peng, L., Stumpe, M.C., 2018. Impact of deep learning assistance on the histopathologic review of lymph nodes for metastatic breast cancer. *The American journal of surgical pathology* 42, 1636.
- Su, A., Lee, H., Tan, X., Suarez, C.J., Andor, N., Nguyen, Q., Ji, H.P., 2022. A deep learning model for molecular label transfer that enables cancer cell identification from histopathology images. *NPJ precision oncology* 6, 1–11.
- Sun, C., Shrivastava, A., Singh, S., Gupta, A., 2017. Revisiting unreasonable effectiveness of data in deep learning era, in: Proceedings of the IEEE international conference on computer vision, pp. 843–852.
- Sundar, S., Ramani, P., Sherlin, H.J., Ranjith, G., Ramasubramani, A., Jayaraj, G., 2020. Awareness about whole slide imaging and digital pathology among pathologists-cross sectional survey. *Indian Journal of Forensic Medicine & Toxicology* 14.
- Suvarna, S.K., Layton, C., Bancroft, J.D., 2019. Bancroft’s theory and practice of histological techniques. 8 ed., Elsevier.
- Swiderska-Chadaj, Z., Ciompi, F., 2019. Lyon19- lymphocyte detection test set (version v1) [data set]. <https://zenodo.org/record/3385420#.XW-6JygzYuW>. [Accessed 18-Mar-2023].
- Swiderska-Chadaj, Z., Pinckaers, H., van Rijthoven, M., Balkenhol, M., Melnikova, M., Geessink, O., Manson, Q., Sherman, M., Polonia, A., Parry, J., et al., 2019. Learning to detect lymphocytes in immunohistochemistry with deep learning. *Medical image analysis* 58, 101547.
- Syrykh, C., Abreu, A., Amara, N., Siegfried, A., Maisongrosse, V., Frenois, F.X., Martin, L., Rossi, C., Laurent, C., Brousset, P., 2020. Accurate diagnosis of lymphoma on whole-slide histopathology images using deep learning. *NPJ Digital Medicine* 3, 1–8.
- Tabata, K., Uraoka, N., Benhamida, J., Hanna, M.G., Sirintrapun, S.J., Gallas, B.D., Gong, Q., Aly, R.G., Emoto, K., Matsuda, K.M., et al., 2019. Validation of mitotic cell quantification via microscopy and multiple whole-slide scanners. *Diagnostic pathology* 14, 1–9.
- Takahama, S., Kurose, Y., Mukuta, Y., Abe, H., Fukayama, M., Yoshizawa, A., Kitagawa, M., Harada, T., 2019. Multi-stage pathological image classification using semantic segmentation, in: IEEE/CVF International Conference on Computer Vision, pp. 10702–10711.
- Tan, C., Sun, F., Kong, T., Zhang, W., Yang, C., Liu, C., 2018. A survey on deep transfer learning, in: International conference on artificial neural networks, Springer, pp. 270–279.
- Tang, B., Li, A., Li, B., Wang, M., 2019. Capsurv: capsule network for survival analysis with whole slide pathological images. *IEEE Access* 7, 26022–26030.
- Tang, S., Hosseini, M.S., Chen, L., Varma, S., Rowsell, C., Damaskinos, S., Plataniotis, K.N., Wang, Z., 2021. Probeable darts with application to computational pathology, in: IEEE/CVF International Conference on Computer Vision, pp. 572–581.
- Tavolara, T.E., Niazi, M.K.K., Arole, V., Chen, W., Frankel, W., Gurcan, M.N., 2019. A modular cgan classification framework: Application to colorectal tumor detection. *Scientific Reports* 9, 1–8.
- Team, N.L.S.T.R., 2011. The national lung screening trial: overview and study design. *Radiology* 258, 243–253.
- Teh, E.W., Taylor, G.W., 2019. Metric learning for patch classification in digital pathology, in: International Conference on Medical Imaging with Deep Learning—Extended Abstract Track.
- Teh, E.W., Taylor, G.W., 2022. Learning with less labels in digital pathology via scribble supervision from natural images. arXiv preprint arXiv:2201.02627 .
- Teikari, P., Santos, M., Poon, C., Hyynnen, K., 2016. Deep learning convolutional networks for multiphoton microscopy vasculature segmentation. arXiv preprint arXiv:1606.02382 .
- Tellez, D., Balkenhol, M., Otte-Höller, I., van de Loo, R., Vogels, R., Bult, P., Wauters, C., Vreuls, W., Mol, S., Karssemeijer, N., et al., 2018. Whole-slide mitosis detection in h&e breast histology using phh3 as a reference to train distilled stain-invariant convolutional networks. *IEEE Transactions on Medical Imaging* 37, 2126–2136.
- Tellez, D., Höppener, D., Verhoef, C., Grünhagen, D., Nierop, P., Drozdal, M., Laak, J., Ciompi, F., 2020. Extending unsupervised neural image compression with supervised multitask learning , 770–783.
- Tellez, D., Litjens, G., Bández, P., Bulten, W., Bokhorst, J.M., Ciompi, F., Van Der Laak, J., 2019a. Quantifying the effects of data augmentation and stain color normalization in convolutional neural networks for computational pathology. *Medical Image Analysis* 58, 101544.
- Tellez, D., Litjens, G., van der Laak, J., Ciompi, F., 2019b. Neural image compression for gigapixel histopathology image analysis. *IEEE Transactions on Pattern Analysis and Machine Intelligence* 43, 567–578.
- Thagaard, J., Hauberg, S., Vegt, B.v.d., Ebstrup, T., Hansen, J.D., Dahl, A.B., 2020. Can you trust predictive uncertainty under real dataset shifts in digital pathology?, in: International Conference on Medical Image Computing and Computer-Assisted Intervention, Springer, pp. 824–833.
- Thandiackal, K., Chen, B., Pati, P., Jaume, G., Williamson, D.F., Gabrani, M., Goksel, O., 2022. Differentiable zooming for multiple instance learning on whole-slide images. arXiv preprint arXiv:2204.12454 .
- Thiagarajan, P., Khairnar, P., Ghosh, S., 2021. Explanation and use of uncertainty quantified by bayesian neural network classifiers for breast histopathology images. *IEEE Transactions on Medical Imaging* 41, 815–825.
- Thorstenson, S., Molin, J., Lundström, C., 2014. Implementation of large-scale routine diagnostics using whole slide imaging in sweden: Digital pathology experiences 2006–2013. *Journal of pathology informatics* 5, 14.
- Thuy, M.B.H., Hoang, V.T., 2019. Fusing of deep learning, transfer learning and GAN for breast cancer histopathological image classification, in: International Conference on Computer Science, Applied Mathematics and Applications, Springer, pp. 255–266.
- Tian, Y., Yang, L., Wang, W., Zhang, J., Tang, Q., Ji, M., Yu, Y., Li, Y., Yang, H., Qian, A., 2019. Computer-aided detection of squamous carcinoma of the cervix in whole slide images. arXiv preprint arXiv:1905.10959 .
- Tjio, G., Yang, X., Hong, J.M., Wong, S.T., Ding, V., Choo, A., Su, Y., 2020. Accurate tumor tissue region detection with accelerated deep convolutional neural networks. arXiv preprint arXiv:2004.08552 .
- Tokunaga, H., Teramoto, Y., Yoshizawa, A., Bise, R., 2019. Adaptive weight-

- ing multi-field-of-view cnn for semantic segmentation in pathology, in: IEEE/CVF Conference on Computer Vision and Pattern Recognition, pp. 12597–12606.
- Tolkach, Y., Dohmögören, T., Toma, M., Kristiansen, G., 2020. High-accuracy prostate cancer pathology using deep learning. *Nature Machine Intelligence* 2, 411–418.
- Tomaszewski, J.E., 2021. Overview of the role of artificial intelligence in pathology: the computer as a pathology digital assistant, in: Artificial Intelligence and Deep Learning in Pathology. Elsevier, pp. 237–262.
- Tomita, N., Abdollahi, B., Wei, J., Ren, B., Suriawinata, A., Hassanzpour, S., 2019. Attention-based deep neural networks for detection of cancerous and precancerous esophagus tissue on histopathological slides. *JAMA network open* 2, e1914645–e1914645.
- Tran, M., Wagner, S.J., Boxberg, M., Peng, T., 2021. S5cl: Supervised, self-supervised, and semi-supervised contrastive learning for sparsely labeled data.
- Tsutani, Y., Miyata, Y., Nakayama, H., Okumura, S., Adachi, S., Yoshimura, M., Okada, M., 2012. Prognostic significance of using solid versus whole tumor size on high-resolution computed tomography for predicting pathologic malignant grade of tumors in clinical stage ia lung adenocarcinoma: a multicenter study. *The Journal of thoracic and cardiovascular surgery* 143, 607–612.
- Turki, T., Al-Sharif, A., Taguchi, Y., 2021. End-to-end deep learning for detecting metastatic breast cancer in axillary lymph node from digital pathology images. medRxiv.
- Ueno, H., Shirouzu, K., Eishi, Y., Yamada, K., Kusumi, T., Kushima, R., Ikegami, M., Murata, A., Okuno, K., Sato, T., et al., 2013. Study group for perineural invasion projected by the Japanese society for cancer of the colon and rectum (JSCCR). characterization of perineural invasion as a component of colorectal cancer staging. *Am J Surg Pathol* 37, 1542–9.
- Uhlen, M., Zhang, C., Lee, S., Sjöstedt, E., Fagerberg, L., Bidkhor, G., Benfeitas, R., Arif, M., Liu, Z., Edfors, F., et al., 2017. A pathology atlas of the human cancer transcriptome. *Science* 357, eaan2507.
- University of Leeds, . Welcome to the university of leeds virtual pathology project website. Available at: <https://www.virtualpathology.leeds.ac.uk/> (accessed June 10, 2021).
- Uthman, E., 2009. Gastric amyloidosis (congo red stain). URL: https://commons.wikimedia.org/wiki/File:Gastric_Amyloidosis_%28Congo_Red_Stain%29_%28283595839154%29.jpg.
- Vacante, M., Borzì, A.M., Basile, F., Biondi, A., 2018. Biomarkers in colorectal cancer: Current clinical utility and future perspectives. *World journal of clinical cases* 6, 869.
- Vahadane, A., Atheth, B., Majumdar, S., 2021. Dual encoder attention u-net for nuclei segmentation , 3205–3208.
- Valkonen, M., Kartasalo, K., Liimatainen, K., Nykter, M., Latonen, L., Ruusuvuori, P., 2017. Dual structured convolutional neural network with feature augmentation for quantitative characterization of tissue histology, in: IEEE International Conference on Computer Vision Workshops, pp. 27–35.
- Van Eycke, Y.R., Balsat, C., Verset, L., Debeir, O., Salmon, I., Decaestecker, C., 2018. Segmentation of glandular epithelium in colorectal tumours to automatically compartmentalise iHC biomarker quantification: A deep learning approach. *Medical Image Analysis* 49, 35–45.
- Vang, Y.S., Chen, Z., Xie, X., 2018. Deep learning framework for multi-class breast cancer histology image classification, in: International Conference Image Analysis and Recognition, Springer, pp. 914–922.
- Varma, M., 2021. Intraductal carcinoma of the prostate: a guide for the practicing pathologist. *Advances in Anatomic Pathology* 28, 276–287.
- Veeling, B.S., Linmans, J., Winkens, J., Cohen, T., Welling, M., 2018. Rotation equivariant cnns for digital pathology, in: Frangi, A.F., Schnabel, J.A., Davatzikos, C., Alberola-López, C. (Eds.), *Medical Image Computing and Computer Assisted Intervention – MICCAI*, Springer, pp. 210–218.
- Vermij, L., Léon-Castillo, A., Singh, N., Powell, M.E., Edmondson, R.J., Genestie, C., Khaw, P., Pyman, J., McLachlin, C.M., Ghatare, P., et al., 2022. p53 immunohistochemistry in endometrial cancer: clinical and molecular correlates in the portec-3 trial. *Modern Pathology* 35, 1475–1483.
- Veta, M., Heng, Y.J., Stathakis, N., Bejnordi, B.E., Beca, F., Wollmann, T., Rohr, K., Shah, M.A., Wang, D., Rousson, M., et al., 2019. Predicting breast tumor proliferation from whole-slide images: the tupac16 challenge. *Medical Image Analysis* 54, 111–121.
- Veta, M., Van Diest, P.J., Willems, S.M., Wang, H., Madabhushi, A., Cruz-Roa, A., Gonzalez, F., Larsen, A.B., Vestergaard, J.S., Dahl, A.B., et al., 2015. Assessment of algorithms for mitosis detection in breast cancer histopathology images. *Medical Image Analysis* 20, 237–248.
- Vu, Q.D., Graham, S., Kurc, T., To, M.N.N., Shaban, M., Qaiser, T., Koohbanani, N.A., Khurram, S.A., Kalpathy-Cramer, J., Zhao, T., et al., 2019. Methods for segmentation and classification of digital microscopy tissue images. *Frontiers in Bioengineering and Biotechnology* , 53.
- Wahab, N., Khan, A., Lee, Y.S., 2017. Two-phase deep convolutional neural network for reducing class skewness in histopathological images based breast cancer detection. *Computers in Biology and Medicine* 85, 86–97.
- Wahab, N., Miligy, I.M., Dodd, K., Sahota, H., Toss, M., Lu, W., Jahanifar, M., Bilal, M., Graham, S., Park, Y., et al., 2022. Semantic annotation for computational pathology: Multidisciplinary experience and best practice recommendations. *The Journal of Pathology: Clinical Research* 8, 116–128.
- Wang, C., Shi, J., Zhang, Q., Ying, S., 2017a. Histopathological image classification with bilinear convolutional neural networks, in: International Conference of the IEEE Engineering in Medicine and Biology Society (EMBC), IEEE, pp. 4050–4053.
- Wang, F., Oh, T.W., Vergara-Niedermayr, C., Kurc, T., Saltz, J., 2012. Managing and querying whole slide images, in: Medical Imaging 2012: Advanced PACS-Based Imaging Informatics and Therapeutic Applications, SPIE, pp. 137–148.
- Wang, H., Roa, A.C., Basavanhally, A.N., Gilmore, H.L., Shih, N., Feldman, M., Tomaszewski, J., Gonzalez, F., Madabhushi, A., 2014. Mitosis detection in breast cancer pathology images by combining handcrafted and convolutional neural network features. *Journal of Medical Imaging* 1, 034003.
- Wang, L., Dou, X., Liu, T., Lu, W., Ma, Y., Yang, Y., 2018a. Tumor size and lymph node metastasis are prognostic markers of small cell lung cancer in a Chinese population. *Medicine* 97.
- Wang, L., Sun, L., Zhang, M., Zhang, H., Ping, W., Zhou, R., Sun, J., 2021a. Exploring pathologist knowledge for automatic assessment of breast cancer metastases in whole-slide image, in: ACM International Conference on Multimedia, pp. 255–263.
- Wang, L., Zhen, H., Fang, X., Wan, S., Ding, W., Guo, Y., 2019a. A unified two-parallel-branch deep neural network for joint gland contour and segmentation learning. *Future Generation Computer Systems* 100, 316–324.
- Wang, S., Rong, R., Yang, D.M., Fujimoto, J., Yan, S., Cai, L., Yang, L., Luo, D., Behrens, C., Parra, E.R., et al., 2020a. Computational staining of pathology images to study the tumor microenvironment in lung cancer. *Cancer research* 80, 2056–2066.
- Wang, S., Wang, T., Yang, L., Yang, D.M., Fujimoto, J., Yi, F., Luo, X., Yang, Y., Yao, B., Lin, S., et al., 2019b. Convpath: A software tool for lung adenocarcinoma digital pathological image analysis aided by a convolutional neural network. *EBioMedicine* 50, 103–110.
- Wang, S., Yang, D.M., Rong, R., Zhan, X., Xiao, G., 2019c. Pathology image analysis using segmentation deep learning algorithms. *The American journal of pathology* 189, 1686–1698.
- Wang, S., Zhu, Y., Yu, L., Chen, H., Lin, H., Wan, X., Fan, X., Heng, P.A., 2019d. Rmdl: Recalibrated multi-instance deep learning for whole slide gastric image classification. *Medical Image Analysis* 58, 101549.
- Wang, W., Ozolek, J.A., Rohde, G.K., 2010. Detection and classification of thyroid follicular lesions based on nuclear structure from histopathology images. *Cytometry Part A: The Journal of the International Society for Advancement of Cytometry* 77, 485–494.
- Wang, X., Janowczyk, A., Zhou, Y., Thawani, R., Fu, P., Schalper, K., Velcheti, V., Madabhushi, A., 2017b. Prediction of recurrence in early stage non-small cell lung cancer using computer extracted nuclear features from digital h&e images. *Scientific Reports* 7, 1–10.
- Wang, Y., Farnell, D., Farahani, H., Nursey, M., Tessier-Cloutier, B., Jones, S.J., Huntsman, D.G., Gilks, C.B., Bashashati, A., 2020b. Classification of epithelial ovarian carcinoma whole-slide pathology images using deep transfer learning, in: *Medical Imaging with Deep Learning*.
- Wang, Z., Dong, N., Dai, W., Rosario, S.D., Xing, E.P., 2018b. Classification of breast cancer histopathological images using convolutional neural networks with hierarchical loss and global pooling, in: International Conference Image Analysis and Recognition, Springer, pp. 745–753.
- Wang, Z., Hosseini, M.S., Miles, A., Plataniotis, K.N., Wang, Z., 2020c. Focuslenn: High efficiency focus quality assessment for digital pathology, in: Martel, A.L., Abolmaesumi, P., Stoyanov, D., Mateus, D., Zuluaga, M.A. (Eds.), *Medical Image Computing and Computer-Assisted Intervention – MICCAI*, Springer, p. 403–413.
- Wang, Z., Li, R., Wang, M., Li, A., 2021b. Gpdbname: deep bilinear network integrating both genomic data and pathological images for breast cancer prognosis prediction. *Bioinformatics* 37, 2963–2970.

- Wang, Z., Yu, L., Ding, X., Liao, X., Wang, L., 2022. Lymph node metastasis prediction from whole slide images with transformer-guided multi-instance learning and knowledge transfer. *IEEE Transactions on Medical Imaging* .
- Wanless, I.R., et al., 1995. Terminology of nodular hepatocellular lesions. *Hepatology* 22, 983–993.
- Wei, J., Suriawinata, A., Ren, B., Liu, X., Lisovsky, M., Vaickus, L., Brown, C., Baker, M., Nasir-Moin, M., Tomita, N., et al., 2021a. Learn like a pathologist: curriculum learning by annotator agreement for histopathology image classification, in: *IEEE/CVF Conference on Computer Vision*, pp. 2473–2483.
- Wei, J., Suriawinata, A., Ren, B., Liu, X., Lisovsky, M., Vaickus, L., Brown, C., Baker, M., Tomita, N., Torresani, L., et al., 2021b. A petri dish for histopathology image analysis, in: *International Conference on Artificial Intelligence in Medicine*, Springer. pp. 11–24.
- Wei, J.W., Tafe, L.J., Linnik, Y.A., Vaickus, L.J., Tomita, N., Hassanpour, S., 2019a. Pathologist-level classification of histologic patterns on resected lung adenocarcinoma slides with deep neural networks. *Scientific Reports* 9, 1–8.
- Wei, J.W., Wei, J.W., Jackson, C.R., Ren, B., Suriawinata, A.A., Hassanpour, S., 2019b. Automated detection of celiac disease on duodenal biopsy slides: A deep learning approach. *Journal of Pathology Informatics* 10.
- Weng, W.H., Cai, Y., Lin, A., Tan, F., Chen, P.H.C., 2019. Multimodal multitask representation learning for pathology biobank metadata prediction. *arXiv preprint arXiv:1909.07846*.
- Wetstein, S.C., Onken, A.M., Luffman, C., Baker, G.M., Pyle, M.E., Kensler, K.H., Liu, Y., Bakker, B., Vlutters, R., van Leeuwen, M.B., et al., 2020. Deep learning assessment of breast terminal duct lobular unit involution: Towards automated prediction of breast cancer risk. *PloS one* 15, e0231653.
- Willemink, M.J., Koszek, W.A., Hardell, C., Wu, J., Fleischmann, D., Harvey, H., Folio, L.R., Summers, R.M., Rubin, D.L., Lungren, M.P., 2020. Preparing medical imaging data for machine learning. *Radiology* 295, 4–15.
- Williams, B.J., Hanby, A., Millican-Slater, R., Nijhawan, A., Verghese, E., Treanor, D., 2018. Digital pathology for the primary diagnosis of breast histopathological specimens: an innovative validation and concordance study on digital pathology validation and training. *Histopathology* 72, 662–671.
- Woerl, A.C., Eckstein, M., Geiger, J., Wagner, D.C., Daher, T., Stenzel, P., Fernandez, A., Hartmann, A., Wand, M., Roth, W., et al., 2020. Deep learning predicts molecular subtype of muscle-invasive bladder cancer from conventional histopathological slides. *European urology* 78, 256–264.
- Wolff, A.C., Hammond, M.E.H., Allison, K.H., Harvey, B.E., McShane, L.M., Dowsett, M., 2018. Her2 testing in breast cancer: American society of clinical oncology/college of american pathologists clinical practice guideline focused update summary. *Journal of oncology practice* 14, 437–441.
- Wolpert, D.H., Macready, W.G., 1997. No free lunch theorems for optimization. *IEEE transactions on evolutionary computation* 1, 67–82.
- Wong, A.N.N., He, Z., Leung, K.L., To, C.C.K., Wong, C.Y., Wong, S.C.C., Yoo, J.S., Chan, C.K.R., Chan, A.Z., Lacambra, M.D., et al., 2022. Current developments of artificial intelligence in digital pathology and its future clinical applications in gastrointestinal cancers. *Cancers* 14, 3780.
- World Health Organization, . Cancer. Available at: <https://www.who.int/news-room/fact-sheets/detail/cancer> (accessed June 10, 2021).
- Wright, A.I., Dunn, C.M., Hale, M., Hutchins, G., Treanor, D., 2020. The effect of quality control on accuracy of digital pathology image analysis. *IEEE Journal of Biomedical and Health Informatics* .
- Wright, J.L., Dalkin, B.L., True, L.D., Ellis, W.J., Stanford, J.L., Lange, P.H., Lin, D.W., 2010. Positive surgical margins at radical prostatectomy predict prostate cancer specific mortality. *The Journal of urology* 183, 2213–2218.
- Wu, B., Zhao, S., Sun, G., Zhang, X., Su, Z., Zeng, C., Liu, Z., 2019. P3sgd: Patient privacy preserving sgd for regularizing deep cnns in pathological image classification, in: *IEEE/CVF Conference on Computer Vision and Pattern Recognition*, pp. 2099–2108.
- Wu, F., Liu, P., Fu, B., Ye, F., 2022a. Deepgcnmil: Multi-head attention guided multi-instance learning approach for whole-slide images survival analysis using graph convolutional networks. in: *2022 14th International Conference on Machine Learning and Computing (ICMLC)*, pp. 67–73.
- Wu, H., Wang, Z., Song, Y., Yang, L., Qin, J., 2022b. Cross-patch dense contrastive learning for semi-supervised segmentation of cellular nuclei in histopathologic images, in: *Proceedings of the IEEE/CVF Conference on Computer Vision and Pattern Recognition*, pp. 11666–11675.
- Wu, J., Liu, C., Liu, X., Sun, W., Li, L., Gao, N., Zhang, Y., Yang, X., Zhang, J., Wang, H., et al., 2021. Artificial intelligence-assisted system for precision diagnosis of pd-l1 expression in non-small cell lung cancer. *Modern Pathology* , 1–9.
- Xiang, T., Song, Y., Zhang, C., Liu, D., Chen, M., Zhang, F., Huang, H., O'Donnell, L., Cai, W., 2021. Dsnet: A dual-stream framework for weakly-supervised gigapixel pathology image analysis. *arXiv preprint arXiv:2109.05788*.
- Xie, P., Zuo, K., Zhang, Y., Li, F., Yin, M., Lu, K., 2019. Interpretable classification from skin cancer histology slides using deep learning: A retrospective multicenter study. *arXiv preprint arXiv:1904.06156* .
- Xie, X., Chen, J., Li, Y., Shen, L., Ma, K., Zheng, Y., 2020. Instance-aware self-supervised learning for nuclei segmentation, in: *International Conference on Medical Image Computing and Computer-Assisted Intervention*, Springer. pp. 341–350.
- Xing, G., Lei, J., Xu, X., 2021. Fluid segmentation in oct with an improved convolutional neural network, in: *The Fifth International Conference on Biological Information and Biomedical Engineering*, pp. 1–5.
- Xiong, Z., Zheng, Y., Qiu, J., 2021. Processing tissue micro-array images using machine learning techniques as preparation for determining gleason grade of prostate cancer , 34–41.
- Xu, B., Liu, J., Hou, X., Liu, B., Garibaldi, J., Ellis, I.O., Green, A., Shen, L., Qiu, G., 2019a. Attention by selection: A deep selective attention approach to breast cancer classification. *IEEE Transactions on Medical Imaging* 39, 1930–1941.
- Xu, B., Liu, J., Hou, X., Liu, B., Garibaldi, J., Ellis, I.O., Green, A., Shen, L., Qiu, G., 2019b. Look, investigate, and classify: a deep hybrid attention method for breast cancer classification, in: *IEEE International Symposium on Biomedical Imaging*, IEEE. pp. 914–918.
- Xu, H., Park, S., Clemenceau, J.R., Radakovich, N., Lee, S.H., Hwang, T.H., 2020. Deep transfer learning approach to predict tumor mutation burden (tmb) and delineate spatial heterogeneity of tmb within tumors from whole slide images. *Cold Spring Harbor Lab* 1, 554527.
- Xu, J., Luo, X., Wang, G., Gilmore, H., Madabhushi, A., 2016. A deep convolutional neural network for segmenting and classifying epithelial and stromal regions in histopathological images. *Neurocomputing* 191, 214–223.
- Xu, Y., Jia, Z., Wang, L.B., Ai, Y., Zhang, F., Lai, M., Eric, I., Chang, C., 2017a. Large scale tissue histopathology image classification, segmentation, and visualization via deep convolutional activation features. *BMC bioinformatics* 18, 1–17.
- Xu, Y., Li, Y., Shen, Z., Wu, Z., Gao, T., Fan, Y., Lai, M., Eric, I., Chang, C., 2017b. Parallel multiple instance learning for extremely large histopathology image analysis. *BMC bioinformatics* 18, 1–15.
- Xu, Y., Li, Y., Wang, Y., Liu, M., Fan, Y., Lai, M., Eric, I., Chang, C., 2017c. Gland instance segmentation using deep multichannel neural networks. *IEEE Transactions on Biomedical Engineering* 64, 2901–2912.
- Xu, Y., Mo, T., Feng, Q., Zhong, P., Lai, M., Eric, I., Chang, C., 2014. Deep learning of feature representation with multiple instance learning for medical image analysis, in: *IEEE International Conference on Acoustics, Speech and Signal Processing (ICASSP)*, IEEE. pp. 1626–1630.
- Xu, Z., Moro, C.F., Bozóky, B., Zhang, Q., 2019c. Gan-based virtual restaining: a promising solution for whole slide image analysis. *arXiv preprint arXiv:1901.04059* .
- Yaar, A., Asif, A., E Ahmed Raza, S., Rajpoot, N., Minhas, F., . Cross-domain knowledge transfer for prediction of chemosensitivity in ovarian cancer patients, in: *IEEE/CVF Conference on Computer Vision and Pattern Recognition Workshops*, pp. 928–929.
- Yagi, Y., 2011. Color standardization and optimization in whole slide imaging, in: *Diagnostic pathology*, Springer. pp. 1–12.
- Yamashita, R., Long, J., Banda, S., Shen, J., Rubin, D.L., 2021. Learning domain-agnostic visual representation for computational pathology using medically-irrelevant style transfer augmentation. *IEEE Transactions on Medical Imaging* 40, 3945–3954.
- Yan, C., Nakane, K., Wang, X., Fu, Y., Lu, H., Fan, X., Feldman, M.D., Madabhushi, A., Xu, J., 2020a. Automated gleason grading on prostate biopsy slides by statistical representations of homology profile. *Computer methods and programs in biomedicine* 194, 105528.
- Yan, C., Xu, J., Xie, J., Cai, C., Lu, H., 2020b. Prior-aware cnn with multi-task learning for colon images analysis , 254–257.
- Yan, R., Ren, F., Wang, Z., Wang, L., Ren, Y., Liu, Y., Rao, X., Zheng, C., Zhang, F., 2018. A hybrid convolutional and recurrent deep neural network for breast cancer pathological image classification, in: *IEEE International Conference on Bioinformatics and Biomedicine (BIBM)*, IEEE. pp. 957–962.
- Yan, R., Ren, F., Wang, Z., Wang, L., Zhang, T., Liu, Y., Rao, X., Zheng, C.,

- Zhang, F., 2020c. Breast cancer histopathological image classification using a hybrid deep neural network. *Methods* 173, 52–60.
- Yang, H., Deng, R., Lu, Y., Zhu, Z., Chen, Y., Roland, J.T., Lu, L., Landman, B.A., Fogel, A.B., Huo, Y., 2020. Circlenet: Anchor-free glomerulus detection with circle representation, in: International Conference on Medical Image Computing and Computer-Assisted Intervention, Springer. pp. 35–44.
- Yang, J., Chen, H., Liang, Y., Huang, J., He, L., Yao, J., 2022a. Concl: Concept contrastive learning for dense prediction pre-training in pathology images, in: European Conference on Computer Vision, Springer. pp. 523–539.
- Yang, J., Chen, H., Yan, J., Chen, X., Yao, J., 2022b. Towards better understanding and better generalization of few-shot classification in histology images with contrastive learning. *arXiv preprint arXiv:2202.09059*.
- Yang, S.P., Su, H.L., Chen, X.B., Hua, L., Chen, J.X., Hu, M., Lei, J., Wu, S.G., Zhou, J., et al., 2021. Long-term survival among histological subtypes in advanced epithelial ovarian cancer: population-based study using the surveillance, epidemiology, and end results database. *JMIR Public Health and Surveillance* 7, e25976.
- Yao, H., Zhang, X., Zhou, X., Liu, S., 2019. Parallel structure deep neural network using cnn and rnn with an attention mechanism for breast cancer histology image classification. *Cancers* 11, 1901.
- Yao, J., Zhu, X., Jonnagaddala, J., Hawkins, N., Huang, J., 2020. Whole slide images based cancer survival prediction using attention guided deep multiple instance learning networks. *Medical Image Analysis* 65, 101789.
- Yen, T.A., Hsu, H.C., Pati, P., Gabrani, M., Foncubierta-Rodríguez, A., Chung, P.C., 2020. Ninepins: Nuclei instance segmentation with point annotations. *arXiv preprint arXiv:2006.13556*.
- Yoshizawa, A., Motoi, N., Riely, G.J., Sima, C.S., Gerald, W.L., Kris, M.G., Park, B.J., Rusch, V.W., Travis, W.D., 2011. Impact of proposed iaslcc/ats/ers classification of lung adenocarcinoma: prognostic subgroups and implications for further revision of staging based on analysis of 514 stage i cases. *Modern pathology* 24, 653–664.
- You, Y.N., Hardiman, K.M., Bafford, A., Poylin, V., Francone, T.D., Davis, K., Paquette, I.M., Steele, S.R., Feingold, D.L., et al., 2020. The american society of colon and rectal surgeons clinical practice guidelines for the management of rectal cancer. *Diseases of the Colon & Rectum* 63, 1191–1222.
- Yu, K.H., Zhang, C., Berry, G.J., Altman, R.B., Ré, C., Rubin, D.L., Snyder, M., 2016. Predicting non-small cell lung cancer prognosis by fully automated microscopic pathology image features. *Nature communications* 7, 1–10.
- Zadeh Shirazi, A., Fornaciari, E., Bagherian, N.S., Ebert, L.M., Koszyca, B., Gomez, G.A., 2020. Deepsurvnet: deep survival convolutional network for brain cancer survival rate classification based on histopathological images. *Medical & Biological Engineering & Computing* 58, 1031–1045.
- Zamir, A.R., Sax, A., Shen, W., Guibas, L.J., Malik, J., Savarese, S., 2018. Taskonomy: Disentangling task transfer learning, in: Proceedings of the IEEE conference on computer vision and pattern recognition, pp. 3712–3722.
- Zanjani, F.G., Zinger, S., Bejnordi, B.E., van der Laak, J.A., et al., 2018. Histopathology stain-color normalization using deep generative models, in: 1st Conference on Medical Imaging with Deep Learning (MIDL), pp. 1–11.
- Zarella, M.D., Bowman, D., Aeffner, F., Farahani, N., Xthona, A., Absar, S.F., Parwani, A., Bui, M., Hartman, D.J., 2019. A practical guide to whole slide imaging: a white paper from the digital pathology association. *Archives of pathology & laboratory medicine* 143, 222–234.
- Zhang, F., Yao, S., Li, Z., Liang, C., Zhao, K., Huang, Y., Gao, Y., Qu, J., Li, Z., Liu, Z., 2020. Predicting treatment response to neoadjuvant chemoradiotherapy in local advanced rectal cancer by biopsy digital pathology image features. *Clinical and translational medicine* 10, e110.
- Zhang, H., Meng, Y., Zhao, Y., Qiao, Y., Yang, X., Coupland, S.E., Zheng, Y., 2022. Dtfdf-mil: Double-tier feature distillation multiple instance learning for histopathology whole slide image classification, in: Proceedings of the IEEE/CVF Conference on Computer Vision and Pattern Recognition, pp. 18802–18812.
- Zhang, J., Gold, K.A., Lin, H.Y., Swisher, S.G., Xing, Y., Lee, J.J., Kim, E.S., William Jr, W.N., 2015. Relationship between tumor size and survival in non-small-cell lung cancer (nsclc): an analysis of the surveillance, epidemiology, and end results (seer) registry. *Journal of Thoracic Oncology* 10, 682–690.
- Zhang, Y., Cao, L., Nguyen, D., Lu, H., 2016a. Tp53 mutations in epithelial ovarian cancer. *Translational cancer research* 5, 650.
- Zhang, Y., Ling, H., Gao, J., Yin, K., Lafleche, J.F., Barriuso, A., Torralba, A., Fidler, S., 2021. Datasetgan: Efficient labeled data factory with minimal human effort, in: IEEE/CVF Conference on Computer Vision and Pattern Recognition, pp. 10145–10155.
- Zhang, Y., Yang, Q., 2021. A survey on multi-task learning. *IEEE Transactions on Knowledge and Data Engineering*.
- Zhang, Z., Chen, P., McGough, M., Xing, F., Wang, C., Bui, M., Xie, Y., Sapkota, M., Cui, L., Dhillon, J., et al., 2019. Pathologist-level interpretable whole-slide cancer diagnosis with deep learning. *Nature Machine Intelligence* 1, 236–245.
- Zhang, Z., Fidler, S., Urtasun, R., 2016b. Instance-level segmentation for autonomous driving with deep densely connected mrf, in: IEEE Conference on Computer Vision and Pattern Recognition, pp. 669–677.
- Zheng, X., Wang, R., Zhang, X., Sun, Y., Zhang, H., Zhao, Z., Zheng, Y., Luo, J., Zhang, J., Wu, H., et al., 2022. A deep learning model and human-machine fusion for prediction of ebv-associated gastric cancer from histopathology. *Nature communications* 13, 1–12.
- Zheng, Y., Jiang, Z., Zhang, H., Xie, F., Shi, J., 2020. Tracing diagnosis paths on histopathology wsis for diagnostically relevant case recommendation, in: Martel, A.L., Abolmaesumi, P., Stoyanov, D., Mateus, D., Zuluaga, M.A. (Eds.), Medical Image Computing and Computer Assisted Intervention – MICCAI, Springer. pp. 459–469.
- Zhou, M., 2013. Intraductal carcinoma of the prostate: the whole story. *Pathology* 45, 533–539.
- Zhu, C., Chen, W., Peng, T., Wang, Y., Jin, M., . Hard sample aware noise robust learning for histopathology image classification. *IEEE transactions on medical imaging*.
- Zhu, C., Chen, W., Peng, T., Wang, Y., Jin, M., 2021a. Hard sample aware noise robust learning for histopathology image classification. *IEEE Transactions on Medical Imaging* 41, 881–894.
- Zhu, Y., Zheng, Y., Chen, Z., 2021b. Cell detection by robust self-trained networks, in: International Conference on Pattern Recognition and Intelligent Systems, pp. 64–67.
- Ziae, D., Li, W., Lam, S., Cheng, W.C., Chen, W., 2020. Characterization of color normalization methods in digital pathology whole slide imaging, in: Medical Imaging: Digital Pathology, International Society for Optics and Photonics. p. 1132017.
- Zioga, C., Kamas, A., Patsiaoura, K., Dimitropoulos, K., Barmpoutis, P., Grammalidis, N., 2017. Breast carcinoma histological images from the department of pathology, “agios pavlos” general hospital of thessaloniki. Greece, July .

8. Supplementary Material

8.1. Surveyed Datasets

8.1.1. Table Creation Details

For each dataset recorded in the literature, a collection of information was collected. This information was organized into 10 categories, listed below. The full table is given in Table 8.3:

1. *Dataset Name*: The name of the dataset, if given. If no name is given, then a name was given for book-keeping purposes.
2. *References*: The works that use this dataset are listed.
3. *Availability*: A hyperlink to the dataset, when publicly available or available for request directly is provided.
4. *Stain type*: The type of stain used.
5. *Size*: Describes the number of WSIs, where this information is available, or the number of patches present in the dataset.
6. *Resolution (μm)/ Magnification*: Presents the resolution, in micrometers along with the magnification in the format $\mu\text{m}/\text{Magnification}$. If a piece of information is unavailable (either resolution or magnification) this information is omitted from the table.
7. *Annotation Type*: Describes the annotation granularity present in the dataset (patient, slide, ROI/ROI mask, patch, pixel) where available.
8. *Label Structure*: Whether each image in the dataset has a single label associated with it, or multiple. Datasets, where each image has only a single label associated with it, are labeled with *S*, whereas those with multiple labels are labeled with *M*.
9. *Classes*: The number of classes available, where this count is meaningful. Where it is more helpful to describe the format of ground truth (ex. nucleus pixel locations), this is written instead.
10. *Class Balance (CB)*: Datasets which are balanced are marked with a *B*, whereas those which are imbalanced are marked as *I*. Those where this information is unavailable are marked with an *U*.

8.2. Organ Overview

For each paper recorded in the literature, a collection of information about their specific goal was collected. This information was categorized by organ and arranged into a table, the organs being: Basal/Epithelium, Bladder, Brain, Mouth/Esophagus, Breast, Liver, Lymph Node, Prostate/Ovary, Kidney, Lung, Pancreas, Thyroid, Stomach/Colon. Below will be the explanation of each column in Table 8.3:

1. *References*: Reference number of the paper that involved the specified task.
2. *Tasks*: Specific target goal that the work wanted to achieve, this range from different types of detection, classification, and segmentation to prognosis and diagnosis.
3. *Disease Specification*: Describes the pathology of the target goal of the paper.
4. *Methods*: Define the different machine learning methods used to achieve the proposed target task of the paper.

8.3. Technicalities by Task

For each paper recorded in the literature, a collection of information on the Neural Network architectures used was organized and categorized by its specific task. It was found that across the majority of papers, the following five tasks were the most prevalent: Detection, Disease Diagnosis, Segmentation, WSI Processing, and Patient Prognosis. At the end of the table, an **Other Task** section was added to attach other works that don't follow the selected tasks. Below will be the explanation of each column in Table 8.3:

1. *References*: Reference number of the paper that involved the specified task.
2. *Tasks Specification*: Describes the pathology of the target goal of the paper.
3. *Architecture*: Defines the different Neural Network architectures used to achieve the proposed target task of the paper.
4. *Datasets*: Name of the datasets used for the specified task (see Table 8.3 for information on datasets).

Compilation of all the datasets carefully studied in this survey with its respective information (see Table Creation Details)

Dataset Name	References	Availability	Stain Type	Size	Res(μm)/ Mag	Annotation	Label	Class	CB
Basal/Epithelium									
NKI-VGH	Beck et al. (2011)	Link	H&E	158 ROIs	N/A	Pixel	S	2	U
AJ-Epi-Seg	Janowczyk and Madabhushi (2016)	Link	H&E	42 ROIs	20×	Pixel	S	2	U
TCGA-Phil	Phillips et al. (2018)	TCGA	H&E	50 WSIs	40×	Pixel	S	4	I
MOIC	Jiang et al. (2020b)	N/A	N/A	6 610 MOIs	10×	Slide	S	2	U
MOIS	Jiang et al. (2020b)	N/A	N/A	1 436 MOIs	10×	Pixel	S	2	U
Jiang et al.	Jiang et al. (2020b)	N/A	N/A	128 WSIs	40×	Pixel	S	2	U
MIP	Kulkarni et al. (2020)	N/A	H&E	108 Patients	40×	Patient	S	2	I
YSM	Kulkarni et al. (2020)	N/A	H&E	104 Patients	40×	Patient	S	2	I
GHS	Kulkarni et al. (2020)	N/A	H&E	51 Patients	40×	Patient	S	2	I
DKI	Hekler et al. (2019)	N/A	H&E	695 WSIs	40×	Slide	S	2	I
Y/CSUXH-TCGA	Xie et al. (2019)	N/A	H&E	2 241 WSIs	0.275/40×, 0.5/20×, 1/10×, 5/4×	Slide	S	4	U
BE-Hart	Hart et al. (2019)	N/A	H&E	300 WSIs	40×	Patch	S	2	I
BE-Cruz-Roa	Cruz-Roa et al. (2013)	N/A	H&E	308 ROI, 1 417 Patches	10×	Patch	S	2	U
DLCS	Ianni et al. (2020)	N/A	H&E	5 070 WSIs	0.25/40×	Slide	S	4	U
BE-TF-Florida-MC	Ianni et al. (2020)	N/A	H&E	13 537 WSIs	0.24/20×, 0.5/20×, 0.55/20×	Slide	S	4	U
Bladder									
TCGA+UFHSH	Zhang et al. (2019)	By Req.	H&E	913 WSIs	40×	Slide, ROI	S	2	I
TCGA-Woerl	Woerl et al. (2020)	TCGA	H&E	407 WSIs	40×	ROI	S	4	I
Bla-NHS-LTGU	Brieu et al. (2019)	N/A	IF	75 ROIs	N/A	Pixel	S	2	U
CCC-EMN MIBC	Woerl et al. (2020)	N/A	H&E	16 WSIs	40×	ROI	S	4	I
UrCyt	Levy et al. (2020)	N/A	ThinStrip	217 WSIs	40×	Pixel	S	3	U
AACHEN-BLADDER	Laleh et al. (2022)	N/A	H&E	183 Patients	N/A	Patient	S	2	I
Brain									
TCGA-Shirazi	Zadeh Shirazi et al. (2020)	N/A	H&E	654 WSIs, 849 ROIs	0.5	ROI	M	4	I
TCGA-GBM-Tang	Tang et al. (2019)	TCGA	N/A	209 Patients, 424 WSIs	0.5/20×	Patient	S	2	I
MICCAI14	Kirby; Barker et al. (2016)	N/A	H&E	45 WSIs	N/A	Slide	S	2	B
M-Qureshi	Qureshi et al. (2008)	N/A	H&E	320 ROIs	N/A	ROI	S	4	B
Lai et al.	Lai et al. (2021)	N/A	Amyloid-β antibody	30 WSIs	20×	Slide, Pixel	S	2, 3	I, U
Vessel	Teikari et al. (2016)	Link	H&E, PAS-H, Masson trichrome, Jones	226 WSIs	0.25/40×	ROI	M	3	I
WCM	Liechty et al. (2022)	N/A	H&E	87 WSIs	N/A	Patch	S	2	U
Esophagus									
ESO-DHMC	Tomita et al. (2019)	N/A	H&E	180 WSIs, 379 ROIs	20×	ROI	S	4	U
Kidney									
AIDPATH _A	Bueno et al. (2020b,a)	Link	PAS	31 WSIs	20×	Pixel	S	3	U
AIDPATH _B	Bueno et al. (2020b,a)	Link	PAS	2 ~ 340 Patches	20×	Patch	S	2	B
M-Gadermayr	Gadermayr et al. (2019)	N/A	PAS	24 WSIs	20×	ROI	S	2	U
TCGA-RCC-Lu	Lu et al. (2021d)	TCGA	H&E	884 WSIs	20×, 40×	Slide	S	3	I
BWH-CRCC	Lu et al. (2021d)	N/A	H&E	135 WSIs	10×, 20×	Slide	S	3	I
BWH-BRCC	Lu et al. (2021d)	N/A	H&E	92 WSIs	40×	Slide	S	3	I
BWH-RCC	Lu et al. (2021d)	N/A	H&E	135 WSIs	40×	Slide	S	3	I
Kid-Wu	Wu et al. (2019)	N/A	N/A	1 216 Patients, 60 800 Patches	N/A	Patch	S	2	U
UHZ-Fuchs	Fuchs et al. (2008)	N/A	MB-1	133 Patients	0.23/40×	Patient	S	9	I
WUPAX	Marsh et al. (2018)	N/A	H&E	48 WSIs	0.495	ROI	S	2	I
Pantomics	Tjio et al. (2020)	N/A	H&E	21 349 Patches	0.5/20×	Patch	S	2	U
RUMC	Hermsen et al. (2019)	N/A	PAS	50 WSIs	0.24/20×	Pixel	S	10	I
Mayo	Hermsen et al. (2019)	N/A	PAS	10 WSIs	0.49/20×	Pixel	S	10	I
UHZ-RCC	Bauer et al. (2016)	N/A	MB-1	1 272 Patches	N/A	Patch	S	2	I
Kid-Cicalese	Cicalese et al. (2020)	N/A	PAS	1 503 ROIs	N/A	ROI	S	2	I
Kid-Yang	Yang et al. (2020)	N/A	H&E, PAS, Jones	949 WSIs	0.25	ROI	S	2	U
Kid-BWH-TCGA	Lu et al. (2022)	N/A	H&E	1 184 WSIs	20×	Slide	S	3	I
WTH	Qi et al.	N/A	N/A	3 734 Patients	N/A	Patient	S	3	I
TCGA-RCC-Chen	Chen et al. (2021b)	N/A	N/A	45K ROIs	20×	ROI	S	3	B

Table 8.3 Continued on Next Page

Continuation of Data Compilation Table 8.3									
Dataset Name	References	Availability	Stain Type	Size	Res(μm)/ Mag	Annotation	Label	Class	CB
BWH-RCC-Chen	Chen et al. (2021b)	N/A	N/A	1 661 ROIs	20×	ROI	S	3	I
MC-Gallego	Gallego et al. (2021)	N/A	H&E, PAS	20 WSIs, 1 184 ROIs	20×, 40×	ROI	S	2	I
AACHEN-RCC	Laleh et al. (2022)	N/A	H&E	249 Patients	N/A	Patient	S	3	I
ANHIR	Borovec et al. (2020)	Link	H&E, MAS, PAS, and PASM	50 WSIs	0.1 to 0.2/40×	Slide	S	8	I
Glomeruli renal biopsies	Wu et al. (2022a)	N/A	H&E, PAS or Jones	42 WSIs	0.25	ROI	S	2	I
Hubmap Glom	Lutnick et al. (2022)	Link	H&E, PAS, PAS-H, Silver, Jones, Van Gieson, etc	3712 WSIs	0.13 to 0.25/40×	ROI	S	2	U
KMPM	Lutnick et al. (2022)	Link	PAS-H	26 WSIs	0.25/40×	ROI	M	2	U
Breast									
BreakHis	Spanhol et al. (2015); Bayramoglu et al. (2016)	By Req.	H&E	82 Patients, 7 909 ROIs	40×, 100×, 200×, 400×	ROI	S	2	I
CAMELYON 16	Cam (2016); Bejnordi et al. (2017a); Litjens et al. (2018)	link	H&E	399 WSIs	0.243/20×, 0.226/40×	Slide, ROI	S	3	I
BACH18	Aresta et al. (2019); Nazeri et al. (2018)	Link	H&E	40 WSIs, 400 Patches	0.42, 0.467	Patch, Pixel	S	4	B
TUPAC16	Veta et al. (2019)	Link	H&E	821 WSIs	40×	Slide	S	3	I
TUPAC16-Mitoses	Veta et al. (2019)	Link	H&E	73 WSIs	0.25/40×	ROI	S	2	U
TUPAC16-ROIs	Veta et al. (2019)	Link	H&E	148 WSIs	40×	ROI	S	2	U
CAMELYON 17	Cam (2017); Litjens et al. (2018); Bández et al. (2019)	Link	H&E	1 399 WSIs	0.23, 0.24, 0.25	Patient, Slide, ROI	S	5, 4, 3	I
BioImaging	Araújo et al. (2017); Huang and Chung (2018)	N/A	H&E	285 WSIs	0.42/200×	Slide	S	4	B
Ext-BioImaging	Yan et al. (2018)	N/A	H&E	1 568 WSIs	0.42/200×	Slide	S	4	I
MITOS-ATYPIA14	MIT; Sebai et al. (2020)	Link	H&E	1 696 HPFs	40×	Pixel	S	2	U
MITOS12	Roux et al. (2013); Sebai et al. (2020)	Link	H&E	50 HPFs	0.185/40×, 0.2273/40×, 0.22753/40×, 0.2456/40×	Pixel	S	2	U
AJ-Lymphocyte	Janowczyk and Madabhushi (2016); Lu et al. (2020c)	Link	H&E	100 ROIs	40×	Pixel	S	2	U
MSK	Campanella et al. (2019a); Clark et al. (2013); Campanella et al. (2019b)	Link	H&E	130 WSIs	0.5/20×	Slide	S	2	I
CCB	Naylor et al. (2017)	Link	H&E	33 Patches	40×	Pixel	S	2	U
BIDMC-MGH	Dong et al. (2014)	Link	H&E	167 Patients, 167 WSIs	0.25/40×	Patient	S	4	I
PUIH	Yan et al. (2020c)	N/A	H&E	4 020 WSIs	100×, 200×	Slide	S	4	I
HASHI	Cruz-Roa et al. (2018)	Link	H&E	584 WSIs	0.2456/40×, 0.23/40×	ROI	S	2	U
TNBC-CI	Naylor et al. (2018)	Link	H&E	50 Patches	40×	Pixel	S	2	U
AP	Dimitropoulos et al. (2017); Zioga et al. (2017)	Link	H&E	300 ROIs	40×	ROI	S	3	I
KIMIA Path24	Kieffer et al. (2017)	Link	N/A	28 380 Patches	0.5/20×, 0.25/40×	Patch	S	24	U
BCSC	Breast Cancer Surveillance Consortium; Meric et al. (2017)	By Req.	H&E	240 WSIs	40×	Slide, ROI	M	14	I
AJ-IDC	Janowczyk and Madabhushi (2016); Bidart and Wong (2019); Mohapatra et al. (2019)	Link	H&E	162 WSIs, 277 524 Patches	40×	Patch	S	2	I
PCam	Veeling et al. (2018)	Link	H&E	327 680 Patches	10×	Patch	S	2	I
AJ-N	Janowczyk et al. (2018)	N/A	H&E	141 ROIs	40×	Pixel	S	2	U
TCGA-Cruz-Roa	Cruz-Roa et al. (2017)	TCGA	H&E	195 WSIs	0.25/40×	ROI	M	5	U
TCGA-Jaber	Jaber et al. (2020)	TCGA	H&E	1 142 WSIs	20×	Patch	S	2	I
TCGA-Corvò	Corvo et al. (2020)	TCGA	H&E	91 WSIs	N/A	ROI	S	4	U
TCGA-Lu-Xu	Lu et al. (2020c)	TCGA	H&E	1K WSIs	N/A	ROI	S	2	I
AMIDA13	Veta et al. (2015); Li et al. (2019a)	N/A	H&E	606 ROIs	0.25/40×	Pixel	S	2	U
MICCAI16/17	Hou et al. (2019a)	N/A	H&E	64 WSIs	N/A	Pixel	S	2	U
MICCAI18	Hou et al. (2019a)	N/A	H&E	33 WSIs	N/A	Pixel	S	2	U
RUMC-Litjens	Litjens et al. (2016)	N/A	H&E	271 WSIs	0.24/20×	ROI	S	2	U
ABCTB	Rawat et al. (2020)	N/A	H&E	2 531 WSIs	20×	Patient	S	3	U
NHO-1	Liu et al. (2017)	N/A	H&E	110 WSIs	40×	Slide	S	2	I
RUMC-Bejnordi	Bejnordi et al. (2017b)	N/A	H&E	221 WSIs	0.243/20×	Slide, ROI	S	3	I
UVLCM-UVMC	Ehteshami Bejnordi et al. (2018)	N/A	H&E	2 387 WSIs	0.455/20×	Slide	S	6	I
HUP	Cruz-Roa et al. (2017)	N/A	H&E	239 WSIs	0.25/40×	ROI	M	5	U
UHCMD-CWRU	Cruz-Roa et al. (2017)	N/A	H&E	110 WSIs	0.23/40×	ROI	M	5	U

Table 8.3 Continued on Next Page

Data Compilation (Continued)

Continuation of Data Compilation Table 8.3									
Dataset Name	References	Availability	Stain Type	Size	Res(μm)/ Mag	Annotation	Label	Class	CB
CINJ	Cruz-Roa et al. (2017)	N/A	H&E	40 WSIs	0.25/40×	ROI	M	5	U
Bre-Steiner	Steiner et al. (2018)	N/A	H&E, IHC	70 WSIs	0.25	Slide	S	4	I
NMCSD	Liu et al. (2019)	N/A	N/A	108 WSIs	0.24	Slide	S	4	I
BC-Priego-Torres	Priego-Torres et al. (2020)	N/A	H&E	12 WSIs	0.2524/40×	Pixel	S	2	U
BIRL-SRI	Peikari et al. (2015)	N/A	H&E	65 WSIs, 5 151 Patches	2/5x, 1/10x	ROI	S	2	U
BWH-Lymph	Lu et al. (2021d)	N/A	H&E	133 WSIs	40×	Slide	S	2	B
NHS-Wetstein	Wetstein et al. (2020)	N/A	H&E	92 WSIs	0.16/40×	ROI	S	3	U
BRE-Parvatikar	Parvatikar et al. (2020)	N/A	H&E	93 WSIs, 1 441 ROIs	0.5/20×	ROI	S	2	I
BWH-TCGA-Breast	Lu et al. (2022)	N/A	H&E	2 126 WSIs	20×	Slide	S	2	I
Bre-Brieu	Brieu et al. (2019)	N/A	H&E	30 ROIs	N/A	Pixel	S	2	U
Duke	Narayanan et al. (2019)	N/A	H&E	140 WSIs	0.5/20×	ROI	S	2	U
TransATAC	Narayanan et al. (2019)	N/A	H&E	30 WSIs	0.45/20×	ROI	S	2	U
BRACS	Jaume et al. (2020, 2021b); Brancati et al. (2021)	By req.	H&E	547 WSIs, 4 539 ROIs	0.25/40×	Slide, ROI	S	7	I
Post-NAT-BRCA	Lagree et al. (2021)	Link	H&E	138 Patients	40×	Patient	S	3	I
BCSS	Amjad et al. (2019)	Link	H&E	151 WSIs, 20K ROIs	0.25	ROI	M	20	I
Amjad et al.	Jahanifar et al. (2021)	N/A	H&E	151 WSIs, 20 340 ROIs	0.25/40×	ROI	S	5	U
SMH+OVC	Geread et al. (2021)	N/A	Ki67	30 TMAs, 660 Patches	20×	Pixel	S	2	U
DeepSlides	Geread et al. (2021)	Link	Ki67	452 Patches	40×	Pixel	S	2	U
Protein Atlas	Geread et al. (2021); Uhlen et al. (2017)	Link	Ki67	56 TMAs	20×	Slide	S	3	U
Yale HER2	Geread et al. (2021)	N/A	H&E	188 WSIs	20×	ROI	S	3	U
Yale Response	Geread et al. (2021)	N/A	H&E	85 WSIs	N/A	ROI	S	2	U
TCGA-Farahmand	Geread et al. (2021)	N/A	H&E	187 WSIs	N/A	ROI	S	2	U
Breast Histopathology Images	Thiagarajan et al. (2021)	Link	H&E	162 WSIs	40×	Patch	S	2	I
Colsanitas	Hameed et al. (2022)	N/A	H&E	544 WSIs	0.46/40×	ROI	M	4	I
Pancreas									
Pan-Bai	Bai et al. (2020)	N/A	Ki67 IHC	203 TMAs	Max. of 20×	Pixel	S	3	I
Liver									
SUMC	Kiani et al. (2020)	N/A	H&E	80 WSIs	0.25/40×	Slide	S	2	B
MGH	Bautista and Yagi (2015)	N/A	H&E	10 WSIs	0.46/20×	ROI	S	4	U
Liv-Atupelage	Atupelage et al. (2013)	N/A	H&E	305 ROIs	20×	ROI	S	5	I
IHC-Seg	Lahiani et al. (2018)	N/A	H&E, PD1, CD163/CD68, CD8/CD3, CEA, Ki67/CD3, Ki67/CD8, FoxP3, PRF/CD3	77 WSIs	20×	Pixel	S	4	I
Lung									
TCGA-Gertych	Gertych et al. (2019)	IDs	H&E	27 WSIs, 209 ROIs	0.5/20×, 0.25/40×	ROI, Pixel	S	4	I
TCGA-Brieu	Brieu et al. (2019)	TCGA	H&E	142 ROIs	N/A	Pixel	S	2	U
TCGA-Wang	Albertina et al. (2016); Clark et al. (2013); Wang et al. (2019b)	TCGA	H&E	1 337 WSIs	20×, 40×	ROI	S	3	U
NLST-Wang	Team (2011); Wang et al. (2019b)	By Req.	H&E	345 WSIs	40×	ROI	S	3	U
TCGA-Wang-Rong	Albertina et al. (2016); Clark et al. (2013); Wang et al. (2020a)	TCGA	H&E	431 WSIs	40×	ROI	S	6	U
NLST-Wang-Rong	Team (2011); Wang et al. (2020a)	By Req.	H&E	208 WSIs	40×	Pixel	S	7	U
SPORE	SPO; Wang et al. (2019b)	N/A	H&E	130 WSIs	20×	ROI	S	3	U
CHCAMS	Wang et al. (2019b)	N/A	H&E	102 WSIs	20×	ROI	S	3	U
TCGA-Hou-2	Hou et al. (2019b)	TCGA	H&E	23 356 Patches	0.5/20×	Patch	S	2	I
TCGA-LUSC-Tang	Tang et al. (2019)	TCGA	N/A	98 Patients, 305 WSIs	0.5/20×	Patient	S	2	I
TCGA-CPTAC-Lu	Lu et al. (2021d)	TCGA, CPTAC	H&E	1 967 WSIs	20×, 40×	Slide	S	2	I
DHMC	Wei et al. (2019a)	N/A	H&E	422 WSIs, 4 161 ROIs, 1 068 Patches	20×	Slide, ROI, Patch	M, S, S	6	I
Lung-NHS-LTGU	Brieu et al. (2019)	N/A	IF	29 ROIs	N/A	Pixel	S	2	U
CSMC	Gertych et al. (2019)	N/A	H&E	91 WSIs, 703 ROIs	0.5/20×	ROI, Pixel	S	4	I
MIMW	Gertych et al. (2019)	N/A	H&E	88 WSIs, 1 026 ROIs	0.389/20×	ROI, Pixel	S	4	I

Table 8.3 Continued on Next Page

Continuation of Data Compilation Table 8.3									
Dataset Name	References	Availability	Stain Type	Size	Res(μm)/ Mag	Annotation	Label	Class	CB
NSCLC-Wang	Wang et al. (2017b)	N/A	H&E	305 Patients	20×	Patient	S	2	I
ES-NSCLC	Lu et al. (2021a)	N/A	H&E	434 Patients, 434 TMAs	20×	Patient	S	2	I
BWH-NSCLC-CL	Lu et al. (2021d)	N/A	H&E	131 WSIs	20×	Slide	S	2	I
BWH-NSCLC-BL	Lu et al. (2021d)	N/A	H&E	110 WSIs	40×	Slide	S	2	B
BWH-NSCLC-RL	Lu et al. (2021d)	N/A	H&E	131 WSIs	20×, 40×	Slide	S	2	I
VCCC	Ristanoski et al. (2021)	N/A	N/A	472 Patients	N/A	Patient	S	3	I
Dijon+Caen	Le Page et al. (2021)	N/A	HES	197 WSIs	20×	ROI	S	2	U
PKUCH+TMUCH	Wu et al. (2021)	N/A	IHC	239 WSIs, 677 ROIs	20×	ROI	S	2	U
Lymph Nodes									
LYON19	Swiderska-Chadaj and Ciompi (2019); Koohbanani et al. (2020); Swiderska-Chadaj et al. (2019)	Link	IHC	441 ROIs	0.24	Pixel	S	2	U
AJ-Lymph	Janowczyk and Madabhushi (2016); Brancati et al. (2019)	Link	H&E	374 WSIs	40×	Slide	S	3	I
TUCI-DUH	Strykh et al. (2020)	N/A	H&E	378 WSIs	0.24/20×	Slide	S	2	I
Thagaard-2	Thagaard et al. (2020)	N/A	H&E, IHC	56 Patches	20×	Patch	S	2	I
Thagaard-3	Thagaard et al. (2020)	N/A	H&E, IHC	135 Patches	20×	Patch	S	2	B
Thagaard-4	Thagaard et al. (2020)	N/A	H&E, IHC	81 Patches	20×	Patch	S	2	I
Thagaard-5	Thagaard et al. (2020)	N/A	H&E, IHC	60 Patches	20×	Patch	S	2	I
Zhongshan Hospital	Wang et al. (2022)	N/A	H&E	595 WSIs	0.5/20×	ROI	M	2	I
Mouth/Esophagus									
SKMCH&RC	Shaban et al. (2019a)	N/A	H&E	70 WSIs, 193 ROIs	0.275/40×	ROI	S	2	I
SKMCH&RC-M	Shaban et al. (2019a)	N/A	H&E	30 WSIs	0.275/40×	ROI	S	4	U
ECMC	Folmsbee et al. (2018)	N/A	H&E	143 WSIs	0.172/40x, 0.345/20x, 0.689/10x	Pixel	S	7	U
BCRWC	Das et al. (2018)	N/A	N/A	126 WSIs	1.163/50×	Pixel	S	4	U
LNM-OSSC	Koohbanani et al. (2021)	N/A	H&E	217 WSIs	0.2467/20x, 0.25/40×	ROI	S	2	U
OP-SCC-Vanderbilt	Lu et al. (2021a)	N/A	H&E	50 Patients	40×	Patient	S	2	B
Sheffield University	Shephard et al. (2021)	N/A	H&E	43 WSIs	0.4952/20×	Slide	S	4	I
Prostate/Ovary									
PCa-Bulten	Bulten et al. (2018, 2019)	Link	H&E, IHC	102 WSIs, 160 ROIs	0.24/20×	Pixel	S	2	U
OV-Kobel	Köbel et al. (2010)	Link	H&E, Ki-67, Mammoglobin B, ER, Mesothelin, MUC5, WT1, p16, p53, Vimentin, HNF-1b	168 WSIs, 88 TMAs	N/A	Slide	S	6	I
TCGA-Tolkach	Tolkach et al. (2020)	TCGA	H&E	389 WSIs	0.25/40×	ROI	S	3	U
UHZ	Arvaniti et al. (2018)	Link	H&E	886 TMAs	0.23/40×	ROI	S	5	U
SMS-TCGA	Eminaga et al. (2019)	N/A	H&E	310 WSIs	20×, 40×	ROI	S	2	U
TCGA-Arvaniti	Arvaniti and Claassen (2018)	TCGA	H&E	447 WSIs	20×, 40×	Slide	S	2	I
TCGA-Yaar	Yaar et al.	TCGA	H&E	220 Patients	20×	Patient	S	2	I
Pro-RUMC	Litjens et al. (2016)	N/A	H&E	225 WSIs	0.16/40×	ROI	S	2	B
UHZ-PCa	Bauer et al. (2016)	N/A	MIB-1	826 Patches	N/A	Patch	S	2	I
SUH	Arvidsson et al. (2019)	N/A	H&E	230 WSIs, 1 103 160 Patches	10×	ROI	S	4	I
CSMC	Li et al. (2018b, 2019b)	N/A	H&E	513 Patches	0.5/20×	Pixel	S	4	U
HUH	Khan et al. (2019b)	N/A	H&E	28 WSIs	0.22	Pixel	S	2	U
RCINJ	Ren et al. (2019)	N/A	H&E	83 WSIs	20×	Slide	S	2	I
Pro-Raciti	Raciti et al. (2020)	N/A	H&E	304 WSIs	0.5/20×	Slide, ROI	S	2	I, U
VPC	Karimi et al. (2019)	N/A	H&E	333 TMAs	40×	Pixel	S	4	U
Pro-Campanella	Campanella et al. (2018a)	N/A	H&E	137 376 Patches	20×	Patch	S	6	U
UPenn-Yan	Yan et al. (2020a)	N/A	H&E	43 WSIs	40×	ROI	S	2	U
Pro-Doyle	Doyle et al. (2011)	N/A	H&E	12K ROIs	0.25/40×	ROI	S	2	U
UPenn-Doyle	Doyle et al. (2012)	N/A	H&E	214 WSIs	40×	ROI	S	7	U
RUMC-Bulten	Pinckaers et al. (2021)	N/A	H&E	1 243 WSIs	0.24	Slide	S	2	U
VGH	Wang et al. (2020b)	N/A	H&E	305 WSIs	N/A	ROI	S	5	U
NMCSDF+MML+TCGA	Nagpal et al. (2019)	N/A	H&E	1 557 WSIs	0.25/40x, 0.5/20×	Slide, ROI	S	4	I, U

Table 8.3 Continued on Next Page

Data Compilation (Continued)

Continuation of Data Compilation Table 8.3									
Dataset Name	References	Availability	Stain Type	Size	Res(μm)/ Mag	Annotation	Label	Class	CB
OVCARE	Levine et al. (2020)	N/A	H&E	354 WSIs	40×	ROI	S	5	U
CWU	Schöming-Markiefka et al. (2021)	Link	H&E	478 WSIs, 120K Patches	0.504/20×	Patch	S	3	I
UHC	Schöming-Markiefka et al. (2021)	Link	H&E	157 WSIs, 120K Patches	0.231/40×	Patch	S	3	I
HWN	Schöming-Markiefka et al. (2021)	Link	H&E	51 WSIs, 120K Patches	0.264/40×	Patch	S	3	I
CSMC	Nour et al. (2021)	N/A	N/A	625 Patches	N/A	Pixel	S	4	U
DiagSet-A	Koziarski et al. (2021)	By Req.	H&E	2 604 206 Patches	5×, 10×, 20×, 40×	Patch	S	9	I
DiagSet-B	Koziarski et al. (2021)	By Req.	H&E	4 675 WSIs	0.25/40×	Slide	S	2	I
DiagSet-C	Koziarski et al. (2021)	By Req.	H&E	46 WSIs	0.25/40×	Slide	S	3	U
SICAPv2	Jaume et al. (2021a); Silva-Rodríguez et al. (2020)	Link	H&E	182 WSIs	40×	Slide, Pixel	S	4	I, U
OVCARE-Farahani	Farahani et al. (2022)	N/A	H&E	485 Patients, 948 WSIs	40×	Patient, Slide	S	5	I
University of Calgary	Farahani et al. (2022)	N/A	H&E	60 Patients, 60 WSIs	40×	Patient, Slide	S	5	I
PANDA	Bulten et al. (2020)	Link	H&E	11 000 WSIs	40×	ROI	S	5	I
Thyroid									
UPMC	Wang et al. (2010)	N/A	Feulgen	10-20 WSIs	0.074	Pixel	S	3	U
Chen et al.	Chen et al. (2021a)	N/A	N/A	600 WSIs	40×	Slide	S	3	I
TCGA-Hoechne	Höhne et al. (2021)	TCGA	H&E	482 WSIs	40×	Slide	S	4	I
DEC	Höhne et al. (2021)	N/A	H&E	224 WSIs	40×	Slide	S	4	I
ACQ	Höhne et al. (2021)	N/A	H&E	100 WSIs	40×	Slide	S	4	I
Stomach & Colon									
UMCM	Aresta et al. (2019); Kather et al. (2016b)	Link	H&E	5K Patches	0.495/20×	Patch	S	8	B
GLaS	Sirinukunwattana et al. (2017b, 2015)	Link	H&E	165 WSIs	0.62/20×	ROI	S	5	I
CRCHistoPhenotypes	Sirinukunwattana et al. (2016); Graham et al. (2019b)	Link	H&E	10 WSIs, 100 Patches	0.55/20×	Pixel	S	4	I
DACHS	Schrammen et al. (2022)	N/A	H&E	3 729 WSIs	20×	Slide	S	3	I
NCT-CRC-HE-100K	Kather et al. (2016b, 2019a); Tran et al. (2021)	Link	H&E	86 WSIs, 100K Patches	0.5	Patch	S	9	I
NCT-CRC-HE-7K	Kather et al. (2016b, 2019a); Tran et al. (2021)	Link	H&E	25 WSIs, 7 180 Patches	0.5	Patch	S	9	I
CoNSeP	Graham et al. (2019b)	Link	H&E	16 WSIs, 41 Patches	40×	Pixel	S	7	I
OSU	Tavolara et al. (2019)	Link	H&E, Pan-Cytokeratin	115 WSIs	0.061/40×	ROI	S	2	U
Warwick-CRC	Awan et al. (2017); Shaban et al. (2020)	Link	H&E	139 ROIs	20×	ROI	S	3	I
HUH	Xu et al. (2016)	Link	EGFR	27 TMAs, 1 377 ROIs	20×	ROI	S	2	I
CRAG	Awan et al. (2017)	N/A	H&E	38 WSIs, 139 Patches	0.275/20×	Patch	S	3	I
ULeeds	University of Leeds; Ponzio et al. (2020)	Link	H&E	27 WSIs	N/A	Slide	S	3	B
Kather et al.	Kather et al. (2019b)	Link	H&E	11 977 Patches	0.5	Patch	S	3	U
ZU	Xu et al. (2017a)	By Req.	H&E	717 ROIs	0.226/40×	ROI	S	6	I
KCCH	Kather et al. (2019b)	N/A	H&E	185 Patients	N/A	Patient	S	3	I
SC-Takahama	Takahama et al. (2019)	N/A	H&E	1 019 WSIs	Max. of 20×	Pixel	S	2	U
HUCH	Bychkov et al. (2018)	N/A	H&E	420 Patients	0.22	Patient	S	2	I
RC-Ciompi	Ciompi et al. (2017)	N/A	H&E	74 WSIs	0.455/200×	ROI	S	9	U
DHMC-Korbar	Korbar et al. (2017)	N/A	H&E	1 962 WSIs	200×	Slide	S	6	U
CRC-TP	Javed et al. (2020)	N/A	H&E	20 WSIs, 280K Patches	20×	ROI	S	7	U
CRC-CDC	Javed et al. (2020)	N/A	H&E	256 Patches	20×	Pixel	S	5	I
SC-Xu	Xu et al. (2014)	N/A	N/A	60 WSIs	N/A	ROI	S	2	U
FAHZU-Xu	Xu et al. (2017b)	N/A	H&E	13 838 WSIs	40×	Slide	S	2	I
Bilkent	Sirinukunwattana et al. (2015); Gunduz-Demir et al. (2010)	N/A	H&E	72 Patches	20×	Pixel	S	2	U
DHMC-Wei	Wei et al. (2019b)	N/A	H&E	1 230 WSIs	20×	Slide	S	3	I
Warwick-UHCW	Qaiser et al. (2019)	N/A	H&E	75 WSIs	0.275/40×	ROI	S	2	U
Warwick-Osaka	Qaiser et al. (2019)	N/A	H&E	50 WSIs	0.23/40×	Slide	S	6	I
GNUCH	Kosaraju et al. (2020)	N/A	H&E	94 WSIs, 343 ROIs	N/A	Slide, ROI	S	4, 2	I
SPSCI	Kloeckner et al. (2020)	N/A	H&E	55 WSIs, 251 ROIs	0.19/40×	ROI	S	5	I
WSGI	Wang et al. (2019d)	N/A	H&E	608 WSIs	0.2517/40×	Slide, Pixel	S	3, 2	I, U
TBB	Nguyen et al. (2020)	N/A	H&E	44 TMAs	N/A	Slide	S	3	I
UV	Sali et al. (2019)	N/A	H&E	456 WSIs	40×	Slide	S	4	U
SC-Sali	Sali et al. (2020)	N/A	H&E	1 150 WSIs	N/A	Slide	S	7	I

Table 8.3 Continued on Next Page

Continuation of Data Compilation Table 8.3									
Dataset Name	References	Availability	Stain Type	Size	Res(μm)/ Mag	Annotation	Label	Class	CB
SC-Holland	Holland et al. (2020)	N/A	H&E	10 WSIs, 1K Patches	40×, 100×	Slide	S	2	B
SC-Kong	Kong et al. (2018)	N/A	H&E	272 WSIs	40×	ROI	S	2	U
SSMH-STAD	Cho et al. (2020)	N/A	H&E	50 WSIs	N/A	Slide	S	2	B
HIUH	Iizuka et al. (2020)	N/A	H&E	8 164 WSIs	20×	Slide, ROI	S	3	I
HAH	Iizuka et al. (2020)	N/A	H&E	1K WSIs	20×	Slide	S	3	I
SC-Galjart	Tellez et al. (2020)	N/A	H&E	363 Patients, 1 571 WSIs	0.25	Slide	S	2	U
SC-Zheng	Zheng et al. (2020)	N/A	H&E	983 WSIs, 10 030 ROIs	0.96/10×	ROI	S	5	U
CRC-I-Chikontwe	Chikontwe et al. (2020)	N/A	H&E	173 WSIs	40×	Slide	S	2	I
CRC-II-Chikontwe	Chikontwe et al. (2020)	N/A	H&E	193 WSIs	40×	Slide	S	2	I
PLAGH	Song et al. (2020)	N/A	H&E	2 123 WSIs	0.238/40×	Pixel	S	4	U
QUASAR	Wright et al. (2020)	N/A	H&E	106 268 ROIs	0.5	ROI	S	2	U
CGMH	Gupta et al. (2021)	N/A	H&E	297 WSIs	0.229/40×	ROI	S	2	U
AOEC-RUMC-I	Marini et al. (2021)	N/A	H&E	2 131 WSIs	5×-10×	Slide	M	5	I
AOEC-RUMC-II	Marini et al. (2021)	N/A	H&E	192 WSIs	5×-10×	Slide, ROI	M, S	4	I, U
Lizard	Graham et al. (2021)	Link	H&E	291 WSIs,	0.5/20×	Pixel	S	6	I
YCR-BCIP	Schrammen et al. (2022)	N/A	H&E	889 WSIs	20×	Slide	S	2	I
MHIST	Wei et al. (2021b)	By Req.	H&E	3 152 Patches	40×	Patch	S	2	I
YSMH	Kim et al. (2021)	N/A	H&E	390 WSIs	20×	Slide, ROI	S	5	I, U
ColonPredict-Plus-2	Schuchmacher et al. (2021)	N/A	H&E	200 Patients, 2 537 Patches	N/A	Pixel	S	2	U
PAIP	Bilal et al. (2021)	By Req.	H&E	47 WSIs	N/A	ROI	S	2	U
Li et al.	Li et al. (2021c)	N/A	N/A	10 894 WSIs, 200 Patches	0.5/20×	Slide, Pixel	S	2	I
Stanford Hospital	Su et al. (2022)	Link	H&E, p53 IHC	70 WSIs	20×	Slide	S	2	U
IMP Diagnostics Lab.	Thandiackal et al. (2022); Oliveira et al. (2021)	By Req.	H&E	1133 WSIs	40×	Slide	S	3	I
Chaoyang	Zhu et al.	Link	H&E	6 160 patches	N/A	Patch	S	8	I
BERN-GASTRIC-MSI	Laleh et al. (2022)	N/A	H&E	302 Patients	N/A	Patient	S	2	I
BERN-GASTRIC-EBV	Laleh et al. (2022)	N/A	H&E	304 Patients	N/A	Patient	S	2	I
Bone Marrow									
BM-MICCAI15	Kainz et al. (2015)	Link	H&E	11 WSIs	N/A	Pixel	S	3	U
MICCAI15-Hu	Hu et al. (2018)	N/A	H&E	11 WSIs, 1 995 Patches	N/A	Patch	S	4	I
FAHZU-Hu	Hu et al. (2018)	N/A	H&E	24 WSIs, 600 Patches	N/A	Patch	S	3	B
BM-Hu	Hu et al. (2018)	N/A	H&E	84 WSIs	N/A	Slide	S	2	I
RUMC-Eekelen	van Eekelen et al. (2020)	N/A	PAS	24 WSIs	0.25	Pixel	S	6	U
MSKCC	Ho et al. (2020)	N/A	H&E	1 578 WSIs	0.5025, 0.5031/20×	Pixel	S	7	I
EUH	Chandradevan et al. (2020)	N/A	Wright's Stain	9 230 ROIs	0.25/40×	ROI	S	12	I
Frankel et al.	Frankel et al. (2022)	N/A	H&E	424 WSIs	40×	Slide	S	9	I
Internal-STAD	Zheng et al. (2022)	N/A	H&E	203 WSIs	0.25/40×	ROI	S	N/A	U
MultiCenter-STAD	Zheng et al. (2022)	N/A	H&E	417 WSIs	0.46/40×	ROI	S	N/A	U
Cervix									
TCGA-Idlahcen	Idlahcen et al. (2020)	TCGA	H&E	10 WSIs	2.5×-40×	Slide	S	2	B
XH-FMMU	Tian et al. (2019)	N/A	H&E	800 WSIs	4x-40×	ROI	S	2	U
Pap-Cytology	Koohbanani et al. (2020)	N/A	N/A	42 ROIs	20×	Pixel	S	2	U
Chen et al.	Chen et al. (2021a)	N/A	N/A	372 WSIs	40×	Slide	S	2	I
OAUTHC	Pal et al. (2021)	N/A	H&E	1 331 ROIs	N/A	ROI	S	2	I
Multi-organ									
MoNuSeg	Kumar et al. (2017)	Link	H&E	30 WSIs	40×	Pixel	S	2	U
UHN	Faust et al. (2019)	Link	H&E	1 656 WSIs, 838 644 Patches	0.504/20×	Slide, Patch	S	74	I
CPM-15	Graham et al. (2019b)	Link	H&E	15 Patches	20×, 40×	Pixel	S	2	U
CPM-17	Graham et al. (2019b)	Link	H&E	32 Patches	20×, 40×	Pixel	S	2	U
ADP	Hosseini et al. (2019); Chan et al. (2019)	By Req.	H&E	100 WSIs, 17 668 Patches	0.25/40×	Patch	M	57	I
Bándi-Dev-Set	Bándi et al. (2019)	Link	H&E, Sirius Red, PAS, Ki-67, AE1AE3, CK8-18	100 WSIs	0.2275, 0.2278, 0.2431, 0.25, 0.2525, 0.5034	Pixel	S	6	U

Table 8.3 Continued on Next Page

Data Compilation (Continued)

Continuation of Data Compilation Table 8.3									
Dataset Name	References	Availability	Stain Type	Size	Res(μm)/ Mag	Annotation	Label	Class	CB
Bándi-Dis-Set	Bándi et al. (2019)	Link	H&E, Alcian Blue, Von Kossa, Perls, CAB, Grocott	8 WSIs	0.2431	ROI	S	4	U
PanNuke	Gamper et al. (2019, 2020a)	Link	H&E	20K WSIs, 205 343 ROIs	40×	ROI	S	5	I
Salvi-SCAN	Shaban et al. (2019a)	Link	H&E	270 ROIs	10×, 20×, 40×	Pixel	S	2	U
TCGA-Nuclei	Hou et al. (2020b); Clark et al. (2013); Hou et al. (2019a)	Link	H&E	5 060 WSIs, 1 356 Patches	0.25/40×	Pixel	S	14	U
MO-Khoshdeli	Khoshdeli et al. (2018)	Link	H&E	32 WSIs, 32 Patches	0.5	Pixel	S	2	U
FocusPath	Wang et al. (2020c)	Link	H&E, Trichrome, IRON(FE), Mucicarmine, CR, PAS, AFB, Grocott	9 WSIs, 8 640 Patches	0.25/40×	Patch	S	15	U
Cheng-Jiang	Jiang et al. (2020a)	Link	H&E, TCT, IHC	20 521 WSIs	10×	Slide	4	S	I
Stanford-TMA	Marinelli et al. (2007); Motlagh et al. (2018)	By Req.	H&E, IHC	6 402 TMAs	N/A	Slide	S	4	I
TCGA-Courtio	Courtio et al. (2019)	TCGA	H&E	56 Patients, 56 WSIs	N/A	Patient, Slide	S	3	I
BreCaHAD	Noorbakhsh et al. (2020)	link	H&E	170 ROIs	40×	ROI	S	2	U
TCGA-Hegde	Hegde et al. (2019)	TCGA	H&E	60 WSIs	10×	ROI	S	10	U
TCGA-Diao	Diao et al. (2020)	TCGA	H&E	2 917 WSIs	20×, 40×	ROI, Pixel	S	4, 6	I
TCGA-Levine	Levine et al. (2020)	TCGA	H&E	668 WSIs	N/A	ROI	S	5	U
TCGA@Focus	Wang et al. (2020c)	Link	H&E	1K WSIs, 14 371 Patches	N/A	Patch	S	2	I
TCGA-Shen	Shen and Ke (2020)	TCGA	H&E	1 063 WSIs	20×	Patch	S	3	U
TCGA-Lerousseau	Lerousseau et al. (2020)	TCGA	H&E	6 481 WSIs	20×	Pixel	S	3	U
TCGA-Schmauch	Schmauch et al. (2020)	TCGA	H&E	10 514 WSIs	N/A	Slide	S	28	I
MO-Khan	Khan et al. (2014)	N/A	H&E	60 WSIs	20×, 40×	Pixel	S	3	U
MESOPATH/ MESOBANK	Courtio et al. (2019)	N/A	HES	2 981 Patients, 2 981 WSIs	40×	Patient, Slide	S	3	U
Mo-Campbell	Campanella et al. (2018a)	N/A	H&E, SDF-1, TOM20	249 600 Patches	20×	Patch	S	6	U
BWH-TCGA-MO	Lu et al. (2021b)	N/A	H&E	25 547 WSIs	N/A	Slide	S	18	I
BWH-Lu	Lu et al. (2021c)	N/A	H&E	19 162 WSIs	20×, 40×	Slide	2	I	
Feng et al.	Feng et al. (2021a)	N/A	H&E, IHC	500 WSIs	20×	Slide	S	10	B
SegSet	Koziarski et al. (2021)	N/A	H&E	30 WSIs	0.25/40×	Pixel	S	2	U
LC25000	Borkowski et al.	Link	H&E	25 000 Patches	N/A	Patch	S	5	B
OCELOT-CELL	Ryu et al. (2023)	Link	H&E	306 WSIs, 673 Patches	0.2	ROI	S	2	I
OCELOT-TISSUE	Ryu et al. (2023)	Link	H&E	306 WSIs, 673 Patches	0.2	Pixel	S	3	I
Other									
MUH	Tran et al. (2021); Matek et al. (2019)	N/A	N/A	18 365 Patches	14.14/100×	Patch	S	15	I
UPenn	Nirschl et al. (2018)	N/A	H&E	209 Patients	20×	Patient	S	2	I
CMTHis	Kumar et al. (2020a)	N/A	H&E	352 ROIs	40×, 100×, 200×, 400×	ROI	S	2	I
Heidelberg University	Höhn et al. (2021)	N/A	H&E	431 WSIs	N/A	ROI	S	2	U
CHOA	Giuste et al. (2020)	N/A	H&E	43 WSIs	10×	Slide	S	4	I
Han-Wistar Rats	Freyre et al. (2021)	N/A	H&E, ISH	349 WSIs	40×	Slide	S	2	U
Osteosarcoma	Tang et al. (2021)	Link	H&E	1 144 ROIs	10×	ROI	S	3	I
UPenn+OSU+UH	Peyster et al. (2021)	N/A	H&E	2 358 WSIs	40×	Slide	S	4	I
Kaggle 2018 Data Sci- ence Bowl	Caicedo et al. (2019)	Link	DAPI, Hoechst, H&E	670 WSIs	N/A	Pixel	S	2	U
ALL-IDB2	Labati et al. (2011); Genovese et al. (2021)	By Req.	N/A	260 ROIs	300× - 500×	Slide	S	2	B

End of Table 8.3

References	Tasks	Disease Specification	Methods
Basal/Epithelium			
Jiang et al. (2020b)	Detection	Metastasis	End-to-end classifier using cascaded CNNs
Cruz-Roa et al. (2013)	Detection	Metastasis	Unsupervised learning via auto-encoder
Xie et al. (2019)	Disease diagnosis	Melanoma, intra-dermal, compound, junctional nevus	CNN-based patch classifier
Failmezger et al. (2020)	Nuclei subtype classification	lymphocyte, stromal, artefact, cancer	CRImage and TTG/CNx for cell identification and classification
Al-Milaji et al. (2019)	Tissue subtype classification	Epithelial, stromal tissues, Spitz, conventional melanocytic lesions	Integration of CNN and HFCM segmentation
Hart et al. (2019)	Tissue subtype classification	Epithelial, stromal tissues, Spitz, conventional melanocytic lesions	CNN-based classifier with transfer learning
Courtial et al. (2019)	Patient prognosis	Epithelioid, sarcomatoid, biphasic in mesothelium, distant metastatic recurrence	ResNet classifier with transfer learning
Saltz et al. (2018)	Patient prognosis	Epithelioid, sarcomatoid, biphasic in mesothelium, distant metastatic recurrence	Combination of DNN and RNN for feature processing
Phillips et al. (2018)	Tumor segmentation	Tumor, epidermis, dermis, background	FCN based segmentation
Hekler et al. (2019)	Classification	Nevi, melanoma	CNN-based classifier
Bladder			
Zhang et al. (2019)	Classification	Papillary urothelial carcinoma LG/HG	Combination of CNN and LSTM
Brieu et al. (2019)	Segmentation	Voronoi objects, edges, background regions	CycleGAN with U-Net segmentation
Kumar et al. (2017)	Nuclei Segmentation	Nuclear, Non-nuclear, Boundary	CNN-based classifier with AJI evaluation
Woerl et al. (2020)	Tissue Subtype Classification	Double negative, basal, luminal, luminal p53-like	ResNet variation classifier
Brain			
Barker et al. (2016)	Classification	Glioblastoma multiforme, LG glioma	Elastic net classifier with weighted voting
Ertosun and Rubin (2015)	Classification	LGG Grade II/III, GBM	Modular CNN-ensemble network
Xu et al. (2017a)	Classification	LGG and GBM	CNN-based classifier with transfer learning
Rathore et al. (2020)	Classification	Glioma grading III,IV,V	SVM classifier
Faust et al. (2019)	Classification	Tissue feature correlation analysis	CNN-based classifier with transfer learning
Liechty et al. (2022)	Patient prognosis	Tissue feature correlation analysis	Densenet121 classifiers, initialized with imageNet pre-trained weights
Mobadarsany et al. (2018)	Patient prognosis	IDH mutation	Survival CNN with genetic biomarker data integration
Zadeh Shirazi et al. (2020)	Patient prognosis	Survival period for glioblastoma	CNN-based patch classifier
Hao et al. (2019)	Patient prognosis	GBM prognostic index	Fusion network of genome, histopathology, and demography
Tang et al. (2019)	Patient prognosis	Glioblastoma Multiforme	Custom CNN classifier
Rathore et al. (2019)	Patient prognosis/Tissue subtype classification	Oligodendroglioma, IDH-mutant/wild type astrocytoma	CNN-based classifier
Lai et al. (2021)	Segmentation	Superior Middle Temporal Gyri in the temporal cortex	Semi-supervised active learning(SSL)
Mouth/Esophagus			
Folmsbee et al. (2018)	Tissue subtype classification	Stroma, lymphocytes, tumor, mucosa, kerClassificationin pearls, blood, adipose	Modified AlexNet patch classifier with active learning
Tomita et al. (2019)	Disease Diagnosis	Barrett esophagus no dysplasia, esophageal adenocarcinoma, normal, Barrett esophagus with dysplasia	Attention based classifier
Lewis Jr et al. (2014)	Patient prognosis	Oropharyngeal squamous cell carcinoma	Computational cell cluster graph
Shephard et al. (2021)	Segmentation	Oral epithelial dysplasia (OED)	HoVer-Net+, a deep learning framework consists of an encoder branch, and three decoder branches
Breast			
Tellez et al. (2019a); Thuy and Hoang (2019)	Detection	Benign, malignant	CNN-based patch classifier
Kumar et al. (2020a); Kassani et al. (2019a); Khan et al. (2019a)	Detection	Benign, malignant	CNN classifier with transfer learning
Cruz-Roa et al. (2017)	Detection	Benign, malignant	CNN-based pixel classifier
Qi et al. (2018)	Detection	Benign, malignant	Pre-trained AlexNet with automatic label query
Budak et al. (2019)	Detection	Benign, malignant	Pre-trained AlexNet with Bi-LSTM classifier
Pimkin et al. (2018)	Detection	Benign, malignant	Combination of CNN classifier and U-Net segmentation
Spanhol et al. (2017)	Detection	Benign, malignant	CNN-based classifier
Xu et al. (2019b)	Detection	Benign, malignant	3 stage LSTM-RNN classifier
Patil et al. (2019)	Detection	Benign, malignant	Attention-based MIL model
Bidart and Wong (2019)	Detection	Benign, malignant	Tri-branched ResNet model
Bardou et al. (2018)	Detection	Benign, malignant	Combination of CNN and hand-crafted features
Cruz-Roa et al. (2018)	Detection		Custom CNN classifier with Quasi-Monte Carlo sampling
Lu et al. (2020c)	Detection, Patient Prognosis	Tumor, Normal/ Tumor-infiltrating lymphocytes	U-Net based classifier

Table 8.3 Continued on Next Page

Organ Overview (Continued)

Continuation of Organ Overview Table 8.3			
References	Tasks	Disease Specification	Methods
Kausar et al. (2020)	Detection	Mitosis	Multi-scale custom CNN classifier
Thiagarajan et al. (2021)	Detection	Invasive Ductal Carcinoma	Bayesian Convolution Neural Networks
Turki et al. (2021)	Binary classification	Breast cancer to axillary lymph nodes (ALNs)	Pre-trained architectures: DenseNet121, ResNet50, VGG16, Xception and lightweight convolutional neural network (LCNN)
Wang et al. (2021a)	Tumor Segmentation and Classification	Breast Cancer Metastases	SOTA methods, designed MLVDeepLabV3+
Lagree et al. (2021)	Segmentation	Segmentation of the malignant nuclei within each tumor bed	Mask regional convolutional neural network (Mask R-CNN)
Ho et al. (2021)	Segmentation	Segmentation of multiple subtypes on breast images	Deep Multi Magnification Network (DMMN), CNN architecture
Lee and Paeng (2018)	Detection	Metastasis/ Micro, Macro	CNN-based pixel classifier
BenTaieb and Hamarneh (2018)	Detection	Metastasis/ Micro, Macro	Resnet with transfer learning
Valkonen et al. (2017)	Detection	Metastasis/ Micro, Macro	Combination of CNNs with LSTM-RNN, DCNN-based classifier
Li and Ping (2018)	Detection	Cancer metastasis detection	MIL+RNN classifier, Neural conditional random field
Liang et al. (2019)	Detection	Cancer metastasis detection	CNN with attention mechanism
Chen et al. (2016b)	Detection	Metastasis in sentinel lymph node	CNN with Random Forest classifier
Cruz-Roa et al. (2014)	Detection	Invasive ductal carcinoma	CNN-based patch classifier
Celik et al. (2020)	Detection	Invasive ductal carcinoma	ResNet with transfer learning
Mohapatra et al. (2019)	Detection	Invasive ductal carcinoma	CNN-based random forest classifier
Brancati et al. (2019)	Detection	Invasive ductal carcinoma	Autoencoder network
Liu et al. (2019)	Detection	Macrometastasis, micrometastasis, isolated tumor cells, negative	Customized InceptionV3 classifier
Wahab et al. (2017)	Detection	Mitosis detection	CNN classifier with two-phase training
Tellez et al. (2018)	Detection	Mitosis detection	Task-based CNN ensemble
Wang et al. (2014)	Detection	Mitosis detection	CNN-based random forest classifier
Jiménez and Racoceanu (2019)	Detection	Mitosis detection	CNN classifier with transfer learning
Li et al. (2018a)	Detection	Mitosis detection	Multi-stage RCNN classifier
Li et al. (2019a)	Detection	Mitosis detection	FCN classifier
Sebai et al. (2020)	Detection	Mitosis detection	Adaptive Mask RCNN
Akram et al. (2018)	Detection	Mitosis detection	CNN-based patch classifier
Otálora et al. (2019)	Detection	Mitosis detection	Combination of DCNN network
Alom et al. (2020)	Detection	Mitosis detection	R2U-Net based regression model
Bayramoglu et al. (2016)	Classification	Epithelium, Stroma	Magnification invariant CNN classifier
Li et al. (2020b)	Classification	Benign, malignant	CNN classifier interleaved with squeeze-excitation modules (SENet)
Alom et al. (2019)	Classification	Adenosis, fibroadenoma, phyllodes tumors, tubular adenoma, ductal, lobular, mucinous, papillary	Inception Recurrent Residual Convolutional Neural Network (IRRCNN)
Nawaz et al. (2018)	Classification	Adenosis, fibroadenoma, phyllodes tumors, tubular adenoma, ductal, lobular, mucinous, papillary	Custom DenseNet classifier
Hameed et al. (2022)	Classification	normal tissue, benign lesion, in situ carcinoma, and invasive carcinoma	Custom multiclass dense layer classifier based on Xception network
Gandomkar et al. (2018)	Disease diagnosis	Adenosis, fibroadenoma, phyllodes tumors, tubular adenoma, ductal, lobular, mucinous, papillary	Two-stage ResNet classifier (MuDeRN)
Kassani et al. (2019b)	Disease diagnosis	Benign, malignant	Ensemble of CNN classifiers
Saxena et al. (2020)	Disease diagnosis	Adenosis, fibroadenoma, phyllodes tumors, tubular adenoma, ductal, lobular, mucinous, papillary	CNN-based classifier with transfer learning
Han et al. (2017)	Disease diagnosis	Adenosis, fibroadenoma, phyllodes tumors, tubular adenoma, ductal, lobular, mucinous, papillary	Class structured DCNN
Xu et al. (2019a)	Disease diagnosis	Adenosis, fibroadenoma, phyllodes tumors, tubular adenoma, ductal, lobular, mucinous, papillary	Two stage classification and selection network
Alirezazadeh et al. (2018)	Disease diagnosis	Adenosis, fibroadenoma, phyllodes tumors, tubular adenoma, ductal, lobular, mucinous, papillary	Domain adaptation based on representation learning
Meng et al. (2019)	Disease diagnosis	Benign, in-situ, invasive carcinoma	CNN-based classifier with gravitational loss
Rakhlin et al. (2018)	Disease diagnosis	Benign, in-situ, invasive carcinoma	CNN ensemble with LightGBM
Vang et al. (2018)	Disease diagnosis	Benign, in-situ, invasive carcinoma	InceptionV3 classifier using dual path network
Dong et al. (2014)	Disease diagnosis	Usual ductal hyperplasia, ductal carcinoma in situ	Logistic regression with Lasso regularization
Pati et al. (2018)	Disease diagnosis	Proliferation score (1, 2, or 3)	Encoder-decoder with Gaussian Mixture model
Parvatikar et al. (2020)	Disease diagnosis	Low risk/High risk	Logistic regression using morphological features
Alzubaidi et al. (2020)	Disease diagnosis	normal, benign, in situ carcinoma, invasive carcinoma	Hybrid CNN classifier
Ehteshami Bejnordi et al. (2018)	Disease diagnosis	Proliferative without atypia, atypical hyperplasia, ductal / lobular carcinoma in situ, invasive carcinoma	Cascade of VGG-Net like classifier

Table 8.3 Continued on Next Page

Continuation of Organ Overview Table 8.3

References	Tasks	Disease Specification	Methods
Nahid and Kong (2018)	Disease diagnosis	Benign, malignant	CNN-based classifier with fourier pre-processing
Nahid et al. (2018)	Disease diagnosis	Benign, malignant	Combination of CNN and LSTM classifiers
Teh and Taylor (2019)	Disease diagnosis	Tumour, normal	Metric learning using similarities
Aresta et al. (2019)	Classification	Clinically relevant classes	CNN-based patch classifier with aggregation
Araújo et al. (2017)	Classification	Benign, in-situ, invasive carcinoma	Scale-based CNN classifier
Nazeri et al. (2018)	Classification	Normal, benign, in situ, invasive carcinoma	Combination of patch and image level CNN
Bejnordi et al. (2017b)	Classification	Normal, benign, DCIS, invasive ductal carcinoma (IDC)	Context-aware stacked CNN
Awan et al. (2018)	Classification	Benign, in-situ, invasive carcinoma	CNN-based classifier with dimensionality reduction
Lu et al. (2020a)	Classification	Benign, in-situ, invasive carcinoma	MIL with auto-regression
Yao et al. (2019)	Classification	Benign, in-situ, invasive carcinoma	Parallel network with CNN-RNN
Yan et al. (2018)	Classification	Benign, in-situ, invasive carcinoma	Hybrid Convolutional and Recurrent NN
Wang et al. (2018b)	Classification	Benign, in-situ, invasive carcinoma	CNN-based patch classifier
Iesmantas and Alzbutas (2018)	Classification	Benign, in-situ, invasive carcinoma	Convolutional capsule network
Huang and Chung (2018)	Classification	Benign, in-situ, invasive carcinoma	Combination of residual and spatial model
Roy et al. (2019)	Classification	Benign, in-situ, invasive carcinoma	Custom CNN patch classifier
Yan et al. (2020c)	Classification	Benign, in-situ, invasive carcinoma	CNN classifier with bidirectional LSTM
Lei et al. (2020)	Classification	Tumor, non-tumor	Custom CNN-based classifier
Hou et al. (2019a)	Nuclei segmentation	N/A	UNet segmentation with GAN patch refinement
Brieu et al. (2019)	Nuclei segmentation	N/A	UNet segmentation with CycleGAN domain transfer
Naylor et al. (2017)	Nuclei segmentation	N/A	Ensemble of several CNNs with different architectures
Kumar et al. (2017)	Nuclei segmentation	Normal, malignant, dysplastic epithelial, fibroblast, muscle, inflammatory, endothelial, miscellaneous	Sequential CNN network
Janowczyk et al. (2018)	Nuclei segmentation	Normal, malignant, dysplastic epithelial, fibroblast, muscle, inflammatory, endothelial, miscellaneous	Custom encoder-decoder model
Narayanan et al. (2019)	Detection, Segmentation	DCIS and invasive cancers	IM-Net for DCIS detection and segmentation
Takahama et al. (2019)	Tumour segmentation	Tumor, Normal	U-Net segmentation with GoogleNet patch level feature extraction
Li et al. (2019c)	Tumour segmentation	Normal, benign, in situ carcinoma or invasive carcinoma	Global and local ResNet feature extractors, FCN with auto zoom
Dong et al. (2018)	Tumour segmentation	Normal, benign, in situ carcinoma or invasive carcinoma	Global and local ResNet feature extractors, FCN with auto zoom
Jahanifar et al. (2021)	Segmentation	Breast cancer	U-Net, Residual Multi-Scale (RMS)
Geread et al. (2021)	Segmentation	Ki67 detection for breast cancer	U-NET, piNET
Priego-Torres et al. (2020)	Tumour segmentation	Non-tumor, ductal carcinoma in situ (DCIS), invasive ductal carcinoma (IDC), lobular carcinoma in situ (LCIS), invasive lobular carcinoma (ILC)	Ensemble of CNN with atrous spatial pyramid encoding
Farahmand et al. (2022)	Classification	Prediction of HER2 status and trastuzumab response	CNN classifier with Inception v3, Transfer learning
Alharbi et al. (2021)	Tissue subtype classification	Classifying cancerous tissues	weakly supervised approach, Multiple Instance Learning (MIL) model, Transfer learning pre-trained models (Trans-AMIL), VGG, DenseNet, ResNe
Kieffer et al. (2017)	Tissue subtype classification	24 different tissues	Ensemble of different CNN architectures with transfer learning
Mercan et al. (2017)	Tissue subtype classification	Proliferative without atypia, atypical hyperplasia, ductal / lobular carcinoma in situ, invasive carcinoma	Multi-class MIL
Jaume et al. (2020)	Disease Diagnosis	Normal, Benign, Atypical, Ductal Carcinoma In Situ, Invasive	CNN-based classifier using graphical representation
Rawat et al. (2020)	Tissue subtype classification	Estrogen, Progesterone, Her2 receptor	Style invariant ResNet classifier
Steiner et al. (2018)	Tissue subtype classification	Negative, micrometastasis, macrometastasis, isolated tumor cell cluster (ITC)	Custom CNN-based classifier
Wetstein et al. (2020)	Tissue subtype classification	Adipose regions, TDLU regions, acini centroid	UNet based CNN classifier
Jaume et al. (2021b)	Classification, Segmentation	Benign, Atypical (flat epithelial atypia, atypical ductal hyperplasia), Malignant (ductal, in situ, invasive)	Graphical neural networks
Jaber et al. (2020)	Tissue subtype classification	Basal-like, HER2-enriched, Luminal A, and Luminal B	CNN-based classifier with PCA
Khan et al. (2020)	Classification	Malignant, normal	CNN classifier with transfer learning
Shaban et al. (2019b)	Segmentation	Stain normalization	Style transfer using CycleGAN, Relevance vector machine
Claudio Quiros et al. (2021)	Segmentation	Realistic patch generation	GAN based architecture
Ziae et al. (2020)	Classification	Processing technique comparison	Comparison of color normalization methods
Lu et al. (2020b)	Classification	19 histological types, HER2-, HER2+, PR+, PR-	Graph CNN slide level classifier
Senousy et al. (2021)	Classification	normal, benign, in situ, and invasive	Dynamic Deep Ensemble CNN
Shao et al. (2021)	Binary Classification	Breast cancer	Transformer based MIL (TransMIL)

Liver

Table 8.3 Continued on Next Page

Organ Overview (Continued)

Continuation of Organ Overview Table 8.3			
References	Tasks	Disease Specification	Methods
Atupelage et al. (2013)	Disease diagnosis, Nuclei segmentation	G0, G1, G2, G3, G4 (HCC grade)	BoF-based classifier
Kiani et al. (2020)	Disease diagnosis	Hepatocellular/cholangio carcinoma	CNN-based end to end diagnostic tool
Levy et al. (2020)	Nuclei segmentation	N/A	CycleGAN based segmentation
Lahiani et al. (2018)	Tissue segmentation	Background, tumor, tissue and necrosis	UNet with color deconvolution
Guo et al. (2019)	Tissue segmentation	Steatosis droplet	Mask-RCNN segmentation
Bautista and Yagi (2015)	Classification	Stain normalization	Relevance vector machine
Lahiani et al. (2019a)	Classification	Hematoxylin, eosin, unstained RBC	Linear discriminant classifier
Lahiani et al. (2019b)	Classification	Stain style transfer	CycleGAN based architecture, CycleGAN with perceptual embedding consistency loss
Lymph Nodes			
Guerrero and Oliveira (2021)	Detection	Detection and quantification of Lymphocytes	U-Net and SegNet with VGG16 and Resnet50 and pre-trained weights of ImageNet
Bejnordi et al. (2017a)	Detection	Metastasis	Ensemble of CNNs with different architectures
Huang and Chung (2019)	Detection	Metastasis	Custom CNN for discriminative feature learning
Bandi et al. (2018)	Detection	Metastasis	DCNN classifier
Liu et al. (2017)	Detection	Metastasis	CNN-based patch classifier
Özeturk and Akdemir (2019)	Detection	Metastasis (Isolated / micro / macro)	Variants of ResNet/GoogleNet
Syrikh et al. (2020)	Disease diagnosis	Hyperplasia, small B cell lymphomas	Bayesian NN with dropout variance
Das et al. (2018)	Tissue segmentation	Keratin, subepithelial, epithelial, background	Custom CNN model
Agarwalla et al. (2017)	Tumor segmentation	normal, metastatic	Representation-Aggregation Network with LSTM
Stacke et al. (2019)	Classification, Segmentation	Domain shift analysis for breast tumour	Comparison of CNN models, data augmentation, and normalization techniques
Zanjani et al. (2018)	Classification, Segmentation	Stain normalization	Deep Gaussian mixture color normalization model
Cho et al. (2017)	Classification, Segmentation	Stain normalization	GAN, stain-style transfer network
Gildenblat and Klaiman (2019)	Classification, Segmentation	Similar image retrieval	Siamese network
Carse et al. (2021)	Classification	metastatic tissue	Contrastive predictive coding, Autoregressor PixelCNN
Wang et al. (2022)	Prognosis of lymph node metastasis	lymph node metastasis of papillary thyroid carcinoma	Transformer-Guided Multi-instance Learning, Attention-based mutual knowledge distillation
Prostate/Ovary			
Xiong et al. (2021)	Tissue subtype classification	Gland, Gland border region, or Stroma	SVM with RBF kernel, CNN classifiers
Nour et al. (2021)	Tissue subtype classification	stromal areas (ST), benign/normal (BN), low-grade pattern (G3) and high-grade pattern (G4) cancer	CNN classifiers using a modified U-Net architecture
Bayat et al. (2021)	Detection	Tumor, No-tumor	Generative Adversarial Network named GAN-CS
Khan et al. (2019b); Pinckaers et al. (2021)	Detection	Tumor, Normal	CNN-based classifier with transfer learning, MIL model
Chang et al. (2017b)	Detection	Pancreatic adenocarcinoma	Custom CNN classifier
Doyle et al. (2011)	Detection	Probabilistic boosting tree with active learning	
Schömig-Markiewka et al. (2021)	Detection	benign glandular, nonglandular, tumor tissue	Pre-trained and validated model based on InceptionResNetV2 convolutional architecture
Li et al. (2018b)	Disease diagnosis	Prostate cancer (benign, LG, HG)	Region based CNN classifier
Otálora et al. (2020)	Disease diagnosis	Gleason Score (G6-G10)	Comparison of commonly used CNN models
Otálora et al. (2020)	Disease diagnosis	Gleason Score (0-5)	Active Learning Framework
Tolkach et al. (2020)	Disease diagnosis	Invasive carcinoma, Benign (glandular, non-glandular, stromal, seminal vesicles, ejaculatory ducts, high-grade prostatic intraepithelial neoplasia, HGPIN), intraductal carcinoma	NASNetLarge classifier with transfer learning
Arvaniti and Claassen (2018)	Disease diagnosis	Gleason grading (3, 4, 5)	ResNet classifier with symmetric domain adaptation
Nagpal et al. (2019)	Disease diagnosis	Gleason grading (3, 4, 5)	Two-stage deep learning system
Li et al. (2017)	Disease diagnosis	Gleason grading (3, 4, 5)	Multi-scale U-Net for pixel-wise Gleason score prediction
Arvidsson et al. (2019)	Disease diagnosis	Gleason grading (3, 4, 5)	CNN classifier with CycleGAN
Li et al. (2019b)	Disease diagnosis	Gleason grading (3, 4, 5)	Attention-based MIL classifier
Karimi et al. (2019)	Disease diagnosis	Benign, Gleason Grades 3-5	Ensemble of CNN classifiers
Yan et al. (2020a)	Disease diagnosis	Gleason grades 1-5	K-NN classifier using statistical representation of Homology Profiles
Wang et al. (2020b)	Disease diagnosis	High-grade serous ovarian, clear cell ovarian, endometrioid (ENOC), low-grade serous, mucinous carcinoma	Two-staged CNN with RF classifier
Lara et al. (2020)	Disease diagnosis	Low risk Gleason score (6-7), high risk (8-10)	Information retrieval using TF-IDF
Avenel et al. (2019)	Gland segmentation	Gleason Score (1-5)	Image analysis using mathematical morphology

Table 8.3 Continued on Next Page

Continuation of Organ Overview Table 8.3

References	Tasks	Disease Specification	Methods
Kozierski et al. (2021)	Tissue subtype classification	Diagset A : scan background (BG), tissue background (T), normal, healthy tissue (N), acquisition artifact (A), or one of the 1-5 Gleason grades (R1-R5). Diagset B: presence of cancerous tissue on the scan (C) or lack thereof (NC), Diagset C: containing cancerous tissue (C), not containing cancerous tissue (NC), or uncertain and requiring further medical examination (IHC)	CNNs, a variant of fully-convolutional VDSR networks, AlexNet, VGG16/19, ResNet50, InceptionV3
Sethi et al. (2016)	Tissue subtype classification	Epithelial, stromal	Multiresolution segmentation
Doyle et al. (2012)	Tissue subtype classification	Gleason grade 3-5, Benign Epithelium (BE), Benign stroma (BS), Tissue atrophy (AT), PIN	Cascaded approach
Raciti et al. (2020)	Clinical validation	Cancer, non-cancerous	Two-stage MIL-RNN classifier
Yaar et al.	Prediction of treatment response	Positive, negative (response to platinum chemotherapy)	Ensemble of RBF+SVM and MIL-based CNN classifier
Kidney			
Tjio et al. (2020)	Detection	Tumor, normal	DCNN based classifier
Cicalese et al. (2020)	Detection	Antibody mediated rejection	CNN-based classifier
Qi et al.	Classification	Abnormalities of blood chemistry, Kidney function and dehydration	k Nearest Neighbour (kNN), Long short-term memory (LSTM)
Gallego et al. (2021)	Classification, Segmentation	Cancer	Modified U-Net CNN model
Yang et al. (2020)	Detection	Glomeruli boundaries	CNN-based classifier with center point localization
Nguyen et al. (2021)	Detection	Glomeruli and Nuclei	Anchor Free Backbone + center point localization
Fuchs et al. (2008)	Prognosis	Survival rate for renal cell carcinoma	Random forest classifier for nuclei detection
Almansouri and Zwyera (2020)	Prognosis	Survival rate	Kaplan-Meier analysis
Marsh et al. (2018)	Classification	Sclerosed glomeruli, tubulointerstitium	Laplacian-of-Gaussian method for blob detection
Wu et al. (2019)	Classification	Glomerulus, lymphocytes	Different architectures of standard CNN with patient privacy preservation
Bueno et al. (2020a)	Classification	Non-glomerular tissue, normal glomeruli, sclerosed glomeruli	U-Net based classifier
Guan et al. (2022)	WSI representation and classification	Kidney Chromophobe Renal Cell Carcinoma (KICH), Kidney Renal Clear Cell Carcinoma (KIRC) and Kidney Renal Papillary Cell Carcinoma(KIRP)	hierarchical global-to-local clustering, weakly-supervised
Gadermayr et al. (2019)	Segmentation	Glomeruli	Cascaded UNet model
Hermsen et al. (2019)	Segmentation	Glomeruli, sclerotic glomeruli, empty Bowman's capsules, proximal tubuli, distal tubuli, atrophic tubuli, undefined tubuli, capsules, arteries, interstitium	Ensemble of U-Net
Shao et al. (2021)	Multiple Classification	3 cancer types	Transformer based MIL (TransMIL)
Lung			
Hou et al. (2019b)	Detection	Lymphocyte richness	Unsupervised classifier using convolutional autoencoder
Vu et al. (2019)	Segmentation, Classification	Mitosis,ND, LUAD, LUSC	Deep residual aggregation network with U-Net
Le Page et al. (2021)	Classification	Squamous and non-squamous non-small cell	Inception V3
Wu et al. (2021)	Detection	Tumor, cell Detection	U-Net
Ristanoski et al. (2021)	Classification	Cancer	Decision Tree, AdaBoost and XGBoost
Coudray et al. (2018)	Disease diagnosis	LUAD, LUSC	Deep CNN with transfer learning
Graham et al. (2018)			CNN ensemble with random forest aggregation
Yu et al. (2016)			ML models with Cox hazard model
Vu et al. (2019)			Deep residual aggregation with U-Net
Yao et al. (2020)	Prognosis	Malignant, Normal	MIL-based CNN classifier
Wei et al. (2019a)	Disease diagnosis	Lepidic, acinar, papillary, micropapillary, solid, benign	CNN-based patch classifier
Gertych et al. (2019)	Disease diagnosis	Acinar, micropapillary, solid, cribriform, non-tumor	CNN-based classifier
Coudray et al. (2018)	Prognosis	STK11, EGFR, SETBP1, TP53, FAT1, KRAS, KEAP1, LRP1B, FAT4, NF1	Deep CNN with transfer learning
Corredor et al. (2021)	Segmentation	Characterizing spatial arrangement features of the immune response	Watershed-based model
Hou et al. (2019a); Brieu et al. (2019); Wang et al. (2020a)	Segmentation	N/A	UNet segmentation with GAN patch refinement, UNet segmentation with CycleGAN domain transfer
		Nuclei of tumor cells, stromal cells, lymphocytes, macrophages, blood cells, karyorrhexis	Mask-RCNN based classifier
Wang et al. (2019b)	Classification	Tumor cell, stromal cell, lymphocyte	CNN
Adnan et al. (2020)	Classification	LUAD, LUSC	Pre-trained DenseNet

Table 8.3 Continued on Next Page

Organ Overview (Continued)

Continuation of Organ Overview Table 8.3			
References	Tasks	Disease Specification	Methods
Guan et al. (2022)	WSI representation and classification	Lung Adenocarcinoma (LUAD) and Lung Squamous Cell Carcinoma (LUSC)	hierarchical global-to-local clustering, weakly-supervised
Yu et al. (2016)	Prognosis	Pathology grade, non-small cancer	Various ML models with Cox hazard model
Wang et al. (2017b)		Recurrence prediction for non-small cell cancer	CNN-based classifier
Yu et al. (2016)		Lung squamous cell carcinoma	Custom CNN
Vu et al. (2019)		Tumor cell, stromal cell, lymphocyte	Cox regression model
Chang et al. (2021)	Prognosis	Squamous cell	Self-supervised pre-trained model, HANet
Bug et al. (2017)	Segmentation	Stain normalization	CNN, LSTM based feature aware normalization
Hägele et al. (2020)	Classification	Cancer, normal	High resolution heatmaps from CNN
Shao et al. (2021)	Binary Classification	LUSC/LUAD subtypes classification	Transformer based MIL (TransMIL)
Shao et al. (2021)	Detection	carcinomas and benign tissue	Transfer Learning
Pancreas			
Faust et al. (2019)	Classification	Feature correlation analysis Nuclei, antigen, cytoplasm, blood, ECM	CNN-based classifier with transfer learning Non-linear tissue component discrimination
Bai et al. (2020)	Classification	Immunopositive tumor, immunonegative tumor, non-tumor	U-Net
Lin et al. (2021)	Tissue Classification	benign lung tissues (LN), lung adenocarcinomas (LAC), lung squamous cell carcinomas (LSCC), benign colonic tissues (CN), and colon adenocarcinomas (CAC)	Pyramid Deep-Broad Learning
Thyroid			
Wang et al. (2010)	Classification	Follicular lesion (FA,FTC), normal	Radial based SVM classifier
Höhne et al. (2021)	Classification, Detection	Unknown/have mutation(BRAF+), don't have mutation (BRAF-)/ have fusion(NTRK+), don't have fusion (NTRK-)	Attention-based deep multiple instance learning classifier, DenseNet121
Anand et al. (2021)	Classification, Detection	Tumor, Healthy/papillary, follicular, poorly differentiated, anaplastic/have mutation(BRAF+), don't have mutation (BRAF-)	Multi Instance Learning (MIL)
Stomach/Colon			
Xu et al. (2014); Tavolara et al. (2019); Xu et al. (2017b)	Detection	Cancer	Combination of CNN and MIL, InceptionV3 classifier with conditional GANs, Generalized mean model with parallel MIL
Kather et al. (2019b)	Detection	Microsatellite instability	ResNet with transfer learning
Yao et al. (2020)	Prognosis	Malignant, normal	MIL-based CNN classifier
Sirinukunwattana et al. (2016)	Detection	Nucleus	Space-constrained CNN
Cho et al. (2020)	Detection	Adenocarcinoma, normal	CNN-based classifier
Holland et al. (2020)	Detection	Carcinoma, benign	CNN-based classifier
Song et al. (2020)	Detection	High-grade intraepithelial neoplasia	Deep learning classifier with ResNet backbone
Li et al. (2021c)	Detection	Gastric cancer	DLA34, Hybrid and Weak supervision Learning method
Schrammen et al. (2022)	Detection	Tumor-bearing tissue, Non-tumor tissue	SuffleNet with end-to-end learning method
Saldanha et al. (2022)	Detection	BRAF mutational status and microsatellite instability	Swarm Learning
Tran et al. (2021)	Classification	N/A	Encoder,Resnet18
Schuchmacher et al. (2021)	Classification	Colorectal carcinoma, Colorectal cancer	Weakly supervised neural network named comparative segmentation network (CompSegNet), U-Net
Lin et al. (2021)	Classification of tissue	Cadipose (ADI),background (BACK), debris (DEB), lymphocytes (LYM),mucus (MUC), smooth muscle (MUS), normal colon mucosa (NORM), cancer-associated stroma (STR), and colorectal adenocarcinoma epithelium (TUM)	Pyramid Deep-Broad Learning
Kim et al. (2021)	Segmentation	colorectal cancer	CNN, Sliding window method, U-Net++
Feng et al. (2020)	Segmentation, Classification	Colorectal cancer	U-Net16/19 network with a VGG-16/19 net as backbone
Kloeckner et al. (2020)	Disease diagnosis	Non-epithelial normal, normal gastric epithelium, neoplastic gastric epithelium/tubular gastric adenocarcinoma, solid-type gastric adenocarcinoma, diffuse/discohesive gastric carcinoma	Custom CNN classifier
Xu et al. (2017a)	Disease diagnosis	Adenocarcinoma, mucinous carcinoma, serrated carcinoma, papillary carcinoma, and cribriform comedo-type carcinoma	CNN-based classifier with transfer learning
Iizuka et al. (2020)	Disease diagnosis	Adenocarcinoma, adenoma, non-neoplastic	CNN classifier with RNN aggregation
Shaban et al. (2020)	Disease diagnosis	Colorectal cancer	CNN
Wei et al. (2019b)	Disease diagnosis	Celiac disease, nonspecific duodenitis	ResNet patch classifier
Chikontwe et al. (2020)	Disease diagnosis	Cancer	Multiple instance learning
Kosaraju et al. (2020)	Disease diagnosis	Adenocarcinoma, poorly cohesive carcinoma, normal gastric mucosa	Multi-scale receptive field model

Table 8.3 Continued on Next Page

Continuation of Organ Overview Table 8.3			
References	Tasks	Disease Specification	Methods
Wang et al. (2019d)	Disease diagnosis	Dysplasia, Cancer	Multi-instance deep learning classifier
Yan et al. (2020b)	Disease diagnosis	Healthy, adenomatous, moderately differentiated, moderately-to-poorly differentiated, and poorly differentiated	Multi-task classifier
Ponzi et al. (2020)	Disease diagnosis	Adenocarcinoma (AC), tubulovillous adenoma (AD), healthy (H)	Downstream classifiers (ResNet18, SVM)
Chen et al. (2016a); Marsh et al. (2018); Sirinukunwattana et al. (2015)	Segmentation	Benign, malignant	Deep contour-aware networks using transfer learning, CNN
Nateghi et al. (2016); Graham et al. (2019a)	Segmentation	Carcinoma	Random polygon model, Multi-scale CNN with minimal information loss
Van Eycck et al. (2018); Yan et al. (2020b)	Segmentation	Lumen, cytoplasm, nuclei	SVM classifier with RBF kernel, Regions containing glandular structures, Multi-task classifier
Wang et al. (2019a); Xu et al. (2017c)	Segmentation	Colorectal Cancer	Two-parallel-branch DNN
Kim et al. (2021)	Segmentation	Colon: adenocarcinoma, high-grade adenoma with dysplasia, low-grade adenoma with dysplasia, carcinoid, and hyperplastic polyp	Ensemble method, wavelet transform (WWE)
Graham et al. (2021)	Segmentation, Classification	Epithelial cell, Connective tissue cell, Lymphocytes, Plasma cells, Neutrophils, Eosinophils	ResNet-34 network with contrastive learning, HoVerNet
Bilal et al. (2021)	Segmentation, Classification	high/ low mutation density, microsatellite instability/ stability, chromosomal instability/ genomic stability, CIMP-high/ low, BRAF mutation/wild-type, TP53 mutation/ wild-type, KRAS wild-type/ mutation	ResNet-18 network/ Adapted ResNet34/ HoVerNet, Weakly supervised learning
Gupta et al. (2021)	Classification	Colorectal Cancer	customized CNNs, pretrained model VGG, ResNet, Inception, IRV2
Kashif et al. (2016)	Segmentation	Epithelial, inflammatory, fibroblast, miscellaneous, unassigned	Spatially Constrained CNN
Takahama et al. (2019)	Segmentation	Tumour	U-Net segmentation with GoogleNet patch level feature extraction, Custom CNN with random forest regression
Liu et al. (2018a)	Segmentation	Gastric cancer	CNN models with transfer learning
Qaiser et al. (2019)	Segmentation	colon/ adenoma, adenocarcinoma, signet, and healthy cases	combination of PHPs, CNN features
Wright et al. (2020)	Classification	tumor, stroma	random forests
Kather et al. (2019a)	Prognosis	Stroma	CNN based on neuronal activation in tissues
Bychkov et al. (2018)	Prognosis	Five year survival rate	CNN/LSTM based regression classifier
Zheng et al. (2022)	Prognosis	EBV-associated gastric cancer	deep convolutional neural network backboned by ResNet50
Marini et al. (2021)	Classification	carcinous, high-grade dysplasia, low-grade dysplasia, hyperplastic polyp, normal glands	CNN based classifier with a Multi-Scale Task Multiple Instance Learning (MuSTMIL)
Kather et al. (2016a); Wang et al. (2017a); Rączkowski et al. (2019); Jayachandran and Ghosh (2020); Korbar et al. (2017)	Classification	Hyperplastic polyp, sessile serrated polyp, traditional serrated / tubular / tubulovillous / villous adenoma	Radial based SVM classifier, CNN classifier with dropout variance and active learning, SqueezeNet with transfer learning
Wang et al. (2017a); Rączkowski et al. (2019)	Classification	tumor epithelium, simple stroma, complex stroma, immune cell conglomerates, debris and mucus, normal mucosal glands, adipose tissue, background	ResNet patch classifier
Nguyen et al. (2020)	Classification	Normal epithelium, normal stroma, tumor	Bilinear CNN classifier, Convolutional networks (ConvNets)
Iizuka et al. (2020)	Classification	Adenocarcinoma, adenoma, or non-neoplastic	InceptionV3 patch classifier
Javed et al. (2020)	Classification	Epithelial, Spindle-shaped, Necrotic, Inflammatory	SC-CNN with Delaunay Triangulation
Foucart et al. (2019)	Segmentation	Colorectal cancer, Gastroesophageal junction (dysplastic) lesion, Head and neck carcinoma	DCNN with residual blocks
Ponzi et al. (2020)	Classification	Adenocarcinoma, corresponding to noticeable CRC, Tubulovillous adenoma, a precursive lesion of CRC, Healthy tissue	Bayesian CNNs (B-CNNs),
Su et al. (2022)	Classification	cancer, non-cancer	Transfer Learning
Zheng et al. (2020)	Disease diagnosis	Gastric cancer	GCN-RNN based feature extraction and encoding
Lahiani et al. (2020)	Segmentation	Tumor	GAN
Ji et al. (2020)	Prognosis	Adenocarcinoma, disease-specific survival time	ECA histomorphometric-based image classifier
Deshpande et al. (2022)	Synthesis of large high-resolution images	Colorectal Cancer	Novel framework called SAFRON (Stitching Across the FROntier Network)
Multi-Organ			
Bauer et al. (2016)	Classification	Benign, malignant	CNN based classifier

Table 8.3 Continued on Next Page

Organ Overview (Continued)

Continuation of Organ Overview Table 8.3			
References	Tasks	Disease Specification	Methods
Lu et al. (2021d)	Classification	Kidney, Lymph nodes, Lung/ Chromophobe, clear cell carcinoma, papillary	Weakly supervised ResNet50 with transfer learning
Graham et al. (2019b)	Segmentation	Bladder, Breast, Kidney, Liver, Prostate, Stomach/ Normal, malignant, dysplastic epithelial, fibroblast, muscle, inflammatory, endothelial, miscellaneous	Modified Preact-ResNet50
Kumar et al. (2017)	Segmentation	Nuclear, non-nuclear, boundary	CNN-based classifier with AJI evaluation
Eminaga et al. (2019)	Detection	Liver, Prostate/Tumor, normal	Custom CNN architecture
Xu et al. (2016)	Classification	Epithelial, stromal tissues	DCNN classifier
Chang et al. (2017a)	Classification	Brain, Breast, Kidney/ DCIS, ERBB2+, triple negative	Transfer learning using multi-scale convolutional sparse coding
Motlagh et al. (2018)	Detection	Bladder, Breast, Lymph nodes, Lung	CNN-based classifier with transfer learning
Campanella et al. (2019b)	Detection	Basal, Breast, Prostate/ Cell carcinoma, Metastasis	RNN classifier with multiple instance learning
Litjens et al. (2016)	Classification	Micro/Macro metastasis	RNN classifier with MIL
Kong et al. (2018)	Detection	Breast, Stomach/Tumor, normal	Custom CNN classifier
Lafarge et al. (2019)	Segmentation	Bladder, Breast, Liver, Prostate, Kidney, Stomach/ Edge, foreground, background	Domain-Adversarial Neural Network
Vu et al. (2019)	Segmentation, Classification	Brain, Lung, Esophagus/ Mitosis, Lymphocyte richness, LUAD, LUSC	Deep residual aggregation network with U-Net segmentation
Khan et al. (2014)	Segmentation	Breast, Esophagus, Liver/ Stain normalization	Relevance vector machine
Sarnecki et al. (2016)	Classification	colon, kidney, ovarian cancer, lung adenocarcinoma, gastric mucosa, astrocytoma, skin cutaneous melanoma, breast cancer/ Nuclei, antigen, cytoplasm, blood, ECM	Non-linear tissue component discrimination
Freyre et al. (2021)	Classification	Different organs of rats/Exploring the morphological changes in tissue to biomarker level	CNN, MIL, multi-task learning
Bussola et al. (2021)	Classification	Adrenal gland, Bladder, Breast, Liver, Lung, Ovary, Pancreas, Prostate, Testis, Thyroid, Uterus, Heart	CNN models with transfer learning/ ResNet-152 pretrained on ImageNet and GTEx
Yamashita et al. (2021)	Classification	Colon, Breast/molecular fingerprint of a deficient mismatch (Microsatellite stability(MSS)/ Microsatellite instability (MSI))	CNN models with transfer learning method
Ciga et al. (2022)	Classification, Segmentation	blood, breast, lymph, colon, bone, prostate, liver, pancreas, bladder, cervix, esophagus, head, neck, kidney, lung, thyroid, uterus, bone marrow, skin, brain, stomach, and ovary	Unsupervised contrastive learning, residual networks pretrained with self-supervised learning
Khoshdeli et al. (2018)	Segmentation	Brain, Breast/ Nuclei	Custom encoder-decoder model
Xu et al. (2020)	Prognosis	Bladder/ Lung, Low TMB, Medium TMB, High TMB	Deep transfer learning, SVM with Gaussian kernel
Gueréndel et al. (2021)	Classification	Bladder, Brain, Breast, Bronchus and lung, Connective, subcutaneous and other soft tissues, Kidney, Liver and intrahepatic bile ducts, Pancreas, Prostate gland, Thyroid gland/ Cancer	ResNet18, self-supervised BYOL method, Clustering tiles using k-means clustering
Khened et al. (2021)	Segmentation,Classification	Colon, Liver, lymph node sections	An ensemble of FCNs architectures/U-Net with DenseNet, ResNet
Wu et al. (2022b)	Segmentation cellular nuclei	Multiple	Cross-patch Dense Contrastive Learning
Chen et al. (2020b)	Prognosis, Cancer Grade Classification	brain and kidney	CNN, GCN, SNN
Belharbi et al. (2021a)	Segmentation	Colon, Lymph Node	Kullback-Leibler (KL) divergence with classifier
Tang et al. (2021)	Segmentation	Breast, Bone, Tissue	Performing Neural architecture search(NAS)
Ghahremani et al. (2022)	Segmentation of nuclei and cytoplasm	Lung, Bladder	Multi-task model
Pati et al. (2021b)	Classification	Axillary lymph nodes, Breast/Metastasis, Colorectal cancer	Adversarial autoencoder, Progressive growing algorithm for GANs, Resnet18 with pre-trained ImageNet weights
Diao et al. (2021b)	Classification,Detection	Skin/ cutaneous melanoma(SKCM), Stomach/ adenocarcinoma(STAD), Breast/ cancer(BRCA), Lung/ adenocarcinoma(LUAD), Lung/ squamous cell carcinoma (LUSC)	Convolutional neural networks(CNNs), Birch clustering
Shen et al. (2022)	Classification of tissue	Stomach, Colon, Rectum	CNN+ Pathology Deformable Conditional Random Field
Yang et al. (2022b)	Classification of tissue	Liver, Lung, Colon, Rectum	Contrastive learning (CL) with latent augmentation (LA)
Zhu et al. (2021a)	Classification	Stomach, Intestine, Lymph node, Colon	label correction + NSHE scheme
Lu et al. (2021e)	Detection	Renal/ cell carcinoma (RCC), lung/nonsmall cell cancer (NSCLC), Breast/cancer lymph node metastasis	Attention-based learning, Instance-level clustering
Srinidhi et al. (2022)	Classification	Breast, Colon /Tumor metastasis and Tumor cellularity quantification	ResNet-18
Pati et al. (2021a)	Classification, Detection	Breast cancer, Colorectal adenocarcinoma, Colorectal cancer	Co-representation learning (CoReL), Neighborhood-aware multiple similarity sampling strategy
Qureshi et al. (2008)	segmentations	Nuclei in pancreatic, tubules in colorectal, epithelium in breast	U-net

Table 8.3 Continued on Next Page

Continuation of Organ Overview Table 8.3

References	Tasks	Disease Specification	Methods
Riasatian et al. (2021)	Classification	Brain, Endocrine, Gastro, Gynaeco, Liver, pancreas, Urinary tract, Melanocytic, Pulmonary, Prostate Cancer	DenseNet121, KimiaNet
Zhu et al. (2021b)	Detection	cell nuclear	Robust Self-Trained Network(RSTN) trained on distance maps(DMs)
Jaume et al. (2021a)	Segmentation, Classification	Nuclei in the breast, prostate/Benign,ADH,DCIS	GNN models
Cheng et al. (2022)	Classification, Segmentation	Lung and Skin/nuclei	ResGANet
Lu et al. (2021a)	Prognosis	HPV+, HPV-, survival class	MIL classifier with discriminant analysis
Lu et al. (2021b)	Detection	18 primary organ/Tumor	MIL with attention pooling
Fischer et al. (2018)	Detection	Tumor, normal	Sparse coding and transfer learning
Noorbakhsh et al. (2020)	Detection	Tumor, normal from 23 cohorts	CNN-based classifier with transfer learning
Shen and Ke (2020)	Detection	Loose non-tumor tissue, dense non-tumor tissue, normal tumor tissue	Custom CNN classifier
Lafarge et al. (2021)	Detection	Mitosis centroid	G-CNN for rotational invariance
Yang et al. (2022a)	Detection, Segmentation	Colon, Rectum	Concept Contrastive Learning
Lu et al. (2021c)	Disease diagnosis	Lung, Breast, Colorectal, Glioma, Renal, Endometrial, Skin, Head and neck,Prostate, Bladder, Thyroid, Ovarian, Liver, Germ cell, Cervix, Adrenal/metastatic tumors and Cancer	MIL
Miao et al. (2021)	Segmentation	Breast, Pancreatic, Colon/Cell Nuclei,Tubules,Epithelium	u-net
Vahadane et al. (2021)	Segmentation	prostate, colon, breast, kidney, liver, bladder, stomach/Nuclei	U-Net
Feng et al. (2021a)	Segmentation	Bladder, Breast, Colorectal, Endometrial, Ovarian, Pancreatic, Prostate/Nuclei	Hoovernet on tiles, Nuc2Vec with a ResNet34 with contrastive learning method
Lutnick et al. (2022)	Segmentation	Brain, Kidney,	semantic segmentation+ Xception
Cheng et al. (2021b)	Segmentation	Breast, liver, kidney, prostate, bladder, colon, stomach/Cell boundary pixels,Nuclei	Hard-boundary Attention Network (HBANet) with background weaken module (BWM)
Dogar et al. (2021)	Segmentation,Classification	Bladder, Breast, Colorectal, Endometrial, Ovarian, Pancreatic,Prostate/Nucleus boundaries/Normal epithelial, malignant/dysplastic epithelial, fibroblast, muscle, inflammatory, endothelial, miscellaneous	CNN pretrained on ImageNe/End-to-end learning
Chen et al. (2021a)	Classification	Thyroid frozen sections, Colonoscopy tissue, Cytological cervical pap smear/ benign, non-benign	VGG16bn, ResNet50, U-net, with stochastic selection and attention fusion
Belharbi et al. (2021b)	Classification	Colon, Breast/ non-discriminative and discriminative regions	CNN classifier, ResNet18, Weakly supervised learning, Max-Min uncertainty
Lafarge et al. (2021)	Classification,Segmentation	Nuclear boundaries,Benign, malignant	G-CNN for rotational invariance
Ianni et al. (2020)	Classification	Basaloid, Melanocytic, Squamous	Multi-stage CNN classifier
Graham et al. (2020)	Classification	Colorectal glands,Tumor, normal	Dense steerable filter CNN for rotational invariance
Lerousseau et al. (2020)	Segmentation	Contoured tumor regions	Resnet classifier with transfer learning
Diao et al. (2020)	Classification	Skin melanoma, stomach adenocarcinoma, breast cancer, lung adenocarcinoma, lung squamous cell carcinoma	Custom CNN using human-interpretable image features (HIF)
Nasrin et al. (2020)	Classification	20 classes for muscle, epithelial, connective tissue	Inception Residual Recurrent CNN
Koohbanani et al. (2021)	Tissue subtype classification	Adipose (ADI), background (BACK), debris (DEB), lymphocytes (LYM), mucus (MUC), smooth muscle (MUS), normal colon mucosa (NORM), cancer-associated stroma (STR), colorectal adenocarcinoma epithelium (TUM)	ResNet based classifier
Javed et al. (2021)	Nuclei segmentation	Breast, Colon, Liver, Prostate, Kidney, Stomach, Colorectal, Bladder, Ovarian	CNN model, VGG-19 network
Li et al. (2021a)	Segmentation	Lung, Breast	Multiple Instance Learning (MIL), self-supervised contrastive learning in SimCLR setting, feature vector aggregation
Chen et al. (2021c)	Prognosis	Prediction of cancer rate survival in the Bladder, Breast, Lung, Uterus, Brain	Graph Convolutional Neural Net(GCN)
Vahadane et al. (2021)	Nuclei segmentation	prostate, colon, breast, kidney, liver, bladder, stomach	A convolutional U-Net architecture
Chen et al. (2019)	Nuclei segmentation	Nuclear boundaries	U-net based architecture
Yen et al. (2020)	Nuclei segmentation	Nuclear boundaries	Modified HoVer-Net segmentation
Sahasrabudhe et al. (2020)	Nuclei segmentation	Nuclear boundaries	CNN-based attention network
Chan et al. (2019)	Segmentation	3-level hierarchy of histological types	Pixel level semantic segmentation
Bändi et al. (2019)	Segmentation	Tissue, background, edge artifacts, inner artifacts, inner/external margin	Custom FCNN
Saltz et al. (2018)	Segmentation	Lymphocytes, necrosis	Semantic segmentation CNN classifier
Awan et al. (2017)	Disease diagnosis	usual ductal hyperplasia, ductal carcinoma in-situ	Deep-learning based CAD tool for pathologists
Mahmood et al. (2019)	Nuclei segmentation	Positive/negative in nuclei boundaries	Conditional GAN

Table 8.3 Continued on Next Page

Organ Overview (Continued)

Continuation of Organ Overview Table 8.3			
References	Tasks	Disease Specification	Methods
Chen et al. (2020c)	Nuclei segmentation	Nuclear boundaries	CNN-based Boundary-assisted Region Proposal Network
Abdel-Nasser et al. (2020)	Nuclei segmentation	Nuclei, other	CNN-based multi-branch network classifier
Tellez et al. (2019a)	Detection	Mitosis and metastasis detection	U-Net based normalization
Shin et al. (2016); Koohbanani et al. (2020)	Nuclei segmentation	normal epithelial, myoepithelial, invasive carcinoma, fibroblasts endothelial, adipocytes, macrophages, inflammatory	U-Net with regression loss
Xie et al. (2020)	Nuclei segmentation	Nuclei body, nuclei boundary, background Background removal Nuclei boundary	UNet based classifier with self-supervised learning UNet with transfer learning Custom encoder-decoder network
Gamper et al. (2020b)	Tissue subtype classification	60 types of tissues from a various datasets	ResNet50 feature encoder/decoder for 11 tasks
Thagaard et al. (2020)	Detection	Tumor, normal	ResNet based patch classifier
Chen et al. (2021b)	Classification	Skin/Skin lesions, Chest/ Benign, malignant, Kidney/Chromophobe, clear cell, papillary carcinoma	Conditional Progressive Growing GAN (PG-GAN/ResNet-50)
Tellez et al. (2019b)	Classification	Neural image compression for Rectal carcinoma	CNN classifier with encoder compression network
Alawad et al. (2020)	Pathology report information extraction	Tumor description relating to primary cancer site, laterality, behavior, histological type, and histological grade	Ensemble of multi-task CNN
Campanella et al. (2018a)	Detection	Blur detection	Combination of CNN and Random Forest regressor
Wang et al. (2020c)	Classification	15 types based on focus level	Lightweight CNN
Schmauch et al. (2020)	Segmentation	Molecular feature extraction	Multi-layer perceptron with aggregation
Jiang et al. (2020a)	Classification	Deblurring	Encoder-decoder with VGG-16 blur type classifier
Thandiackal et al. (2022)	Classification	WSI Classification	Multi-scale Context-aware MIL, Multi-level Zooming
Chen et al. (2022)	Classification	BRCA subtyping, NSCLC subtyping, RCC Subtyping	Vision Transformer
Hou et al. (2016)	Classification	Classification of glioma and non-small-cell lung carcinoma cases into subtypes	Two-level model consisting of an Expectation Maximization based method combined with CNN and a decision fusion model
Chen et al. (2022)	Prognosis	Survival prediction of IDC, CCRCC, PRCC, LUAD, CRC, and STAD cancer types	Vision Transformer
Salvi et al. (2020)	WSI Processing	Stain normalization	Combination of segmentation and clustering for nuclear/stroma detection
Mahapatra et al. (2020)	WSI Processing	Stain normalization	Self-supervised cycleGAN
Nadeem et al. (2020)	WSI Processing	Stain normalization	Modified Wasserstein Barycenter approach for multiple referencing
Levine et al. (2020)	WSI Processing	Patch synthesis	Progressive GAN model
Kalra et al. (2020)	WSI Processing	Similar image retrieval	Classifier based on ANN with K-means clustering
Other			
Mirzazadeh et al. (2021)	Detection	Heart/rejection and nonrejection tissue tiles	Progressive Generative Adversarial Network + Inspirational Image Generation with a VGG-19 as a classifier
Nirschl et al. (2018)	Detection	Heart failure	CNN based patch classifier
Peyster et al. (2021)	Classification	Heart/Endomyocardial disease	CACHE-Grader, SVM and K-means clustering
Höhn et al. (2021)	Classification	Skin/Cancer	random forest ensemble learning method, feature extractor using ResNeXt50
Xing et al. (2021)	Detection	Eye/Macular edema	Fully convolutional neural network (FCN), Improved attention U-Net architecture (IAUNet)
Lu et al. (2022)	Prognosis	N/A	Custom MIL framework with attention modules
Hu et al. (2018)	Classification	Bone marrow/Neutrophil, myeloblast, monocyte, lymphocyte	GAN-based classifier
Chandrasevan et al. (2020)	Classification, Detection	Bone marrow/nonneoplastic, myeloid leukemia, myeloma	Two-stage detection and classification model
Mu et al. (2021)	Detection	Bone marrow/aspirate pathology synapses	BERT-based NLP mode, Active learning
Ho et al. (2020)	Segmentation	Viable tumor, necrosis with/without bone, normal bone, normal tissue, cartilage, blank	UNet-based multi-magnification network
Dastidar and Ethirajan (2020)	Diseases diagnosis	Bacterial disease	CNN-based classifier
van Eekelen et al. (2020)	Segmentation	Bone marrow/Myelopoietic cells, erythropoietic cells, matured erythrocytes, megakaryocytes, bone, lipocytes	Custom CNN
Hou et al. (2020b)	Segmentation	10 Cancer types	U-Net, Mask R-CNN for quality control
Hosseini et al. (2019)	Classification	Level 1 (Epithelial, Connective Proper, Blood, Skeletal, Muscular, Adipose, Nervous, Glandular), Level 2 (23 sub-classes from Level 1), Level 3 (36 sub-classes from Level 2 classes)	Ensemble of different CNN architectures
Hegde et al. (2019)	Classification	Arteries, nerves, smooth muscle, fat	InceptionV3, Deep ranking network
Sali et al. (2019)	Disease diagnosis	Duodenum/Celiac	CNN-based classifier
Idlahcen et al. (2020)	Disease diagnosis	Cervical cancer, Squamous cell carcinoma, adenocarcinoma	CNN-based patch classifier
Sali et al. (2020)	Disease diagnosis	Duodenum/Celiac, environmental enteropathy, Esophagus/EoE, Ileum/Crohn's disease	Hierarchical CNN classifier
Tian et al. (2019)	Disease diagnosis	Squamous carcinoma	Combinations of CNN classifiers

Table 8.3 Continued on Next Page

Organ Overview (Continued)

72

Continuation of Organ Overview Table 8.3			
References	Tasks	Disease Specification	Methods
Pal et al. (2021)	Classification	Normal, Cervicitis, Squamous Intra-epithelial Lesion- High, Cancer	Low and Deep multiple instance learning
van Eekelen et al. (2020)	Classification, Segmentation	Bone marrow/Aplasia	SVM classifier with BoW
Corvo et al. (2020)	Detection	Tumor cells, stromal cells, lymphocytes, stromal fibroblasts	k-means,Hierarchical Clustering
Tellez et al. (2020)	Classification	colorectal liver metastasis	Ensemble of 4 MLP and an encoder, supervised multitask learning (MTL)
Li et al. (2020a)	Detection	Mitosis	Feature pyramid network
Genovese et al. (2021)	Detection	Acute Lymphoblastic (or Lymphocytic) Leukemia (ALL), normal/lymphoblast	Transfer Learning, CNN pretrained on a histopathology dataset, ResNet18 and VGG16 as the backbone

End of Table 8.3

Compilation of information and Neural Network architectures found in different Co-Path papers categorized by task (see 8.3)

References	Disease/Organ Specification	Architecture	Datasets
Detection Task			
Litjens et al. (2016); Bejnordi et al. (2017a); Bandi et al. (2018); Campanella et al. (2019b); Cruz-Roa et al. (2014); Liu et al. (2017); Tellez et al. (2019a); Bejnordi et al. (2017b); Celik et al. (2020); Mohapatra et al. (2019); Tellez et al. (2019b); Li and Ping (2018); Lee and Paeng (2018); Brancati et al. (2019); Teh and Taylor (2019); Liang et al. (2019); Liu et al. (2019); Öztürk and Akdemir (2019); Cho et al. (2017); Huang and Chung (2019); Chen et al. (2016b); Kong et al. (2018); Cruz-Roa et al. (2018); Yen et al. (2020); BenTaieb and Hamarneh (2018); Valkonen et al. (2017); Lafarge et al. (2021); Graham et al. (2020); Lu et al. (2021d); Shen and Ke (2020); Khan et al. (2020); Koohbanani et al. (2021); Lu et al. (2021c); Wang et al. (2021a); Turki et al. (2021); Farahmand et al. (2022)	Breast cancer	Custom CNN {15}, Inception {6}, ResNet {14}, VGG {4}, U-Net {2}, Multi-stage CNN {1}, DenseNet {4}, GAN {1}, AlexNet {1}, E-D CNN {1}, CAS-CNN {1}, Attention CNN {3}, HoVer-Net {1}, MLV-DeepLabV3+ {1}, Xception {1}, Lightweight-CNN {1}	RUMC, CAMELYON16, CAMELYON17, MSK, HUP+CINJ, NHO-1, IDC-Moh, AJ-IDC, PCam, NMCS, HASHI, TCGA, Cancer Imaging Archive, TCGA-BRCA, Yale HER2 dataset, Yale response dataset
Litjens et al. (2016); Campanella et al. (2019b); Khan et al. (2019b); Raciti et al. (2020); Doyle et al. (2011); Pinckaers et al. (2021); Tolkach et al. (2020); Lu et al. (2021c); Xiong et al. (2021)	Prostate cancer	Custom CNN {2}, ResNet {4}, Inception {1}, Non-DL {1}, NASNetLarge {1}	RUMC, MSK, HUH, Pro-Raciti, Pro-Doyle, CUH, UHB, Gleason 2019
Campanella et al. (2019b); Jiang et al. (2020b); Saltz et al. (2018); Cruz-Roa et al. (2013); Lu et al. (2021c); Höhn et al. (2021)	Skin cancer	ResNet {3}, Inception {1}, Custom CNN {1}, E-D CNN {1}, ResNeXt {1}	SCMOI, YSM, GHS, MIP, MSK, BE-Cruz-Roa, Private
Xu et al. (2014); Tavolara et al. (2019); Xu et al. (2017b); Iizuka et al. (2020); Chikontwe et al. (2020); Shen and Ke (2020); Lahiani et al. (2020); Gupta et al. (2021); Feng et al. (2020); Marini et al. (2021); Saldanha et al. (2022)	Colon cancer	Custom CNN {2}, Inception {1}, GAN {1}, Novel algorithm {1}, DenseNet {1}, ResNet {2}, Inception-ResNet {1}, U-Net {1}, VGG {1}, Swarm Learning {1}	SC-Xu, FAHZU, OSU, TCGA, CRC-Chikontwe, Novel Dataset, DigestPath 2019, Epi700, DACHS, TCGA-CRC, QUASAR trial, YCR-BCIP
Cho et al. (2020); Kong et al. (2018); Iizuka et al. (2020); Shen and Ke (2020); Song et al. (2020); Kausar et al. (2020); Li et al. (2021c)	Stomach cancer	AlexNet {1}, ResNet {3}, Inception {3}, DenseNet {1}, DeepLab {1}, VGG {1}, DLA {1}, Custom CNN {1}	TCGA, SSMH-STAD, SC-Kong
Xu et al. (2020); Lu et al. (2021c)	Bladder cancer	Inception {1}, ResNet {2}	TCGA
Tian et al. (2019); Lu et al. (2021c)	Cervix cancer	Inception {1}, ResNet {2}, Inception-ResNet {1}	XH-FMMU
Tjio et al. (2020)	Kidney cancer	Custom CNN {1}	Pantomics
Hägle et al. (2020); Lu et al. (2021c); Ristanoski et al. (2021); Wu et al. (2021); Le Page et al. (2021)	Lung cancer	Inception {2}, ResNet {1}, DT {1}, AdaBoost {1}, XGBoost {1}, U-Net {1}	TCGA-(LUAD, LUSC), MedicineInsight, 22c3, Ventana PD-L1, Private
Koohbanani et al. (2021)	Oral cancer	Custom CNN {1}	LNM-OSCC
Lafarge et al. (2019); Tellez et al. (2019a); Wahab et al. (2017); Tellez et al. (2018); Wang et al. (2014); Jiménez and Racóceanu (2019); Li et al. (2018a); Otálora et al. (2019); Li et al. (2019a); Sebai et al. (2020); Akram et al. (2018); Lafarge et al. (2021); Alom et al. (2020); Li et al. (2020a)	Mitosis	Custom CNN {7}, AlexNet {1}, U-Net {2}, Multi-stage CNN {2}, FCN {1}, R-CNN {1}, ResNet {2}	TUPAC16, RUMC, MITOS12, TNBC-JRC, AMIDA13, MITOS-ATYPIA14, CWRU
Brieu et al. (2019); Fuchs et al. (2008); Sirinukunwattana et al. (2016); Li et al. (2018b); Kashif et al. (2016); Shephard et al. (2021); Zhu et al. (2021b); Dawood et al. (2021); Javed et al. (2021); Feng et al. (2021a); Dogar et al. (2021); Corredor et al. (2021)	Nuclei	U-Net {2}, GAN {1}, Non-DL {2}, Custom CNN {2}, Hover-Net {2}, SC-CNN {1}, Robust-Self Trained Network (RSTN) {1}, RCNN {1}, VGG {1}, ResNet {2}, E-D CNN {1}	NHS-LTGU, TNBC-CI, MoNuSeg, UHZ, CRCHistoPhenotypes, TCGA, Private, BCFM, PanNuke, NuCLS, CoNSeP, NCT-CRC-HE-100K, Cleveland Clinic (CC)
Chen et al. (2016a); Wang et al. (2019a)	Colorectal gland	FCN {2}	GLaS
Tellez et al. (2019a)	Epithelial cell	Custom CNN {1}	PCa-Bulten, RUMC
Wu et al. (2019); Yang et al. (2020); Bueno et al. (2020a)	Glomeruli	ResNet {1}, VGG {1}, AlexNet {1}, MobileNet {1}	Kid-Wu, Kid-Yang
Nirschl et al. (2018); Peyster et al. (2021); Mirzazadeh et al. (2021)	Heart failure, Heart Transplant	Custom CNN {1}, K-Means {1}, SVM {1}, VGG {1}, PG-GAN {1}	UPenn, CHOA
Das et al. (2018)	Keratin pearl	Custom CNN {1}	BCRWC
Atupelage et al. (2013); Roy et al. (2021)	Liver, Liver fibrous region	Non-DL {1}, Autoencoder CNN {1}	Liv-Atupelage, PAIP
Hou et al. (2019b)	Lymphocyte-richness	Autoencoder CNN {1}	TCGA
Kather et al. (2019b)	Microsatellite instability	ResNet {1}	TCGA, DACHS, KCCH
Lu et al. (2020c); Narayanan et al. (2019)	Tumor-infiltrating lymphocyte	U-Net {1}, IM-Net {1}, DRDIN {1}	TCGA, DUKE
Fischer et al. (2018); Noorbakhsh et al. (2020); Lu et al. (2021c); Riasatian et al. (2021); Diao et al. (2021b); Cheng et al. (2022)	Multi-organ tumor	KimiaNet {1}, Novel algorithm {1}, ResNet {3}, Inception {1}, DenseNet {1}, Custom CNN {1}, MLV-DeepLabV3+ {1}	AJ-Lymph, TCGA, ISIC2017, LUNA, COVID19-CT
Campanella et al. (2018a); Bautista and Yagi (2009); Wang et al. (2020c)	WSI defect	ResNet {2}, DenseNet {1}, Novel algorithm {1}, Custom CNN {1}	Pro-Campanella, MO-Campanella, MGH, TCGA@Focus, FocusPath
Genovese et al. (2021)	Acute Lymphoblastic (or Lymphocytic) Leukemia (ALL)	Custom CNN {1}, ResNet {1}, VGG {1}	ADP, ALL-IDB2

Table 8.3 Continued on Next Page

Technicalities by Task (Continued)

Continuation of Technicalities by Task Table 8.3			
References	Disease/Organ Specification	Architecture	Datasets
Tissue Subtype Classification Task			
Kather et al. (2019a, 2016a); Ciompi et al. (2017); Tellez et al. (2019a); Korbar et al. (2017); Javed et al. (2020); Wang et al. (2017a); Rączkowski et al. (2019); Jayachandran and Ghosh (2020); Nguyen et al. (2020); Xu et al. (2016); Koohbanani et al. (2021); Su et al. (2022)	Colorectal cancer	Non-DL {1}, FCN {1}, ResNet {3}, VGG {3}, AlexNet {1}, Inception {1}, SqueezeNet {2}, BCNN {1}, Capsule CNN {1}, Custom CNN {5}, U-Net {2}	NCT-CRC-HE-100K, NCT-CRC-HE-7K, RUMC, RC-Ciompi, GLaS, CRC-TP, CRC-CDC, UMCM, DHMC-Korbar, TBB, HUH, Stanford Hospital, TCGA
Rawat et al. (2020); Chang et al. (2017a); Mercan et al. (2017); Steiner et al. (2018); Jaber et al. (2020); Xu et al. (2016); Senousy et al. (2021)	Breast cancer	Custom CNN {1}, ResNet {1}, Novel algorithm {2}, Inception {2}, Novel CNN {1}	US-Biomax, ABCTB, TCGA, Bre-Chang, Bre-Steiner, BCSC, NKG-VGH, BACH
Faust et al. (2019); Chang et al. (2017a); Rathore et al. (2019)	Brain cancer	VGG {1}, Novel algorithm {1}, ResNet {1}	UHN, TCGA
Wei et al. (2019a); Gertych et al. (2019); Wang et al. (2019b)	Lung cancer	ResNet {2}, AlexNet {1}, Inception {1}, Custom CNN {1}	DHMC, CSMC, MIMW, TCGA, NLST, SPORE, CHCAMS
Sethi et al. (2016); Bauer et al. (2016); Doyle et al. (2012)	Prostate cancer	Non-DL {2}, Custom CNN {1}, ResNet {1}	CPCTR, UHZ-PCA, UPenn
Chang et al. (2017a); Bauer et al. (2016); Lu et al. (2021d)	Kidney cancer	Novel algorithm {1}, ResNet {2}	TCGA, UHZ-RCC, BWH
Woerl et al. (2020)	Bladder cancer	ResNet {1}	CCC-EMN MIBC
Kloeckner et al. (2020)	Stomach cancer	Custom CNN {1}	SPSCI
Khan et al. (2014); Kieffer et al. (2017); Hosseini et al. (2019); Bauer et al. (2016); Diao et al. (2020); Nasrin et al. (2020); Lu et al. (2021b); Guéründel et al. (2021); Chen et al. (2022)	Multi-organ	Non-DL {1}, Custom CNN {2}, VGG {2}, Inception {3}, ResNet {4}, K-Means {2}, XGBoost {1}, ViT {1}	MO-Khan, KIMIA Path24, ADP, UHZ, TCGA, KIMIA Path960, MO-Diao, BWH-TCGA-MO, CRC-100K, BCSS, BreastPathQ
Sirinukunwattana et al. (2016); Graham et al. (2019b); Atupelage et al. (2013); Chang et al. (2017b); Shephard et al. (2021); Dawood et al. (2021)	Nuclei	Custom CNN {3}, ResNet {1}, Non-DL {1}, Hover-Net {2}	CRCHistoPhenotypes, CoNSeP, Liv-Atupelage, PHI, Private, PanNuke, NuCLS
Iizuka et al. (2020); Al-Milaji et al. (2019); Shephard et al. (2021)	Epithelial	Inception {1}, Custom CNN {1}, Hover-Net+ {1}	HUH-HH, NKG-VGH, TCGA, Private
Bueno et al. (2020a)	Glomeruli	AlexNet {1}	AIDPATH _A , AIDPATH _B
Hu et al. (2018); van Eekelen et al. (2020); Chandradevan et al. (2020)	Bone marrow	VGG {1}, GAN {1}, FCN {1}	BM-MICCAI15, BM-Hu, FAHZU, RUMC, EUH
Wang et al. (2010); Hart et al. (2019); Parvatikar et al. (2020)	Lesion	Non-DL {2}, Inception {1}	UPMC, BE-Hart, Bre-Parvatikar
Folmsbee et al. (2018)	Oral cavity	AlexNet {1}	ECMC
Disease Diagnosis Task			
Rakhlin et al. (2018); Aresta et al. (2019); Bardou et al. (2018); Araújo et al. (2017); Stacke et al. (2019); Bayramoglu et al. (2016); Li et al. (2020b); Nahid and Kong (2018); Nahid et al. (2018); Nazeri et al. (2018); Kumar et al. (2020a); Bejnordi et al. (2017b); Ehteshami Bejnordi et al. (2018); Lu et al. (2020a); Celik et al. (2020); Jiang et al. (2019); Meng et al. (2019); Pimkin et al. (2018); Vang et al. (2018); Mohapatra et al. (2019); Kassani et al. (2019a); Khan et al. (2019a); Awan et al. (2018); Qi et al. (2018); Budak et al. (2019); Lee and Paeng (2018); Thuy and Hoang (2019); Yao et al. (2019); Yan et al. (2018); Alom et al. (2019); Nawaz et al. (2018); Wang et al. (2018); Iesmantas and Alzbutas (2018); Spanhol et al. (2017); Xu et al. (2019b); Motlagh et al. (2018); Patil et al. (2019); Huang and Chung (2018); Gandomkar et al. (2018); Kassani et al. (2019b); Saxena et al. (2020); Bidart and Wong (2019); Roy et al. (2019); Dong et al. (2014); Yan et al. (2020c); Han et al. (2017); Xu et al. (2019a); Alirezazadeh et al. (2018); Alzubaidi et al. (2020); Jaume et al. (2020, 2021b); Lu et al. (2022)	Breast cancer	ResNet {14}, VGG {7}, Inception {9}, Custom CNN {12}, AlexNet {3}, XGBoost {1}, MobileNet {1}, Xception {1}, DenseNet {7}, Multi-stage CNN {3}, Capsule CNN {1}, SENet {1}, Inception-ResNet {1}, VGGNet {2}, Attention CNN {3}, RCNN {1}, CafefNet {1}, TriResNet {1}, Class Structured Deep CNN {1}, Non-DL {1}	BACH18, BreakHis, BioImaging, Ext-BioImaging, CAMELYON16, CAMELYON17, CMTHis, AP, AJ-IDC, BIDMC-MGH, PUIH, BRACS, TCGA
Arvidsson et al. (2019); Li et al. (2017, 2018b); Arvaniti and Claassen (2018); Li et al. (2019b); Nagpal et al. (2019); Ren et al. (2019); Otálora et al. (2019); Karimi et al. (2019); Yan et al. (2020a); Otálora et al. (2020); Tolkach et al. (2020); Lara et al. (2020)	Prostate cancer	Custom CNN {3}, U-Net {1}, ResNet {2}, VGG {2}, Inception {1}, AlexNet {2}, Non-DL {1}, MobileNet {1}, DenseNet {1}, DCNN {1}, NASNetLarge {1}	SUH, CSMC, TCGA, NMCS-MML-TCGA, VPC, UPenn, RCINJ
Shaban et al. (2020); Xu et al. (2017a); Holland et al. (2020); Yan et al. (2020b); Ponzio et al. (2020)	Colon cancer	Inception {1}, ResNet {4}, SqueezeNet {1}, AlexNet {2}, MobileNet {1}, Xception {1}	Warwick-CRC, Ext-Warwick-CRC, SC-Holland, GLaS, ZU, ULeeds
Coudray et al. (2018); Graham et al. (2018); Yu et al. (2016); Vu et al. (2019); Lu et al. (2021d); Adnan et al. (2020); Lu et al. (2021a)	Lung cancer	Inception {1}, ResNet {3}, Non-DL {2}, DenseNet {1}, GCNN {1}	TCGA, MICCAI17, Stanford-TMA, NYU LMC, BWH, DHMC, ES-NSCLC
Barker et al. (2016); Xu et al. (2017a); Ertosun and Rubin (2015); Rathore et al. (2020)	Brain cancer	Non-DL {2}, Custom CNN {1}, AlexNet {1}	TCGA, MICCAI14
Kiani et al. (2020); Atupelage et al. (2013)	Liver cancer	DenseNet {1}, Non-DL {1}	TCGA, SUMC, Liv-Atupelage
Kosaraju et al. (2020); Wang et al. (2019d)	Stomach cancer	Custom CNN {1}, Multi-stage CNN {1}	GNUCH, WSGI
Hekler et al. (2019); Xie et al. (2019); Ianni et al. (2020)	Skin cancer	ResNet {2}, VGG {1}, Multi-stage CNN {1}	DKI, Y/CSUXH-TCGA, DLCS, BE-TF-Florida-MC
Zhang et al. (2019)	Bladder cancer	Custom CNN {1}, Inception {1}, Multi-stage CNN {1}	TCGA+UFHSH
Idlahcen et al. (2020)	Cervix cancer	VGG {1}	TCGA

Table 8.3 Continued on Next Page

Technicalities by Task (Continued)

Continuation of Technicalities by Task Table 8.3			
References	Disease/Organ Specification	Architecture	Datasets
Tomita et al. (2019)	Esophagus cancer	ResNet {1}, Attention CNN {1}	DHMC
Lu et al. (2022)	Kidney cancer	Custom CNN {1}	TCGA
Motlagh et al. (2018); Chen et al. (2021a)	Multi-organ cancer	Inception {1}, ResNet {2}, Custom CNN {1}, U-Net {1}, VGG {1}	Stanford-TMA, BIDMC-MGH, Private
Lu et al. (2021a)	Oral cancer	Custom CNN {1}	OP-SCC-Vanderbilt
Wang et al. (2020b)	Ovarian cancer	VGG {1}, Multi-stage CNN {1}	VGH
Wei et al. (2019b); Sali et al. (2019, 2020)	Non-cancer GI tract disorder	ResNet {2}, VGG {1}	DHMC-Wei, UV, SC-Sali
Syrykh et al. (2020); Brancati et al. (2019)	Lymphoma	E-D CNN {1}, Custom CNN {1}	TUCI-DUH, AJ-Lymph
Segmentation Task			
Hou et al. (2019a); Lafarge et al. (2019); Naylor et al. (2017); Kumar et al. (2017); Shin et al. (2016); Graham et al. (2019b); Vu et al. (2019); Hou et al. (2019b); Hu et al. (2018); Mahmood et al. (2019); Levy et al. (2020); Chen et al. (2019); Atupelage et al. (2013); Hou et al. (2020b); Khoshdeli et al. (2018); Janowczyk et al. (2018); Yen et al. (2020); Lafarge et al. (2021); Graham et al. (2020); Koohbanani et al. (2020); Wang et al. (2020a); Abdel-Nasser et al. (2020); Sahasrabudhe et al. (2020); Bai et al. (2020); Chen et al. (2020c); Xie et al. (2020); Nadeem et al. (2020); Dawood et al. (2021); Vahadane et al. (2021); Feng et al. (2021a); Dogar et al. (2021); Cheng et al. (2021b); Corredor et al. (2021)	Nuclei	U-Net {6}, Custom CNN {8}, FCN {1}, ResNet {5}, GAN {4}, Non-DL {2}, Multi-stage CNN {1}, E-D CNN {4}, Autoencoder CNN {1}, PangNet {1}, DeconvNet {1}, Hover-Net {3}, multi-branch CNN {1}, Attention(EP, SM) CNN {1}, HBA-Net {1}	MICCAI15-18, TCGA, TNBC-CI, MoNuSeg, CPM-15, CPM-17, CCB, CRCHistoPhenotypes, CoNSeP, BM-Hu, FAHZU, Liver-Atupelage, DHMC, MO-Khoshdeli, AJ-N, Kumar-TCGA, TCGA-Nuclei, SOX10, UrCyt, NLST, Pan-Bai, PanNuke, NuCLS, Cleveland Clinic (CC)
Chen et al. (2016a); Sirinukunwattana et al. (2015); Marsh et al. (2018); Nateghi et al. (2016); Graham et al. (2019a); Van Eycck et al. (2018); Yan et al. (2020b); Wang et al. (2019a); Xu et al. (2017c); Graham et al. (2020); Koohbanani et al. (2020)	Gland	FCN {2}, Non-DL {1}, Custom CNN {5}, ResNet {2}, VGG {1}, multi-branch CNN {1}, E-D CNN {1}	GLaS, Bilkent, CRAG, Priv-IHC
Takahama et al. (2019); Pimkin et al. (2018); Cruz-Roa et al. (2017); Agarwalla et al. (2017); Li et al. (2019c); Priego-Torres et al. (2020); Dong et al. (2018); Pati et al. (2018); Wang et al. (2021a); Jahanifar et al. (2021); Farahmand et al. (2022); Ho et al. (2021)	Breast tumor	Custom CNN {2}, Inception {2}, U-Net {3}, FCN 1, E-D CNN {1}, RAN {1}, DA-RefineNet {1}, DeepLab {1}, MLV-DeepLabV3 {1}	CAMELYON16, CAMELYON17, BACH18, TCGA, UHCMC-CWRU, BC-Priego-Torres, TUPAC16, AMGrad, TCGA-BRCA, Yale HER2 dataset, Yale response dataset
Qaiser et al. (2019); Xu et al. (2017a); Kim et al. (2021); Feng et al. (2020)	Colon tumor	Custom CNN {1}, VGG {1}, U-Net {2}, Non-DL {1}, AlexNet {1}	Warwick-UHCW, Warwick-Osaka, ZU, DigestPath 2019, Yeouido
Eminaga et al. (2019); Lahiani et al. (2018); Roy et al. (2021)	Liver tumor	PlexusNet {1}, U-Net {1}, Autoencoder CNN {1}	TCGA, IHC-Seg, PAIP
Wu et al. (2021)	Lung tumor	U-Net {1}	22c3, Ventana PD-L1
Eminaga et al. (2019); Avenel et al. (2019); Nour et al. (2021)	Prostate tumor	PlexusNet {1}, Non-DL {1}, U-Net {1}	SMS-TCGA, UUH, Private
Takahama et al. (2019); Liu et al. (2018a)	Stomach tumor	Inception {1}, U-Net {1}, ResNet {1}	SC-Takahama, SC-Liu
Xu et al. (2017a)	Brain tumor	AlexNet {1}	MICCAI14
Ho et al. (2020)	Bone tumor	U-Net {1}	MSKCC
Phillips et al. (2018); Cheng et al. (2022)	Skin tumor	FCN {1}, ResNet {1}, ResGANet {1}	TCGA, ISIC2018
Lerousseau et al. (2020)	Multi-organ tumor	ResNet {1}	TCGA
Marsh et al. (2018); Gadermayr et al. (2019); Hermsen et al. (2019); Gallego et al. (2021)	Kidney tissue structure	Custom CNN {1}, U-Net {1}, cascaded CNN {1}	WUPAX, M-Gadermayr, RUMC, Mayo, AIDPATH
van Eekelen et al. (2020)	Bone marrow cell	FCN {1}	RUMC
Wetstein et al. (2020)	Breast tissue subtype	U-Net {1}	NHS
Chan et al. (2019)	Histological tissue type	Custom CNN {1}	ADP
Guo et al. (2019)	Liver steatosis	ResNet {1}	Liv-Guo
Jiménez and Racoceanu (2019); Kausar et al. (2020)	Mitosis	U-Net {1}, FCN {1}	MITOS12, MITOS-ATYPIA14, AMIDA13
Das et al. (2018); Shephard et al. (2021)	Oral mucosa, Oral Epithelial Dysplasia	Custom CNN {1}, Hover-Net+ {1}	BCRWC, Private
Saltz et al. (2018); Narayanan et al. (2019); Guerrero and Oliveira (2021)	Lymphocytes(Tumor-infiltrating,segmentation)	E-D CNN {1}, IM-Net {1}, DRDIN {1}, U-Net {1}, SegNet {1}	TCGA, DUKE, Lymphocyte Detection(from Andrew Janowczyk and Anant Madabhushi)
Bándi et al. (2019); Xing et al. (2021)	Tissue region, Fluid Lesions	Custom CNN {1}, FCN {1}, IAUNet {1}	Bándi-Dev-Set, Bándi-Dis-Set, RETOUCH
WSI Processing Task			
Brieu et al. (2019); Shaban et al. (2019b); Ren et al. (2019); Lahiani et al. (2019a,b); Levy et al. (2020); Otálora et al. (2019)	Domain adaptation	GAN {5}, U-Net {1}, AlexNet {1}, Custom CNN {1}, ResNet {5}	NHS-LTGU, MITOS-ATYPIA14, RCINJ, Roche, Liv-Lahiani, TUPAC16, TCGA, DHMC, SOX10, UrCyt
Arvidsson et al. (2019); Bug et al. (2017); Khan et al. (2014); Bautista and Yagi (2015); Zanjani et al. (2018); Salvi et al. (2020); Mahapatra et al. (2020); Nadeem et al. (2020)	Stain normalization	Custom CNN {2}, ResNet {1}, VGG {1}, U-NET {1}, GAN {3}, E-D CNN {1}, Multi-stage CNN {1}, Non-DL {4}	SUH, Leica Biosystems, MO-Khan, MGH, Lym-Bejnordi, Salv SCAN, MITOS-ATYPIA14

Table 8.3 Continued on Next Page

Technicalities by Task (Continued)

Continuation of Technicalities by Task Table 8.3			
References	Disease/Organ Specification	Architecture	Datasets
Hou et al. (2019a); Thuy and Hoang (2019); Mahmood et al. (2019); Claudio Quiros et al. (2021); Levine et al. (2020); Chen et al. (2021b); Deshpande et al. (2022)	Patch synthesis	Custom CNN {2}, GAN {5}, PG-GAN {2}, ResNet {1}, VGG {1}, U-Net {2}	MICCAI16/17/18, Kumar-TCGA, BreakHis, NKI-VGH, TCGA, OV-CARE, ISIC 2020, ChestXray-NIHCC, CRAG, Digestpath
Tellez et al. (2019a); Cho et al. (2017); Ziae et al. (2020); Nadeem et al. (2020)	Processing technique comparison	U-Net {1}, Custom CNN {2}, GAN {2}	RUMC, CAMELYON16, MITOS-ATYPIA14
Tellez et al. (2019b, 2020)	WSI compression	Custom CNN {2}, E-D CNN {1}, GAN {1}	N/A
Ponzio et al. (2020)	Data cleaning	ResNet {1}	ULEeds
Sarnecki et al. (2016)	Stain augmentation	VGG {1}	Kid-Cicalese
Sarnecki et al. (2016)	Tissue component discrimination	Non-DL {1}	TCGA, MO-JHU/US/UB
Nahid and Kong (2018)	WSI transformations	Custom CNN {1}	BreakHis
Thandiackal et al. (2022)	WSI Classification	MIL {1}	IMP Diagnostics Lab., BRIGHT, CAMELYON16
Patient Prognosis Task			
Mobadersany et al. (2018); Zadeh Shirazi et al. (2020); Hao et al. (2019); Tang et al. (2019); Rathore et al. (2019)	Brain cancer	Inception {1}, VGG {1}, Custom CNN {2}, Capsule CNN {1}, ResNet {1}	TCGA
Yu et al. (2016); Tang et al. (2019); Wang et al. (2019b, 2020a); Yao et al. (2020); Lu et al. (2021a); Chang et al. (2021)	Lung cancer	Custom CNN {2}, Non-DL {2}, Attention-MIL {1}, MI-FCN {1}, HANet {1}	Stanford-TMA, TCGA(-LUSC), CHCAMS, NLST, ES-NSCLC
Kather et al. (2019a); Bychkov et al. (2018); Ji et al. (2020); Yao et al. (2020)	Colon cancer	VGG {2}, Inception {1}, ResNet {1}, Non-DL {1}, AlexNet {1}, SqueezeNet {1}, AttentionMIL {1}, MI-FCN {1}	NCT-CRC-HE-100K, NCT-CRC-HE-7K, HUCH, WRH-WCH, MCO
Fuchs et al. (2008); Almansouri and Zwyera (2020); Lu et al. (2022)	Kidney cancer	Non-DL {2}, AttentionMIL {1}	UHZ, TCGA, HPA
Lu et al. (2020c, 2022)	Breast cancer	U-Net {1}, AttentionMIL {1}	AJ-Lymph, TCGA
Nagpal et al. (2019)	Prostate cancer	Inception {1}	NMCSD+MML+TCGA
Saltz et al. (2018)	Melanoma	Multi-stage CNN {1}	MIP, YSM, GHS
Courtiol et al. (2019)	Mesothelioma	ResNet {1}	MESOPATH, TCGA
Chen et al. (2021c, 2022)	Multi-Organ	AttentionMIL {1}, GCN {1}, ViT {1}	TCGA, CRC-100K, BCSS, BreastPathQ
Wang et al. (2017b); Lewis Jr et al. (2014)	Recurrence prediction	Custom CNN {1}, Non-DL {1}	NSCLC-Wang, ROOHNS
Other Tasks			
Kiani et al. (2020); Steiner et al. (2018); Raciti et al. (2020); Hekler et al. (2019); Schömöig-Markiewka et al. (2021); Schuchmacher et al. (2021)	Clinical validation, Stress Test, Quality Control, Explainability	DenseNet {1}, ResNet {2}, Inception {1}, Inception-ResNet {1}, Extended U-Net {1}	SUMC, Bre-Steiner, Pro-Raciti, DKI, TCGA, Private
Kumar et al. (2020a); Hosseini et al. (2019); Hou et al. (2020b); Yan et al. (2020c); Miao et al. (2021); Jaume et al. (2021a); Graham et al. (2021); Bussola et al. (2021); Bayat et al. (2021); Schrammen et al. (2022); Koziarski et al. (2021); Yamashita et al. (2021); Brancati et al. (2021); Khened et al. (2021)	Dataset creation/curation and annotation, Integrated API and (End-to-End) Toolkits	Custom CNN {1}, GNN {1}, VGG {3}, Inception {3}, AlexNet {1}, FCN {2}, U-Net {4}, ResNet {6}, Hover-Net {1}, DenseNet {1}, MobileNet {1}, DeepLab {1}, SLAM {1}	CMTHis, ADP, TCGA, TCGA-Nuclei, PUIH, BRACS, BACH, UZH, SICAPv2, Lizard, GTEx Dataset(V8), BreakHis, HF(Heart failure) Dataset, DACHS, YCR-BCIP, Diagset-A, Diagset-B, Diagset-C, Painter by Numbers, miniImageNet, CRC(DX), CAMELYON(16,17), DigestPath, PAIP, Private
Hägele et al. (2020); Foucart et al. (2019); Thagaard et al. (2020)	Data deficiency study	Inception {1}, Custom CNN {1}, ResNet {1}	TCGA, GLaS, CAMELYON16, CAMELYON17, Thagaard
Hegde et al. (2019); Gildenblat and Klaiman (2019); Zheng et al. (2020); Lara et al. (2020); Jewsbury et al. (2021); Kim et al. (2021); Guéréndel et al. (2021); Freyre et al. (2021)	Image retrieval/compression, Representation Learning	ResNet {1}, Inception {1}, Non-DL {2}, GCN {1}, AttnMIL {1}, Custom CNN {2}, U-Net++ {1}, Barcodes {1}, XGBoost {1}, K-Means {1}	TCGA, CAMELYON16, SC-Zheng, CRA, Han-Wistar Rats
Gamper et al. (2020b); Tellez et al. (2020); Lai et al. (2021); Li et al. (2021a); Chen et al. (2021c); Tran et al. (2021); Srinidhi and Martel (2021); Lu et al. (2021e); Srinidhi et al. (2022); Boyd et al. (2021); Dawood et al. (2021); Belharbi et al. (2021b); Ciga et al. (2022); Pal et al. (2021); Freyre et al. (2021); Marini et al. (2021); Li et al. (2021c); Schrammen et al. (2022); Feng et al. (2021a); Alharbi et al. (2021); Höhne et al. (2021); Bilal et al. (2021); Anand et al. (2021); Shao et al. (2021)	Multi-(task,instance) learning(MT,MIL), (Weak,Semi,Self)-Supervised Learning, Contrastive Learning	ResNet {9}, GCN {1}, AttentionMIL {2}, MuSTML {1}, SimCLR {3}, MIL {2}, D(S)MIL {1}, Pretext-RSP {1}, MoCo {1}, MLP {1}, CLAM {1}, GAN {1}, VGG {2}, DenseNet {2}, Hover-Net {2}, Custom CNN {2}, SLAM {1}, DLA {1}, TransMIL {1}	UHC-WNHST, PanNuke, AJ-Epi-Seg, OSCC, TCGA(-CRC-DX, -THCA, -NSCLC, -RCC), CAMELYON16, CAMELYON17, NCT-CRC-HE-100K, NCT-CRC-HE-7K, CPM-17, AJ-Lymph, M-Qureshi, SKMCH&RC, SKMCH&RC-M, OV-Kobel, MT-Tellez, TUPAC16, SC-Galjart, CT-CRC-HE-100K, Munich AML, MSK, MHIST, CPTAC, Kather multi-class, BreastPathQ, CRC, Novel, PanNuke, NuCLS, GlA, OAHTC, DACHS, YCR-BCIP, BreakHis, DEC, TH-TMA17
Tellez et al. (2018, 2019b); Geread et al. (2021)	Proliferation scoring	Custom CNN {2}, piNET {1}	TUPAC16, DeepSlides
Hu et al. (2018)	Cell clustering	ResNet {1}	MICCAI15, BM-Hu, FAHZU
Hu et al. (2018)	Chemosensitivity prediction	Non-DL {1}	TCGA
Tang et al. (2021)	Neural Architecture Search	DARTS {1}	ADPBCCS,BACH, Osteosarcoma
Faust et al. (2019); Gildenblat and Klaiman (2019); Carse et al. (2021); Roy et al. (2021); Diao et al. (2021b); Feng et al. (2021a)	Feature extraction/analysis, Unsupervised Learning	VGG {1}, Custom CNN {2}, Hover-Net {1}, PixelCNN {1}, AutoEncoder CNN {1}	CAMELYON16, UHN, TCGA, Private
Coudray et al. (2018); Höhne et al. (2021); Bilal et al. (2021); Anand et al. (2021)	Gene mutation prediction	VGG {1}, Inception {1}, AttentionMIL {2}, DenseNet {1}, ResNet {1}, Hover-Net {1}	TCGA(-CRC-DX, -THCA), DEC, PAIP, TH-TMA17, Private

Table 8.3 Continued on Next Page

Technicalities by Task (Continued)

Continuation of Technicalities by Task Table 8.3			
References	Disease/Organ Specification	Architecture	Datasets
Meng et al. (2019); Wu et al. (2019); Pati et al. (2021a); Feng et al. (2020); Javed et al. (2021)	Novel loss function, Novel optimizer	ResNet {3}, VGG {3}, MobileNet {1}, DenseNet {1}, U-Net {1}	BACH18, AJ-Lymphocyte, CRCHistoPhenotypes, CoNSeP, ICPR12, AMIDA13, Kather Multi-class, DigestPath 2019, CT-CRC-HE-100K
Xu et al. (2016); Srinidhi and Martel (2021)	Patch triaging	Non-DL {1}, ResNet {1}, Pretext-RSP {1}, MoCo {1}, MLP {1}	BIRL-SRI, CAMEYTHON16, MSK, MHIST
Alawad et al. (2020); Mu et al. (2021)	Pathology report information extraction	BERT {1}, Custom CNN {1}	LTR
Lu et al. (2020b)	Receptor status prediction	Custom CNN {1}	TCGA
Xu et al. (2020)	TMB prediction	Inception {1}	TCGA
Tellez et al. (2018); Lagree et al. (2021)	Tumor grading	Mask R-CNN {1}, Custom CNN {1}, Non-DL {1}	TUPAC16, Post-NAT-BRCA, ILC
Corvo et al. (2020)	Visual analytic tool	Non-DL {1}	TCGA

End of Table 8.3

8.4. Model Card Categorization

8.4.1. Template

Model-Card for Categorizing Computational Pathology Papers

Step-1) Paper Summarization:

Summarize the paper in terms of (A) Goal/Problem of the paper to be solved; (B) Why the problem introduced by the authors is important to the community in terms of Technical Novelty, Comprehensive Experiment, New Insights, Explainability; and (C) Overall conclusion of the paper.

Step-2) Model Card Table Categorization:

The following is a model-card for each paper to populate the table accordingly. Find relevant information within each category that is reported in the paper. Try to compile it efficiently and populate each sub-type within each category.

Keywords	comma separated list
Organ Application	Organ: Task:
Dataset Compilation	Name: Availability: Dataset Size: (#patches/#slides/#images) Image Resolution: Staining Type: Annotation Type: (region/patch/slide-level) Histological Type: (cellular/tissue ROI/etc, I.e., on what basis is it labeled) Label Structure: (single label/multi label) Class Balance: (is size of dataset balanced across each classes)
Technicity	Model: (architecture/transfer learning/output format) Training Algorithm: (end-to-end/separately staged) Code Availability: (give source)
Data Processing	Image Pre-processing: (patching, data augmentation, color normalization) Output Processing:
Performance Summary	Evaluation Metrics: Notable Results: Numerical result for strongest performing model. Comparison to Other Works: Comparison to state-of-the-art models (one sentence)
Novelty	Medical Applications/Perspectives: Technical Innovation: (algorithms for processing or deep learning, new metrics)
Explainability	Visual Representations: (feature distribution, heatmaps, tsne, gradCAM, pseudocode, etc.)
Clinical Validation	Usage in Clinical Settings: Has the work been used by pathologists in clinical setting? Suggested Usage: How can the work be used by pathologists? Performance Comparison: Has the model performance been compared to that of pathologists?
Caveats and Recommendations	<ul style="list-style-type: none"> • Personal comments on the paper • Relevant info from other papers • Criticism and limitations of the work

Step-3) Citation: BibTeX Citation.

8.4.2. Samples

Paper: Pathologist-level classification of histologic patterns on resected lung adenocarcinoma slides with deep neural networks

Summary:

Classification of histological structures in lung adenocarcinoma tissue is important for patient prognosis and treatment plans. Some histological patterns (such as lepidic patterns) are associated with better survival rates, whereas others (micropapillary and solid patterns) are associated with poor prognoses. The identification of these histological patterns is a challenge, as 80% of adenocarcinoma tissue samples contain a mixture of different patterns, and the qualitative classification criteria can result in variance in diagnosis between different pathologists. Automated analysis and classification of tissue structures through convolutional neural networks has been a compelling area of research. This paper presents a variant of ResNet, ResNet18 to perform a patch-based classification amongst the different lung adenocarcinoma histological patterns. A heatmap for the entire WSI is made using the probability score per patch, with low-confidence patches being discarded. The performance of the model is compared with 3 expert pathologists to determine relative performance. The study concludes that the model has high performance, with results on par with expert pathologists.

Categorization:

Keywords	Deep learning, convolutional neural networks, lung adenocarcinoma, multi class, ResNet
Organ Application	Organ: Lung Task: Histologic pattern classification in lung adenocarcinoma
Dataset Compilation	Name: Dartmouth-Hitchcock Medical Centre in Lebanon, New Hampshire Availability: Unavailable due to patient privacy constraints. Anonymized version available upon request. Dataset Size: 422 WSIs, 4 161 training ROIs, 1 068 validation patches Image Resolution: 20x magnification Staining Type: H&E Annotation Type: Region-level training set, patch-level validation set, slide-level test set Histological Type: Lepidic, acinar, papillary, micropapillary, solid, and benign. Label Structure: Single label Class Balance: Imbalanced, with significantly fewer papillary patterns in all data.
Technicity	Model: ResNet model with 18 layers Training Algorithm: <ul style="list-style-type: none"> • Multi-class cross-entropy loss • Initial learning rate of 0.001 • Learning rate decay by factor of 0.9 per epoch Code Availability: https://github.com/BMIRDS/deepslide
Data Processing	Image Pre-processing: <ul style="list-style-type: none"> • Created training ROIs by selectively cropping regions of 245 WSIs. • Spliced 34 validation WSIs into 1 068 224x224 patches. • Colour channel normalization to mean and standard deviation of entire training set. • Data augmentation by rotation; flipping; and random colour jittering on brightness, contrast, hue, and saturation. Output Processing: Low-confidence predictions filtered out for predictions below a threshold. Thresholds are determined by a grid search over classes, optimizing for similarity between the trained model and the validation data.
Performance Summary	Evaluation Metrics: F1-Score, AUC Notable Results: F1-Score of 0.904 on validation set, AUC greater than 0.97 for all classes. Comparison to Other Works: ResNet18, 34, 50, 101, 152 compared for performance to choose optimal depth. All had similar accuracies on validation set, so chose ResNet18 for lower model complexity.
Novelty	Medical Applications/Perspectives: Potential platform for quality assurance of diagnosis and slide analysis. Technical Innovation: First paper to attempt to classify based on histological lung adenocarcinoma subtypes.
Explainability	Visual Representations: Heatmaps for patterns detected, AUC curve for each class
Clinical Validation	Usage in Clinical Settings: N/A Suggested Usage: <ul style="list-style-type: none"> • Could be integrated into existing lab information management systems to provide second opinions to diagnoses. • Visualization of a slide could highlight important tissue structures. • Could help facilitate tumour diagnosis process by automatically requesting genetic testing based on histological data for patient. Performance Comparison: <ul style="list-style-type: none"> • On par with pathologists for all evaluated metrics • Model in agreement 66.6% of the time with pathologists on average, with robust agreement (agreement with 2/3 of the pathologists) 76.7% of the time. • WSI region annotation differences between pathologist and model are compared for a sample slide.
Caveats and Recommendations	<ul style="list-style-type: none"> • Data taken from one medical centre, so may not be representative of lung adenocarcinoma morphology • Dataset relatively small compared to other deep learning datasets, with some classes having very few instances

Citation:

```
@article{wei2019pathologist,
title={Pathologist-level classification of histologic patterns on resected lung adenocarcinoma slides with deep neural networks},
author={Wei, Jason W and Tafe, Laura J and Linnik, Yevgeniy A and Vaickus, Louis J and Tomita, Naofumi and Hassanpour, Saeed},
journal={Scientific reports},
volume={9},
number={1},
pages={3358},
year={2019},
publisher={Nature Publishing Group UK London}
}
```

Paper: Classification of lung cancer histology images using patch-level summary statistics**Summary:**

The classification of non-small cell lung cancer WSIs as either lung adenocarcinoma (LUAD) or lung squamous cell carcinoma (LUSC) is an important task in diagnosis and treatment planning. Manually classifying these WSIs is a laborious and subjective task that is often complicated by poorly differentiated tissue structures within the slide. Automated classification of WSIs may facilitate the analysis of non-small cell lung cancers. This paper proposes a new 3-class network for effective classification of tissue regions within a WSI. It uses a modification of the ResNet50 architecture, ResNet32 to create probability maps of LUAD/LUSC/non-diagnostic pixels in the WSI. Features from these probability maps are next extracted and fed into a random forest classifier for the final classification. The model achieves the greatest accuracy of 0.81 in the Computational Precision Medicine Challenge and provides a new method of classification for non-small lung cancer histological images.

Categorization:

Keywords	Non-small cell lung cancer, histology image classification, computational pathology, deep learning
Organ Application	Organ: Lung Task: Classification between non-small cell lung cancer types
Dataset Compilation	Name: Computational Precision Medicine at MICCAI 2017 Availability: Unavailable, link on MICCAI 2017 website unreachable Dataset Size: 64 WSIs Image Resolution: 20× magnification Staining Type: H&E Annotation Type: Pixel-level and Slide-level Histological Type: <ul style="list-style-type: none"> At pixel-level, classifies as lung adenocarcinoma (LUAD), lung squamous cell carcinoma (LUSC), and non-diagnostic (ND) At slide-level, LUAD or LUSC Label Structure: Single label Class Balance: Balanced dataset at the slide level, 32 LUAD and 32 LUSC
Technicity	Model: <ul style="list-style-type: none"> Ensemble ML model Variant of ResNet50, called ResNet32 with 32 layers and 3x3 kernel, as compared to 7x7 kernel with ResNet50. 50 statistical and morphological features extracted from probability maps generated by ResNet32. The top 25 are selected for best class separability and used as input to a random forest. Training Algorithm: Separately staged, ResNet32 creates probability maps, then random forest generates final prediction for each WSI Code Availability: Unavailable
Data Processing	Image Pre-processing: <ul style="list-style-type: none"> Splicing of slides into 256×256 patches, then random cropping into 224×224 patches Reinhard stain normalization Random crop, flip, rotation data augmentation Output Processing: N/A
Performance Summary	Evaluation Metrics: Accuracy Notable Results: <ul style="list-style-type: none"> ResNet32 with Random Forest achieves 0.81 accuracy over WSI Results superior to ResNet32 with Maximum Vote, which had 0.78 accuracy. Features for the random forest are tailored for WSI classification, and so can achieve higher performance. Comparison to Other Works: Compared ResNet32 to VGG, GoogLeNet, and ResNet50, with higher average classification accuracy.
Novelty	Medical Applications/Perspectives: Automated distinguishing of LUAD tissue from LUSC could be done at scale to assist pathologists in diagnosis and treatment planning for patients. Technical Innovation: <ul style="list-style-type: none"> First 3-class network for classification of WSI into diagnostic/nondiagnostic areas Ensemble method resulted in greatest accuracy at the MICCAI 2017 competition.
Explainability	Visual Representations: Probability maps for each pixel-level class
Clinical Validation	Usage in Clinical Settings: N/A Suggested Usage: Automated distinguishing of LUAD and LUSC slides could aid pathologists in treatment planning. Performance Comparison: N/A
Caveats and Recommendations	<ul style="list-style-type: none"> Because features for random forest training are chosen based on categorization of lung tissue samples, may not be able to generalize well to other tissue types.

Citation:

```
@inproceedings{graham2018classification,
title={Classification of lung cancer histology images using patch-level summary statistics},
author={Graham, Simon and Shaban, Muhammad and Qaiser, Talha and Koohbanani, Navid Alemi and Khurram, Syed Ali and Rajpoot, Nasir},
booktitle={Medical Imaging 2018: Digital Pathology},
volume={10581},
pages={327–334},
year={2018},
organization={SPIE}
}
```

Paper: Digital pathology and artificial intelligence (Review)

Summary:

The advent of cheaper storage solutions, faster network speed, and digitized WSIs has greatly facilitated the presence of digital pathology in modern pathology. Particularly, WSIs allow for the development and integration of automated AI tools for histopathological analysis into the pathologist's workflow. AI tools have the potential to increase the efficiency of diagnostics and improve patient safety and care. However, histological analysis comes with several challenges, including the large size, different potential image magnifications, presence, and variation of stain color information, and z-axis information (in the thickness of the slide). These challenges make it difficult for a human viewer to extract all available information and provide important issues that an AI tool must overcome. This paper outlines several different areas in which AI may be applied in digital pathology, namely education, quality assurance (QA), clinical diagnosis, and image analysis. The potential uses are outlined as follows:

- Education: Through the digitization of slides, education can be enhanced. As slides no longer need to be viewed through a microscope, and images can be zoomed into and panned, convenience can be increased without sacrificing the quality of education. Synthetic tissue sample images using GANs can be used to easily create test material in trainees, as well as evaluate cognitive biases in practicing pathologists.
- Quality Assurance: Can help pathologists remain updated in their field and check for lab proficiency of diagnoses, as well as monitor for inter-observer variance.
- Clinical Diagnosis: AI can aid in the preparation of digital slide imagery, such as in reducing the frequency of out-of-focus areas in slides. Color and stain normalization methods using AI-based models are another possible area of application.
- Image Analysis: AI can be used to process the data, including in nuclear segmentation and ROI detection.

AI systems have several different limitations. AI models have been criticized as being black box models. Explainability of decisions will need to be increased. While visualization techniques are being developed, these tend to reduce performance. Additionally, regulatory and economic effects of AI-based systems are unknown at this time. Some areas of future research for AI applications in computational pathology include one-shot learning and reinforcement learning.

Citation:

```
@article{niazi2019digital,
title={Digital pathology and artificial intelligence},
author={Niazi, Muhammad Khalid Khan and Parwani, Anil V and Gurcan, Metin N},
journal={The lancet oncology},
volume={20},
number={5},
pages={e253–e261},
year={2019},
publisher={Elsevier}
}
```